Improved wideband coaxial methods for dielectric measurements on nitrogen ceramics

Abu Bakar Ahmad

IMPROVED WIDEBAND COAXIAL METHODS

FOR

DIELECTRIC MEASUREMENTS ON NITROGEN CERAMICS

A Thesis submitted to the University of Durham

by

Abu Bakar Ahmad, M.Sc. (Leeds)

for the degree of

Doctor of Philosophy

Department of Applied Physics

and Electronics, Science Laboratories,

Durham City, England

MARCH 1983

To my wife: Fawzia

and sons: Imran-Faisal

& Imran-Firdauz

ABSTRACT

Two methods of measuring the dielectric properties of materials - matched termination and coaxial line resonance - have been developed and used to study the properties of two groups of nitrogen ceramics, namely, silicon nitrides and oxynitride glasses. In these methods advantage is taken of the wide frequency range, from 500 MHz up to about 9 GHz, covered by a single apparatus - the General Radio slotted coaxial line. Previous measurements in this Department have indicated the difficulties in the determination of the loss tangent of low to medium loss samples ($\tan \delta \sim 10^{-3} - 10^{-2}$). The two methods developed reduced these difficulties. The applicability of these methods was assessed using known materials including the high loss liquids water and chlorobenzene, medium loss solutions of chlorobenzene in cyclohexane and the low loss solids polymethyl methacrylate and polytetrafluoroethylene.

The silicon nitride ceramics were in various degrees of nitridation given by the weight gain which ranged from 38% for partially-nitrided to a maximum of 63.2% for the fully-nitrided samples. The dielectric constant at 1 GHz increased from 4.51 for fully-nitrided to about 9.9 for the 38% weight gain samples. The fully-nitrided material has a loss factor of 7.6×10^{-3}; this increased to 1.85×10^{-1} as the weight gain decreased to 38% . These values have been

extrapolated to 'zero weight gain' and compared with pure silicon for which the dielectric constant is 11.7 and the loss factor approximately 0.2. The oxynitrides have dielectric constants between 6.5 and 7.5 depending on the cation present and the percentage of nitrogen substituted for oxygen in the glasses. ε' increased in the cation order Mg, Y, Ca and increased with increasing nitrogen substitution in each cation series. The loss factor, however, depends not only on these cation types but also on the other constituents of the glasses.

The dielectric constant of both the silicon nitride ceramics and oxynitride glasses fitted the Jonscher universal law of dielectric response $(\varepsilon' - \varepsilon_\infty) \propto \omega^{n-1}$, where the exponent $n \simeq 1$ for all the samples. Similarly, the loss factor for these materials showed a frequency dependence $\varepsilon'' \propto \omega^{n-1}$, again with n approximately 1. This is a limiting case of dielectric behaviour corresponding to a frequency independent loss where most dipolar processes have been eliminated.

ACKNOWLEDGEMENTS

I am most grateful to my supervisors, Dr. J.S. Thorp and Dr. B.J.J. Kulesza for their guidance, advice and encouragement, and who were always very keen to help in every possible way throughout my work.

I would like to express my gratitude to the University of Malaya for the award of a scholarship and for the grant of study leave from January 1980 until May 1983.

My sincere thanks are due to Prof. G.G. Roberts for giving me access to the facilities of the Department, and to the technical staff of the Department, especially Mr. R.T. Harcourt, for his help in the sample preparation, and to Messrs. W. Mounsey and P.J.E. Richardson, for their assistance in the construction of apparatus.

I would also like to thank Prof. K.H. Jack of the University of Newcastle-upon-Tyne and members of his group for supplying the oxynitride glass samples.

Last, but not least, I am grateful to my wife, Fawzia, whose patience and encouragement throughout my work made it possible for me to produce this Thesis.

CONTENTS

CHAPTER 1

INTRODUCTION

1.1 OBJECTIVES

One of the prime interests of the present work is to extend and develop previous measurements on the dielectric properties of two groups of nitrogen ceramics, namely (a) silicon nitrides and (b) oxynitride glasses. In previous work carried out in this Department the studies on these materials were restricted in two ways, i.e. in general to the low frequency range (1×10^3 to 5×10^4 Hz) and by the fact that the dielectric constant could be fairly well measured while various problems were encountered in the determination of the loss factor. Hence this research project developed in two complimentary ways. Firstly, the development of techniques, especially of the loss factor at high frequencies, and secondly their applications to the two groups of materials mentioned.

A general review of conventional methods currently employed in dielectric property measurements in the frequency range from 100 MHz up to 10 GHz was undertaken to establish which lines of approach would be more appropriate and this is given in section 1.2 below. The choice of the methods to be used would depend on the possibility of the same equipment providing coverage over a wide frequency range. Preference would also be given to the potential use of few or just one

sample configuration over the whole frequency range of interest.

1.2 GENERAL REVIEW

1.2.1 Microwave Dielectric Measurements

Microwave dielectric property measurements have been traditionally associated with the fields of electrical engineering and telecommunications. Recently however, a variety of techniques have been developed for the non-destructive determination and control of the thickness, dielectric constant and moisture content of slab-like materials in production environments [1.1, 1.2] . Extensive use of microwaves in domestic and industrial food processing and the general problem of electromagnetic pollution have resulted in increasing research into the biological effects of microwave radiation [1.3] . In agriculture, data on the frequency dependence of dielectric properties of grains and insects are useful for the determination of the optimum frequency range for selective dielectric heating of stored-grain insects with microwave energy [1.4] . Other applications in this area that depend upon the dielectric properties of grains and seeds include microwave treatment of hard seeds to assist germination [1.5] and the electrical determination of moisture content in grains [1.6] . Microwave dielectric measurements may be an invaluable non-invasive technique for investigating some properties of proteins [1.7] , for example some dielectric

properties of lipoproteins of normal and sick individuals exhibit significant differences; similarly differences have been observed between sera or erythrocytes of normal individuals and those of solid-tumor patients [1.8]. Together with the development of in vivo measurement methods [1.9, 1.10] these microwave techniques appear potentially able to provide diagnostic and therapeutic treatments [1.3, 1.8].

Various microwave dielectric property measurement techniques employing coaxial lines, hollow waveguides, open transmission lines and resonant cavities have been described in the literature in both the frequency and time domains [e.g 1.11 - 1.20]. It is not intended here to elaborate on nor to give an exhaustive list of these techniques. However, the coaxial line reflection methods, in particular the short-circuit termination method, will be described to some extent (see later). In the coaxial line methods (and for waveguides in general) the structure to be measured may be viewed as the termination or transmission type depending on whether it possesses one or more accessable ports or terminal pairs in its network representation [1.21]. The termination-type structure can be represented as a one port equivalent network whose parameters can be obtained from a single input measurement. The transmission-type structure, on the other hand, can be analyzed by terminating the structure on the output side with various known loads.

1.2.2 Coaxial Line Reflection Methods

1.2.2.1 Sample Configurations

In the coaxial line reflection methods the permittivity is either calculated from measurements of the input impedance or the reflection coefficient (or the scattering parameter S_{11} [1.21 - 1.23]) on the input side of the sample holder. A reference plane is initially defined, this usually being located at the input interface of the dielectric sample (the plane A-A in Fig.1.1(a), say). In the case of the slotted coaxial lines, measurements of the voltage standing-wave ratio (VSWR) and the position of the voltage standing-wave minimum with respect to a reference plane yield the reflection coefficient for the sample [1.12, 1.13, 1.17]. The reflection coefficient can also be determined by other means, for example, by using a network analyzer [1.24, 1.25] and by forming a resonator terminated by the sample [1.24]. Possible sample configurations for the coaxial line reflection methods are illustrated in Fig.1.1. The samples are denoted by the complex relative permittivity ε^* and finite sample thicknesses are denoted by d. Wherever it is indicated that an equivalent electrical length should be infinity, the sample should be sufficiently long for the electric field to be at least two orders of magnitude less behind the sample than its value at the interface with the coaxial line. In all cases the sample is placed at or near the end of a coaxial line of internal diameter a, outer

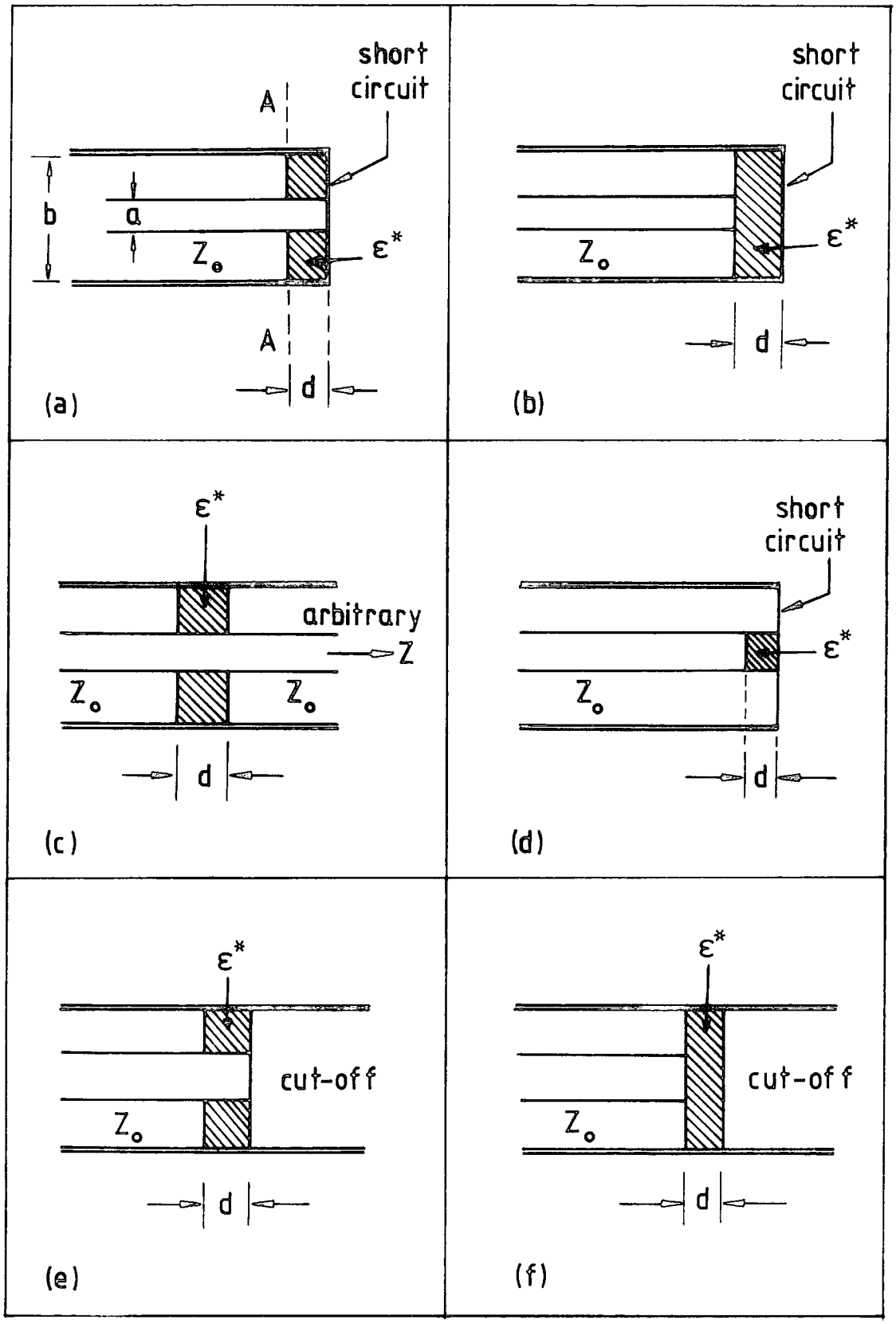

Fig. 1-1 Coaxial line sample configurations

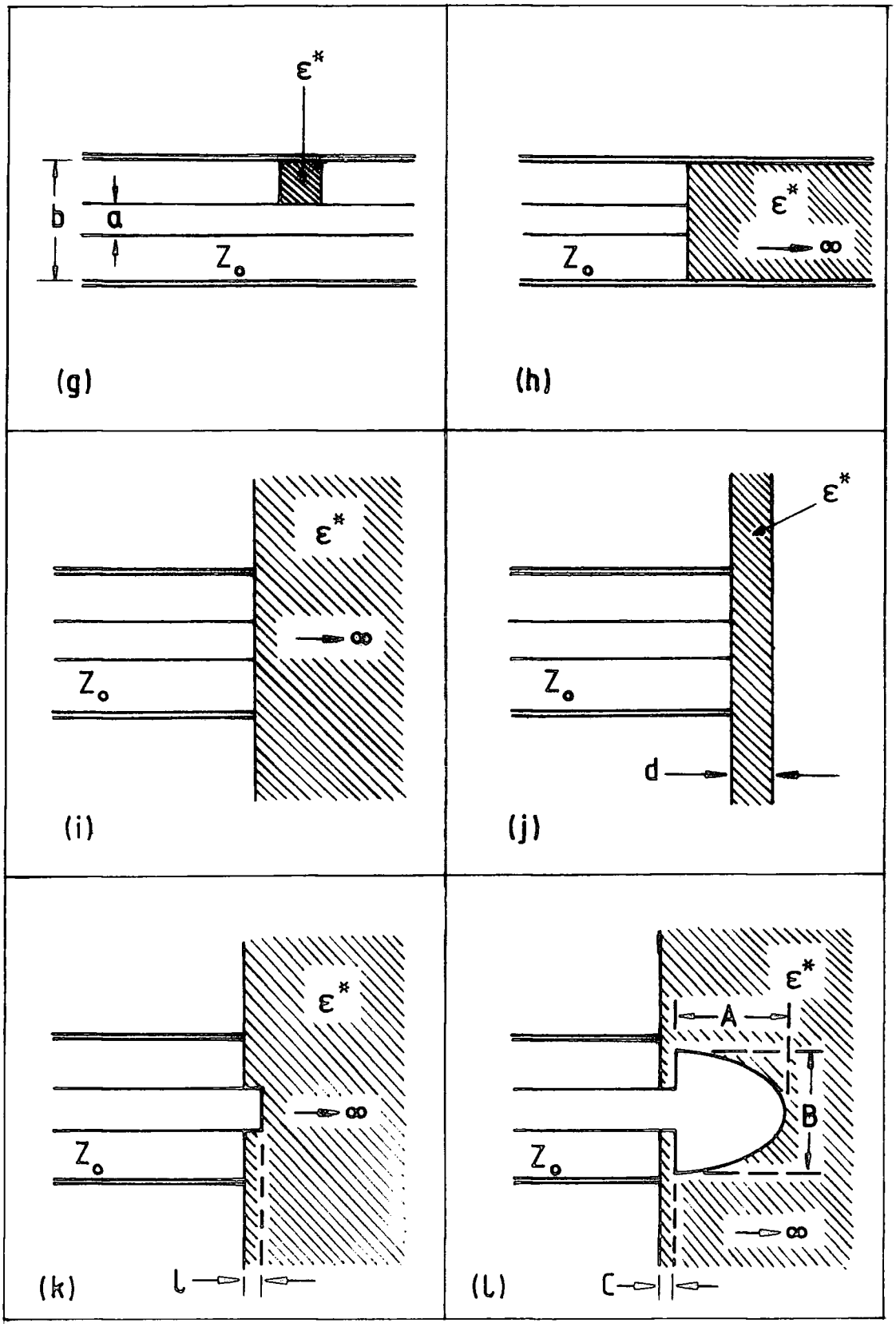

Fig. 1-1 (continued)

diameter b and of characteristic impedance Z_o . Some of the samples may be machined to the internal dimensions of the coaxial line cross-section and constitute part of it, as for example in Fig.1.1(a), (c) and (e). In other cases they may terminate the coaxial line, like those in Fig.1.1(i), (j) and (k). Some of the configurations allow easy monitoring and control of the sample temperature; this is generally true for those in which the sample is placed against a short-circuit, examples of which are furnished by Fig.1.1(b) and (d). The coaxial line operates in the transverse electromagnetic (TEM) mode and does not support higher order modes.

1.2.2.2 Equivalent Circuits

Fig.1.2 shows some of the useful equivalent circuits [1.13, 1.14, 1.27] for the sample configurations given in Fig.1.1. The equivalent circuits illustrated in Fig. 1.2(a) are very general and are also applicable to other waveguides [1.13]. For low microwave power (small signal theory) it can be assumed that the dielectric properties of the samples are linear. The samples can be taken as symmetric [1.21] and so are their impedance (Z), admittance (Y) and scattering (S) representations. In this case the circuit elements $Z_{22} = Z_{11}$, $Z_{21} = Z_{12}$, $Y_{22} = Y_{11}$ and $Y_{21} = Y_{12}$. Similarly the scattering parameters $S_{22} = S_{11}$ and $S_{21} = S_{12}$. In general the equivalent circuit shown in Fig.1.2(b) can be applied to all the sample configurations when the sample

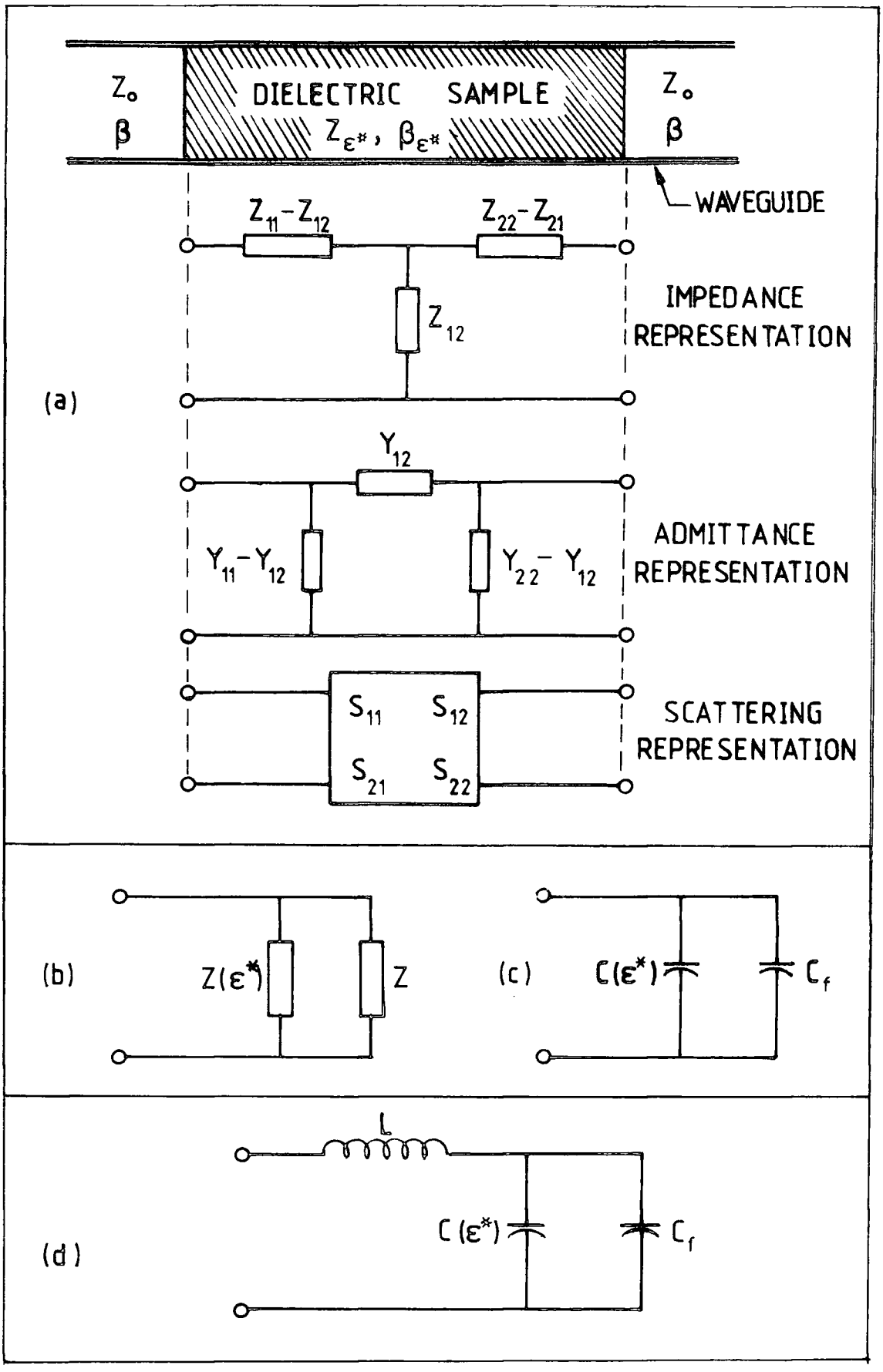

Fig. 1·2 Equivalent circuits for the sample configurations in Fig. 1·1

thickness d is small compared to the guide wavelength λ_g, [1.28]. With restrictions, the simplified version given in Fig.1.2(c) applies to all but the configurations shown in Fig.1.1(c) and (g). When the coaxial line and sample are terminated by a circular waveguide, Fig.1.1(e) and (f), the equivalent circuit may be given as in Fig.1.2(d), [1.19, 1.24]. For a lossy dielectric the capacitance $C(\varepsilon^*)$ in Fig.1.2(c) also includes the conductance due to the losses [1.28]. The equivalent circuit for samples terminating the coaxial lines, as in Fig.1.1(i) - (l), contains an additional element, say R, which represents the radiation conductance in parallel with the circuit elements in Fig.1.2(c). The dielectric properties of liquids and powders may be measured using all the configurations except those in Fig.1.1(d) and (g), by placing suitable 'windows' at the coaxial line - sample interfaces and by choosing the appropriate equivalent circuit representations. Significant errors may be introduced, however, unless the windows are constructed of very thin low dielectric constant materials. Both frequency and time domain techniques have been applied to the various sample configurations, but that given in Fig.1.1(a) gives poor accuracy [1.28]. For all the configurations in which the size of the sample can be controlled there is an optimum sample size, for a given frequency and permittivity, that will give the smallest uncertainty of the measurements [1.12, 1.13, 1.15, 1.19]. There is thus an optimum value of the capacitance $C(\varepsilon^*)$ for which small changes in ε' will result in relatively large

changes in the reflection coefficient.

1.2.3 General Comparison

Of all the configurations shown in Fig.1.1, only those in (d) and (g) have the advantage of requiring small amounts of material. The sample preparation techniques in these cases are also relatively simple. Nevertheless, configuration (g) is seldom used, due in part to difficulties in accurately locating the sample in the coaxial line. On the other hand, the configuration (d) has recently been widely used to study biological materials [1.17, 1.18, 1.23]. The calculations of the relative permittivity using (d) and (g) are simple. For the configuration shown in Fig.1.1(d) it has been shown [1.17] that there is an optimum capacitance $C(\varepsilon^*)$ for minimum uncertainty of the measurements for a frequency range as broad as one tenth to ten times the frequency at which the optimum capacitance is selected.

Next in order of simplicity of sample preparation are the configurations in Fig.1.1(b) and (f). Those given in Fig.1.1(a), (c) and (e) require careful machining to ensure that the sample-air interfaces are parallel and perpendicular to the length of the coaxial line. Also, close dimensional tolerances between the coaxial line and sample are essential. A slight air space between the sample and inner conductor is more serious than when there is a similar air space between the sample and the outer conductor and proper

corrections may have to be applied [1.12, 1.13]. It is thus more important to have a better fit at the inner rather than at the outer conductor. These air gap errors become increasingly more important with increasing dielectric constant [1.13]. A sliding fit is thus essential for these sample configurations, and a force fit may become necessary in some cases.

The classical method illustrated in Fig.1.1(a) provides for good accuracy in a narrow frequency range [1.12, 1.13] only when the sample thickness is an odd number of a quarter-wavelength in the sample. Due to the transcendental equation involved there exists theoretically an infinite number of possible solutions for the dielectric constant. Hence it may become necessary to know an approximate value of the dielectric constant beforehand. Alternatively, two sample lengths have to be used to pin-point the right solution. This can be a serious drawback when besides an approximate value of the dielectric constant not being known only a limited amount of the material is available. The configuration in Fig.1.1(c) offers no advantage over that in (a) except for the simpler calculations since no transcendental equation is involved.

For the coaxial line opened into a circular waveguide, Flg.1.1(e) the equivalent circuit of Fig.1.2(d) has been employed [1.29]. Formulae for the fringing-field capacitance C_f are available [1.30, 1.31] and hence the calculations of the dielectric parameters should be straight-

forward. A similar sample configuration to that above is the one given in Fig.1.1(f), (or Fig.1.1(h)), the difference being that in this case the sample is placed on the circular waveguide side, hence the sample preparation is relatively simpler. This is very suitable for measuring the dielectric properties of liquids and powders when a proper window is placed at the coaxial line and circular waveguide interface. Analytical solutions for the dielectric parameters are available [1.8] and the calculations are not difficult although some reference standards must be used. A shielded open-circuit termination configuration [1.19, 1.32] may be considered as a special case of the coaxial line opened into a circular waveguide. This is again very suitable for measurements of liquids and powders and the calculations are not too difficult [1.24]. Formulae for the calculation of the effective position of the open-circuit for coaxial lines of different characteristic impedances and different geometries of the inner conductor ends may be found in references [1.19 and 1.33].

The sample configurations shown in Fig.1.1(i), (j) and (k) provide for simplicity in sample preparation; for samples that are already flat in an area as large as the coaxial line outer conductor, very little preparation is needed for the configuration (i). Similarly, a parallel-sided slab may be used straight away as in case (j). One disadvantage of these configurations is that the samples must be available in rather large quantities. Nevertheless, these are potentially suitable

for in vivo measurements, as in the case of biological specimens. Again Fig.1.1(l) offers the same advantage as above except that it may only be suitable for liquids or powdered samples since it is very difficult to ensure that the space within the region C is properly filled by the samples.

Table 1.1 summarizes qualitatively the relative merits of the various measurement methods in the frequency range 100 MHz to 10 GHz. The relative complex permittivity is indicated in terms of its components where $\varepsilon^* = \varepsilon' - j\varepsilon''$. Here ε' or the relative dielectric constant is associated with the ability of the material to store electrical energy. In a similar fashion, ε'' or the loss factor is associated with the dielectric losses that occur in the material.

1.3 SUMMARY OF THESIS

The foregoing general survey of the coaxial line methods was carried out to identify the most suitable techniques of measuring the dielectric properties of the two groups of nitrogen ceramics in the frequency range 500 MHz to 9 GHz. As only relatively small quantities of the oxynitride glasses were available and since their cross-sections were very much smaller than that of the coaxial line available (14-mm General Radio GR 874 LBB slotted coaxial line), there was, in practice, little choice of the measurement methods in this case. Preliminary tests indicated that the oxynitride glasses were of low loss, while the silicon nitrides comprised of a

Table 1.1 Comparison of the Various Measurement Methods

Sample Configuration	Sample Preparation	Temperature Control	Frequency Range	Computation of ε' and ε''	Accuracy	References
Fig.1.1(a)	moderately difficult	easy	100 MHz - 10 GHz	difficult (transcendental equation)	good only for appropriate sample length	1.12, 1.13
Fig.1.1(b)	easy	easy	100 MHz - 5 GHz	fairly easy	good if C_f can be determined accurately	1.12, 1.13
Fig.1.1(c)	moderately difficult	moderately difficult	100 MHz - 10 GHz various sample lengths	fairly easy	moderate	1.12, 1.13 1.18, 1.23
Fig.1.1(d)	very easy	easy	100 MHz - 5 GHz can be extended up to 18 GHz	very easy	good for optimum capacitance	1.12, 1.13 1.14, 1.15
Fig.1.1(e)	moderately difficult	difficult	100 MHz - 5 GHz	easy	good for optimum length	1.19, 1.31 1.33
Fig.1.1(f)	easy	difficult	100 MHz - 5 GHz	difficult (transcendental equation)	good for optimum length	1.19, 1.24 1.28, 1.31

Table 1.1 (continued)

Sample Configuration	Sample Preparation	Temperature Control	Frequency Range	Computation of ε' and ε''	Accuracy	References
Fig.1.1(g)	easy	difficult	100 MHz - 5 GHz	easy	fairly good depends on sample volume	1.12
Fig.1.1(h)	easy	easy	narrow range	difficult	good only in narrow freq. range	1.8, 1.29
Fig.1.1(i)	very easy	very easy	100 MHz - 10 GHz	easy	good within narrow freq. range	1.9, 1.28
Fig.1.1(j)	easy	moderately difficult	-	very difficult analytical solution not available	not known	1.9, 1.28
Fig.1.1(k)	easy	very easy	100 MHz - 10 GHz various sample lengths	easy	good	1.10, 1.28, 1.33
Fig.1.1(l)	difficult	easy	-	very difficult	not known	1.10, 1.28

range of materials from high to low loss. The short-circuit termination method was adequate for measurements of the dielectric constant. It has been assumed in general that there is a high uncertainty in measuring the loss factor of low loss materials by this method [1.13] although quantitative estimates are not available. A considerable proportion of time was therefore devoted to the development, analysis and assessment of techniques. Thus Chapter 2 describes the short-circuit termination method while Chapters 3 and 4 discuss the matched termination and resonance methods which were found necessary and advantageous in accurate measurements of the dielectric loss.

In addition to the coaxial line techniques the cavity perturbation method was also employed at the X-band frequency of 9.34 GHz. This was to provide the high frequency end of the measurement range since the coaxial line methods could not be used up to this frequency due to the onset of higher order modes and for various other reasons which will be given later. Chapter 7 describes the experimental results on the silicon nitrides and their interpretation. The study on the oxynitride glass systems are given in Chapter 8. Chapter 9 gives some overall conclusions.

1.4 REFERENCES

1.1 Bosisio R.G., Giroux M. and Couderc D.,"Paper sheet moisture measurement by microwave phase perturbation techniques", J. Microwave Power, vol.5,no.1,25(1970)

1.2 Chudobiak W.J., Syrett B.A. and Hafez H.M.,"Recent advances in broadband VHF and UHF transmission line methods for moisture content and dielectric constant measurements", IEEE Trans.Instrum.Meas, vol.28,284(1979)

1.3 IEEE Trans.Microwave Theory and Techniques, Special Issue, vol.26(1978)

1.4 Nelson S.O. and Stetson L.E.,"Possibilities of controlling insects with microwaves and lower frequency RF energy", IEEE Trans.Microwave Theory and Techniques, vol.22,1303(1974)

1.5 Nelson S.O.,"Use of microwave and lower frequency RF energy for improving alfalfa seed germination", J.Microwave Power vol.11,271(1976)

1.6 Nelson S.O.,"Electrical properties of agricultural products - a critical review", Trans.ASAE, vol.6,384(1973)

1.7 Essex C.G., Grant E.H., Sheppard R.J., South G.P., Symonds M.S., Mills G.L. and Slack J.,"Dielectric properties of normal and abnormal lipoproteins in aqueous solutions", Ann. N.Y.Acad.Sci., no.303,142(1977)

1.8 Bianco B., Drago G.P., Marchesi M., Martini C., Mela G.S. and Ridella S.,"Measurements of complex dielectric constant of human sera and erythrocytes", IEEE Trans.Instrum.Meas., vol.28,290(1979)

1.9 Her C.,"Measures dielectriques in vivo de la peau humaine par TDS", Second Int.T.D.S. Meeting, Bordeaux, France, Sept.8 - 10 (1975)

1.10 Burdette E.C., Cain F.L. and Seals J.,"In vivo probe measurement technique for determining dielectric properties at VHF through microwave frequencies", IEEE Trans. Microwave Theory and Techniques, vol.29,176(1980)

1.11 Roberts S. and Von Hippel A.R.,"A new method for measuring dielectric constant and loss in the range of centimeter waves", J.Appl.Phys., vol.17,61(1946)

1.12 Westphal W.B. in "Dielectric Materials and Applications", Von Hippel A.R.(Ed.), Wiley,N.Y.(1954)

1.13 Sucher M and Fox J.,"Handbook of Microwave Measurements", Vol.II,3rd edn., Polytechnic Press, Brooklyn, N.Y.(1963)

1.14 Fellner-Feldegg H.,"The measurements of dielectrics in the time domain", J.Phys.Chem., vol.73,616(1969)

1.15 Nakamura H., Mashimo S. and Wada A.,"Application of time domain reflectometry covering a wide frequency range to the dielectric study of polymer solutions", Jap.J.Appl.Phys., vol.21, no.3,467(1982)

1.16 Chamberlain J. and Chantry G.W.(Eds.),"High Frequency Dielectric Measurements", IPC Science and Technology Press, Guildford (1972)

1.17 Iskander M.F. and Stutchly S.S.,"A time-domain technique

for measurements of the dielectric properties of biological substances", IEEE Trans.Instrum.Meas., vol.21, 425(1972)

1.18 Van Gemert M.J.C.,"High-frequency time-domain methods in dielectric spectroscopy", Philips Res.Rep., vol.R844, 530(1973)

1.19 Bussey H.E.,"Microwave dielectric measurements of lunar soil with a coaxial line resonator method", in Proc. Tenth Lunar Planetary Conf., Houston, Texas, TX, Geochimia Physica Acta, Supp.11,2175(1979)

1.20 Akyel C. and Bosisio R.G.,"Wide-range complex dielectric constant measurements using microprocessor control techniques", IEEE Trans.Instrum.Meas., vol.28,272(1979)

1.21 Felsen L.B. in "Handbook of Microwave Measurements", VOL.I, 3rd.edn., Polytechnic Press, Brooklyn, N.Y.(1963)

1.22 "S-Parameters", Hewlett-Packard Application Note 95(1968)

1.23 Kwok B.P., Nelson S.O. and Bahar E.,"Time-domain measurements for the determination of the dielectric properties of agricultural materials", IEEE Trans.Instrum.Meas., vol. 28,109(1979)

1.24 Bussey H.E.,"Dielectric measurements in a shielded open circuit coaxial line", IEEE Trans.Instrum.Meas., vol.29 120(1980)

1.25 Schepps J.R., Friend Jr. A.W. and Foster K.R.,"Tissue impedance measurements using the microwave network

for measurements of the dielectric properties of biological substances", IEEE Trans.Instrum.Meas., vol.21, 425(1972)

1.18 Van Gemert M.J.C.,"High-frequency time-domain methods in dielectric spectroscopy", Philips Res.Rep., vol.R844, 530(1973)

1.19 Bussey H.E.,"Microwave dielectric measurements of lunar soil with a coaxial line resonator method", in Proc. Tenth Lunar Planetary Conf., Houston, Texas, TX, Geochimia Physica Acta, Supp.11,2175(1979)

1.20 Akyel C. and Bosisio R.G.,"Wide-range complex dielectric constant measurements using microprocessor control techniques", IEEE Trans.Instrum.Meas., vol.28,272(1979)

1.21 Felsen L.B. in "Handbook of Microwave Measurements", VOL.I, 3rd.edn., Polytechnic Press, Brooklyn, N.Y.(1963)

1.22 "S-Parameters", Hewlett-Packard Application Note 95(1968)

1.23 Kwok B.P., Nelson S.O. and Bahar E.,"Time-domain measurements for the determination of the dielectric properties of agricultural materials", IEEE Trans.Instrum.Meas., vol. 28,109(1979)

1.24 Bussey H.E.,"Dielectric measurements in a shielded open circuit coaxial line", IEEE Trans.Instrum.Meas., vol.29 120(1980)

1.25 Schepps J.R., Friend Jr. A.W. and Foster K.R.,"Tissue impedance measurements using the microwave network

analyzer", in Bioelectromagnetics Symp.Program and Abstracts, 1979 URSI Spring Meeting, Seattle W.A., June 18 - 22, p.372

1.26 Stutchly S.S., Stutchly M.A. and Carraro B.,"Permittivity measurements in a resonator terminated by an infinite sample", IEEE Trans.Instrum.Meas., vol.27,436(1978)

1.27 Kolodziej H. and Sobczyk L.,"Investigation of the dielectric properties of potassium hydrogen maleate", Acta Phys.Polon. (A), vol.39,59(1971)

1.28 Stutchly M.A. and Stutchly S.S.,"Coaxial line reflection methods for measuring dielectric properties of biological substances at radio and microwave frequencies - a review", IEEE Trans.Instrum.Meas., vol.29,176(1980)

1.29 Stutchly S.S., Mladek J., Stutchly M.A. and Parasien B.,"A method for measurement of the permittivity of thin samples", J.Microwave Power, vol.14,7(1979)

1.30 Razaz M. and Davis J.B.,"Capacitance of the abrupt transition from coaxial to circular waveguide", IEEE Trans. Microwave Theory and Techniques, vol.27.564(1979)

1.31 Risley E.W.,"Discontinuity capacitance of a coaxial line terminated in a circular waveguide", IEEE Trans.Microwave Theory and Techniques, vol.17,86(1969)

1.32 Jesch R.L.,"Dielectric measurements of five different soil textural types as functions of frequency and moisture content", Nat.Bur.Stand.Inst.Res., NBSIR 78,879(1978)

1.33 Somlo P.I.,"The discontinuity capacitance and the effective position of a shielded open circuit in a coaxial line", Proc. Inst.Radio Elec.Eng., Australia, vol.28,7(1967).

CHAPTER 2

THE SHORT-CIRCUIT TERMINATION METHOD

2.1 GENERAL OUTLINE

In this chapter attention will be focussed on the method utilizing the sample configuration (d) in Fig.1.1 since it is employed in this work. It is re-emphasised that this configuration is particularly useful for measuring the dielectric properties of materials that are available only in small quantities. Furthermore, it has the advantage over others in that it requires only simple VSWR measuring equipment that is available commercially and the sample requires relatively straightforward preparation techniques. In addition, the calculation of the real and imaginary components of the relative complex permittivity is relatively simple to carry out.

When a transmission line carrying a sinusoidal wave is operated with a mismatched termination or load that provides a reflected wave, the incident and reflected waves combine to produce a resultant that varies in amplitude along the line. At some points along the line the incident and reflected waves will be in time phase with one another and the resultant will be a maximum. Similarly, points will exist where the two waves will be in anti-phase with one another and at these points the resultant will be a minimum.

This results in a standing-wave pattern in which the minimum points (or nodes) and the maximum points (or antinodes) alternate along the line and occur a quarter of a wavelength apart. The voltage standing-wave ratio, denoted by the symbol S, is usually defined as [2.1]

$$S = \frac{|V|_{max}}{|V|_{min}} = \frac{1 + |\Gamma|}{1 - |\Gamma|} \qquad (2\cdot1)$$

so that S lies in the range $1 \leq S \leq \infty$.

$|V|_{max}$ and $|V|_{min}$ are the maximum and minimum voltage amplitudes respectively. The magnitude of the reflection coefficient $|\Gamma|$ can be derived from the VSWR as

$$|\Gamma| = \frac{S - 1}{S + 1} \qquad (2\cdot2)$$

The reflection coefficient at a distance ℓ from the load is expressed as

$$\Gamma = |\Gamma| \exp(-j\theta) \qquad (2\cdot3)$$

where its phase angle

$$\theta = 2\beta\ell - (2n + 1)\pi \qquad (2\cdot4)$$

Here $\beta = 2\pi / \lambda_g$ is the phase constant, λ_g is the guide wavelength and the integer n denotes the number of the voltage nodes in front of the sample. In principle the

measurements consist of measuring the VSWR and the positions of the voltage standing-wave minima with and without the sample. This yields the reflection coefficient which can then be related to the dielectric properties of the material via a suitable equivalent circuit representation. A reference plane for the measurements of the phase shifts is usually obtained by short-circuiting the sample-holder and locating the voltage minimum nearest to it (n = 1). Then when the sample is introduced into the sample-holder the phase shift ℓ will be given by the distance of the nearest voltage minimum from the reference plane. However, since the minimum repeats every half a wavelength these minima are equivalent points and in practice a more accurate value of the phase shift is obtained by averaging the displacements of a few minima locations with the sample from those without it in the sample-holder.

2.2 DERIVATION OF THE DIELECTRIC CONSTANT AND LOSS FACTOR

The equivalent circuit for this method is as shown in Fig.1.2(c). For the sample-holder without the test material the capacitance $C(\varepsilon^*) = C_o$ can be taken as the parallel plate capacitance formed by the inner conductor and the terminating short-circuit while C_f is the fringing-field capacitance [2.2 - 2.4]. When a test sample is inserted into the sample-holder the capacitance $C(\varepsilon^*) = C_o \varepsilon^*$ and the total capacitance is given by [2.4, 2.5]:

$$C = C_o\varepsilon^* + C_f = \frac{\pi a^2}{4d}\varepsilon_o\varepsilon^* + 2a\varepsilon_o \ell n\left(\frac{b-a}{2d}\right) \qquad (2.5)$$

provided that this satisfies the conditions $\lambda_g \ll (b - a)$ and $d \ll (b - a)$ where $\varepsilon_o = 8.854 \times 10^{-12}$ F m^{-1} is the permittivity of free space. The impedance looking into the terminal plane of the sample-holder is

$$Z = \frac{1}{j\omega C} \qquad (2.6)$$

where $\omega = 2\pi f$ is the radian frequency and f is the frequency in Hz. From transmission line theory the reflection coefficient [1.14] is then given by

$$\Gamma = |\Gamma|\exp(-j\theta) = \frac{Z - Z_o}{Z + Z_o} = \frac{1 - j\omega Z_o[\,C(\varepsilon^*) + C_f\,]}{1 + j\omega Z_o[\,C(\varepsilon^*) + C_f\,]} \qquad (2.7)$$

where the symbols have all been previously defined. It is assumed that the introduction of the test material into the parallel plate capacitor causes only a negligibly small variation in the fringing-field capacitance C_f [1.19, 2.4]. From equation (2.7) we have

$$j\omega Z_o[\,C(\varepsilon^*) + C_f\,] = \frac{1 + |\Gamma|\exp(-j\theta)}{1 - |\Gamma|\exp(-j\theta)} \qquad (2.8)$$

Substituting for $\varepsilon^* = \varepsilon' - j\varepsilon''$ and solving for the dielectric constant ε' and the loss factor ε'' we obtain

$$\varepsilon' = \frac{2|\Gamma|\sin(-\theta)}{\omega C_o Z_o [1 + 2|\Gamma|\cos(\theta) + |\Gamma|^2]} - \frac{C_f}{C_o}$$

$$\varepsilon'' = \frac{1 - |\Gamma|^2}{\omega C_o Z_o [1 + 2|\Gamma|\cos(\theta) + |\Gamma|^2]} \qquad (2.9)$$

It is seen that the effect of the fringing-field is to decrease the value of the dielectric constant by C_f/C_o while the loss factor remains unaffected. The loss tangent, which is proportional to the ratio of the power lost in heat to the energy stored per cycle of the applied field, is then simply calculated from the expression

$$\tan\delta = \frac{\varepsilon''}{\varepsilon'} \qquad (2.10)$$

When the direct current conductivity is comparitively negligible, the high frequency conductivity can then be obtained from the equation

$$\sigma = \omega \varepsilon_o \varepsilon'' \qquad (2.11)$$

It has been pointed out that the calculation of the real and imaginary components of the complex permittivity for this capacitance method, as originally suggested in reference [1.12], is not very accurate. A full analysis of the method and a more rigourous derivation of ε' and ε'' have been given in references [1.27 and 2.6]. With suitable

modifications and when certain conditions are satisfied the method may be extended up to 18 GHz.

2.3 ANALYSIS OF THE METHOD

This method has been used for the measurements of the dielectric properties of lossy materials [e.g. 1.14, 1.19, 2.7] and that is its traditional area of application. An analysis of this method has been carried out in this work with the view of choosing the optimum sample dimensions, minimizing the fringing-field effects and to evaluate the suitability of the method for measuring the dielectric properties from medium to low loss materials in the frequency range from 100 MHz to 10 GHz. For a given material at a given frequency of measurement and uncertainty in the measurement of the reflection coefficient it can be shown that the uncertainty in the measured value of ε^* may be minimized by a proper selection of the parallel plate capacitance C_o (Appendix A). This optimum capacitance has been calculated to be

$$C_{opt} = \frac{1}{2\pi f Z_o} \cdot \frac{1}{\sqrt{\varepsilon'^2 + \varepsilon''^2}} \qquad (2.12)$$

Fig.2.1 illustrates the optimum capacitance values over the frequency range 100 MHz to 10 GHz for a coaxial line of characteristic impedance 50 ohms and for values of $|\varepsilon^*| = \sqrt{\varepsilon'^2 + \varepsilon''^2}$ up to 100. The values of ε' has actually been used in the calculations, since for medium ($\varepsilon'' \lesssim 10^{-1}$) to low losses substitution of ε' for $|\varepsilon^*|$ when $\varepsilon' \gtrsim 5$ has

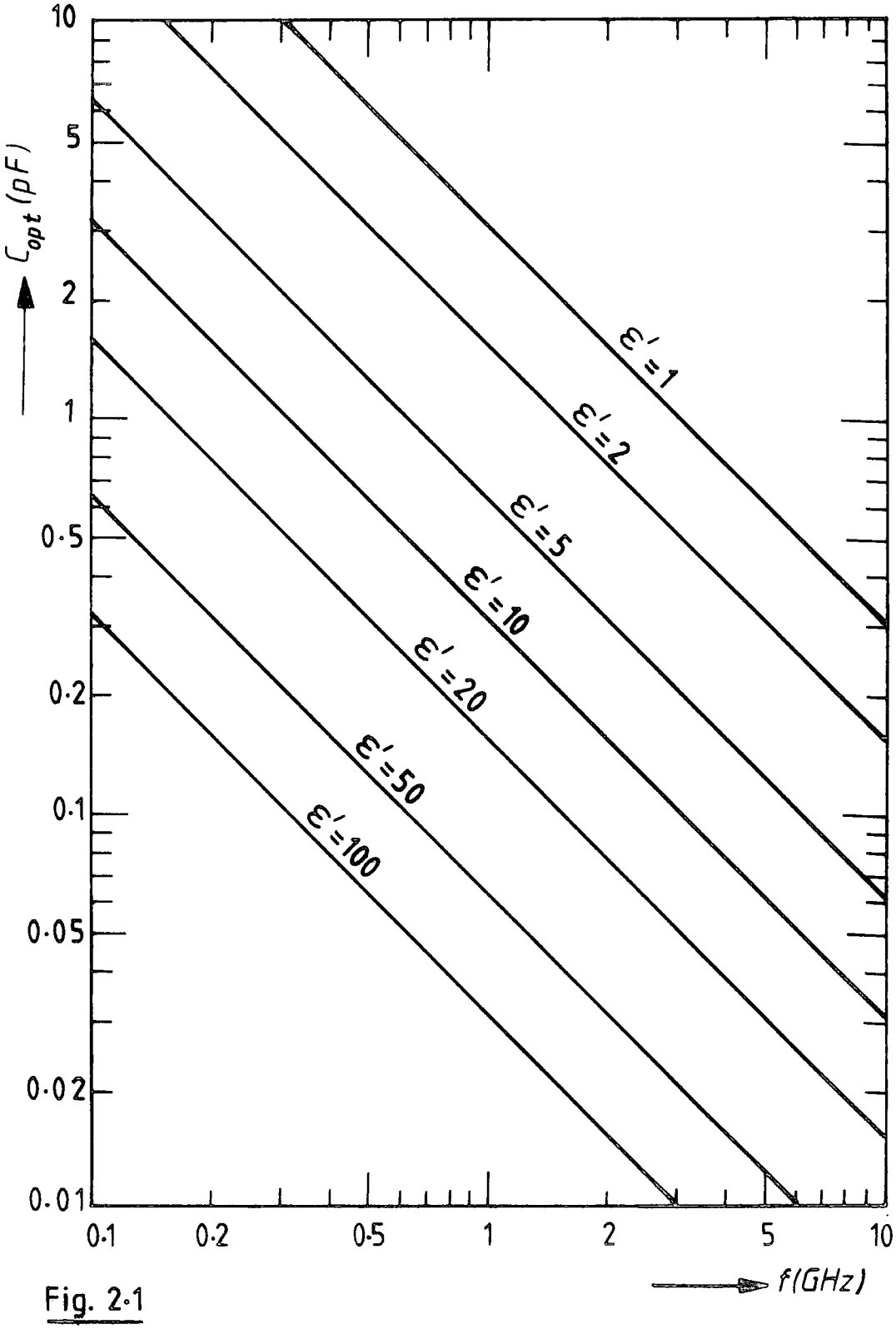

Fig. 2·1

Optimum capacitance for the short-circuit termination method

a negligible effect on the results. Since $|\varepsilon^*| > 1$ when a material is inserted into the sample-holder, the electric field lines tend to concentrate into the material, hence the value of the fringing-field capacitance C_f given in equation (2.5) is probably an overestimate and represents an upper limit of the fringing-field effect [1.14, 2.4]. The lower bound of the capacitance of the empty sample-holder may be estimated as follows: for example, by requiring that C_f should be less than 5 percent of the value of $C_o|\varepsilon^*|$, for a coaxial line having an internal conductor diameter $a \simeq 6.2$ mm and assuming for convenience $|\varepsilon^*| \sim 10$, we have $C_o \gtrsim 0.4$ pF. This implies that the sample thickness $d \lesssim 0.67$ mm.

In Fig.2.2 the values of the capacitance of the empty sample-holder and the ratio C_f/C_o are plotted as functions of the sample thickness and the ratio $(b - a)/d$, where, as before, a and b are the inner and outer conductor diameters respectively. The percentage contribution of the fringing-field effect can be found by dividing the ratio C_f/C_o given in percentage by the dielectric constant. Since the sample thickness must satisfy the inequalities following equation (2.5) for the fringing-field effect assumption to be valid, this sets an upper limit of about 2.5 mm. This corresponds to an empty sample-holder capacitance of $C_o > 0.1$ pF. With this restriction and referring to Fig.2.1 it will be noted that these values of sample

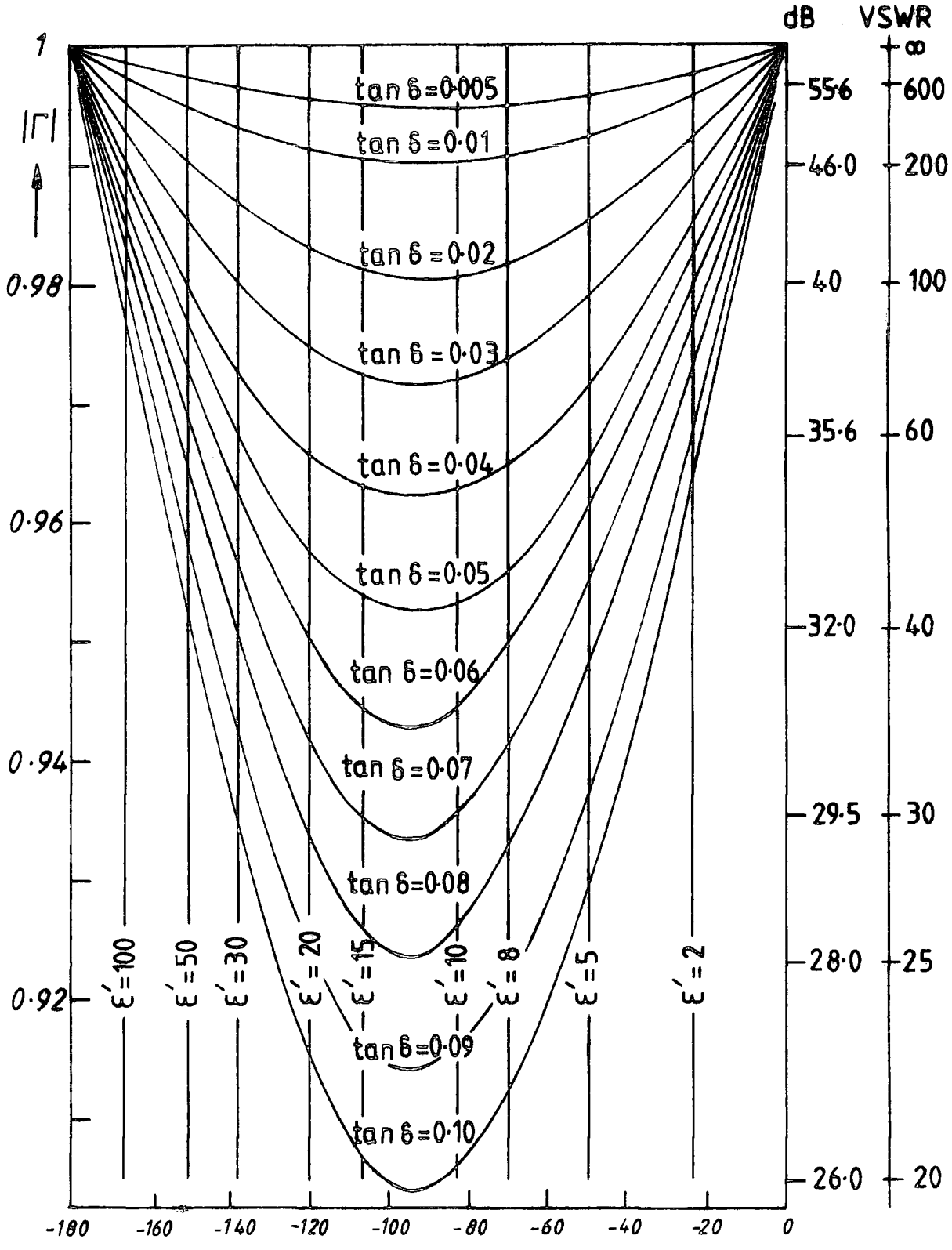

Fig. 2·3

The dielectric constant and loss tangent as functions of the reflection coefficient for an air-capacitance of $C_o = 0.54$ pF at 500 MHz

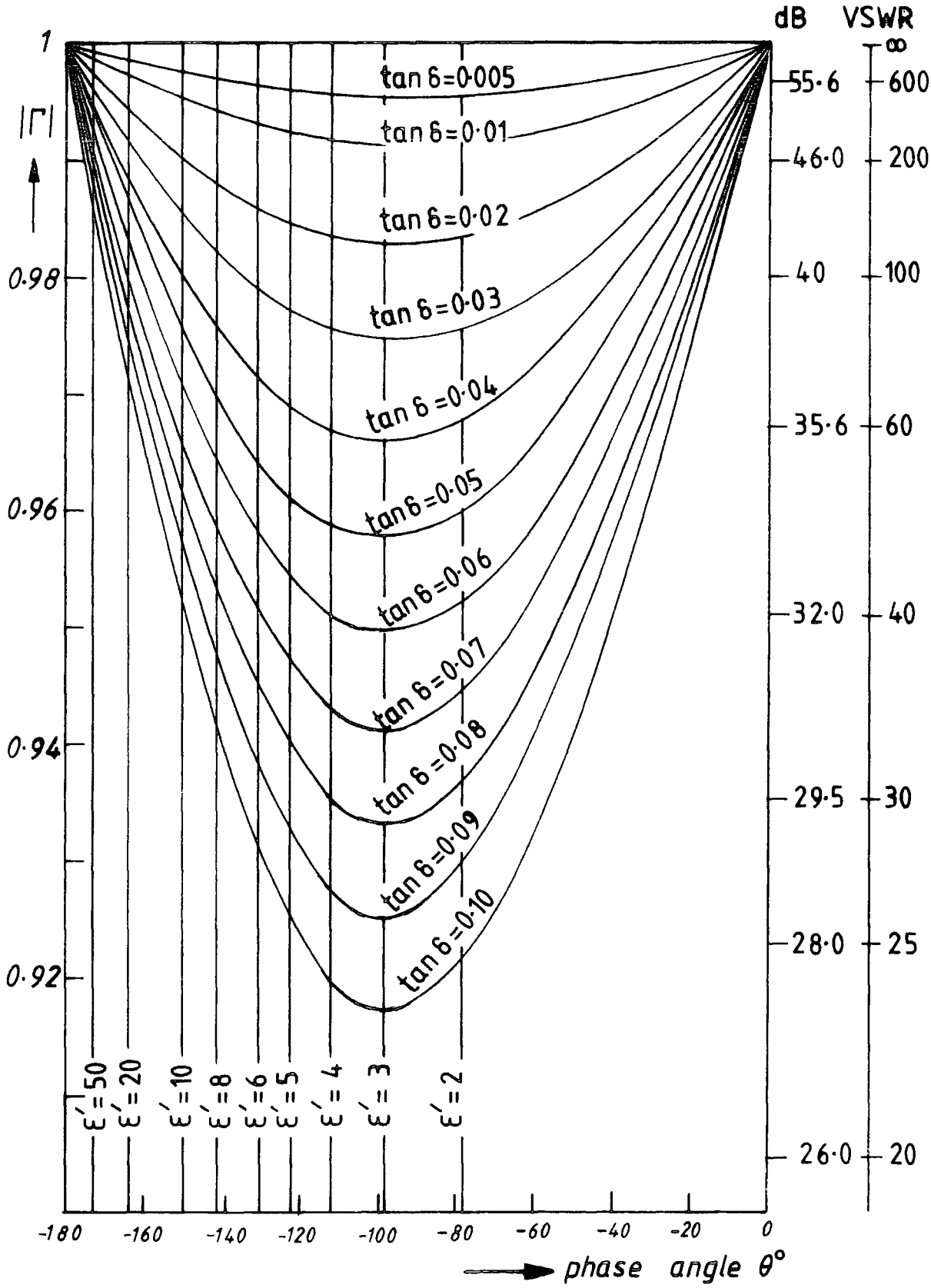

Fig. 2·4

Plots of the quantities in Fig. 2·3 at 2 GHz

thickness and air-capacitance give optimum measurements of materials with dielectric constant $\varepsilon' \sim 10$ in the frequency range up to about 5 GHz.

Fig.2.3 is a typical multi-parameter plot of the variations of the dielectric constant and loss tangent with the reflection coefficient magnitude $|\Gamma|$ and its phase angle θ for medium to low loss materials. The reflection coefficient magnitude is also given in terms of the VSWR and its equivalent in decibels. It can be seen that maximum sensivities of $|\Gamma|$ as indicated by maximum separations of the $\tan\delta$ curves occur for samples having ε' values between about 5 and 25. The phase angles of the reflection coefficients are also well spaced apart for dielectric constant values up to about 25. Going on to Fig.2.4 one sees similar trends in the $\tan\delta$ curves but the ε' curves are now displaced towards higher $(-\theta)$ values. This similarity in the $\tan\delta$ curves and the shift of the ε' curves with respect to the phase angle of the reflection coefficient with increasing frequency for a constant sample thickness has been found to hold generally. From this it can be seen that on going to higher frequencies the highest sensitivities in the reflection coefficient measurements will be found in materials having lower ε' values. Thus this will indicate the limiting high frequency at which a material with a given dielectric constant and thickness can be accurately measured with the short-circuit method.

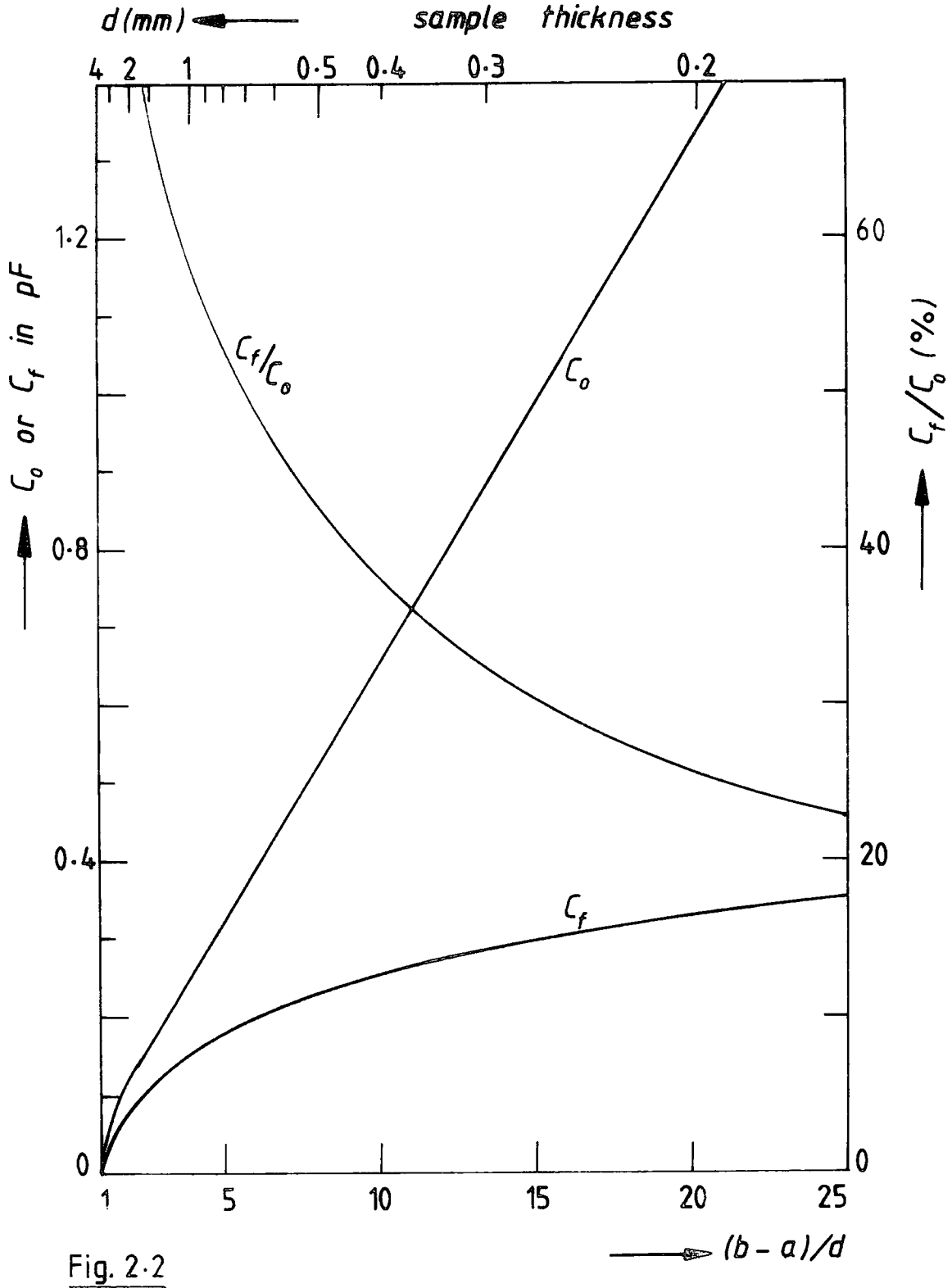

Fig. 2·2

Empty sample-holder and fringing-field capacitances, C_o and C_f, and the ratio C_f/C_o as functions of sample thickness and (b-a)/d

Another important point observed from Figures 2.3 and 2.4 is that of the lower loss tangents that can be readily measured. One sees that, in Fig.2.3 for example, for $\tan\delta \lesssim 10^{-2}$ the VSWR is greater than about 300. For low loss materials, $\tan\delta \sim 10^{-3}$ say, the VSWR that would have to be measured then would be very high ($\sim 10^{3}$ to $\sim 10^{4}$). Not only is there a large uncertainty in measuring high values of VSWR, it could also be time consuming to carry out [2.8].

2.4 EXPERIMENTAL

2.4.1 Slotted Coaxial Line Principle

Since the standing-wave pattern provides a direct comparison between the incident and reflected waves on a transmission line, the measurement of VSWR can provide accurate values of the reflection coefficient and effective impedance at any particular frequency. A radial electric-field probe is usually used to map the standing-wave pattern in a coaxial line. The probe must be mounted on a sliding carriage so that it can be moved axially along the line over a distance of at least one half-wavelength, in order to ensure that at least one maximum and minimum of the pattern can be measured. At low frequencies, where the wavelength is too large to allow a half-wavelength section to be used, the effective length of the measurement section may be increased by inserting additional sections of line

of known length in order to be able to locate the maximum and minimum of the pattern.

A field probe can be inserted into a coaxial line through a narrow slot cut axially along the outer conductor as indicated in Fig.2.5. The presence of the slot does not disturb the field patterns appreciably as the electric field is entirely radial and the current flow in the conductors is axial. A diode is used to rectify the voltage induced in the probe and the system is tuned to resonance by a short-circuited stub, which also provides a return path for the rectified diode current. The depth of penetration of the probe must be kept as small as possibly, consistent with measurement sensitivity, to minimise the power extracted and the reflections due to the presence of the probe itself. In the General Radio GR874 LBB slotted line used in this work the probe penetration depth of 1.55 mm from the inner surface of the outer conductor was found to give a symmetrical standing-wave pattern about the minimum. A power meter was connected to the end of the slotted section of the coaxial line while the probe depth was adjusted in order to ensure that the presence of the probe has only a negligibly small effect. Although it is possible to use the rectified voltage or current from the diode directly, a large increase in sensitivity can be obtained by using a modulated microwave signal generator, so that the diode output can be fed to a narrow-band audio-frequency amplifier. Since the

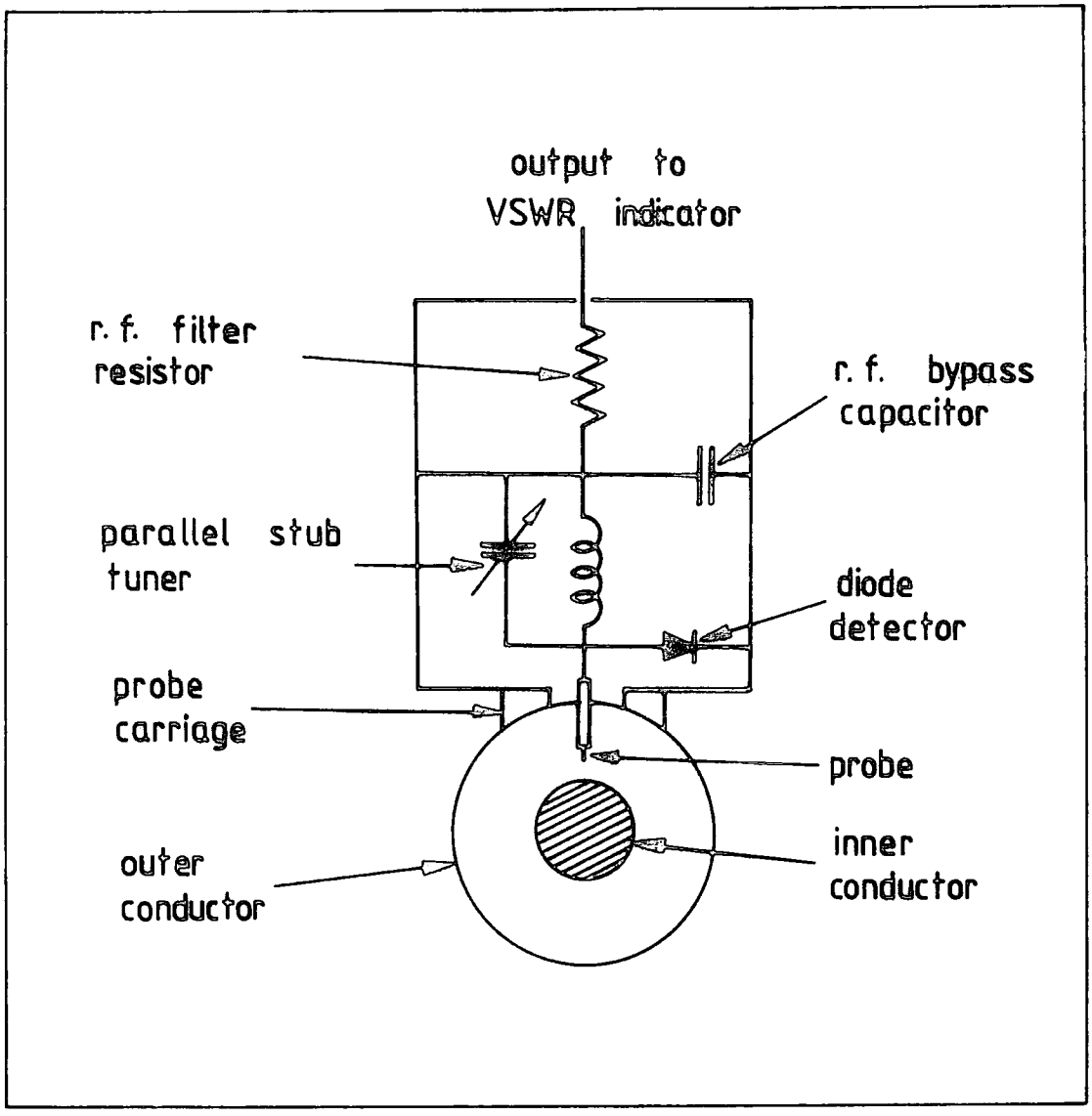

Fig. 2·5 Slotted coaxial line probe and detector assembly

microwave generators use direct modulation of the oscillator stage a square-wave modulation was used to reduce frequency modulation of the resulting microwave signal. The signal generators employed in this work consisted of a Marconi TF 1060 operating between 500 MHz and 1.25 GHz, a Flan Microwave Instruments PCLS for the range 1.5 GHz to 5 GHz and another Flan Microwave Instruments PCLX source covered the range 4 GHz to 12 GHz. All of the signal generators can be square-wave modulated at 1 kHz and 3 kHz; normally the 1 kHz modulation was used.

A satisfactory signal-to-noise ratio can be obtained at microwave power levels of a few milliwatts and at these power levels the diode output voltage is proportional to the square of the electric field strength. The calibrated VSWR scale of commercial indicators, including that of the Marconi Type 6503A used here, is normally based on this assumption. Under such a condition the VSWR measurement can be made by setting the gain to give full-scale deflection at a voltage maximum and then reading off the indicated value directly at a voltage minimum. If there is any doubt about the detector characteristic it can be checked quite easily since the standing-wave pattern for a short-circuit section of line varies sinusoidally with distance from the minimum. A plot of detector voltage against $\sin^2(2\pi x/\lambda_g)$, where x is the distance measured from a pattern minimum, will reveal any departure from the square-law characteristic. Such plots

were constructed in the initial calibration and preparatory procedure and the square law characteristic of the diode employed was found to occur at power levels corresponding to 2 mV or less.

A block diagram of the short-circuit termination method is illustrated in Fig.2.6. In practice the sample-holder is usually an extended inner conductor protruding into an open circuit component. The sample-holder used here, shown in Fig.2.7, consisted of an inner conductor element extended by a copper piece and a General Radio open circuit element, the GR 874 WO. Harmonics in the signal generator output can mask the actual standing-wave pattern and a suitable low-pass filter is required if the harmonic output from the generator is significant. The fundamental operating frequency was checked by measuring the distance between successive minima which should be exactly one half-wavelength. Next is the matched attenuator pad which provide at least 10 dB of attenuation in order to isolate the generator from variations in the effective load impedance by attenuating the reflected wave from the load under test. In practice it was found that even a 10 dB attenuator resulted in an output level too low to give satisfactory results when the Marconi TF 1066 was operating between 500 MHz and 750 MHz. Otherwise, at least 16 dB of attenuation was required to ensure proper isolation of the signal sources.

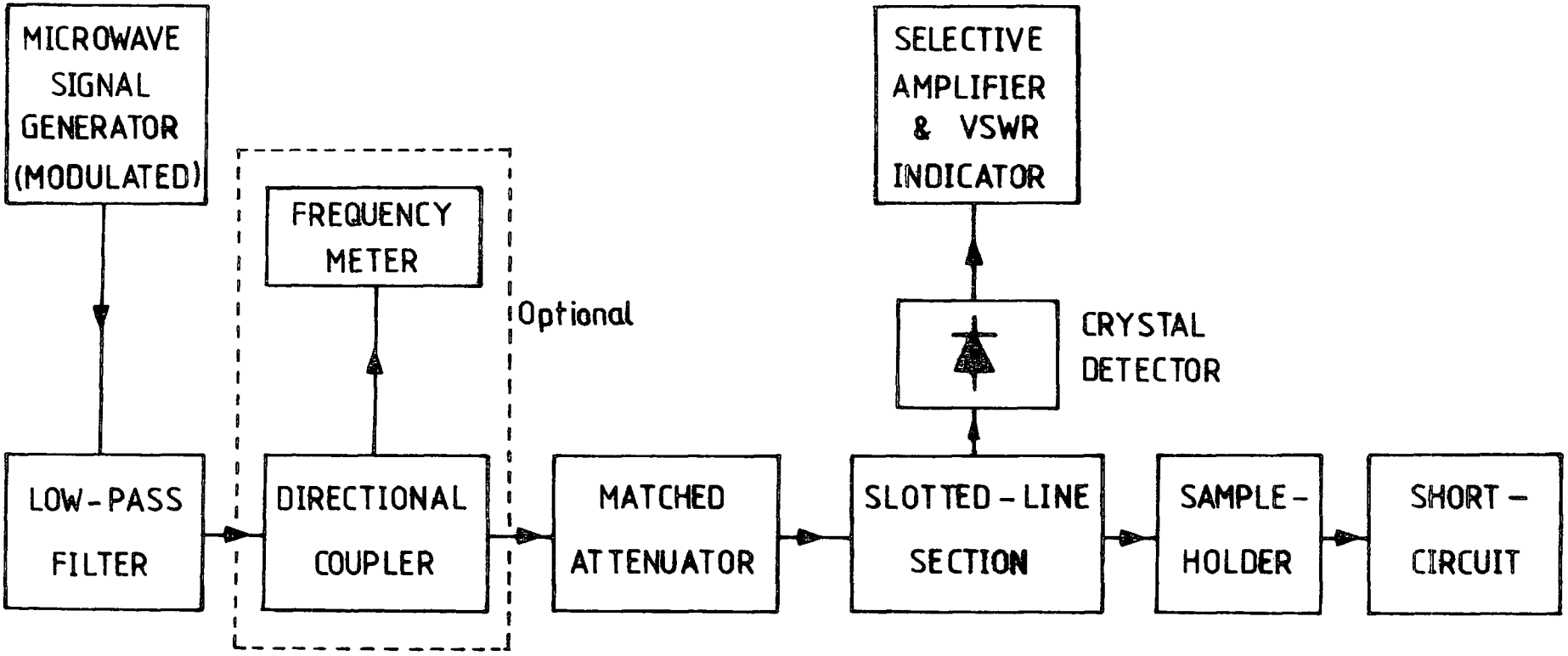

Fig.2·6 Block diagram of set-up for the coaxial line short-circuit termination method

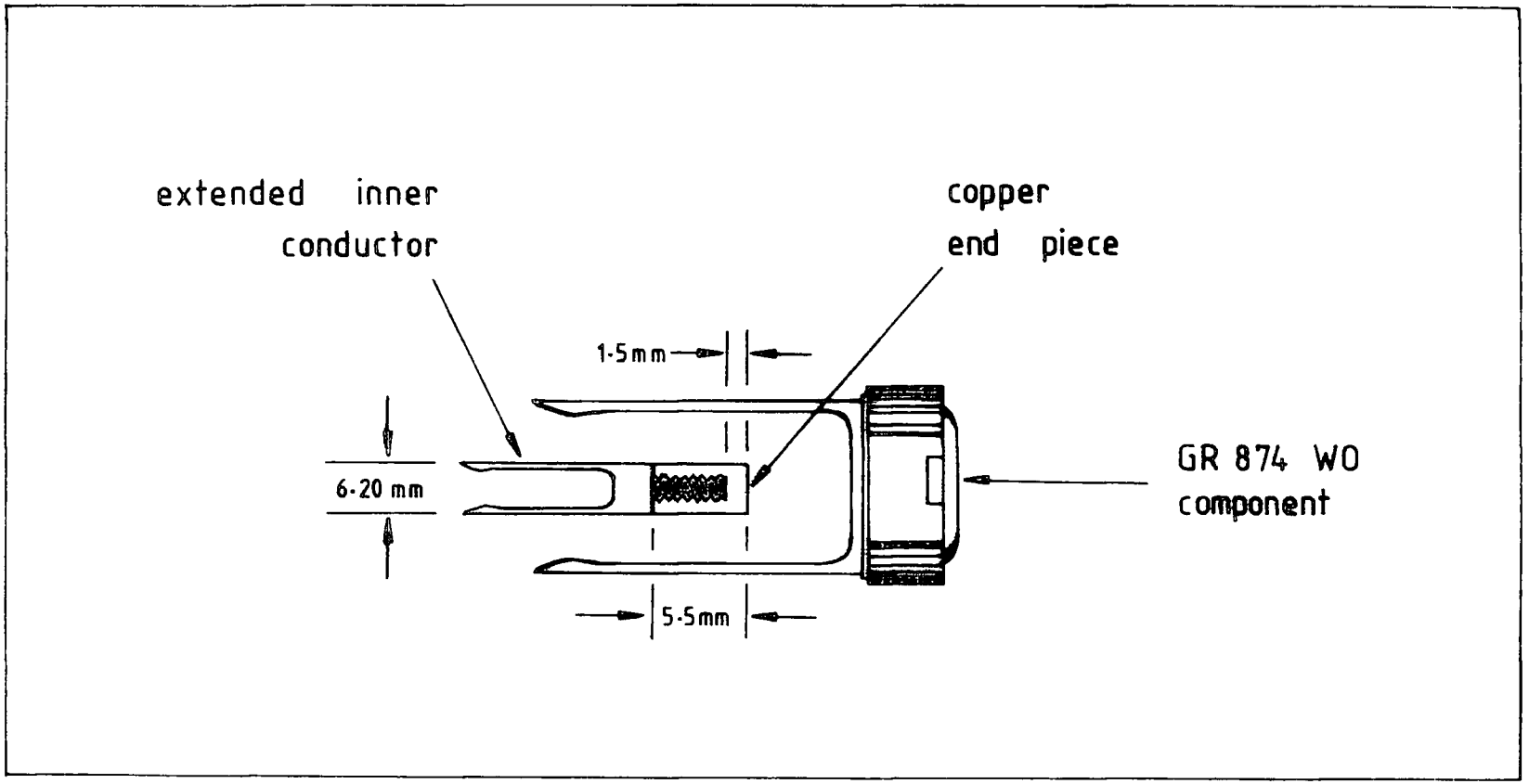

Fig. 2·7 Sample-holder for the short-circuit termination method

There are various methods of measuring the VSWR and which one is suitable depends on the magnitude to be measured. Basically three different methods are usually used, namely (a) the direct method which employs the VSWR indicator directly, within the square-law characteristic of the diode detector, (b) the attenuation method which measures the difference in decibels between the maximum and minimum, since the VSWR is given by

$$SWR(dB) = 20 \log(VSWR) \tag{2.13}$$

or $$VSWR = \text{antilog}(dB/20)$$

and (c) the twice-minimum-voltage method. The direct method is the easiest, nevertheless, it is not suitable for VSWR values greater than about 50. In the second method a calibrated attenuator may be included in place of the fixed attenuator pad or in addition to it, so that the VSWR can be measured by altering the attenuator setting so as to maintain a fixed output at the VSWR indicator when the probe carriage is moved from a voltage maximum to a voltage minimum. This method of measurement eliminates the possibility of error due to non-linearity of the characteristics of the detector and the VSWR indicator as they are operated at constant signal levels. The last method mentioned will be described in the next section. All of these methods are utilized in this project since the VSWR values measured spanned the range from below ten to the order of a thousand. However,

the second method was limited by the availability of suitably calibrated attenuators and the lack of calibration below 3 dB (the smallest attenuator) was made up by adjustments in the VSWR indicator attenuator; thus this gave only approximate values. The third method was found suitable for high VSWR values and at the low frequencies; at higher frequencies when the wavelengths become short, the width of the curve around the minimum was found to be the limiting factor for high VSWR measurements (see Fig.2.8).

2.4.2 Measurements of Extreme Values of VSWR

When the standing-wave ratio becomes small it becomes increasingly difficult to locate the position of the pattern minimum with accuracy. The error in the measurement can be considerably reduced by the process of bracketting as indicated in Fig.2.8(a). Points on either side of the pattern minimum, corresponding to a fixed voltage amplitude, are located at x_1 and x_2. The point midway between x_1 and x_2 then represents a first approximation to the position of the minimum, x_{min}. This approximation can be improved by repeating the process for several voltage amplitudes and drawing the locus of the mid-points to intersect the pattern at x_{min}.

When the VSWR is very large it is very difficult to make accurate measurements of the maximum and minimum amplitudes on one range of the measuring instrument. Hence

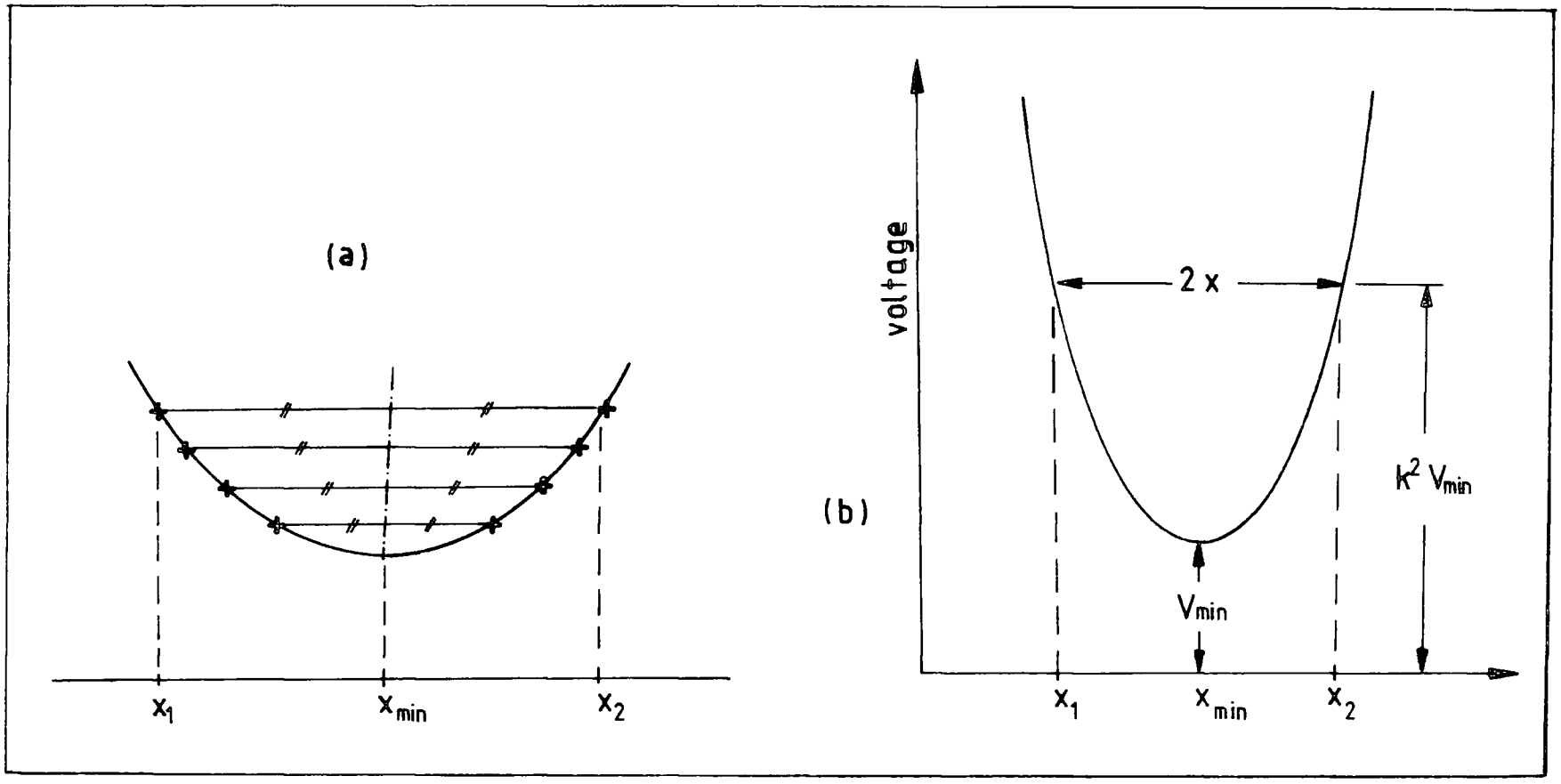

Fig. 2·8 (a) Locating the voltage standing-wave minimum by the process of bracketting (b) determination of large values of VSWR

errors are introduced because of the inaccuracy of the range attenuators or due to the large voltage amplitudes at the detector. An alternative method of measurement is indicated in Fig.2.8(b). This depends on the measurements of the voltage standing-wave pattern near the minimum and uses a restricted voltage range [2.1, 2.9]. It can be shown that the VSWR can be calculated using an arbitrary value k^2 times the voltage minimum from the relation

$$S = \frac{\sqrt{k^2 - \cos^2(2\pi x/\lambda_g)}}{\sin(2\pi x/\lambda_g)} \qquad (2.14)$$

where x is the half-width of the pattern for an arbitrary voltage $k^2 V_{min}$. The successful application of this relationship depends upon accurate measurements of k^2 and x. Once again a better value can be obtained by repeating the measurement for several values of k^2. On choosing the value $k^2 = 2$ equation (2.14) becomes

$$S = \sqrt{1 + 1/\sin^2(2\pi x/\lambda_g)} \qquad (2.15)$$

This relationship is plotted out in Fig.2.9. When x is small the above expression is further reduced to

$$S \simeq \lambda_g/2\pi x \qquad (2.16)$$

This method was found to be very useful when the VSWR values were in excess of 100 and when the frequency of measurement was low.

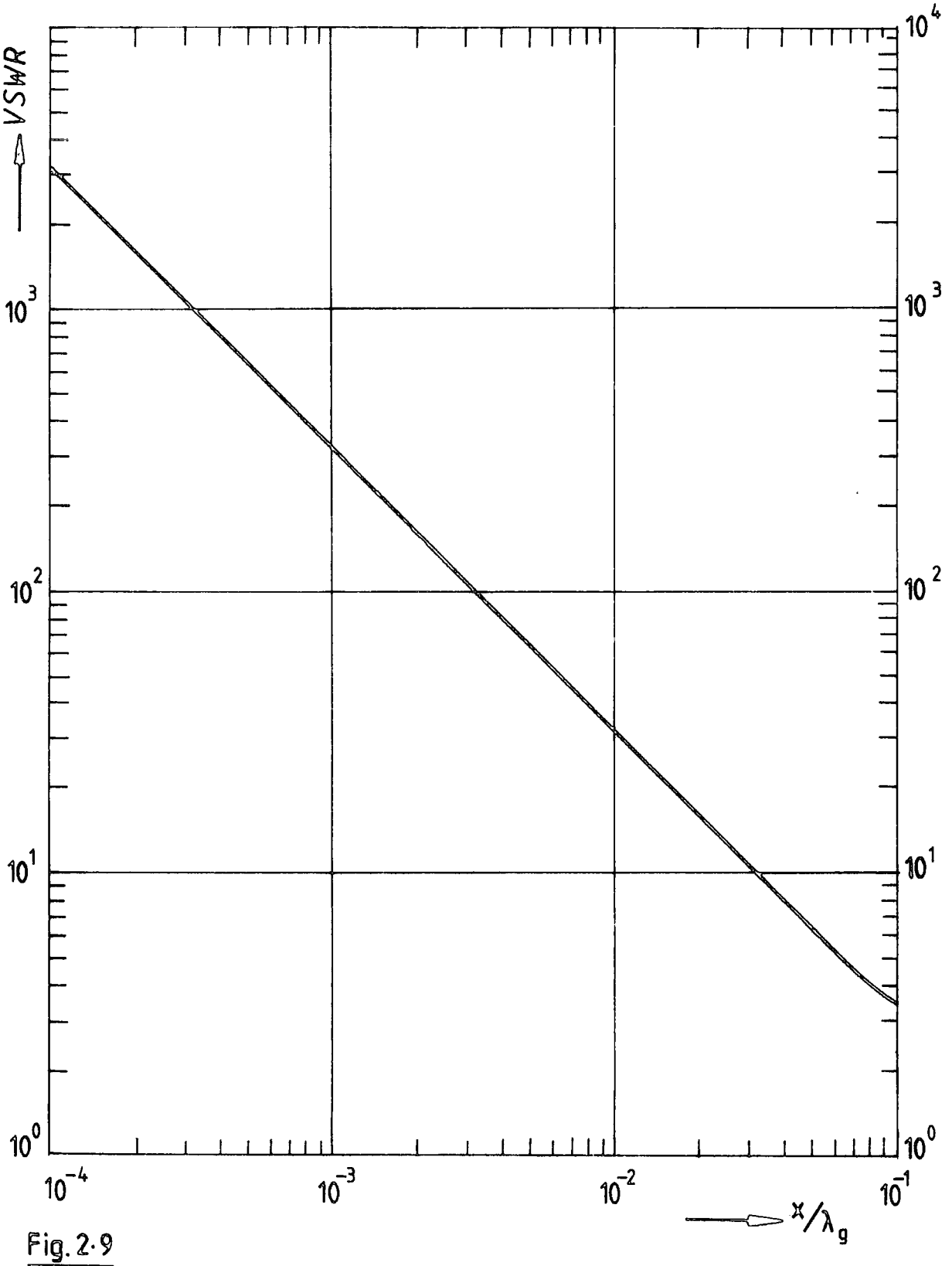

Fig. 2·9

VSWR as a function of the width of the curve at k^2 equals twice the minimum voltage

2.4.3 Correction Due to Line Attenuation

When the load is inaccessible or the wavelength too long, so that the measurement of the VSWR has to be made far from the end of a long section of line, the effect of attenuation can be significant. However, as the reflection coefficient is reduced by a constant factor both when the load is connected and when it is replaced by a short-circuit, a correction can be applied to give the true VSWR and the impedance at the load. For example, let us suppose that when a short-circuit is connected in place of the load the VSWR at the measurement position is some value S'_{∞} instead of infinity, the VSWR with the load connected is S_L and the normalised impedance with the load is given by the point $z = (a + jb)$ on a Smith chart. The line attenuation between the load and the measurement position can be found by drawing the S'_{∞} circle on the Smith chart and projecting downwards from the point of intersection with the real axis on to the transmission-loss scale. This construction is illustrated in Fig.2.10. Under short-circuit conditions the VSWR should correspond with the perimeter of the chart, so that the line attenuation is the number of dB steps between the chart perimeter and the S'_{∞} circle, shown as N dB in Fig.2.10. The true value of the VSWR at the load is greater than the measured value and can be found by increasing the radius of the measured load VSWR circle by N dB to compensate for the known loss. The

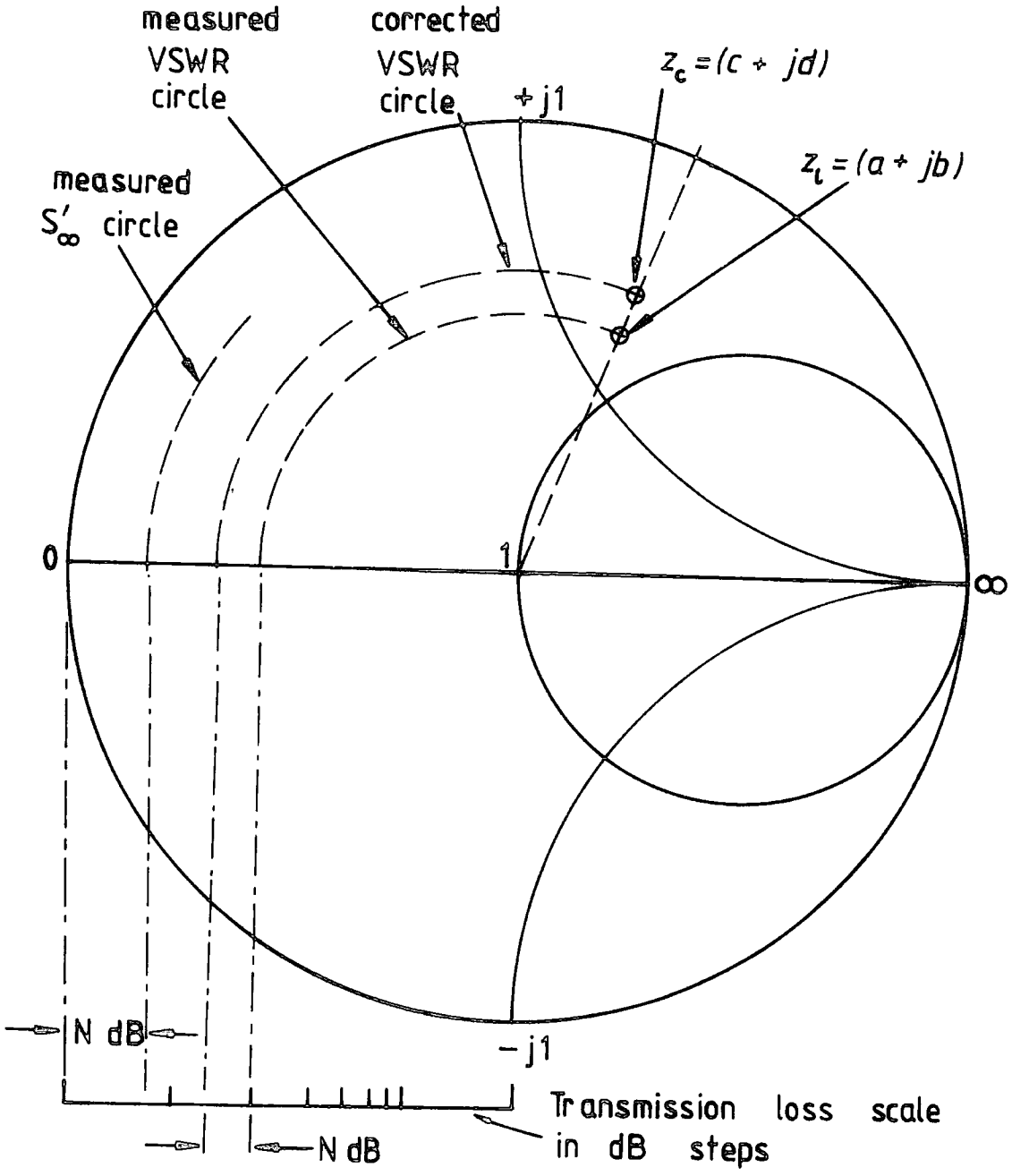

Fig. 2·10

Measured VSWR corrected for line attenuation

corrected impedance is then represented by the point $z_c = (c + jd)$ corresponding to the corrected VSWR.

2.4.4 Errors Due to Connector Mismatch

If a connector or adaptor is used between the slotted line section and the load, the small discontinuity introduced may have a significant effect on the measurement accuracy. When the reflection coefficients due to the connector and load are small their effects are basically additive, but their relative phase is unknown. Hence, if the magnitudes of the reflection coefficients for the connector and load are $|\Gamma_c|$ and $|\Gamma_l|$ respectively, the total reflection coefficient can vary over the range $(|\Gamma_c| \pm |\Gamma_l|)$ with a corresponding variation in the phase angle. Maximum error occurs when the two reflected waves are either exactly in phase or in anti-phase with each other. Fig.2.11 indicates the uncertainty due to a connector with a VSWR of 1.05 and serves to emphasize the importance of minimizing the number of connectors or adaptors between the load and measurement section when accurate measurements must be made.

2.5 COMMENTS AND CONCLUSIONS

The optimum capacitance values for the sample has been examined; Fig.2.1 provides a useful quick guide for

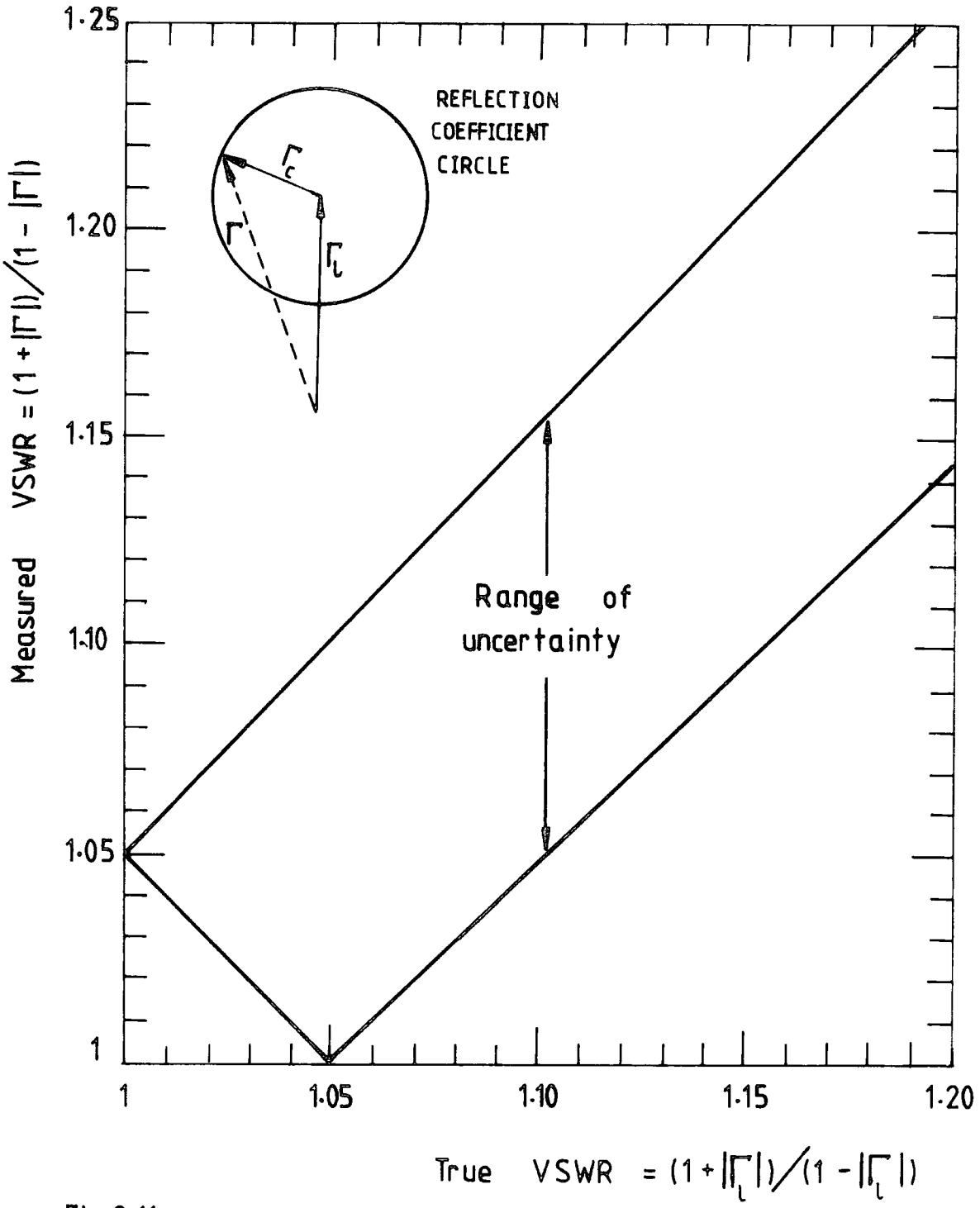

Fig. 2·11

Errors due to connector mismatch

choosing the best sample thickness and it gives an estimation of the high frequency limit up to which measurements of the dielectric properties using the coaxial line short-circuit termination method can be applied. Initially a first approximation to the dielectric constant can be obtained fairly easily by neglecting the effects of the fringing field and then Figures 2.1 and 2.2 can be used as a guide for more accurate determinations. In addition examination of the plots such as those given in Figures 2.3 and 2.4 would reveal the maximum sensitivity region for the loss factor determination. These last two figures also indicate that the angles of the reflection coefficients, θ, hence the phase shifts, for medium to low loss materials do not appreciably affect the value of the dielectric constant for different degrees of losses (this is indicated by the parallel vertical lines for ε'). An important conclusion drawn from this is that this method can be used to determine only the dielectric constant after it is satisfied that the material is not lossy (as would be indicated by checking that the VSWR is rather large when it is placed in the sample-holder). For low loss materials, say $\tan\delta < 10^{-2}$, the VSWR that has to be measured would be of the order of 500 or greater. A considerable amount of difficulties would be encountered in measuring this high VSWR as can be deduced from Fig.2.8. If a method can be found to measure just the loss (with ε' determined from the above method) it would avoid the

difficulties mentioned. The next two chapters explore this possibility and will describe proposals for alternative means of measuring the complex dielectric permittivity and the loss tangent.

2.6 REFERENCES

2.1 Sucher M. and Fox J. (Eds.), "Handbook of Microwave Measurements", 3rd. edn., Vol.I, Polytechnic Press, Brooklyn, N.Y. (1963)

2.2 Green H.E.,"The numerical solution of some important transmission line problems", IEEE Trans. Microwave Theory and Techniques, vol.5,576(1965)

2.3 Marcuvitz N., "Waveguide Handbook", M.I.T. Rad. Lab. Series, Vol.10, McGraw-Hill, N.Y. (1951)

2.4 Van Gemert M.J.C.,"Theoretical analysis of the lumped capacitance method in dielectric time-domain spectroscopy", Adv. Molec. Relaxation Processes, vol.6,123(1974)

2.5 Iskander M.F. and Stutchly S.S., "Fringing field effect in the lumped capacitance method of permittivity measurement", IEEE Trans.Instrum.Meas., vol.27,107(1978)

2.6 Kolodziej H.,"Dielectric relaxation in ferroelectrics of the order - disorder type", in Dielectric and Related Molecular Processes, Davis M.(Ed.), Vol.II, Chem.Soc., London (1972)

2.7 Stutchly S.S., Rzepecka M.A. and Iskander M.F.,"Permittivity measurements at microwave frequencies using lumped elements", IEEE Trans.Instrum.Meas., vol.23,56(1974)

2.8 Rad N.E.,"The Radio Frequency and Microwave Dielectric Properties of Doped Magnesium Oxide", Ph.D. Thesis, University of Durham (1980)

2.9 Davidson C.W.,"Transmission Lines for Communications", MacMillan Press Ltd., London (1978) p.105

2.10 Fellner-Feldegg H.,"The measurements of dielectrics in the time-domain", J.Phys.Chem., vol.73,616(1969).

CHAPTER 3

THE MATCHED TERMINATION METHOD

3.1 INTRODUCTION

The analysis of the method described in the last chapter indicated that high VSWR values have to be measured for low loss materials. In the present chapter a method aimed at reducing this difficulty, by using a termination matched to the characteristic impedance of the coaxial line, will be investigated. This method requires simple conventional apparatus for measuring VSWR and is applicable both to solids and liquids without any modification to the coaxial sample-holder. For solid samples the inner conductor is spring-loaded to ensure good electrical contact between the sample and conductor. When non-volatile liquids are measured the spring can be unloaded and thin layers of the liquid are simply held between the inner conductor gap by their viscosity forces and surface tensions.

3.2 GENERAL PRINCIPLE

In this method the sample is placed between a gap in the inner conductor of a coaxial sample-holder. The measurement consists of determining the VSWR and the voltage standing-wave minima nearest the sample-holder when the sample is inserted into it. Maintaining the same gap spacing as with

the sample the VSWR and the corresponding voltage standing-wave minimum position are then measured without the sample. As before, whenever the situation permits, a few minima positions may be necessary and advantageous in providing average values of the standing-wave minima displacement. The difference in the standing-wave minima locations and the VSWR values are then used to calculate the relative dielectric constant and loss factor of the sample.

3.3 THEORY

A capacitive gap in the inner conductor of a coaxial line finds common applications in filter circuits at radio and microwave frequencies [3.1, 3.2]. The distribution of the electric field lines in the vicinity of a gap in the inner conductor of a coaxial line is shown in Fig.3.1(b). A simple series capacitance representation of the gap has been found to be inadequate in explaining the behaviour of the line section or filter circuit [3.2, 3.3]. The distortion of the normal transverse electromagnetic field lines around the gap may be described in terms of a fringing-field capacitance [3.3 - 3.6]. It is assumed that the redistribution of the field is negligible outside a region about the gap approximately the size of the coaxial line cross-section [3.4, 3.6]. Thus a more appropriate equivalent circuit for the gap is a π-network of capacitors as shown in Fig.3.2.

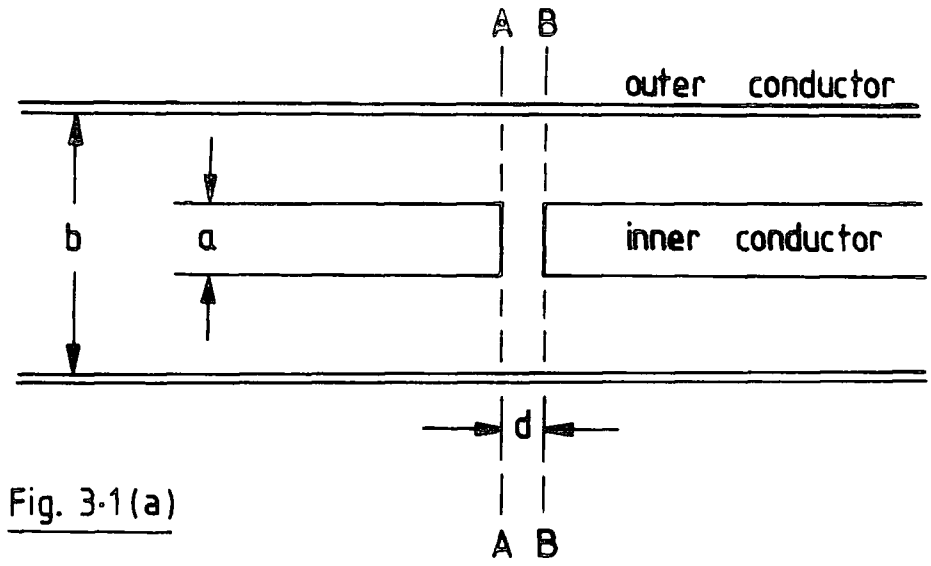

Fig. 3·1(a)

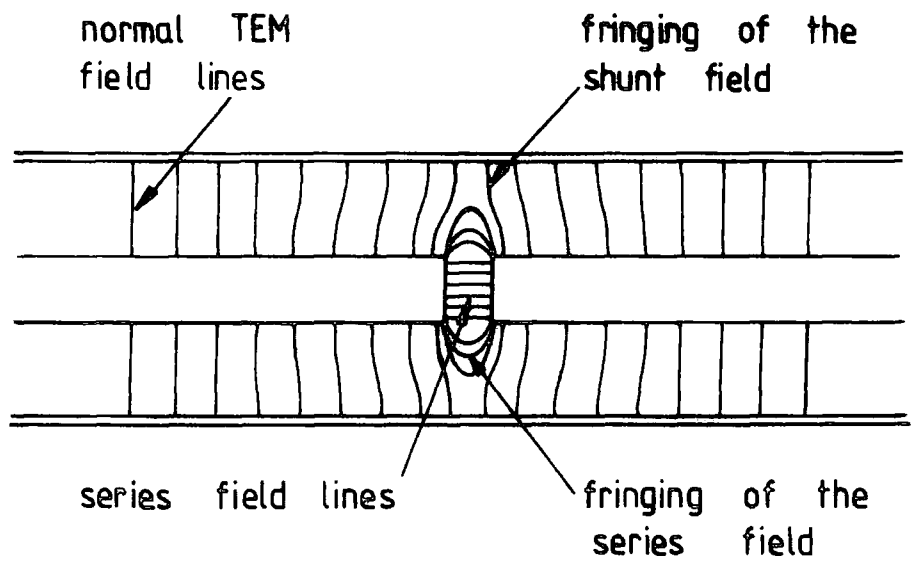

Fig. 3·1(b)

Fig. 3·1 (a) Capacitive gap in the inner conductor of a coaxial line

(b) Electric field lines in the vicinity of the gap

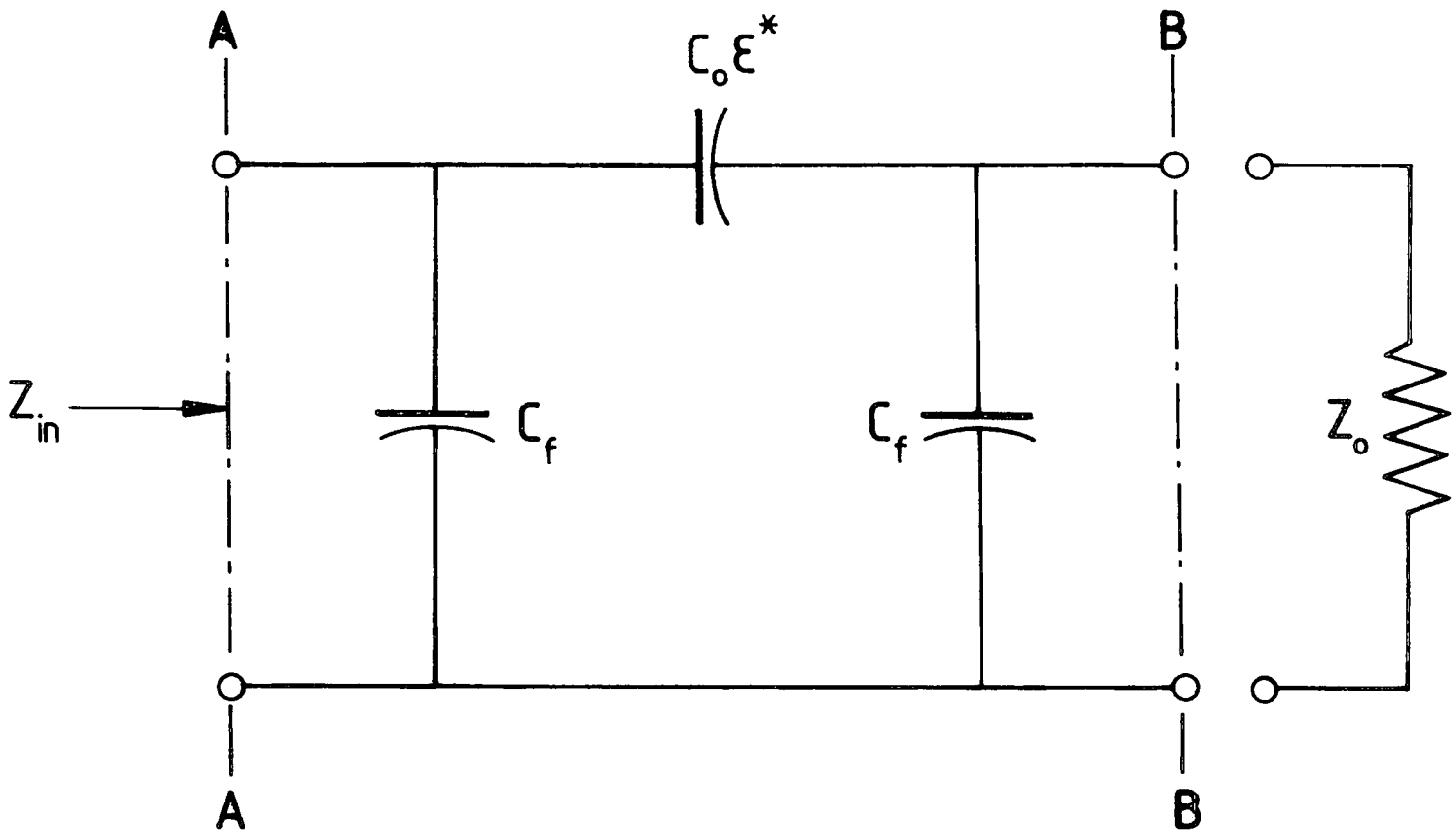

Fig. 3.2 The π-network of capacitors equivalent circuit for the gap in the inner conductor of the coaxial line section of Fig. 3.1

The sample-holder constructed and used in the present work is based on such a gap and its π-network of capacitors equivalent circuit representation. It is evident that when a sample is introduced into the sample-holder the series capacitance would be given by $C_o \varepsilon^*$ where ε^* is the complex relative permittivity of the sample. C_o is the series capacitance of the empty sample-holder calculated from the inner conductor and gap dimensions and C_f represents the fringing-field capacitance associated with the discontinuities of the inner conductor. For reasons similar to those given in chapter 2, the fringing-field capacitance is assumed to be an upper limit. When a load matched to the characteristic impedance of the coaxial line is connected to the output of the sample-holder, and assuming $\omega Z_o C_f \ll 1$ for most practical purposes [3.7], the impedance looking into the sample-holder at the plane A - A of Fig.3.2 may be approximated by

$$Z = \frac{1 + j\omega Z_0 (C_0 \varepsilon^* + C_f)}{j\omega (C_0 \varepsilon^* + C_f)} \qquad (3.1)$$

where $\omega = 2\pi f$ is the radian frequency and f is the frequency in Hz. When air is the dielectric in the inner conductor gap, the series capacitance may be taken as the vacuum capacitance C_o and the reflection coefficient [3.8] at the plane A - A is then given by

$$|\Gamma_a| \exp(-j\theta) = \frac{Z_a - Z_0}{Z_a + Z_0} = \frac{1}{1 + j2\omega Z_0 (C_0 + C_f)} \qquad (3.2)$$

where $|\Gamma_a|$ is the reflection coefficient magnitude,

θ_a is the phase angle of the reflection coefficient,

Z_a is the input impedance at the plane A - A.

Similarly, when a sample of complex relative permittivity ε^* is introduced into the sample-holder the reflection coefficient at the plane A - A can be written as

$$|\Gamma_s| \exp(-j\theta_s) = \frac{Z_s - Z_0}{Z_s + Z_0} = \frac{1}{1 + j2\omega Z_0(C_0\varepsilon^* + C_f)} \qquad (3.3)$$

where the subscript s denotes quantities similar to the ones defined above but in this case pertaining to the sample. On dividing eqn(3.2) by eqn(3.3) and substituting for $\varepsilon^* = \varepsilon' - j\varepsilon''$ we have

$$|\Gamma_a|/|\Gamma_s| \exp j(\theta_s - \theta_a) = \frac{1 + 2\omega Z_0 C_0 \varepsilon'' + j2\omega Z_0 C_0(\varepsilon' + C_f/C_0)}{1 + j2\omega Z_0 C_0(1 + C_f/C_0)} \qquad (3.4)$$

Expanding the left-hand side of the above equation and transposing results in

$$|\Gamma_a|/|\Gamma_s|[\cos(\theta_s - \theta_a) + j\sin(\theta_s - \theta_a)][1 + j2\omega Z_0 C_0(1 + C_f/C_0)]$$

$$= 1 + 2\omega Z_0 C_0 \varepsilon'' + j2\omega Z_0 C_0(\varepsilon' + C_f/C_0) \qquad (3.5)$$

Equating real and imaginary parts, solving for ε' and ε'' and simplifying we obtain

$$\varepsilon' = \frac{|\Gamma_a|}{|\Gamma_s|}\left[(1 + C_f/C_0)\cos 2\beta(\ell_s - \ell_a) + \frac{\sin 2\beta(\ell_s - \ell_a)}{2\omega Z_0 C_0}\right] - \frac{C_f}{C_0} \qquad (3.6)$$

$$\varepsilon'' = \frac{|\Gamma_a|}{|\Gamma_s|}\left[\frac{\cos 2\beta(\ell_s - \ell_a)}{2\omega Z_0 C_0} - (1 + C_f/C_0)\sin 2\beta(\ell_s - \ell_a)\right] - \frac{1}{2\omega Z_0 C_0} \qquad (3.7)$$

where the phase constant $\beta = 2\pi/\lambda_g$ with λ_g as the guide wavelength; ℓ_a and ℓ_s are respectively the voltage standing-wave minima locations with air and the sample as the dielectric. The phase angle of the reflection coefficient with air, θ_a, is related to β and ℓ_a through the equation [3.8]

$$\theta = 2\beta\ell - (2n + 1)\pi \qquad (3.8)$$

where the integer n refers to the number of the standing-wave nodes in front of the terminal plane A - A. A similar definition applies to the phase angle of the reflection coefficient θ_s when the material under test is introduced into the sample-holder. Once the dielectric constant and loss factor are known, the loss tangent and conductivity can be calculated in the usual way.

3.4 SAMPLE-HOLDER DESIGN AND CONSTRUCTION

3.4.1 Line Parameters and Characteristic Impedance

The geometry of the coaxial line leads to particularly simple forms for the electric and magnetic fields.

For the TEM mode the electric field is entirely radial and the magnetic field forms a series of concentric circles around the inner conductor as indicated in Fig.3.3. This permits easy calculations of the basic line parameters: the shunt capacitance and conductance, which are determined by the line geometry and the dielectric medium between the conductors, and their series inductance and resistance. At high frequency, when the skin effect is important, current flow is restricted to the adjacent surfaces of the conductors and the magnetic field to the space between them. The dominant line parameters, the inductance L and capacitance C per unit length of line, which control its high frequency characteristic impedance, can easily be shown to be given by [3.10, 3.11]:

$$L = \frac{\mu_r}{2\pi} \ell n(b/a) \tag{3.9}$$

and

$$C = 2\pi\varepsilon_r / \ell n(b/a) \tag{3.10}$$

where ε_r and μ_r are respectively the permittivity and permeability of the medium filling the space between the conductors. The high frequency resistance of the conductors is the resistance of the appropriate surface layers, i.e.

$$R = \frac{R_s}{2\pi}\left[\frac{1}{a} + \frac{1}{b}\right] \tag{3.11}$$

where the equivalent surface resistance of the conductors is given by $R = 1/\sigma\delta$ with σ the conductivity and δ the skin depth of the conductor material. As R_s is

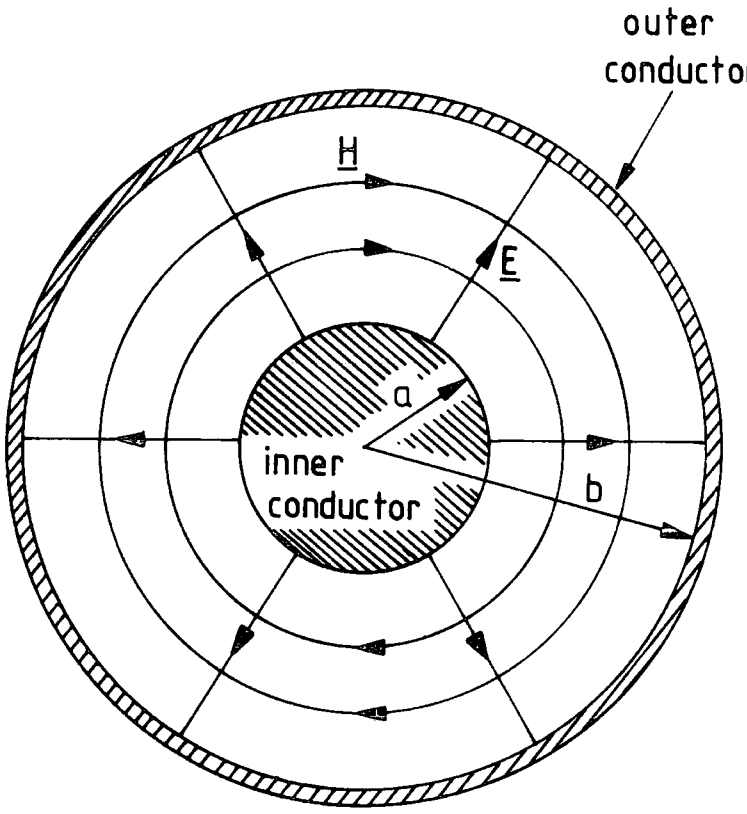

Fig. 3.3 Cross-section of a coaxial line showing the TEM field distributions

proportional to the square root of the frequency, the line loss tends to be proportional to $\sqrt{f}$. For a low loss line R must be minimized. It is then necessary to make R_s small and to choose large values of the conductor diameters a and b [3.9] . The characteristic impedance of a low loss line can be calculated from the values of the distributed inductance and capacitance using the equation [3.10] :

$$Z_o = \sqrt{L/C} = \frac{1}{2\pi}\sqrt{\mu_r/\varepsilon_r}\,\ell n(b/a) \qquad (3.12)$$

The sample-holder used in this work was constructed of brass; the external diameter of the inner conductor a was 6.20 mm while the internal diameter of the outer conductor b was 14.29 mm. This gave a diameter ratio of 2.305 and would theoretically yield a characteristic impedance very close to 50 ohms, [3.9 - 3.11] ; Table 3.1. Fig.3.4 shows the dominant line parameters L and C and the characteristic impedance Z_o as a function of the diameter ratio b/a .

Table 3.1 50 Ω Coaxial Line Conductor Diameters [3.12]

	14-mm line		7-mm line	
	mm	in.	mm	in.
Outer diameter of inner conductor	14.2875	0.5625	7.000	0.2756
Inner diameter of outer conductor	6.2041	0.24425	3.040	0.1197

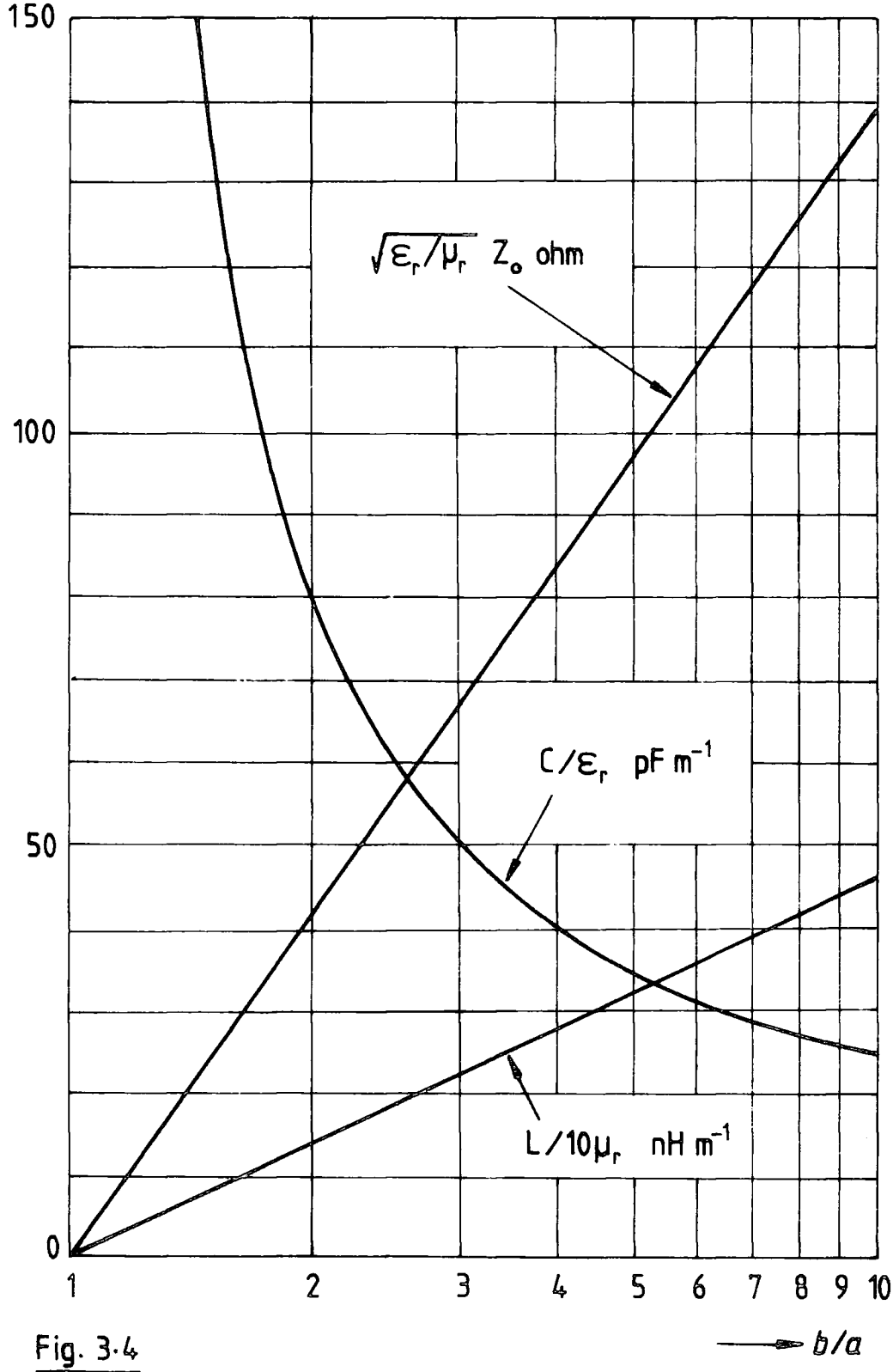

Fig. 3.4

The impedance and capacitance per unit length, and the characteristic impedance of a coaxial line as a function of the diameter ratio b/a

The size of the internal conductor of the sample-holder chosen was appropriate for most practical situations since samples of this cross-section can be readily obtained. This was also consistent with minimizing the conductor losses mentioned earlier and for minimizing the error in length measurements. Another advantage in this case was that the main line used had identical diameter sizes, thus the additional problem associated with step discontinuities when transforming to different conductor diameters [3.4, 3.6] was avoided.

3.4.2 Inner Conductor Supports

For reasons of mechanical stability and alignment, it would be better in principle to have some kind of support for the inner conductor of the sample-holder. Fig.3.5 illustrates schematically some of the possible ways of supporting the inner conductor while minimizing the reflections of the electromagnetic waves due to the supports themselves. The presence of such supports increases the characteristic impedance at the points of support since the capacitance per unit length increases at those points. Hence it is desirable to keep the dielectric constant and losses of such supports as low as possible to minimize the reflections. Table 3.2 below lists some of the potential materials for the inner conductor supports.

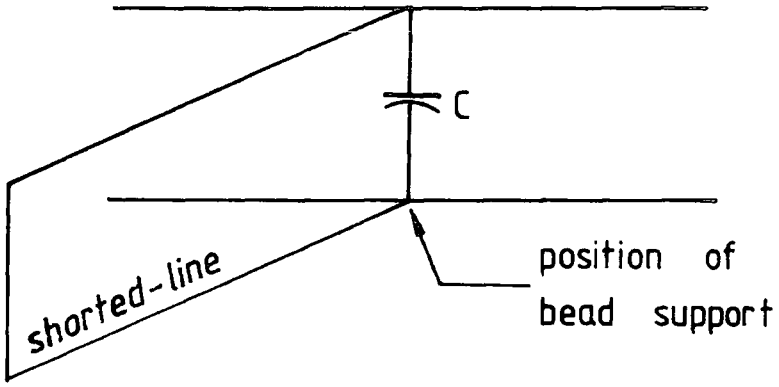

(a) Shorted length of line connected in parallel to coaxial line at the point of support

(After reference 3·17)

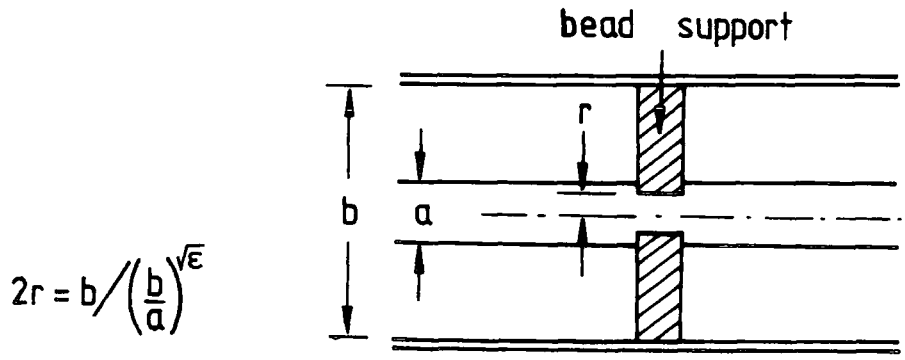

(b) Undercut bead: radius of inner conductor of coaxial line reduced at the point of support

(After references 3·16, 3·17)

Fig. 3·5 Some ways of minimising reflections due to bead supports for the inner conductors of coaxial lines

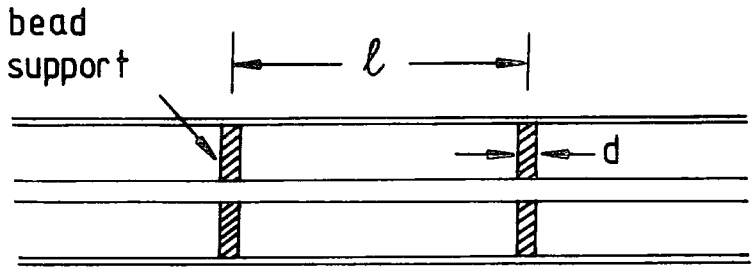

$$\ell = \frac{\lambda_g}{2\pi} \tan^{-1}\left[\frac{2\sqrt{\epsilon}}{1+\epsilon} \cot\left(\frac{2\pi\sqrt{\epsilon}\, d}{\lambda_g}\right)\right]$$

(c) Two bead supports for a coaxial line inner conductor showing separation ℓ for minimum reflections

(After references 3·16, 3·17)

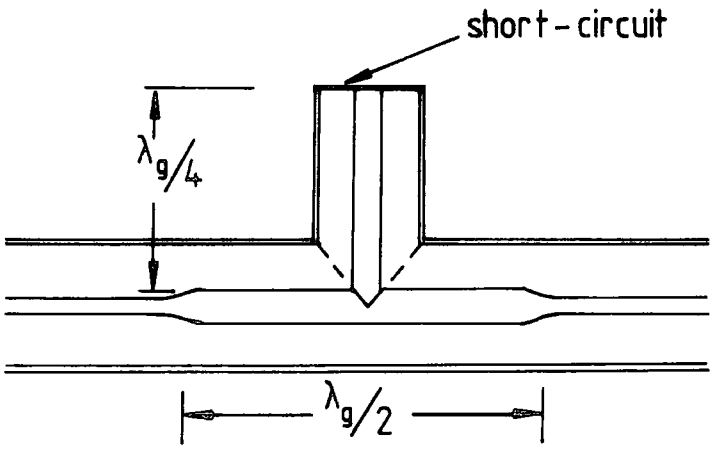

(d) A quarter-wavelength side-arm for a coaxial line inner conductor support

(After references 3·10, 3·16, 3·17)

Fig. 3·5 (Continued)

Table 3.2 Candidate Materials for Coaxial Line Inner Conductor Supports [3.13 - 3.15]

Properties	Materials		
	Polyethylene (PE)	Polytetrafluoroethylene (PTFE)	Polystyrene (PS)
Dielectric constant, ε' (at 23°C and from 1 - 10^{10} Hz)	2.25 - 2.30	$\varepsilon' = \frac{1 + 0.238D}{1 - 0.119D}$ ($\sim$ 2.1 - 2.3) where D = density	ε'(amorph) = 2.49 - 2.56 ε'(cryst) = 2.45 - 2.65
Loss tangent, $\tan\delta$ (at 23°C and from 1 - 10^{10} Hz)	10^{-4} - 10^{-3}	$\sim 2 \times 10^{-4}$	$\tan\delta$(amorph) = 10^{-3} $\tan\delta$(cryst) = 3×10^{-4} (flat from 1 - 10^{10} Hz)

The effect of a single support may be represented by an extra capacitance at that point and if its thickness $d \ll \lambda_g$ we may say that the capacitance is concentrated at a point. Over a limited frequency range this effect may be cancelled by incorporating a shorted length of line as shown in Fig.3.5(a). In addition, where the situation permits, the effect of the support can be further reduced by placing it at the node of a voltage standing-wave. For small values of $2\pi\sqrt{\varepsilon}\, d/\lambda_g$ where ε is the dielectric constant of the supporting material the reflection Γ introduced by the support is given by [3.16]:

$$\Gamma = -j(\varepsilon - 1)\pi d/\lambda_g \qquad (3.13)$$

Another way of minimizing the reflections introduced by the supporting beads while maintaining a constant characteristic impedance is to use undercut beads as illustrated in Fig.3.5 (b). To achieve this the outer radius of the inner conductor should be reduced to a value r given by the expression [3.16, 3.17]

$$2r = b \Big/ \left(\frac{b}{a}\right)^{\sqrt{\varepsilon}} \qquad (3.14)$$

If it becomes necessary to support the inner conductor with more than one bead, as in Fig.3.5(c), then these beads should be placed a distance ℓ apart [3.16, 3.17] such that:

$$\ell = \frac{\lambda_g}{2\pi} \tan^{-1}\left[\frac{2\sqrt{\varepsilon}}{1+\varepsilon} \cot\left(\frac{2\pi\sqrt{\varepsilon}\, d}{\lambda_g}\right)\right] \qquad (3.15)$$

Alternatively if C is the capacitance due to one support the distance ℓ may be expressed as [3.17]

$$Z_o \tan\left(\frac{2\pi\ell}{\lambda_g}\right) = \frac{2}{\omega C} \qquad (3.16)$$

It is also possible to maintain the characteristic impedance constant at the points where the supports are placed by making the outer conductor slightly larger at those points [3.6] . The inner conductor may also be supported by a quarter-wavelength stub as illustrated in Fig. 3.5(d). This produces low reflections in a narrow frequency range. Alternatively, the stub support can be made half a wavelength long so that the transformation ratio in a limited frequency range is independent of the characteristic impedance.

Some of the schemes like those described above have been considered, nevertheless problems remained which were

(i) schemes (a) and (d) were found suitable only for a limited frequency range

(ii) supports like those shown in Fig. 3.5(c) were inconvenient as the separation ℓ can be very long at lower frequencies and it has to be

continuously adjusted for different frequencies

(iii) The problems in maintaining a uniform cross-section, straight edges over a long length of coaxial sample-holder and the mechanism for moving the bead supports smoothly along it presents considerable difficulties and could not be overcome satisfactorily.

Initially the scheme illustrated in Fig.3.5(b) was adopted and tests indicated that the residual VSWR values (see later) of the sample-holder were still quite high. A combination of undercut and overcut beads gave an improvement although the residual VSWR values could still be reduced; the inability of minimizing the VSWR values very much further might actually be an inherent limitation [3.18] of this kind of bead support itself. By trial and error a line section about 10 cm long was found to be suitable. Nevertheless, two inner conductor supports of the overcut and undercut type machined from polytetrafluoroethylene (trade name Teflon) were used and modified by trial to produce lower reflections. Commercial 14-mm line supports were actually incorporated into the sample-holder as they were compensated [3.18, 3.19] . The final working construction is shown in Fig.3.6, the various parts labelled being:

A and E : fixed sections of inner conductor

B : removable portion of inner conductor

C : thin-walled sliding tube

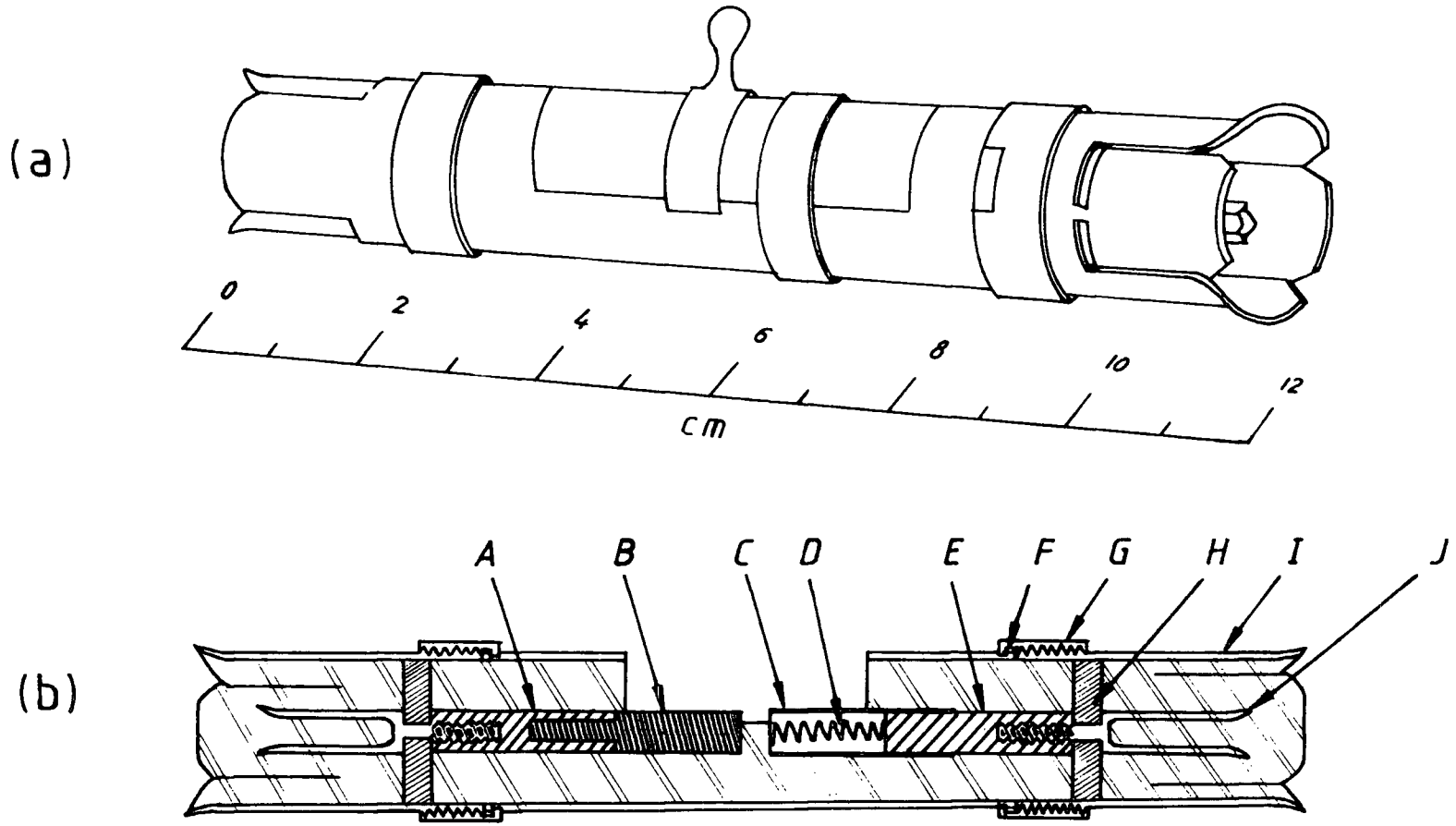

Fig. 3·6 (a) External view and (b) cross-section of sample-holder used in this work

D : compression spring

F : retaining ring

G : linking annulus

H : Teflon bead support

I and J : GR 874 connector set.

One portion of the inner conductor, section B, is removable to facilitate the loading and unloading of the compression spring. Access to the inner conductor gap is via a window, approximately 3.5 cm by 120^{o} of arc, on the outer conductor. When the sample-holder is in use a sliding close-fitting ring clamps the cover of the access window onto the outer conductor.

3.5 SAMPLE-HOLDER VSWR AND CALIBRATION

The block diagram of the measurement set-up is very similar to the conventional arrangement of measuring VSWR's as shown in Fig.2.6, except that in place of the short-circuit is a matched termination (GR 874 WN was used here). The overall performance of the sample-holder may be given in terms of the residual VSWR. By this is meant the VSWR values obtained when the inner conductor gap is closed (or a dummy metal piece of similar cross-section as the inner conductor inserted into the gap) and the sample-holder terminated with a matching load. In view of the fact that the line losses increase with increasing frequency [3.9] and that most general purpose commercial components

have residual VSWR values of the order 1.05 in the 1 - 10 GHz range of frequencies, a requirement level of residual VSWR of about 1.05 to 1.15 from about 500 MHz to 10 GHz was assumed to be sufficiently suitable. Silver coating of the surfaces bounding the electromagnetic field was found to give only marginal improvements in the residual VSWR's. Hence in the final sample-holder the internal surfaces were not silver coated but were simply polished to a smooth shiny finish. Measured values of the residual VSWR are compared with the requirement level in Fig.3.7.

The variations of the VSWR of the empty sample-holder (air dielectric) with air capacitance C_o (or gap spacing) for various frequencies are shown in Fig.3.8. With the spring unloaded the gap spacing was set to a particular value by means of a feeler-gauge. This was carried out slowly, to allow sufficient time for air to get into or out of the close-fitting sliding tube C, in order to ensure that the gap was set to the correct spacing. For a particular gap spacing and frequency the measured value is compared with the calculated ones, as shown in Fig.3.8. This serves both as a check against the approximations assumed in the calculations of the reflection coefficients and as a calibration for later calculations of ε' and ε''. It will be observed that for the lower frequencies considerable deviations between 5 and 10 from the calculated values

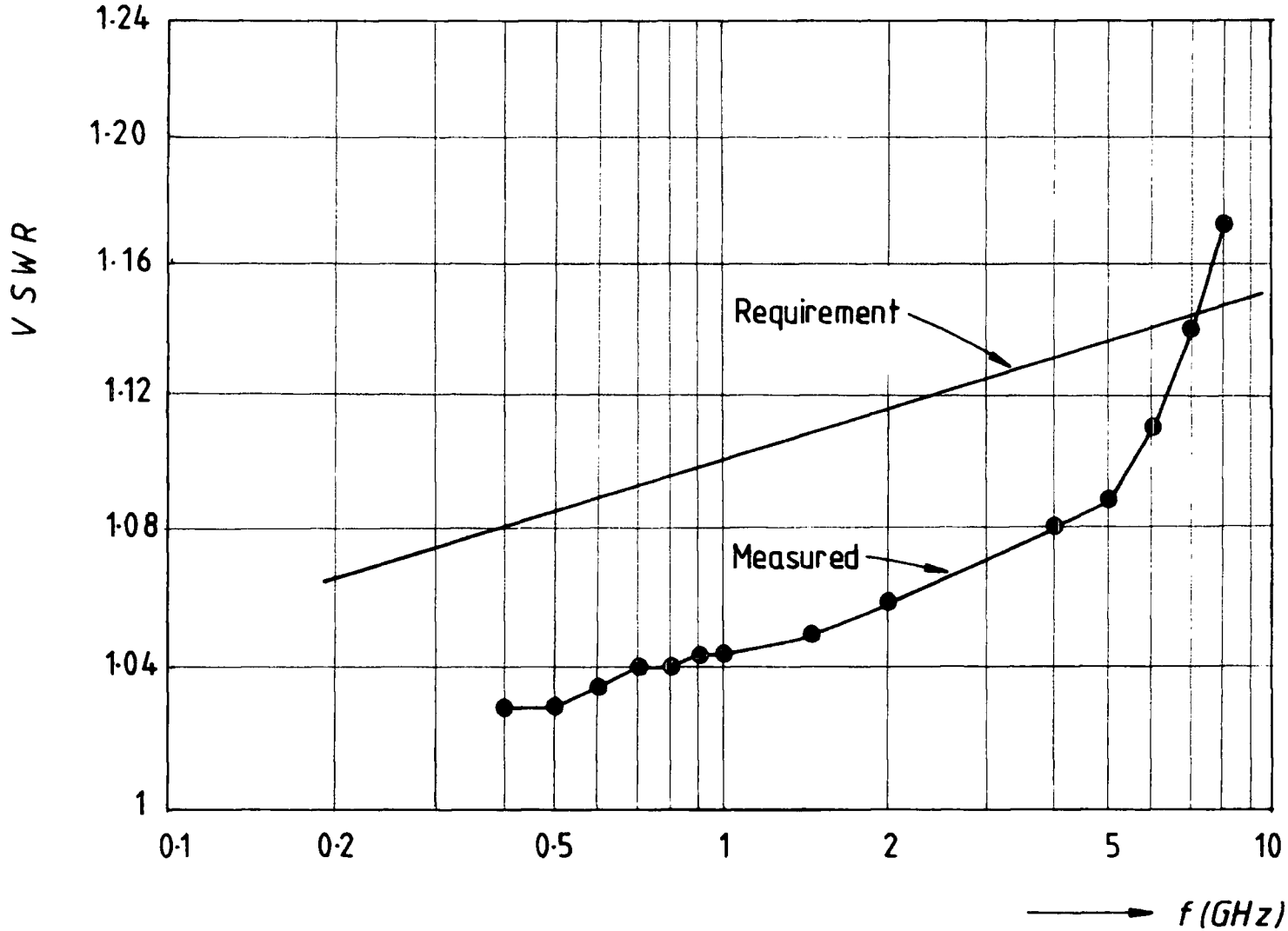

Fig.3·7 VSWR of sample-holder terminated with a 50Ω load (gap closed)

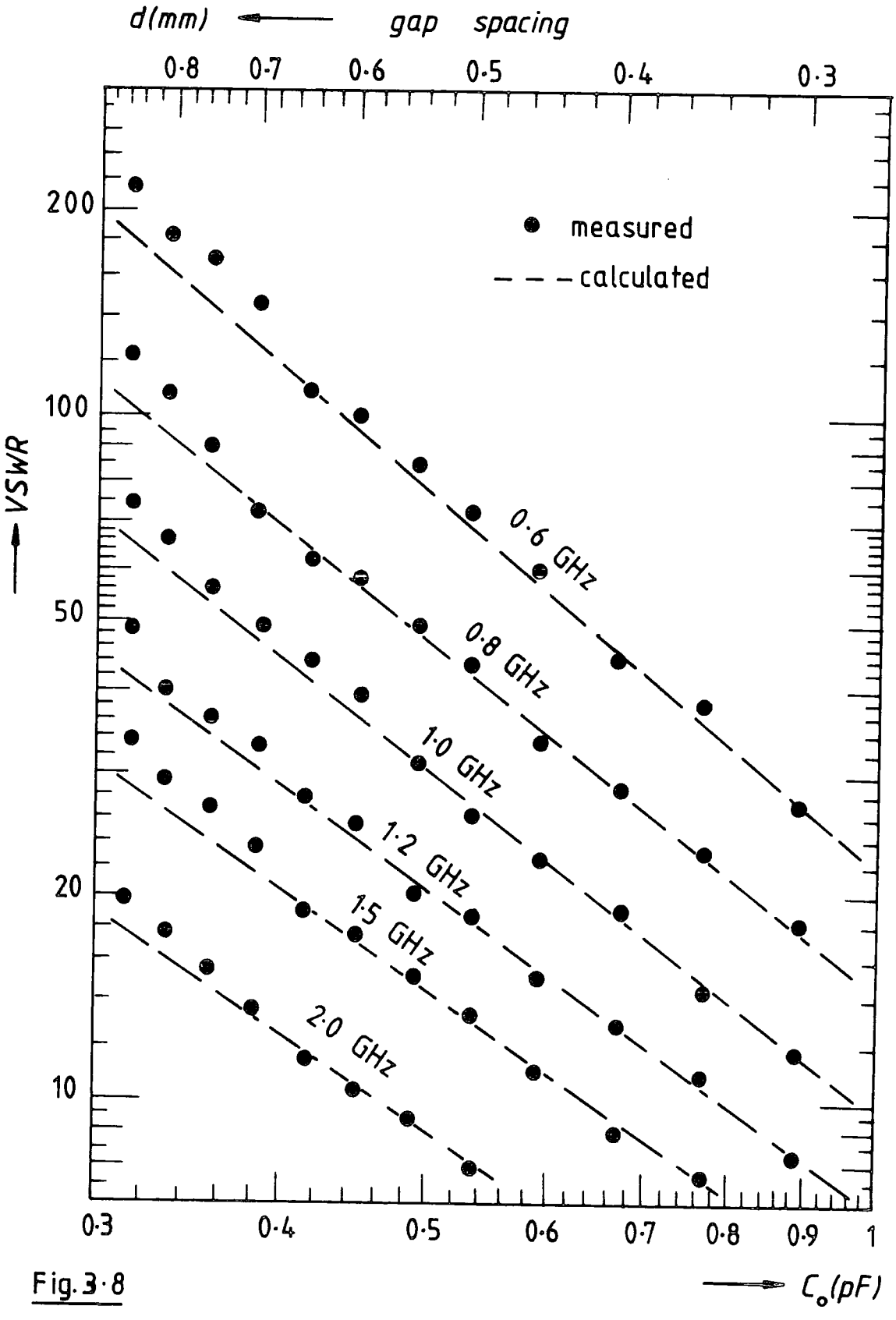

Fig. 3·8

VSWR of empty sample-holder for various gap spacings and frequencies

occur for gap spacings greater than about 0.8 mm, ($C_o \lesssim 0.35$ pF). For smaller gap spacings corresponding to air capacitances $C_o \gtrsim 0.35$ pF, the measured VSWR's can be said to be in satisfactory agreement with the calculated values.

3.6 COMMENTS AND CONCLUSIONS

Equations relating the dielectric constant and loss factor to the ratio of reflection coefficient magnitudes and the difference in their phase angles with and without the sample were derived on certain assumptions. Thus the dielectric properties of a material can be found from measurements on a disc sample placed within a gap in the inner conductor of a sample-holder. Various geometries of the sample-holder and schemes of supporting the inner conductor were studied. The criteria for a suitable sample-holder were firstly that it should provide coverage over a wide frequency range so as to take advantage of a similar feature of coaxial lines and secondly, that the characteristic impedance should remain within a certain level in the entire frequency range. A sample-holder which met these requirements was satisfactorily constructed partly using commercially available connectors and bead supports. This considerably reduced the problems associated with coaxial line discontinuities due to geometrical factors and was also compatible with the existing line cross-sectional dimensions.

However, due to increasing line losses in general and the losses due to connectors at higher frequencies, the residual VSWR value was found to exceed the requirement level above about 8 GHz. The VSWR plots illustrated in Fig.3.8 indicate that suitable values of the gap spacing can be chosen so as to lower the VSWR.

3.7 REFERENCES

3.1 Young L.," The practical realization of series capacitive couplings for microwave filters", Microwave J., vol.5,79 (1962)

3.2 Matthaei C.L., Young L. and Jones E.M.T. (Eds.),"Microwave Filters, Impedance-Matching Networks, and Coupling Structures", McGraw-Hill, New York (1974)

3.3 Dawirs H.N.," Equivalent circuit of a series gap in the centre conductor of a coaxial transmission line", IEEE Trans.Microwave Theory and Techniques, vol.17,127(1969)

3.4 Whinnery J.R., Jamieson H.W. and Robbins T.E.," Coaxial line discontinuities", Proc.IRE, vol.32,695(1944)

3.5 Marcuvitz N.," Waveguide Handbook ", Vol.10, M.I.T. Rad. Lab. Series, McGraw-Hill, New York (1951)

3.6 Green H.E.," The numerical solutions of some important transmission-line problems ", IEEE Trans. Microwave Theory and Techniques, vol.13,676(1965)

3.7 Iskander M.F. and Stutchly S.S.," Fringing field effect in the lumped-capacitance method of permittivity measurement ", IEEE Trans. Instrum. Meas., vol.27,107 (1978)

3.8 Sucher M. and Fox J. (Eds.), " Handbook of Microwave Measurements ", Vol.I, 3rd edn., Polytechnic Press, Brooklyn, New York (1963) Chapt.2

3.9 Davidson C.W.," Transmission Lines for Communications ", MacMillan, London (1978) Chapt.1

3.10 Saad T.s.," Microwave Engineers' Handbook ", Vol.1, Artech House Inc., Mass. (1971)

3.11 Kraus J.D. and Carver K.R.," Electromagnetics ", 2nd edn., McGraw-Hill Kogakusha, Tokyo (1973) Chapt. 13

3.12 Winschel B.O.," Standardization of precision coaxial connectors ", Proc. IEEE, vol.55,923(1967)

3.13 Boundy R.H. and Boyer R.F. (Eds.)," Styrene, Its Polymers, Co-polymers and Derivatives ", Reinhold Pub. Co., New York (1962)

3.14 Sheratt S. and Ottmer K.," Encyclopedia of Chemical Technology ", 2nd edn., Vol.9,805(1966)

3.15 Brandrup J. and Immergut T. (Eds.)," Polymer Handbook ", 2nd edn., John Wiley, New York (1955), V-13, V-29, V-59

3.16 Moreno T.," Microwave Transmission Design Data ", Dover Publications (1948)

3.17 Mooijwear H.," Microwave Techniques ", Philip Technical Library, Eindhoven (1971)

3.18 Bussey H.E.," Dielectric measurements in a shielded open circuit coaxial line ", IEEE Trans. Instrum. Meas. vol.29,120(1980)

3.19 General Radio Co. Handbook (1966)

CHAPTER 4

THE COAXIAL LINE RESONANCE METHOD

4.1 INTRODUCTION

The matched termination method described in the last chapter indicates that the high frequency limit up to which the method may be employed is about 3 GHz since at this frequency the VSWR before a dielectric is introduced into the sample-holder is of the order of 10. When a sample is inserted into the sample-holder the VSWR would then drop to a value close to between one and two thus increasing the uncertainty in the locations of the voltage standing-wave minima. An increase in the VSWR value such that it can be measured accurately while at the same time not sacrificing the accuracy in locating the standing-wave minima, with and without the sample, may be achieved if the 50 ohm termination is reduced to a lower value, say 20 ohms. This would then extend the usefulness of the method to a higher frequency limit. Nevertheless, the calculations of ε' and ε'' become complicated [see equations (3.2) and (3.3)] and cannot be solved in a straightforward manner as cross products of ε' and ε'' appear implicitly in the ensuing equations. In addition it is rather difficult to produce a purely resistive termination without introducing some small inductive or capacitive effects at the high frequencies [4.1, 4.2] .

4.2 GENERAL PRINCIPLE

An alternative way to overcome the shortcomings mentioned above is to use a purely reactive termination instead of a resistive one. A whole range of continuously variable reactive load in a coaxial line system can be provided by a stub tuner [4.3] . In this case the stub tuner can be adjusted so as to cancel the reactive component of the impedance due to the dielectric when it is placed in the sample-holder. The resulting purely resistive impedance seen at the input terminal of the sample-holder can then be used to calculate the dielectric loss of the sample. The same sample-holder used in the matched termination method can be used directly in this case without any modification.

4.3 THEORY OF THE METHOD

When a variable reactive load is connected to the output terminal of the sample-holder, the equivalent circuit may be given as in Fig.4.1. Let the impedance due to the sample be

$$Z = \frac{1}{j\omega C_o \varepsilon^*}$$

$$= \frac{1}{j\omega C_o(\varepsilon' - j\varepsilon'')} = \frac{\varepsilon'' - j\varepsilon'}{\omega C_o(\varepsilon'^2 + \varepsilon''^2)} \qquad (4.1)$$

where the symbols have their usual meanings. When the variable reactive termination is adjusted such that it

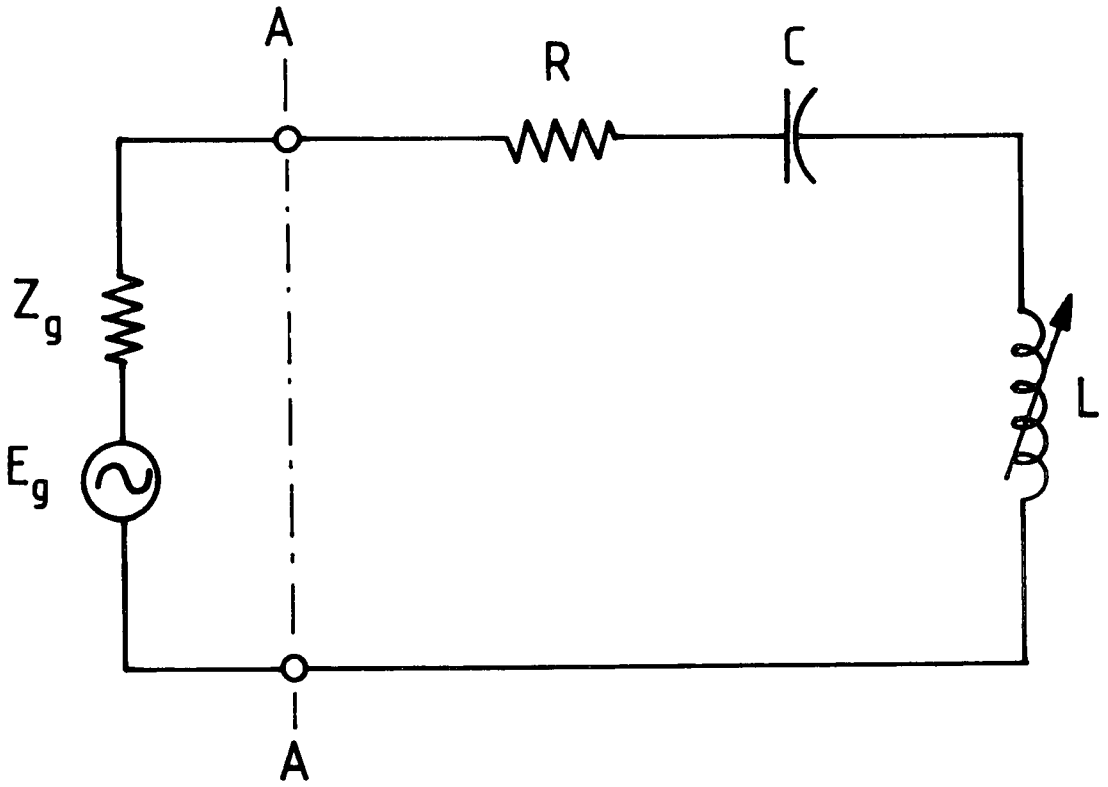

Fig. 4·1 Equivalent circuit for the coaxial line resonance method

cancells off the reactive component due to the sample, the resultant impedance looking into the input terminal of the sample-holder would be purely resistive and at its minimum value. This results in a resonance condition and will produce a maximum value of the VSWR detected on the slotted-line section. If we write the impedance due to the sample in the form $R + jX$, then at the resonance condition when X is cancelled off, the net impedance will be just R. Thus we may write

$$R = \frac{\varepsilon''}{\omega C_o(\varepsilon'^2 + \varepsilon''^2)} \tag{4.2}$$

Since the loss factor is related to the loss tangent through the relation $\varepsilon'' = \varepsilon' \tan\delta$, on substituting this into the above equation we have

$$R = \frac{\tan\delta}{\omega C_o \varepsilon'(1 + \tan^2\delta)} \tag{4.3}$$

Therefore

$$\omega R C_o \varepsilon' \tan^2\delta - \tan\delta + \omega R C_o \varepsilon' = 0 \tag{4.4}$$

Since the frequency, air capacitance, dielectric constant and resistance R are all real positive quantities, the practical solution of equation (4.4) can be shown to be

$$\tan\delta = A - \sqrt{A^2 - 1} \tag{4.5}$$

subject to the condition $A \geq +1$ (for similar reasons as above), where

$$A = \frac{1}{2\omega R C_o \varepsilon'} \qquad (4.6)$$

A purely resistive impedance falls on the real axis of the Smith chart [4.4] and the normalized value of R is then given by the reciprocal of the VSWR at the resonance condition; hence $R = Z_o / \text{VSWR}$. In practice there will be a small resistance associated with the connector of the reactive load. The value of R would then include this resistance in addition to the resistive component of the impedance due to the sample. An estimate of the resistance due to the connector can be made by measuring the VSWR at the resonance condition without the sample. Assuming that this resistance is in series with the resistive part of the impedance due to the sample, the latter can be found from the difference of the resistances with and without the sample.

4.4 EFFECTS OF SAMPLE-HOLDER LOSSES

Since the resistance at the resonance condition is given by the expression $R = Z_o / \text{VSWR}$, if we let the VSWR at the resonant condition with and without the sample be S_s and S_a respectively, the net resistance due to the sample is then

$$Z_o\left(\frac{1}{S_s} - \frac{1}{S_a}\right) \tag{4.7}$$

Equation (4.3) can be written as:

$$Z_o\left(\frac{1}{S_s} - \frac{1}{S_a}\right) = \frac{\tan\delta}{\omega C_o \varepsilon'(1 + \tan^2\delta)} \tag{4.8}$$

Substituting $\omega = 2\pi f$ and rearranging we obtain:

$$\text{Constant.}\, f C_o \varepsilon' \left\{\frac{1 + \tan^2\delta}{\tan\delta}\right\} = 1 \Big/ \left(\frac{1}{S_s} - \frac{1}{S_a}\right) \tag{4.9}$$

Plots of the function on the right-hand side of the above equation against the loss tangent for various values of $fC_o\varepsilon'$ are given in Fig.4.2. A proper selection of the values of $fC_o\varepsilon'$ and the capacitance of the empty sample-holder can be made so as to lower the VSWR values when the dielectric is inserted into the sample-holder.

When the resistance due to the connectors and line losses are significant, the VSWR at resonance without the sample would be finite. This can actually be advantageous if its value is not too close to that when the material under test is inserted into the sample-holder. Fig. 4.3 illustrates the variation of the VSWR of the sample at resonance for cases when the VSWR of the empty sample-holder, under a similar condition, are finite, together with the ideal lossless case when the VSWR, S_a, is infinite.

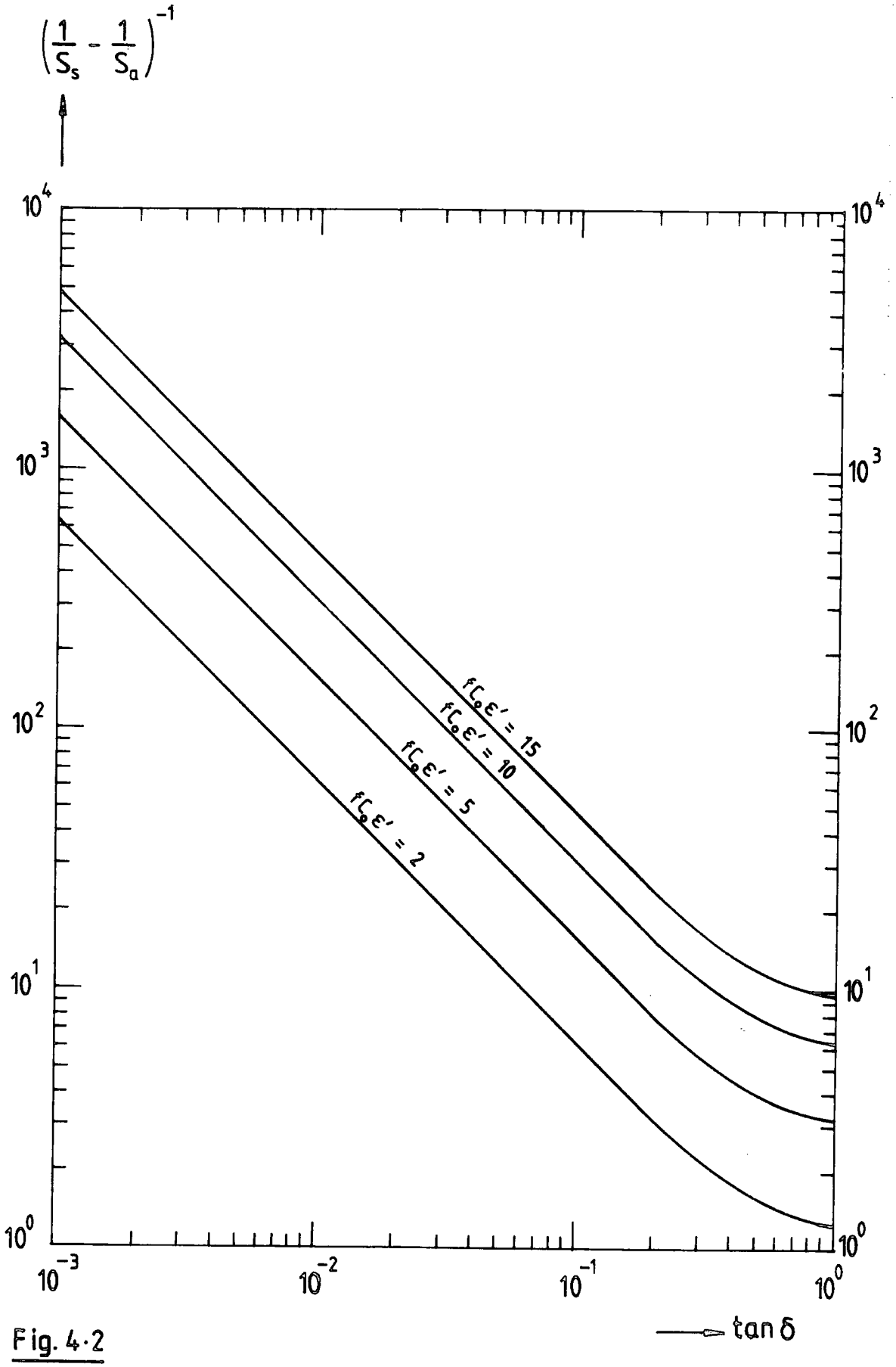

Fig. 4·2

Reciprocal of normalised resistance versus loss tangent for various values of $f C_o \varepsilon'$

Relatively large errors can result if, without measuring it, one assumes that the VSWR of the empty sample-holder at the resonance condition is infinite, even when its value is as large as $\sim$ 10,000. For example, assuming an ideal situation the resistance of the sample is say 0.05 ohms, corresponding to a VSWR of 1000. If the VSWR value at the resonant condition without the sample is actually 10,000, this would have meant that the true resistance of the sample is 0.045 ohms ; the error in assuming an infinite VSWR without the sample would amount to $\sim$ 10 % . Plots similar to those given in Fig.4.3 may also be used as calibration curves. If the VSWR at resonance without the sample in the holder becomes too high, hence the usual difficulties in measurements, a known standard sample - for example quartz or polytetrafluoroethylene (PTFE) - may be used for comparison, in which case appropriate adjustments must be made in the calculations of the loss tangent of the material under test.

4.5 DISCUSSION

A coaxial line resonance method of measuring the loss tangent of a material with corrections for losses due to the connector of a variable reactive load has been suggested. Since this method uses the same sample-holder as the matched termination method, it is again applicable to both solids and liquids. As long as the VSWR values at resonance with

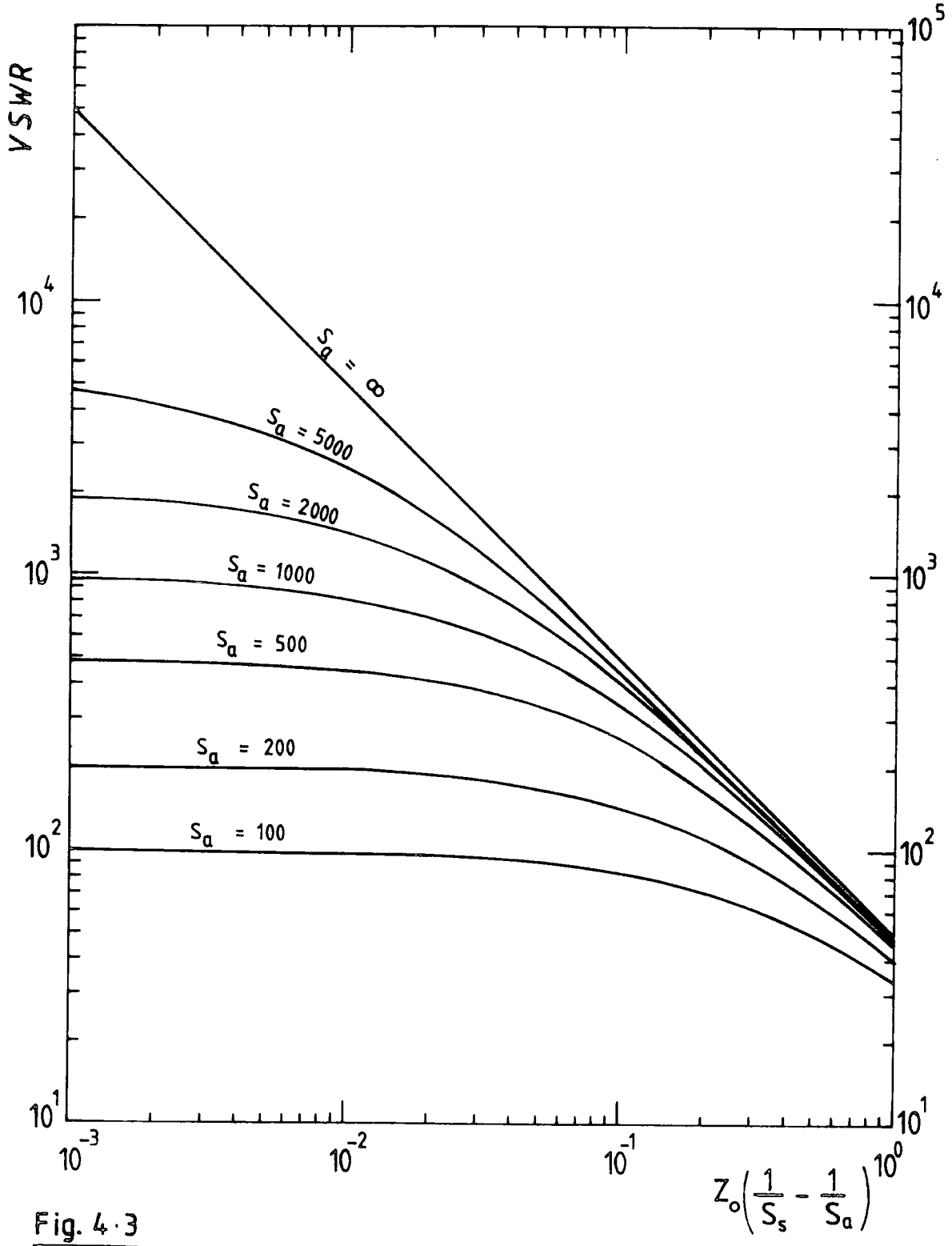

Fig. 4·3

VSWR as a function of resistance for various losses of the empty sample-holder

and without the sample are not too close the method is apparently not restricted to any specific degree of loss. In addition, if identical geometrical conditions can be met the method lends itself to a comparison type of measurement using known samples as the standard.

4.6 REFERENCES

4.1 Davidson C.W.," Transmission Lines for Communications ", MacMillan, London (1978) Chapt.3

4.2 Magnusson P.C.," Transmission Lines and Wave Propagation ", 2nd edn., Allyn and Bacon Inc., Boston (1970)

4.3 Oliner A.A., in Proc. Symp. Modern Advances in Microwave Technology, Polytechnic Press, Brooklyn, New York (1954) p.271

4.4 Smith P.H.," An improved transmission-line calculator ", Electronics, vol.17,130(1944)

CHAPTER 5

ASSESSMENT OF METHODS

5.1 INTRODUCTION

Experimental evaluation of the measurement methods described in Chapters 3 and 4 may be readily carried out using liquids since the air capacitance of the empty sample-holder C_o can be conveniently set to any suitable value by carefully setting the appropriate gap spacing. The liquids used should have the proper combination of physical and chemical properties, for example, their surface tensions and viscosities should allow them to be easily placed into the inner conductor of the coaxial sample-holder; and, of course, they should not react with the metallic conductors. Similarly, an assessment of the methods using known or standard solids can be performed with samples in the form of thin circular discs machined from the bulk. There is , however, a lack of flexibility with regard to the thickness of solid samples in comparison to the liquids whose thickness can be continuously varied.

5.2 MEASUREMENTS OF KNOWN MATERIALS

5.2.1 LIQUID SAMPLES

5.2.1.1 Matched Termination Method

Chlorobenzene * (of chemical formula C_6H_5Cl) was

* Chemical laboratory grade

chosen for the assessment of measurements on liquids since it met the physical and chemical property requirements. Among other factors taken into consideration were that its pure form has been recommended as a standard calibration liquid [5.1 - 5.3] and its effects on contact with the skin were within the safety limits [5.4, 5.5] . Measurements using this method were made between 500 MHz and 3 GHz . The liquid to be measured was carefully placed into the sample-holder by means of a fine-tipped dropper, care being taken to wipe off excess liquid that smeared other parts of the inner conductor. Since the liquid was held in place by its surface tension, the gap spacing was chosen such that the weight of the liquid was observed not to distort its shape. A value between about 0.50 mm and 0.80 mm was found suitable; this corresponds to an empty sample-holder capacitance of between 0.54 pF and 0.36 pF. Although a smaller gap spacing was desirable in order to reduce the fringing-field effects, this was found more difficult to set accurately and insertion of the sample was time consuming (this was in view of the fact that chlorobenzene was rather volatile).

The VSWR of the empty sample-holder was either read off the calibration curves in Fig.3.8 or separately measured if it was not given there. Positions of the voltage standing-wave minima were located on the slotted coaxial line by the process of bracketting (section 2.4.2) ; this was especially essential when measurements with the liquids were

carried out. The measured guide wavelength, voltage standing-wave minima shift and the VSWR values with and without the liquid in the sample-holder were then used to calculate the real and imaginary components of the relative permittivity from equations (3.6) and (3.7). Fig.5.1 shows the VSWR values with and without pure chlorobenzene for an empty sample-holder capacitance of 0.45 pF in the frequency range investigated. In Table 5.1 the values of ε' and ε'' averaged over empty sample-holder capacitances of 0.38, 0.45 and 0.54 pF are compared with those from the literature. These averaged values are plotted over the frequency range of

Table 5.1 Complex Permittivity of Chlorobenzene Determined by the Matched Termination Method ($\simeq 20^{o}C$)

Matched Termination Method			Literature values			
f(GHz)	ε'	ε''	f(GHz)	ε'	ε''	References
0.5	5.65	0.1122	0.5	5.72	0.158	5.1, 5.3 ($20^{o}C$)
1.0	5.51	0.2127				
1.5	5.50	0.3029	0.4	5.58	0.0762	5.6 ($23^{o}C$)
2.0	5.45	0.4005	1.0	5.55	0.146	
2.4	5.48	0.4800	3.0	5.48	0.653	

measurements in Fig.5.2. A plot illustrating maximum differences in the phase angles of the reflection coefficients with and without the sample together with the ratio of

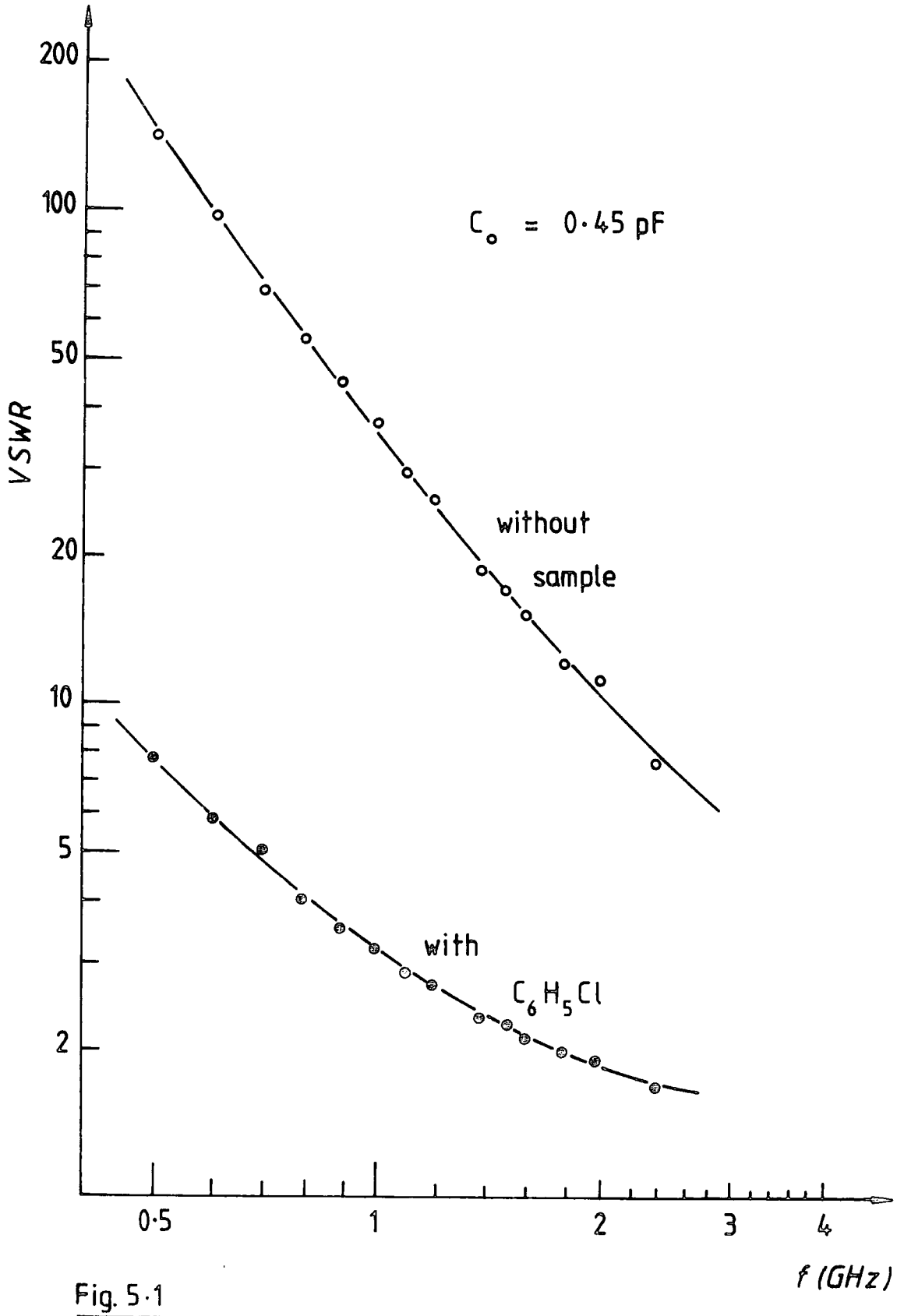

Fig. 5·1

VSWR versus frequency for chlorobenzene and empty sample-holder in the matched termination method

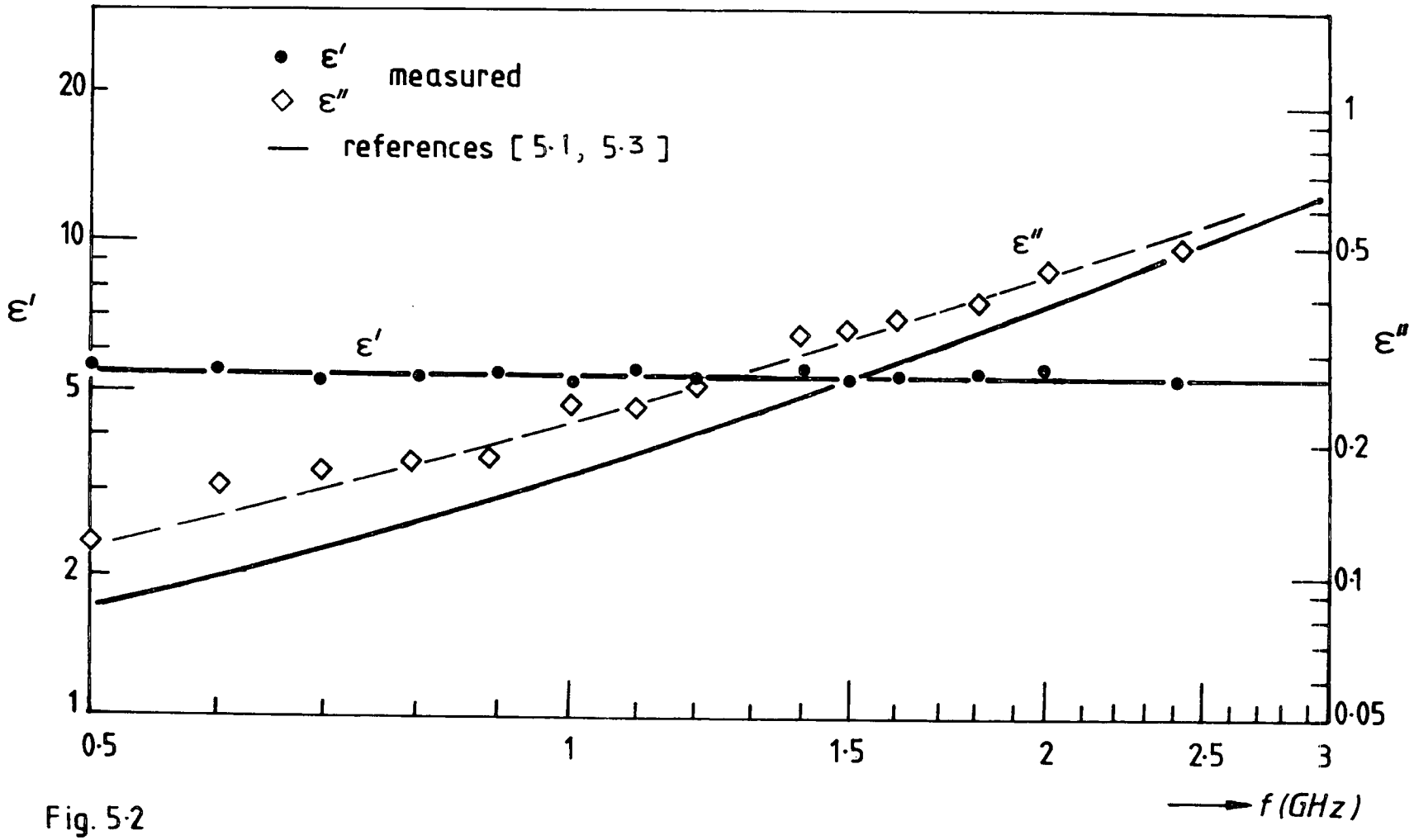

Fig. 5·2

Complex permittivity of chlorobenzene determined by the matched termination method

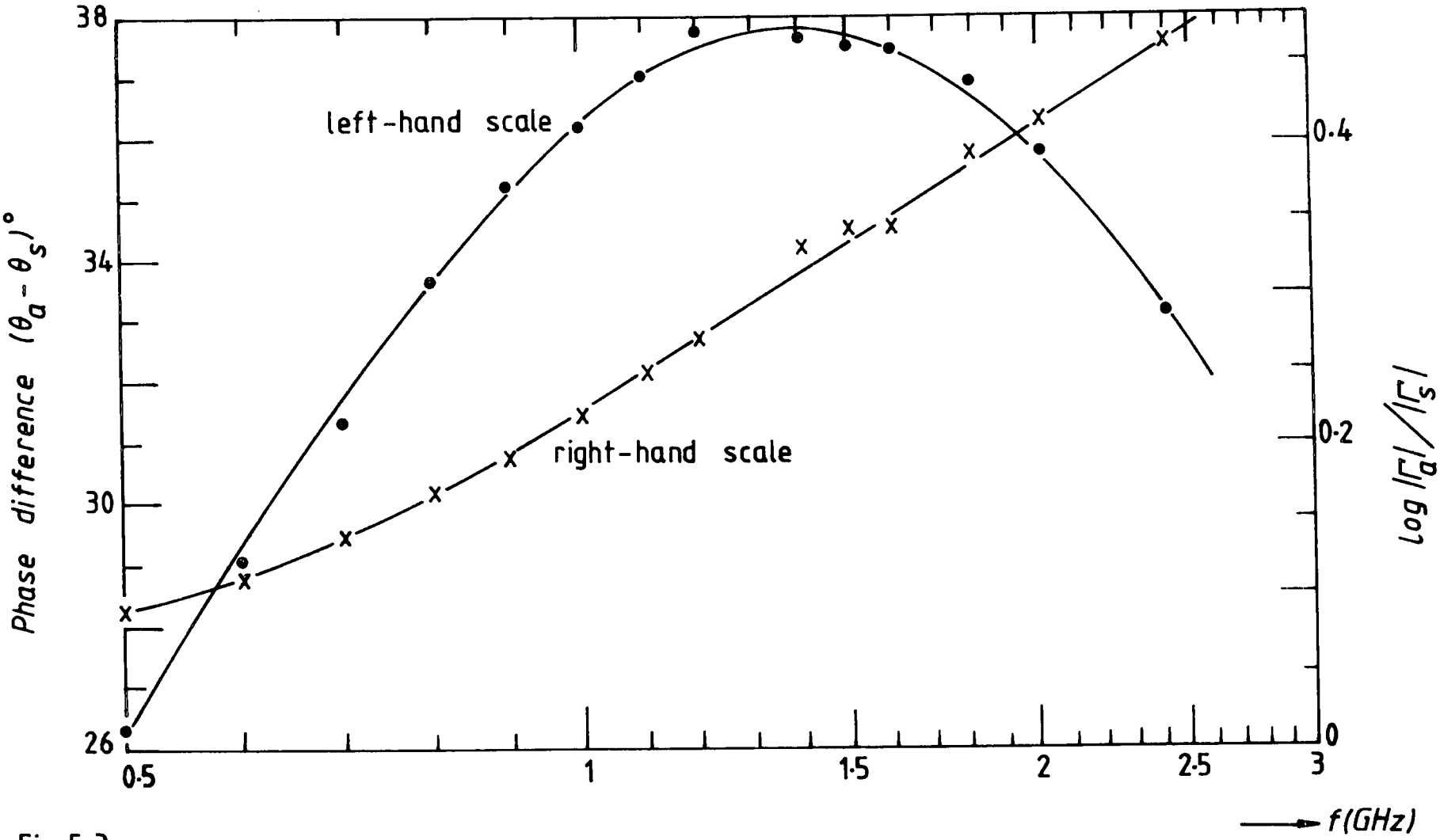

Fig. 5·3

Phase difference and reflection coefficient ratio of chlorobenzene as a function of frequency

reflection coefficient magnitudes are shown in Fig.5.3 for the case C_o = 0.45 pF.

5.2.1.2 Coaxial Line Resonance Method

With this method of measurement the frequency range covered was much wider (from 500 MHz up to about 8 GHz). Chlorobenzene was again found suitable and, in addition, a mixture of 10.6 molar percent of chlorobenzene in cyclohexane (C_6H_{12}) was used. In this method sample thicknesses ranged from 0.50 mm up to 0.80 mm. Plots of the maximum VSWR values at resonance in the frequency range 500 MHz up to 7.2 GHz are given in Fig.5.4. The dielectric constants required for the loss tangent calculations were taken from the matched termination measurements and from the short-circuit method, together with those from the literature [5.6, 5.7]. The measured values of the loss tangents are compared with those from various sources in Table 5.2 below.

Table 5.2 Loss Tangents of Chlorobenzene Determined from the Coaxial Line Resonance Method ($\simeq 20^{\circ}C$)

Coaxial Resonance Method		Literature values		
f (GHz)	tan δ	f (GHz)	tan δ	References
0.5	0.0148	0.5	0.0276	5.1, 5.3 ($20^{\circ}C$)
1.0	0.0278	1.0	0.0264	
2.0	0.0638	3.0	0.1182	5.6 ($23^{\circ}C$)
5.0	0.1974	5.0	0.2028	
7.2	0.2860	7.52	0.2680	5.8 ($22^{\circ}C$)

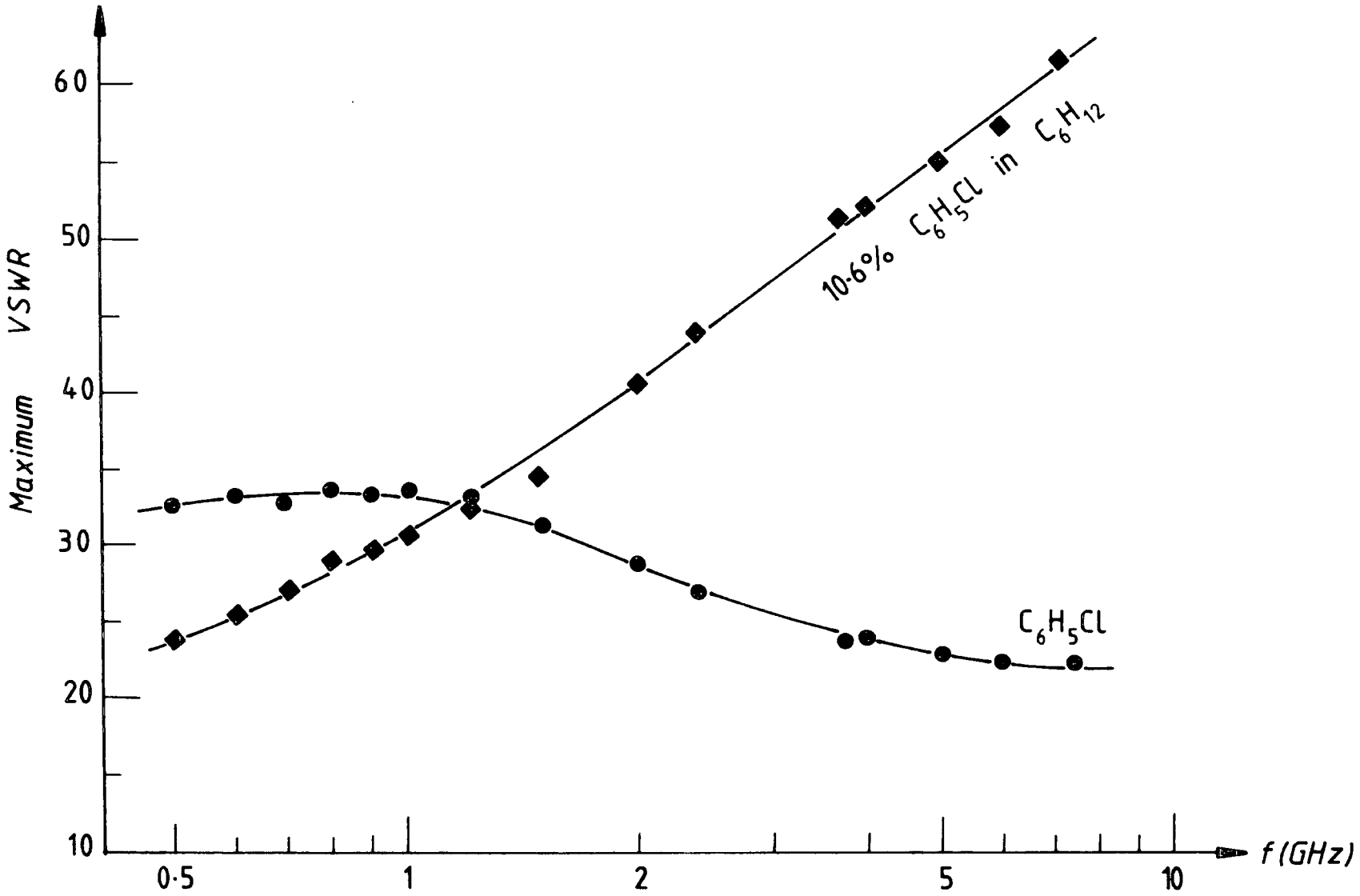

Fig. 5·4 Maximum VSWR for chlorobenzene and 10·6 molar per cent of chlorobenzene in cyclohexane

Variations of the loss tangents of the pure chlorobenzene and the 10.6 percent chlorobenzene solution in cyclohexane with frequency are plotted in Fig.5.5.

The coaxial resonance method of determining the loss tangent was also evaluated using a relatively high dielectric constant liquid - pure water.* Experimental data for pure water are known to fit well [5.10 - 5.16] the Cole-Cole equation [5.17] :

$$\varepsilon^* = \varepsilon'_\infty + \frac{\varepsilon'_s - \varepsilon'_\infty}{1 + (j\omega\tau)^{1-\alpha}} \qquad (5.1)$$

where ε'_s and ε'_∞ are the static and high frequency dielectric constants respectively, τ the relaxation time and α the relaxation time spread parameter. After normalization one can readily show from equation (5.1) that:

$$\varepsilon' = \varepsilon'_\infty + \frac{(\varepsilon'_s - \varepsilon'_\infty)\left[1 + (\omega\tau)^{1-\alpha}\sin(\alpha\pi/2)\right]}{1 + 2(\omega\tau)^{1-\alpha}\sin(\alpha\pi/2) + (\omega\tau)^{2(1-\alpha)}} \qquad (5.2)$$

Table 5.3 lists some dielectric quantities for pure water at

Table 5.3 Quoted Dielectric Data for Pure Water ($20^{\circ}C$)

Quantity	Value
Static dielectric constant, ε'_s	80.4
High frequency dielectric constant, ε'_∞	4.42
Relaxation time constant, τ	9.3×10^{-12} s
Relaxation time spread parameter, α	0.013

* freshly distilled water

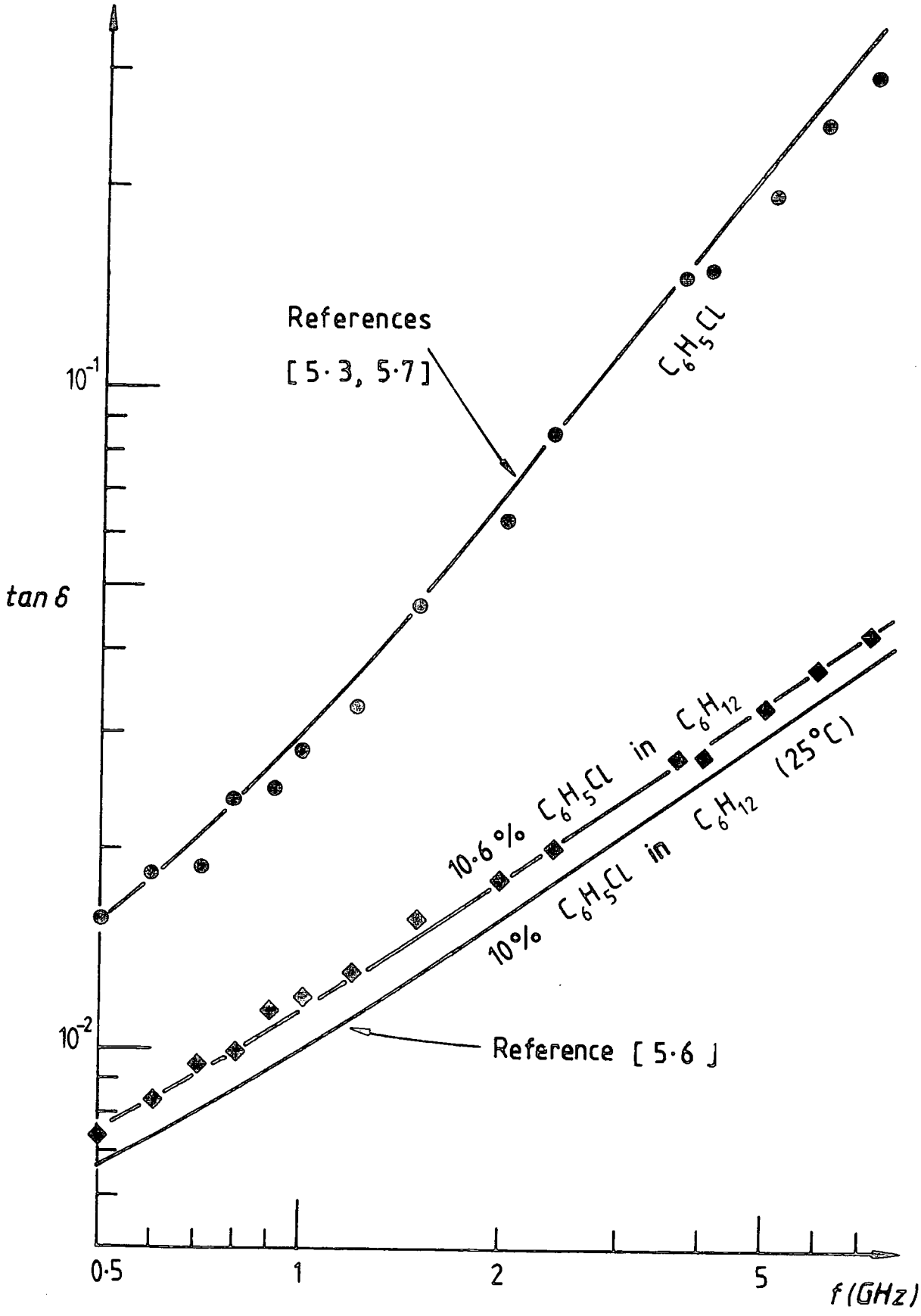

Fig.5·5 Loss tangent of chlorobenzene and its 10·6 molar per cent solution in cyclohexane obtained by the coaxial line resonance method

$20^{o}C$ taken from various sources [see for example, 5.13 - 5.16] . Together with the experimental data in Table 5.3, e quation (5.2) was used to provide the dielectric constant values at the measurement frequencies shown in Table 5.4 below. Values of the VSWR at resonance for samples of

Table 5.4 Dielectric Constant of Pure Water Used For the Loss Tangent Determination ($20^{o}C$)

Frequency f(GHz)	Dielectric constant	Frequency f(GHz)	Dielectric constant
0.8	80.0	2.4	78.5
0.9	79.9	3.7	76.4
1.0	79.8	4.0	75.8
1.2	79.7	5.0	73.7
1.5	79.5	6.0	71.3
1.8	79.2	7.2	68.2
2.0	78.9		

pure water for three different empty sample-holder capacitances are plotted in Fig.5.6 for the frequency range given in Table 5.4. In Table 5.5 the measured loss tangent values are compared with those from the literature. The averaged values of $\tan\delta$ calculated from the measured VSWR values in Fig.5.6 are plotted against frequency in Fig.5.7.

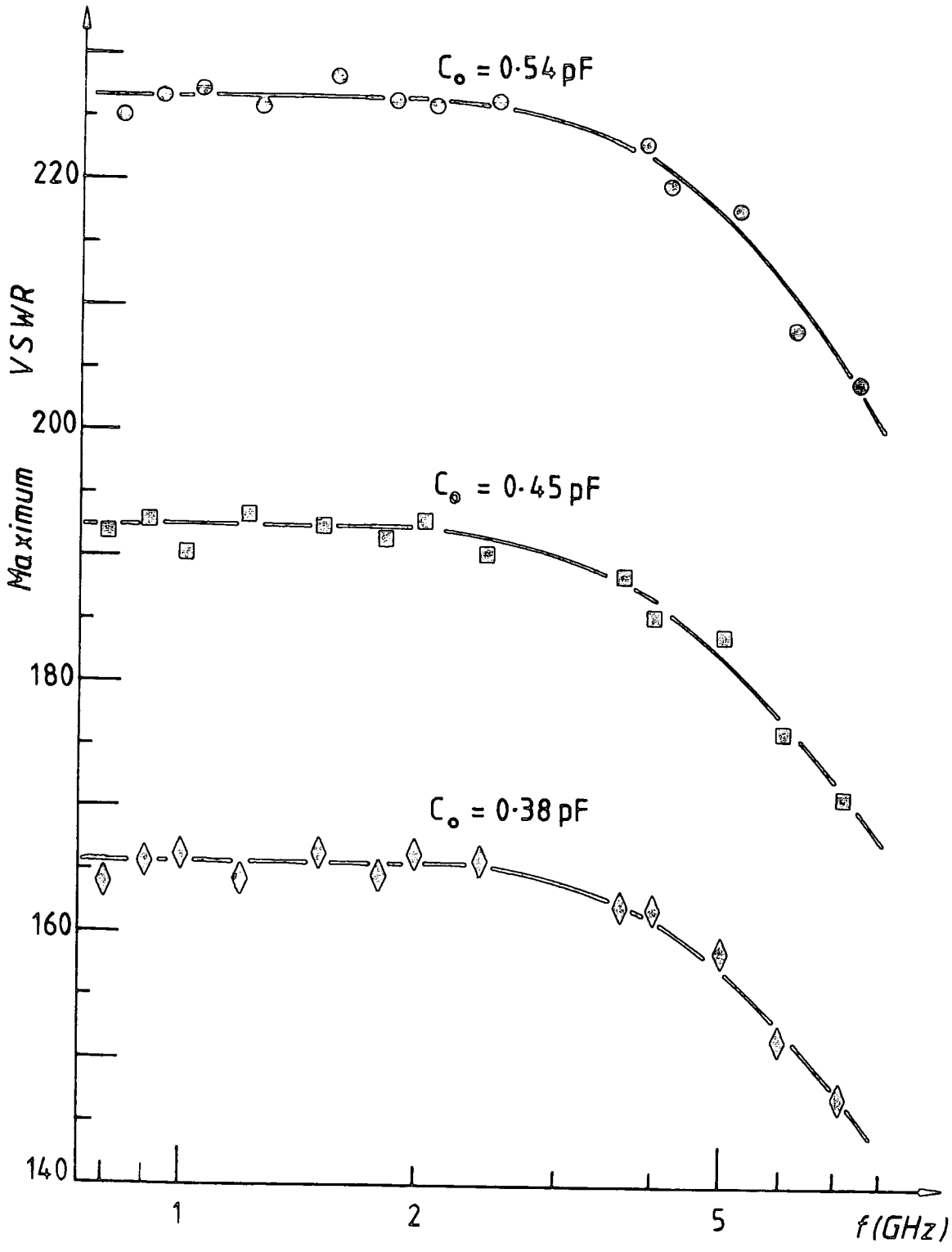

Fig.5·6 Maximum VSWR for various thicknesses of pure water samples in the coaxial line resonance method

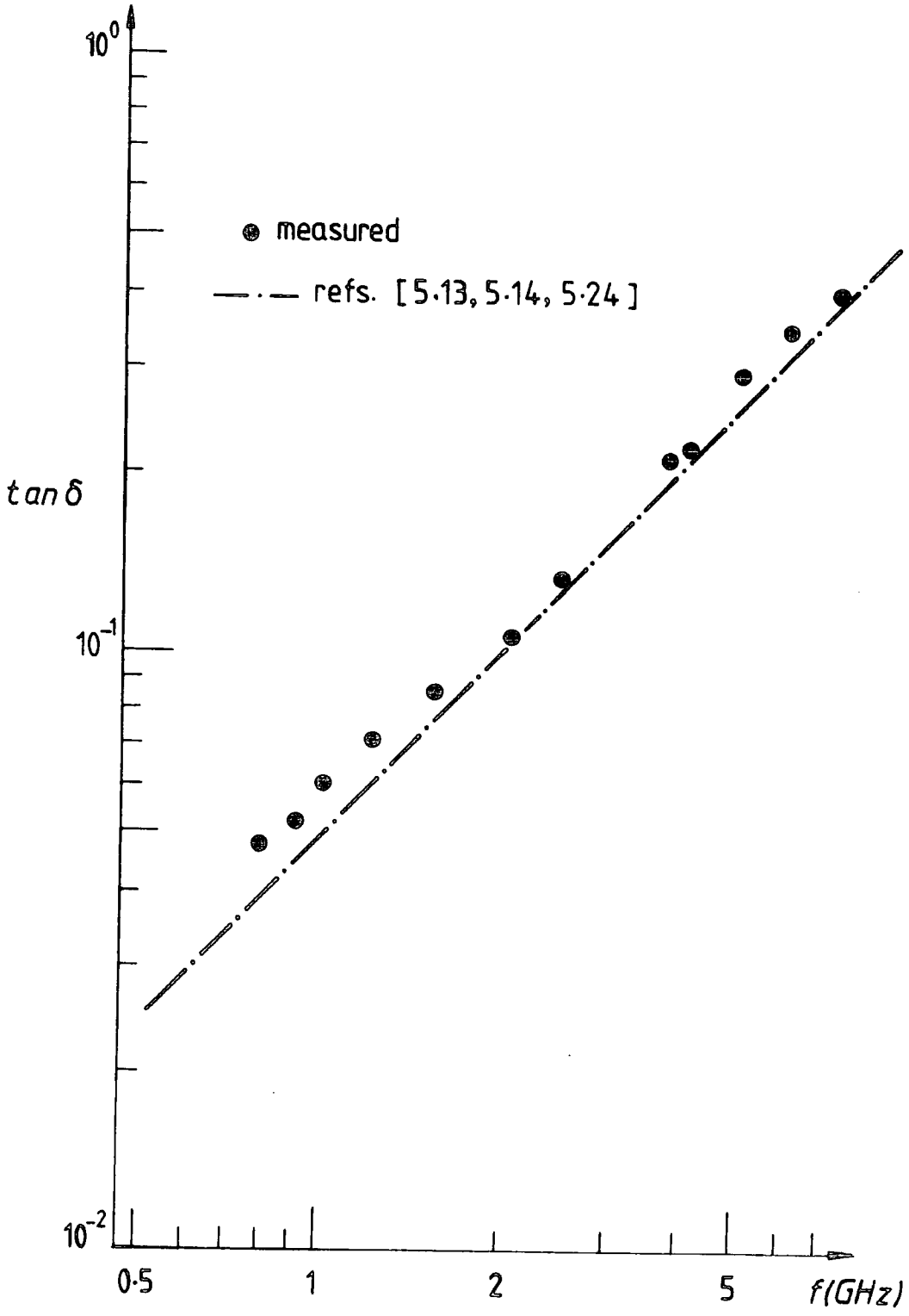

Fig. 5·7 Loss tangent of pure water calculated from the data in Fig. 5·6

Table 5.5 Loss Tangent of Pure Water Determined from the Coaxial Line Resonance Method ($\simeq 20^{o}$)

Coaxial Resonance Method		Literature values		
f (GHz)	tan δ	f(GHz)	tan δ	References
1.0	0.0586	1.0	0.0556	5.18 (20^{o}C)
2.0	0.1154	2.0	0.1040	5.20 (23^{o}C)
3.7	0.2113	3.65	0.2045	5.12 (20^{o}C)
4.0	0.2289	4.0	0.2212	5.18 (20^{o}C)
7.2	0.4031	7.95	0.3810	5.14 (25^{o}C)

5.2.2 SOLID SAMPLES

5.2.2.1 Matched Termination Method

Experimental evaluation of this method for solids was carried out using samples machined from the bulk material. Circular discs of polymethylmethacrylate (PMMA) about 6.5 mm in diameter and of various thicknesses were used. The measurement procedure involved was similar to that for the case of the liquid samples, except that in this case the inner conductor was spring loaded when measurements with the solid samples were being taken. The average values of the dielectric constant and loss tangent from 500 MHz up to 2 GHz are given in Table 5.6 below. These may be compared with the literature values of 2.59 - 2.60 for the dielectric constant and 5.7×10^{-3} - 6.7×10^{-3} for the loss tangent

between 100 MHz and 10 GHz [5.21, 5.22].

Table 5.6 The Dielectric Constant and Loss Tangent of PMMA Measured by the Matched Termination Method

Frequency f (GHz)	Dielectric constant	Loss tangent $\tan\delta \times 10^3$
0.5	2.59	5.67
0.6	2.58	5.21
0.7	2.58	5.26
0.8	2.60	5.48
0.9	2.62	4.94
1.0	2.63	5.87
1.2	2.60	5.58
1.5	2.55	5.08
2.0	2.58	5.64

5.2.2.2 Coaxial Line Resonance Method

The PMMA samples above were also used in the coaxial line resonance method of determining the loss tangent. A typical curve of the variation of the VSWR along the slotted coaxial line when the reactive load was continuously varied, for an empty sample-holder capacitance of 0.32 pF at a frequency of 2 GHz, is illustrated in Fig.5.8. In this instance the maximum value of the VSWR was about 93

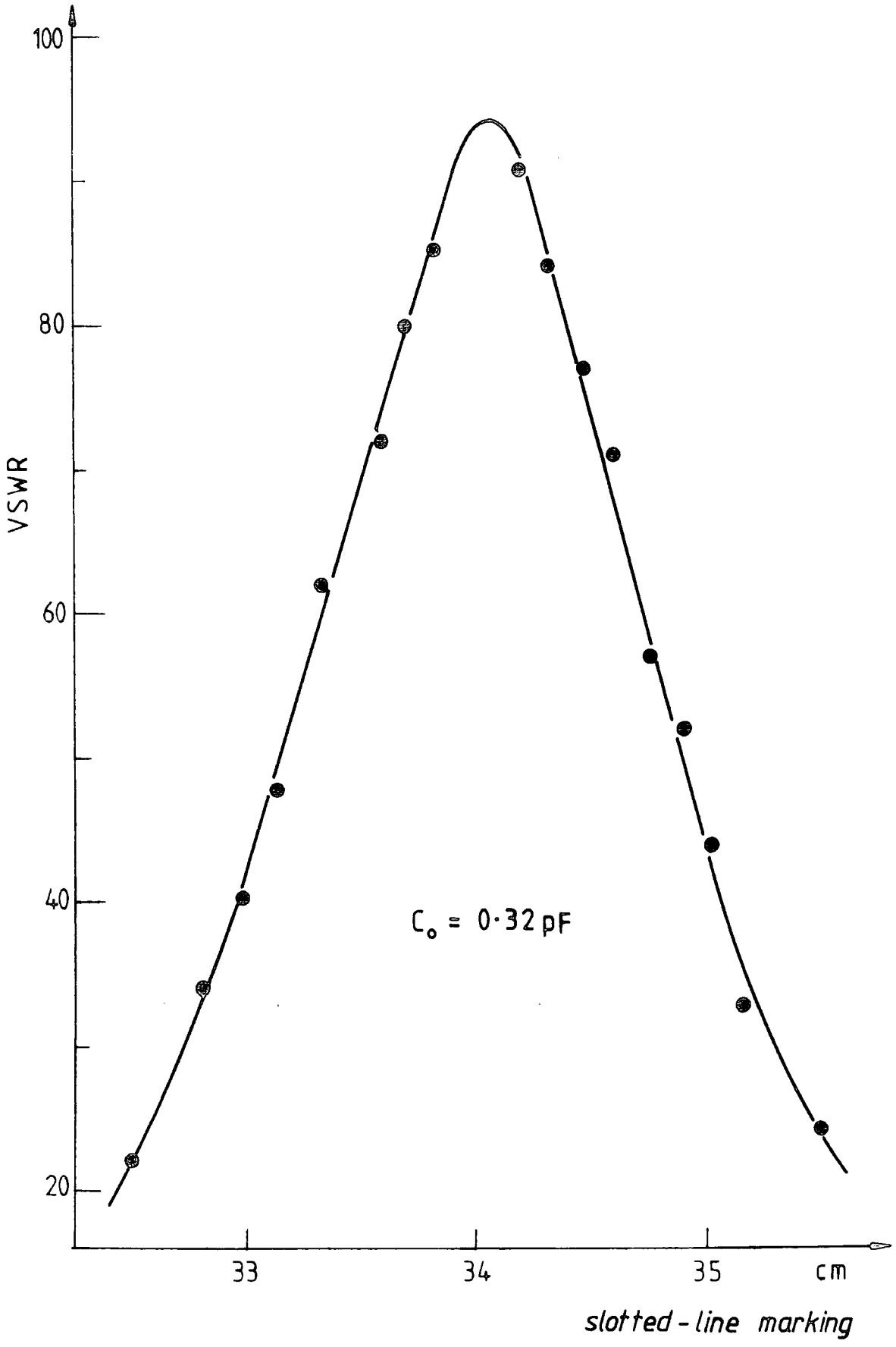

Fig. 5·8 Resonance peak for a PMMA sample at 2 GHz

giving a loss tangent value of 5.73×10^{-3}. Since the high frequency literature values of the loss tangent for PMMA are scarce and far between those from 1 MHz to 138 GHz [5.21 - 5.23] have been plotted out separately. The values determined by this method are then compared with the literature values in the high frequency region, Fig.5.9.

5.3 COMMENTS AND CONCLUSIONS

The matched termination and coaxial resonance methods of measuring the dielectric properties described in chapters 3 and 4 have been applied to known solid and liquid samples. It was found that the first method was applicable to the frequency range from 500 MHz up to about 3 GHz, while the second method could be used up to about 8 GHz. The onset of higher order modes ($\simeq$ 9.3 GHz) for 14-mm coaxial lines [3.10, 3.12] and the validity of lumped circuit element representations when the sample thickness becomes comparable to the wavelength set the upper frequency limit of measurement in the second case. In practice, when there was no material in the sample-holder the VSWR was found to be very high and thus assumed infinite such that the resistance could be taken to be zero in comparison to the situations with chlorobenzene, water and the PMMA samples. Nevertheless, this VSWR was estimated from measurements on different thicknesses of PMMA samples to be of the order of 15000. This has a negligibly small effect on the measured

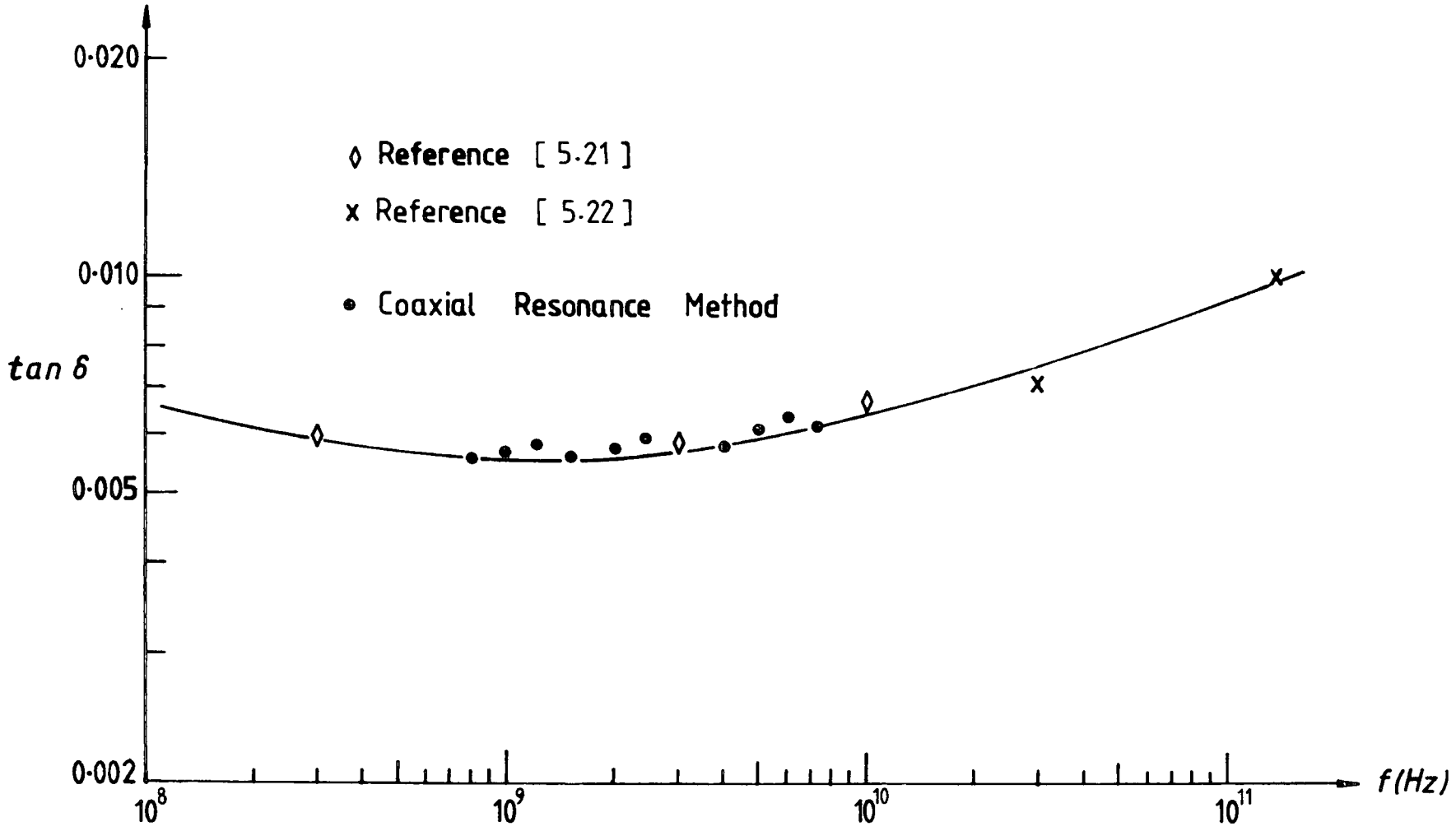

Fig. 5.9 Loss tangent of PMMA measured by the Coaxial Line Resonance Method

values of the loss tangents of the samples and thus may be taken to be infinite in most practical situations. The overall agreement of the measured quantities with those from the literature for the known samples was reasonable; in conclusion it may be said that the two methods proposed provide alternative means of determining the dielectric properties of materials between about 500 MHz and 10 GHz. The overall accuracy obtainable with the coaxial line methods was about 10 % ; this being determined primarily in the matched termination method by difficulties in locating the minima and in the coaxial resonance method by the high value of VSWR.

5.4 REFERENCES

5.1 Weast R.C. (Ed.)," Handbook of Chemistry and Physics ", 57th edn., The Chemical Rubber Co., Ohio (1976/77)

5.2 Kaye G.W.C. and Laby T.H.," Tables of Physical and Chemical Constants ", 14th edn., Longmans, London (1973)

5.3 Maryott A.A. and Smith E.R.," Tables of Dielectric Constants of Pure Liquids ", Nat. Bur. Stand., Washington D.C., NBS Circular No. 514 (1951)

5.4 Lowenheim F.A. and Moran M.K.," Kayes and Clark's Industrial Chemicals ", Wiley Interscience (1975)pp.258, 298

5.5 Sax N.I.," Dangerous Properties of Industrial Chemicals ", 4th edn., Van Nostrand (1975)pp.542, 590

5.6 Bussey H.E.," Dielectric measurements in a shielded open circuit coaxial line ", IEEE Trans. Instrum. Meas., vol.29,20(1980)

5.7 Buckley F. and Maryott A.A.," Tables of Dielectric Dispersion Data for Pure Liquids and Dilute Solutions ", Nat. Bur. Stand., Washington D.C., NBS Circular No. 589 (1958)

5.8 Afsar M.N., Bellemans A., Birch J.R., Chantry G.W., Clarke R.N., Cook J.R., Finsy R., Göttman O., Goulon J., Jones R. G., Kaatze U., Kestemont E., Kilp H., Mandel M., Pottel R., Rivail J-L., Rosenberg C.B. and Van Loon R.," A

comparison of dielectric measurement methods for liquids in the frequency range 1 GHz to 4 THz ", IEEE Trans. Instrum. Meas., vol.29,283(1980)

5.9 Nicol E.A. and Hill N.E.," Dielectric properties of simple liquids at high frequencies ", J. Phys. C, vol.3 no.11,2207(1970)

5.10 Colie C.H., Hastead J.B. and Ritson D.M.," The dielectric properties of water and heavy water ", Proc. Phys. Soc., vol.60,145(1948)

5.11 Grant E.H., Buchanan T.J. and Cook H.F.," Dielectric behaviour of water at microwave frequencies ", J. Chem. Phys., vol.26,1561(1957)

5.12 Harvey A.F.," Microwave Engineering ", Academic Press, New York (1963)p.248

5.13 Bottreau A.M., Moreau J.M., Laurent J.M. and Marzat C., " A method of analyzing the dielectric relaxation spectra of mixtures by decomposition into Debye elementary domains. Application to the study of water spectrum ", J.Chem. Phys., vol.62,360(1975)

5.14 Hastead J.B. in " Water: A Comprehensive Treatise ", Vol. I, Franks F. (Ed.), Plenum Press, New York (1972) Chapt.7

5.15 Pottel R. in " Water: A Comprehensive Treatise ", Vol.II, Franks F. (Ed.), Plenum Press, New York (1973)Chapt.17

5.16 Hastead J.B.," Aqueous Dielectrics ", Chapman and Hall, London (1973)Chapt.2

5.17 Cole R.H. and Cole K.S.," Dispersion and absorption in dielectrics ", J. Chem. Phys., vol.9,341(1941)

5.18 Stuchly M.A. and Stuchly S.S.," Coaxial line reflection methods for measuring the dielectric properties of biological substances at microwave frequencies - a review ", IEEE Trans. Instrum. Meas., vol.29,176(1980)

5.19 Mosig J.R., Besson J.G.E., Gex-Fabry M. and Gardiol F.E., " Reflection of an open ended coaxial line and application to non-destructive measurements of materials ", IEEE Trans. Instrum. Meas., vol.30,146(1980)

5.20 Stuchly M.A., Brady M.M., Stuchly S.S. and Gajda G., " Equivalent circuit of an open-ended coaxial line in a lossy dielectric ", IEEE Trans. Instrum. Meas., vol. 31, 146(1981)

5.21 Von Hippel A.R. (Ed.)," Dielectric Materials and Applications ", M.I.T. Press, Cambridge, Mass. (1954)p.334

5.22 Wunderlich W. ," The physical properties of polymethyl methacrylate ", in "Polymer Handbook ", Brandrup J. and Immergut E.H. (Eds.), 2nd edn., Wiley-Interscience (1975) p. V-55

5.23 Ishida Y.," Relaxation in polymethyl methacrylate ", J. Polym. Sci., Part A-2, vol.7,1835(1969)

5.24 Nightingale N.R.V., Szwarnowski S., Sheppard R.J. and Grant E.H.," A coaxial line cell for measuring the permittivity of medium to high loss liquids in the frequency range 2 to 15 GHz ", J. Phys. E, vol.14,156(1981)

CHAPTER 6

DIELECTRIC THEORY

6.1 DEFINITIONS AND BASIC IDEAS

The application of an electric field to a dielectric material results in the appearance of a net dipole moment per unit volume, known as the polarization P. For simplicity, consider a dielectric material in the form of a parallel-sided slab. The external manifestation of the polarization is the appearance of a charge $q_d = P$ on the surface of the material. Assuming that the field E is produced by the application of a potential difference between two electrodes attached to opposite faces of the slab, the total charge Q at the electrodes is given by

$$Q = q_o + q_d = D \qquad (6.1)$$

where q_o is the charge due to the free space between the electrodes in the absence of the material and the field vector D is defined as the dielectric induction. Most dielectric measurements are concerned essentially with the determination of the charge Q. The dielectric behaviour is described by the time dependence of the charge Q(t) under excitation of a time-varying electric field E(t). For simplicity, first consider a delta function excitation $\delta(t)$ at time $t = 0$. The strength of this delta function is given by the product

of the amplitude of the field E and its duration Δt in the limit $\Delta t \to 0$. The dielectric response function $f(t)$ may be defined as the response of the polarization of the medium to the delta function excitation

$$P(t) = \varepsilon_o E \, \Delta t \, f(t) \tag{6.2}$$

where ε_o is the permittivity of free space. The physical cause of the time dependence of $P(t)$ is the inevitable "inertia" of any material medium that cannot instantaneously follow arbitrary rapid variations of the exciting field. Since there can be no reaction before the cause and since we do not expect any permanent polarization after an infinite time without the external field, the function $f(t)$ has the properties:

$$\begin{aligned} f(t) &= 0 \qquad \text{for} \quad t < 0 \\ f(t) &\to 0 \qquad \text{for} \quad t \to \infty \end{aligned} \tag{6.3}$$

Making the assumption that the system is linear (hence the superposition principle holds), the response to consecutive excitations is the sum of the responses due to individual excitations. Thus the polarization due to a time-varying field $E(t)$ may be written in the form of a convolution integral

$$P(t) = \varepsilon_o \int_0^\infty f(\tau) E(t - \tau) \, d\tau \tag{6.4}$$

If $E(t)$ is now a step function with amplitude E and

$f(t) = 0$ for $t < 0$, then equation (6.4) becomes

$$P(t) = \varepsilon_o E \int_o^t f(\tau)\, d\tau \tag{6.5}$$

By definition, the charge q_o due to the response of free space is instantaneous so that

$$q_o(t) = \varepsilon_o E \tag{6.6}$$

regardless of the form of $E(t)$. The total dielectric induction $D(t)$ is the sum of q_o and $P(t)$. It is evident that the total charge q_d arising from the steady-state polarization of the dielectric material must be recovered in the process of discharge, so that

$$q_d = \varepsilon_o E \int_o^\infty f(t)\, dt \tag{6.7}$$

The basis of dielectric response in the frequency domain is the application of a harmonically variable field $E(t) = \hat{E} \sin \omega t$ at a radian frequency ω. Let the physical quantities $E(t)$, $P(t)$ and $D(t)$ have complex Fourier transforms $\mathcal{E}(\omega)$, $\mathcal{P}(\omega)$ and $\mathcal{D}(\omega)$ respectively. Applying the Fourier transform to equation (6.4) the convolution integral transforms to the simple product of the form

$$\mathcal{P}(\omega) = \varepsilon_o \chi(\omega)\, \mathcal{E}(\omega) \tag{6.8}$$

This shows the simplicity of the response of a linear system

in that every Fourier component of the driving field $\mathcal{E}(\omega)$ causes its own response of the polarization component $\mathcal{P}(\omega)$ through the transfer function $\chi(\omega)$, which is referred to as the dielectric susceptibility

$$\chi(\omega) = \chi'(\omega) - j\chi''(\omega) \tag{6.9}$$

The real and imaginary components of $\chi(\omega)$ are respectively the cosine and sine Fourier transforms of $f(t)$, where

$$\chi(\omega) = \int_0^\infty f(t) \exp(-j\omega t)\, dt \tag{6.10}$$

The imaginary component $\chi''(\omega)$ is the dielectric loss since the electric current due to this component is in phase with the driving field while the real part $\chi'(\omega)$ defines the energy of polarization stored in the material. The susceptibility function $\chi(\omega)$ defines the dielectric response of the material medium between the electrodes and the total response of the system is given by the sum of this and the free space contribution, thus from equations (6.1), (6.6) and (6.8)

$$\mathcal{D}(\omega) = \varepsilon_o \left[1 + \chi(\omega) \right] \mathcal{E}(\omega) \tag{6.11}$$

The ratio $\mathcal{D}(\omega)/\mathcal{E}(\omega)$ is defined as the dielectric permittivity so that

$$\mathcal{D}(\omega) = \varepsilon(\omega)\mathcal{E}(\omega) = \varepsilon_o \varepsilon_r(\omega)\mathcal{E}(\omega) \tag{6.12}$$

where $\varepsilon_r(\omega)$ is known as the relative dielectric permittivity or dielectric constant. For brevity, the term 'relative' is often omitted and the relative complex permittivity is henceforth simply referred to as the complex permittivity. The unity in brackets in equation (6.11) represents the free space contribution and is purely real. The entire loss comes from the material medium and we may write for the real and imaginary components of the complex permittivity

$$\varepsilon'(\omega) = 1 + \chi'(\omega), \qquad \varepsilon''(\omega) = \chi''(\omega) \tag{6.13}$$

The transforms may be inverted to give

$$\begin{aligned} f(t) &= \frac{2}{\pi}\int_0^\infty \chi'(\omega)\cos\omega t\, dt \\ &= \frac{2}{\pi}\int_0^\infty \chi''(\omega)\sin\omega t\, dt \end{aligned} \tag{6.14}$$

Recalling the properties of Fourier transforms, we note from equation (6.9) that $\chi'(\omega)$ is an even function; the static value is obtained by setting $\omega = 0$ in equation (6.10)

$$\chi(0) = \int_0^\infty f(t)\, dt \tag{6.15}$$

which corresponds directly to equation (6.7). Similarly, $\chi''(\omega)$ is an odd function of ω and has a series expansion of the form

$$\chi''(\omega) = \sigma_0/\omega + a\omega + [\text{higher odd powers}] \tag{6.16}$$

where the first term on the right-hand side (that gives a singularity at the origin) arises from a finite value of the d.c. conductivity, necessarily present in measurements, and does not belong to the actual dielectric response.

Equations (6.9) and (6.14) show that $\chi'(\omega)$ and $\chi''(\omega)$ are interrelated and may be expressed as Hilbert transforms and known as the Kramers-Kronig relations:

$$\chi'(\omega) = \frac{2}{\pi}\int_0^\infty \frac{s\chi''(s)}{s^2 - \omega^2}\, ds$$
$$\chi''(\omega) = \frac{-2}{\pi}\int_0^\infty \frac{\omega\chi'(s)}{s^2 - \omega^2}\, ds \qquad (6.17)$$

Since $\varepsilon(\omega)$ is related to $\chi(\omega)$ through equation (6.13) and that the Hilbert transform of a constant is zero, the integral relations in equations(6.17) are also true for $\varepsilon(\omega)$.

6.2 MECHANISMS OF POLARIZATION

An atom comprises a positively charged inner core surrounded by electron clouds having symmetries determined by their quantum states. On application of an electric field, the electron clouds are displaced slightly with respect to the positive cores, causing atoms to take up an induced dipole moment. This phenomenon is termed electronic polarization.

Consider next a diatomic molecule made of atoms X

and Y. The interaction between the constituent atoms results in a redistribution of the electrons which would generally be axially symmetrical along XY. One would expect the diatomic molecule to possess a dipole moment in the direction XY, except where X and Y are identical, when the dipole moment should vanish for reasons of symmetry. Molecules of this kind are true dipoles and termed as polar; a typical example being hydrochloric acid in which there is a displacement of the charge in the bonding between the H and Cl atoms. Under the influence of an applied field the polarization of a polar material can change in two ways. Firstly, the field may cause the atoms to be displaced resulting in a change in the dipole moment, this may be called atomic polarization. Secondly, the whole molecule may rotate and try and align itself with the field. This is referred to as orientational polarization.

In real crystals there exist a large number of defects such as lattice vacancies, impurity centres, dislocations, etc. Free charge carriers migrating through the crystal, under the influence of an applied field, may be trapped or pile up against a defect. This results in a localized accumulation of charge which will induce its image charge on an electrode and gives rise to a dipole moment. This constitute a separate polarization mechanism known as interfacial polarization.

In an ionic or partially ionic solid, under the influence of an external field, the positive and negative ions are displaced from their equilibrium positions. This gives rise to ionic polarization.

There may exist several polarization mechanisms in any particular material, each characterized by its own frequency dependence. The dielectric response of the material is obtained by summing the individual contributions, thus

$$\varepsilon(\omega) = \varepsilon_o \left\{ 1 + \sum_k \left[\chi'_k(\omega) - j\chi''_k(\omega) \right] \right\} \qquad (6.18)$$

The losses due to some of the mechanisms become insignificant in certain frequency ranges below the respective loss peaks, so that the particular $\chi(0)$ values may be added to ε_o to give an effective high-frequency permittivity ε_∞, hence

$$\varepsilon(\omega) = \varepsilon_\infty + \varepsilon_o \sum_{k \geq k_1} \left[\chi'_k(\omega) - j\chi''_k(\omega) \right] \qquad (6.19)$$

where k_1 is now the first mechanism with a non-vanishing loss in the frequency range under consideration. This is schematically illustrated in Fig.6.1 for a hypothetical material having three non-overlapping polarization mechanisms. For most purposes the electronic polarization is so rapid, $\sim 10^{-15}$sec, that it may be regarded as instantaneous. The same may be said of ionic polarization, with response times of the order 10^{-13}sec. Both mechanisms can thus be said to

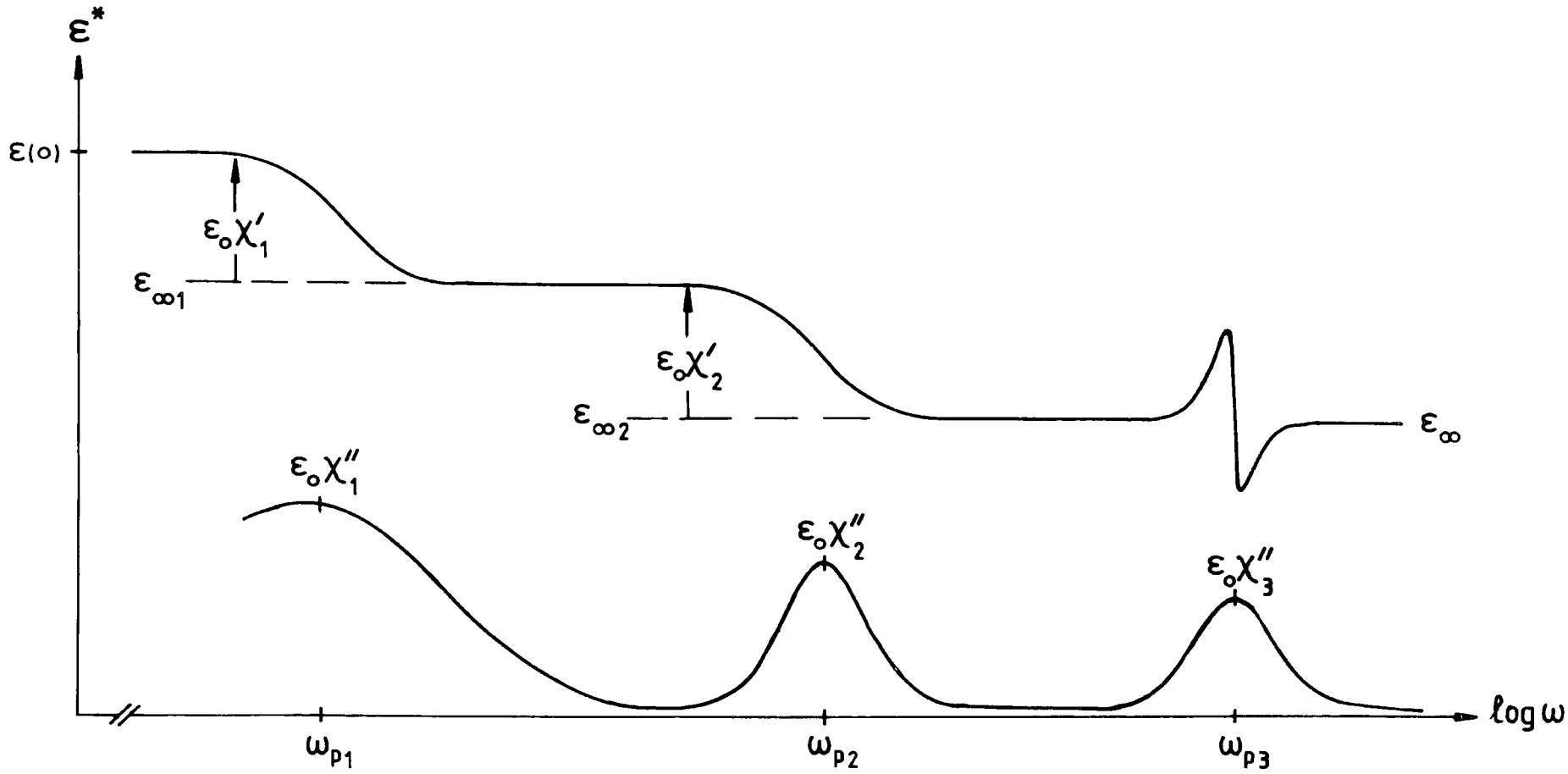

Fig. 6·1 The frequency dependence of the dielectric permittivity $\varepsilon'(\omega)$ and the corresponding losses for three non-overlapping polarisation mechanisms

simply contribute to ε_∞.

6.3 EMPIRICAL CHARACTERIZATION OF DIELECTRIC RESPONSE

The study of dielectric response of materials is simplified if the various polarization mechanisms are sufficiently well separated in frequency so that they do not overlap, which is often found in practice. The dielectric behaviour in particular regions of the frequency spectrum is then best represented in terms of the dielectric susceptibility

$$\chi(\omega) = \chi'(\omega) - j\chi''(\omega) = \varepsilon(\omega) - \varepsilon_\infty \qquad (6.20)$$

The frequency dependence is the most fundamental manner of presenting the dielectric response and in this respect the imaginary component $\varepsilon''(\omega)$ is the more sensitive indicator, being an odd function of frequency and shows more features than the even function $\varepsilon'(\omega)$. Since we are dealing with the frequency dependence of a complex parameter, there are several ways of representing the experimental information, e.g. by the $\chi'' - \chi'$ plot and the linear plots of $\chi'(\omega)$ and $\chi''(\omega)$ against $\log \omega$. These representations are very useful for the study of the neighbourhood of loss peaks which are emphasised in these graphs, but the details of the response away from the loss peaks are lost to a large extent.

The conventional starting point in the approach

to the dielectric response in materials is through the classical Debye model [6.1] described by the expression

$$\chi(\omega) = \frac{A}{1 + j\omega\tau} \qquad (6.21)$$

where A is a constant and τ the relaxation time. The dielectric loss $\chi''(\omega)$ represents a symmetric peak at $\omega_p = 1/\tau$ with a width at half-height of $\lambda_D = 1.144$ decades, Fig.6.2. Although a response of the Debye type may be an acceptable approximation to the behaviour of some liquids and solutions of simple polar molecules [6.2] , the overwhelming majority of materials, particularly solids, do not follow such a response [6.3, 6.4].

Attempts to explain departures from the Debye model take many forms. From a very early stage distributions of relaxation times (DRT's) have been proposed, when one alone is inadequate [6.2, 6.3]. Amongst the principal empirical relations suggested are the Cole-Cole circular function with depressed centres [6.5] , the skewed-arc function of Cole-Davidson [6.6] , the Fuoss-Kirkwood function [6.7] , the Havriliak-Negami equation [6.8, 6.9] and the William-Watts dipole correlation function [6.10] . These equations will not be detailed here as they have already been discussed in detail elsewhere [e.g. 6.2 - 6.4]. The manner of presenting of dielectric data reflects, consciously or otherwise, certain assumptions about the expected model

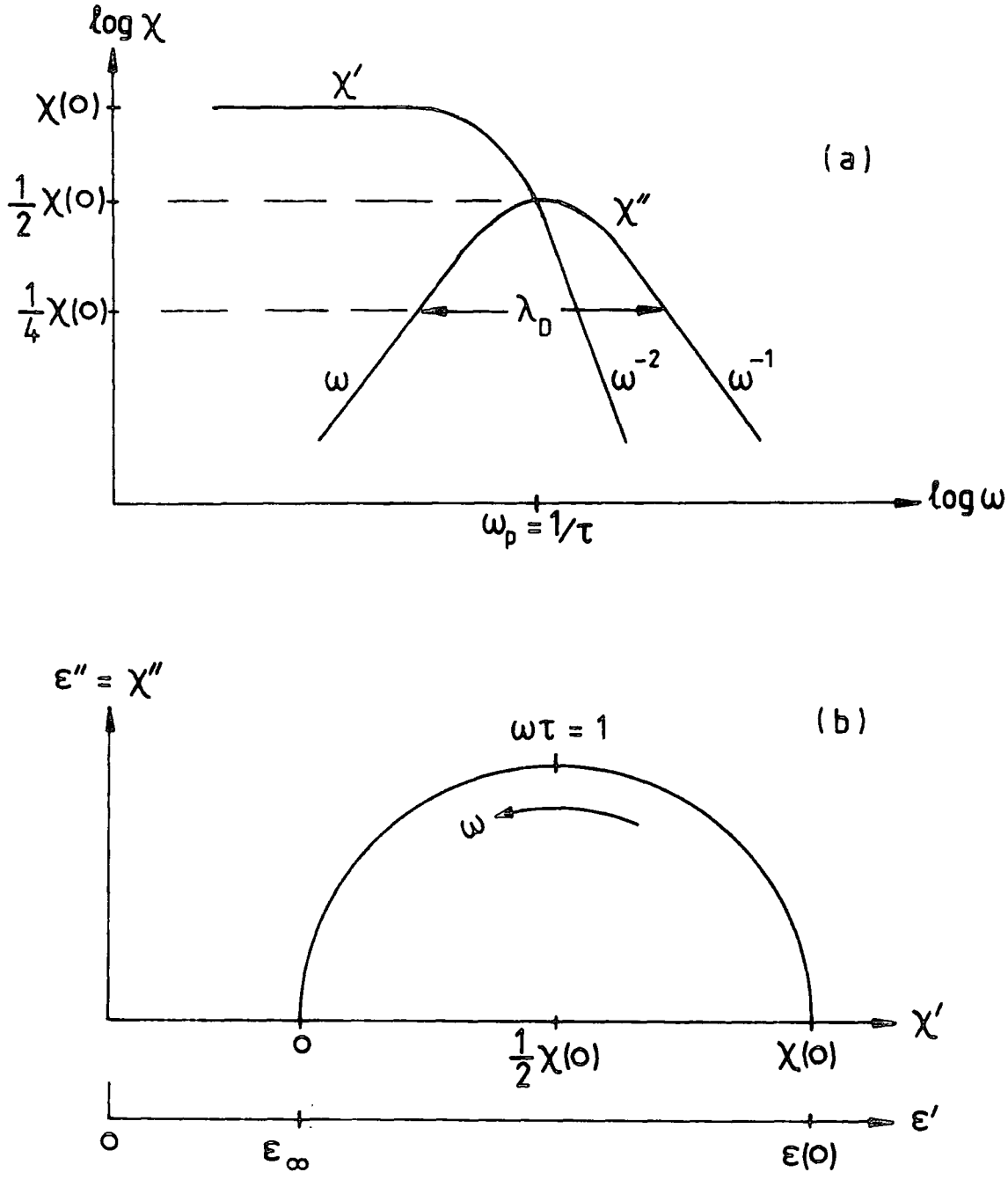

Fig. 6·2 (a) The frequency dependence of the real and imaginary components of the complex susceptibility for an ideal Debye response.

The $\chi'' - \chi'$ plot in (b) shows the relationship with the complex permittivity ε.

which is to be used in their interpretation. It often appears that the original assumptions made about a particular model are subsequently forgotten and that the same presentation is later applied to systems which do not obey the original model [6.12] thereby "force-fitting" the experimental results with the model. The choice of the model thus seems arbitrary. Recently Jonscher [6.13] and Hill [6.14] noted that an overwhelming majority of experimental evidence, when presented in the form of a $\log\chi''$ - $\log\chi'$ plot, can be approximated by the expression

$$\chi''(\omega) \propto \frac{1}{(\omega\tau)^{-m} + (\omega\tau)^{1-n}} \qquad (6.22)$$

with the parameters m and n in the range 0 and 1; while the real part of the susceptibility follows the relations

$$\chi'(\omega) \propto \omega^{n-1} \quad \text{for} \quad \omega \gg \omega_p$$

$$\chi'(\omega) = \text{constant} \quad \text{for} \quad \omega \ll \omega_p \qquad (6.23)$$

ω_p is the frequency at which the loss peak occurs. Hill [6.15] has collected one hundred sets of data on polar solids and liquids and showed that the exponents m and n are uncorrelated and concluded that they must therefore represent independent physical mechanisms. The above expression for the loss may be regarded as a generalization of the Fuoss-Kirkwood equation to which it reduces for $m = 1 - n = \alpha$.

For m different from 1 - n it yields an asymmetric loss peak with limiting power law dependences as $(\omega/\omega_p)^{-(1-n)}$ for $\omega \gg \omega_p$ and $(\omega/\omega_p)^m$ for $\omega \ll \omega_p$; thereby resembling the other empirical equations as special cases. Jonscher has described the pattern of behaviour in Hill's examples and many others [e.g. 6.4, 6.11] as the "universal law of dielectric response" and concluded that it was necessary to seek a universal framework within which all these materials would find a common interpretation.

6.4 THE UNIVERSAL DIELECTRIC RESPONSE

A wide-ranging study of dielectric behaviour of various materials by Jonscher and co-workers [6.4, 6.11 - 6.17] has led to a formulation of a general classification of all known types of dielectric response in the wide frequency range below the quantum regimes. This is shown schematically in Fig.6.3 which gives the $\log \chi'(\omega)$ and $\log \chi''(\omega)$ against $\log \omega$ plots and the complex $\chi''(\omega) - \chi'(\omega)$ plots. On the right is the ideal Debye response, which is hardly seen in solids. Moving to the left, we go through a range of increasingly 'non-Debye' types of responses with increasing widths of the loss peaks. The near-Debye response peaks found in many ferroelectrics at gigahertz frequencies are approximated by the Cole-Cole equation; the symmetric peaks may also be represented by the Fuoss-Kirkwood equation. Next, the asymmetric peaks with the accepted Cole-Davidson and

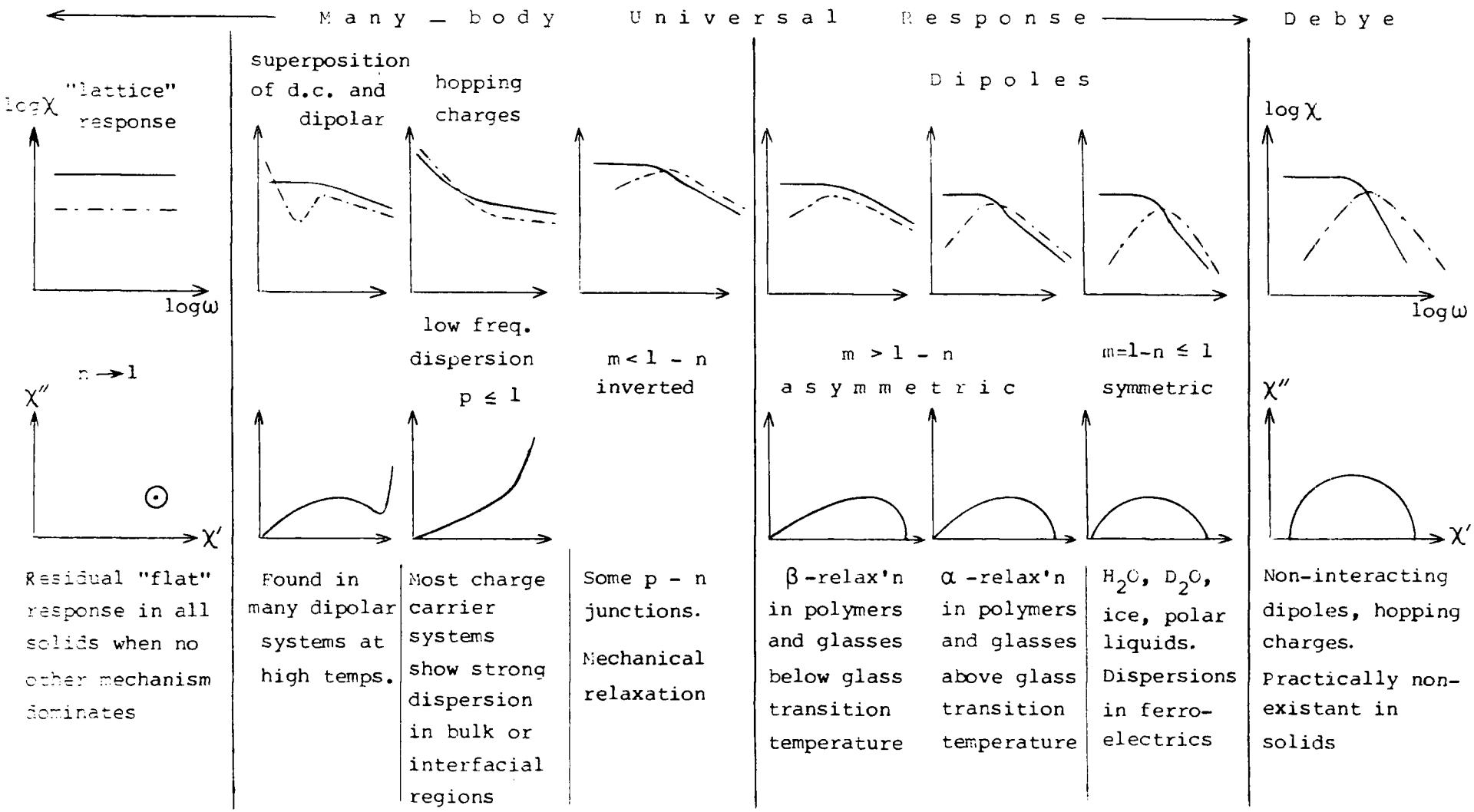

Fig 6.3 A general classification of all observed types of dielectric response in the entire range of solids. The upper diagrams represent the $\log\chi - \log\omega$ curves while the lower ones represent the $\chi'' - \chi'$ plots. (After reference [6.11]).

William-Watts formalisms, and further still towards the left in which the polarization is dominated by hopping electronic or ionic charge carriers with the absence of loss peaks. This is followed by a region of strong low-frequency dispersion obeying the Kramers-Kronig relations; then finally on the extreme left is the limiting case of flat frequency and temperature independent loss, ($n \rightarrow 1$).

The high-frequency limit of both the Cole-Cole and Cole-Davidson expressions,

$$\chi(\omega) = \frac{\chi(0)}{1 + (j\omega\tau)^{1-\alpha}} \tag{6.24}$$

and

$$\chi(\omega) = \frac{\chi(0)}{(1 + j\omega\tau)^{1-\alpha}} \tag{6.25}$$

respectively, of the form

$$\chi(\omega) \propto (j\omega)^{n-1} = \left[\sin\left(\frac{n\pi}{2}\right) - j\cos\left(\frac{n\pi}{2}\right)\right]\omega^{n-1} \tag{6.26}$$

is referred to as the universal law of dielectric response. The characteristic feature of this law of frequency dependence is the fact that the real and imaginary components of the complex susceptibility are the same functions of frequency so that their ratio is frequency independent

$$\chi''(\omega)/\chi'(\omega) = \frac{\varepsilon''(\omega)}{\varepsilon'(\omega) - \varepsilon_\infty} = \cot\left(\frac{n\pi}{2}\right) \tag{6.27}$$

This is consistent with the fact that the high-frequency branch of the complex χ plot is a straight line and is also a consequence of the Kramers-Kronig relations - the "universal" function ω^{n-1} has the unique property that it remains invariant, except for a constant, under the Hilbert transformation [6.4]. The constancy of this ratio is in stark contrast with the Debye response, for which it is equal to $\omega\tau$. Equation (6.26) has the physical significance that the ratio of the energy lost per radian to the energy stored in the system at the peak of the polarization is independent of frequency:

$$\frac{\chi''(\omega)}{\chi'(\omega)} = \frac{\text{energy lost per radian}}{\text{energy stored}} = \cot\left(\frac{n\pi}{2}\right) \qquad (6.28)$$

6.5 REFERENCES

6.1 Debye P.," Polar Molecules ", Dover Reprints, N.Y. (1945)

6.2 Cole R.H.," Molecular correlation function approaches to dielectric relaxation ", in " Physics of Dielectric Solids ", Inst. Phys. Conf. Ser. No. 58 (Canterbury, U.K.), (1980)

6.3 Bottcher C.J.F. and Bordewijk P.," Theory of Electric Polarization ", Vol.II, (Elsevier, Amsterdam), (1978)

6.4 Jonscher A.K.,"The universal dielectric response: A review of data and their new interpretation ", Phys. Thin Films, Vol.II,205(1980)

6.5 Cole K.S. and Cole R.H.," Dispersion and absorption in dielectrics ", J. Chem. Phys., vol.9.341(1941)

6.6 Davidson D.W. and Cole R.H.," Dielectric relaxation in glycerine ", J. Chem. Phys., vol.18,1417(1950)

6.7 Fuoss R.M. and Kirkwood J.G.," Electrical properties of solids VIII. Dipole moments in polyvinyl chloride - diphenyl systems ", J. Am. Chem. Soc., vol.63,385(1941)

6.8 Havriliak S. and Negami S.," A complex plane analysis of - dispersions in some polymer systems ", J. Polym. Sci. C, vol.14,99(1965)

6.9 Havriliak S. and Negami S.," A complex plane representation of dielectric and mechanical relaxation

processes in some polymers ", Polymer, vol.8,161(1967)

6.10 Williams G and Watts D.C.," Non-symmetrical dielectric relaxation behaviour arising from a single empirical decay function ", Trans. Faraday Soc., vol.66,80(1970)

6.11 Jonscher A.K.," Review: A new understanding of the dielectric relaxation of solids ", J. Mat. Sci., vol. 16,2037(1981)

6.12 Jonscher A.K.," Presentation and interpretation of dielectric data ", Thin Solid Films, vol.50,187(1978)

6.13 Jonscher A.K.," New model of dielectric loss in polymers ", Colloid Polym. Sci., vol253,231(1975)

6.14 Hill R.M.," Characterization of dielectric loss in solids and liquids ", Nature, vol.275,96(1978)

6.15 Hill R.M.," Characterization of dielectric materials ", J. Mat. Sci., vol.16,118(1981)

6.16 Dissado L.A. and Hill R.M.," Nonexponential decay in dielectrics and dynamics of correlated systems ", Nature, vol.279,685(1979)

6.17 Dissado L.A. and Hill R.M.," Dielectric behaviour of materials undergoing dipole alignment transitions ", Phil. Mag. B, vol.41,625(1980)

CHAPTER 7

DIELECTRIC PROPERTIES OF SILICON NITRIDE CERAMICS

7.1 INTRODUCTION

Increasing interest has been shown in silicon nitride (Si_3N_4) since its technological potentials have been identified. Much effort has been made to investigate its preparation, characterization and properties. Thin film silicon nitride has been extensively described in the literature; the Handbook of Electronic Materials edited by Milek [7.1] and a recent review by Morosanu [7.2] indicate the scope of research in this area. Deposits of Si_3N_4 films are now widely used in the semiconductor and integrated circuit technology [e.g. 7.3 - 7.5] . In bulk form silicon nitride has been identified as a useful refractory ceramic with a combination of properties found in very few others [7.6 - 7.8] It possesses a high specific modulus, a high decomposition temperature, high temperature strength, low coefficient of friction, good oxidation resistance and is highly resistant to corrosive environments. Hence it has been a leading contender for a wide range of high temperature engineering applications such as in gas turbines, flame cans and high temperature gas bearings.

7.1.1 SILICON NITRIDE STRUCTURE

Earlier studies on the crystallography of silicon

nitride were carried out by Hardie and Jack [7.9] , Forgeng and Decker [7.10] , and Huddlesdon and Popper [7.11] using powder and single crystal samples. Silicon nitride is known to exist in two structural phases (α and β) both of which are built up of Si_3N_4 tetrahedra; they both have the hexagonal structure although with slightly different lattice dimensions. The atomic arrangement of β - Si_3N_4 is the same as that of phenacite, Be_2SiO_4 [7.9] , whereas α- Si_3N_4 demonstrates an alternative way of joining Si_3N_4 tetrahedra and gives approximately twice the cell volume of β - Si_3N_4 (Table 7.1; Fig.7.1). From crystallographic studies and C - V measurements it has been reported [7.12] that in view of the two hexagonal forms it is relatively easy to change the α to the β phase; the application of a high electric field may be sufficient. It is also said that at room temperature the two phases may co-inhabit the same crystal.

Table 7.1 The Crystal Structure of Silicon Nitride [7.9 - 7.11]

Phases	alpha	beta
Crystal System	hexagonal	hexagonal
Space Group	Pb 31c	Pb 3/m
Lattice Parameters	a = 7.748 Å b = 5.617 Å	a = 7.608 Å b = 2.911 Å

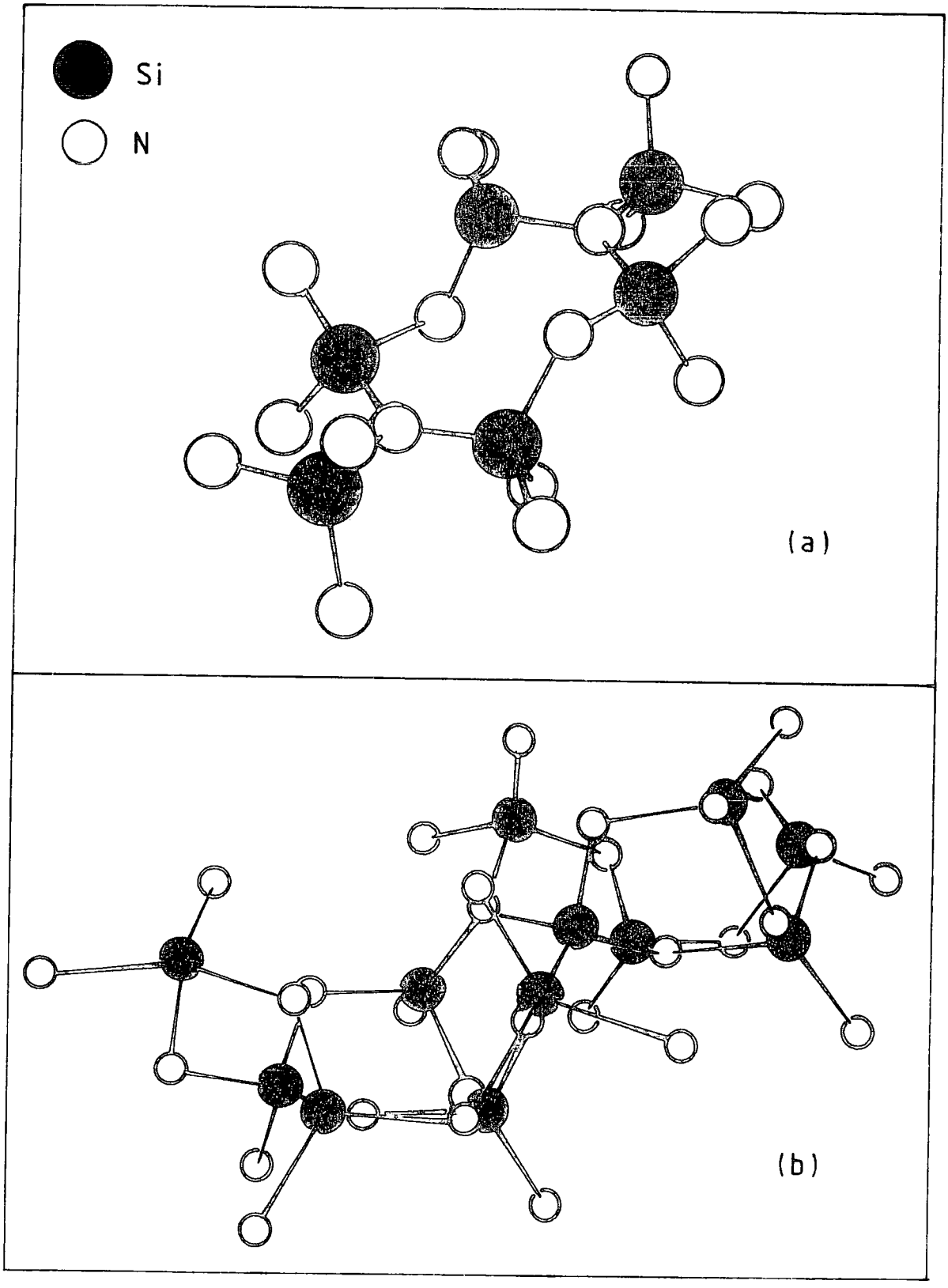

Fig. 7.1 The crystal structure of:

(a) β - silicon nitride, Si_6N_8

(b) α - silicon nitride, $Si_{12}N_{16}$

Recently there has been a discussion [7.13] on the electronic structure of Si_3N_4 based on calculations within the framework of a linear combination of atomic orbitals (LCAO). Each Si atom is thought of as covalently bonded to four N atoms in a tetrahedral arrangement and in turn each N atom is bonded to three Si atoms, with a Si - N - Si bond angle of $\simeq 120^{o}$. On this basis, with a central N atom, a bonding unit composed of nitrogen 2s and 2p states along with three silicon sp^3 hybrids directed towards the N atom is considered; the nitrogen 1s and silicon 1s, 2s and 2p states being taken as core states. These considerations result in a primitive cell consisting of four bonding units, Fig.7.2.

7.1.2 MANUFACTURE OF SILICON NITRIDE CERAMICS

Two main ways of manufacturing silicon nitrides are now used: hot-pressing and reaction-bonding - hence the identification HPSN and RBSN for Hot-pressed and Reaction-bonded Si_3N_4 respectively. The term reaction-bonded has been preferred to reaction-sintered by Moulson [7.14] since the word "sinter" usually implies densification by solid-state diffusion processes which are not significant in the formation of RBSN. HPSN is manufactured from commercial silicon powder which is nitrided directly to give α - Si_3N_4 powder. This is then hot-pressed at $1700^{o}C$ in air at a pressure between 150 MNm^{-2} and 300 MNm^{-2} to give a maximum density

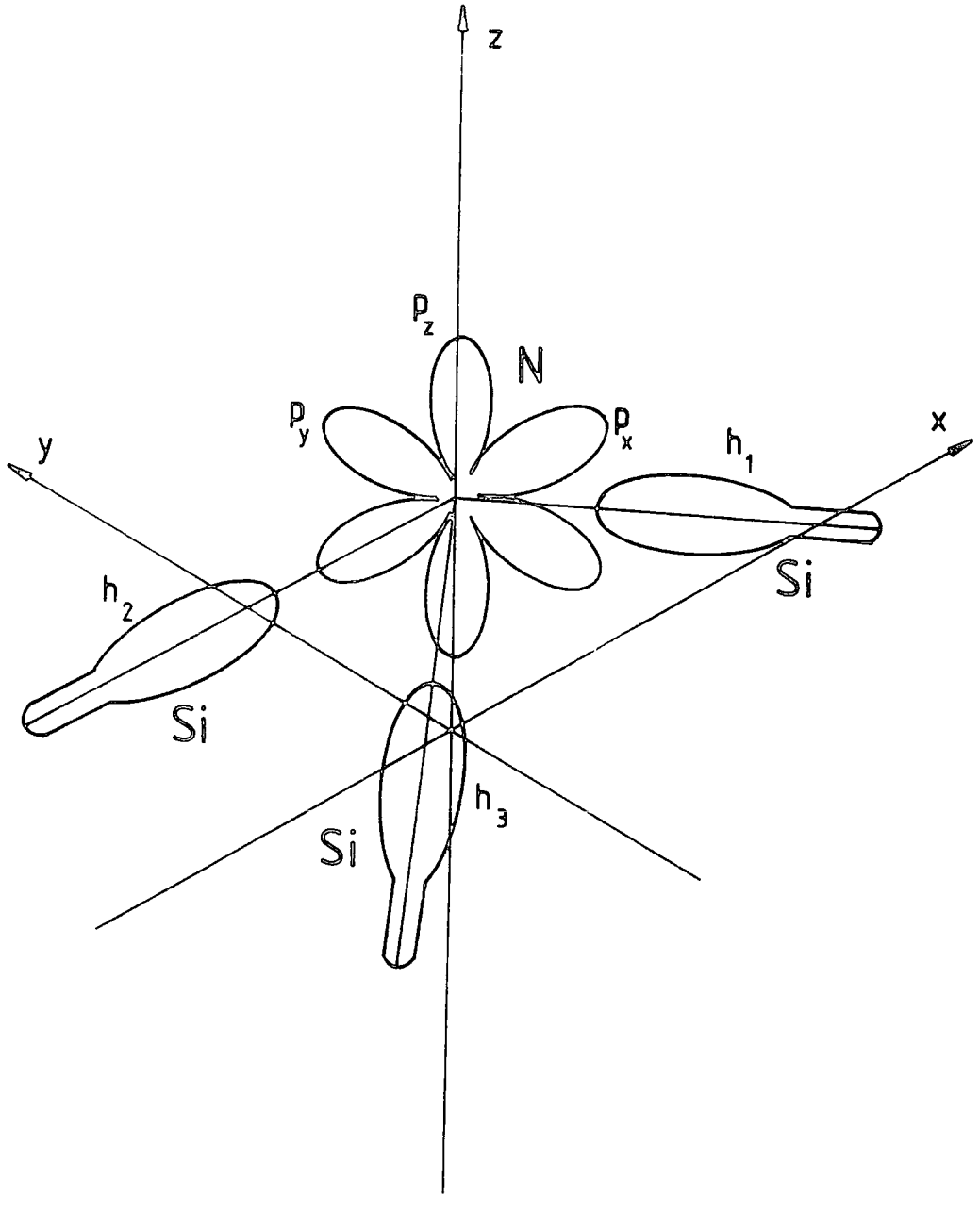

Fig. 7·2 The electronic structure of Silicon Nitride, centred on the nitrogen atom.
(After [7·13])

pore-free $\beta - Si_3N_4$. There is, however, one main disadvantage of this fabrication technique in that it is not possible to hot-press complex shapes. Hence the finishing process is expensive.

The starting material for RBSN is again commercial silicon powder. Initially a silicon powder compact is produced, either as a billet or in the shape of the component being fabricated, by isostatic pressing at up to 200 MNm^{-2} in an argon atmosphere. After shaping the component is heated in nitrogen to between $1250^{o}C$ and $1450^{o}C$ when reaction-bonding occurs. The silicon powder compact might also be formed directly into the component shape by slip-casting, extrusion, injection moulding, die-pressing or flame-spraying. A very attractive feature of this fabrication route is that very little size change is observed during densification and close tolerances (approximately 1%) on the dimensions of a finished component can be readily achieved thereby avoiding expensive machining after firing. However, since Si_3N_4 is covalently bonded it has a low self-diffusivity, hence the desired density cannot be achieved by this method due to the presence of pores. Typically RBSN has a porosity of about 20 - 25 % with roughly four-fifths of the pores less than 0.1 μm in size [7.15] ; this consequently leads to a slight degradation of its oxidation resistance, high temperature strength and resistance to corrosive environments since porosity leads to a higher

effective surface area.

7.1.3 RBSN SAMPLES STUDIED

7.1.3.1 Weight Gain and Impurities

The silicon nitride ceramics studied in the present work were supplied by AME Ltd. (Gateshead) and details of their fabrication are described in a thesis by Bushell [7.16] . These materials were in various degrees of nitridation; to assess this degree of nitridation they are referred to by the "weight gain" of the ceramic, which is the percentage by which the weight of the green ceramic has increased in the reaction. If one assumes that all available silicon is converted to silicon nitride then the maximum weight gain would theoretically be 66.5 % . However, in practice the maximum weight gain that could be achieved was slightly less (63.2 %). There is thus a small amount of unreacted free silicon, due to the inability of nitrogen to reach the remaining silicon as the reaction progresses.

Table 7.2 lists the impurities in the starting material, these being typical of commercially available silicon powders [7.14] . Iron is a major impurity, which usually results from the steel ball mill grinding of the silicon powder. Recently Boyer and Moulson [7.17] and Moulson [7.14] have proposed mechanisms for the formation of RBSN taking into account the effects of Fe as the major

Table 7.2 Impurities in Silicon Powder Used for Manufacturing PBSN Samples

Impurity	Weight Percent of Impurities	
	AME Powder	Commercial Powder
Fe	0.45	0.90
Al	0.25	0.20
Ca	0.052	0.30
Ti	-	0.10
O	-	1.0 (native oxide)
Particle Size	Standard Micronized 90 % < 30 μm	15 μm (mean)

impurity in the starting powder - as was the case with the AME materials used in this study.

The proposed mechanisms are :

(a) the volatization of Si (melting point 1410°C) and its subsequent vapour phase reaction with N_2, a CVD process leading to the formation of α - Si_3N_4 ;

(b) solution of N_2 in alloys which are liquid at the reaction temperature resulting in the formation of β - Si_3N_4.

7.1.3.2 Composition of Samples

The materials studied were manufactured by varying

the firing schedules in the development furnace at AME. These firing cycles and nitrogen partial pressure profiles have been fully described in Bushell's thesis [7.16] . Table 7.3 lists the compositions of the silicon nitrides with an indication of the peak firing temperatures and nitrided densities. It was not possible to produce systematic weight gain intervals over the whole composition range as the variation of firing schedules and temperatures sometimes produces unpredictable results.

The phase composition of RBSN ceramics may be calculated [7.14] using the following equations :

$$\begin{aligned} C_p &= 1 - 0.218\,\rho_g - 0.148\,\rho_n \\ C_{Si} &= 1.072\,\rho_g - 0.643\,\rho_n \\ C_{sn} &= 0.791\,(\rho_n - \rho_g) \end{aligned} \qquad (7.1)$$

where C_p , C_{Si} and C_{sn} are respectively the volume fractions of porosity, silicon and Si_3N_4 in a nitrided compact. In these equations ρ_g is the density of the green ceramic while ρ_n refers to that of the nitrided material. Values of the various volume fractions for the samples are shown in Table 7.3; the porosity vary between about 17 and 26 percent.

Table 7.3 Preparation and Composition Data for Available Silicon Nitride Samples

Firing Run	Mean Weight Gain (%)	Nitrided Density (g/cm^3)	Phase Composition			Green Ceramic Density (g/cm^3)	Peak Firing Temp. (^oC)
			C_{sn}	C_{Si}	C_p		
1	20.0	1.95	0.277	0.461	0.262	1.60	1250
2	33.5	2.15	0.435	0.333	0.232	1.60	1240
3	38.0	2.24	0.506	0.275	0.219	1.60	1150
4	41.5	2.25	0.514	0.268	0.217	1.60	1340
5	46.5	2.35	0.593	0.204	0.203	1.60	1370
6	55.0	2.40	0.683	0.172	0.195	1.60	1440
7	57.0	2.54	0.744	0.082	0.174	1.60	1440
8	63.2	2.52	0.783	0.020	0.197	1.53	1440

7.2 RESULTS: FULLY-NITRIDED SAMPLES

7.2.1 DIELECTRIC CONSTANT

The real part of the complex permittivity of the fully nitrided sample (Run no.8, 63.2 weight gain) was measured from 500 MHz up to 5 GHz with both the matched and short-circuit termination coaxial line methods. Additional measurements were also made at 9.34 GHz using the resonant cavity technique. In this method the resonant frequencies of the cavity with and without the sample were first measured. These frequencies, together with the volumes of the sample and empty cavity, are directly related to the dielectric constant (see Appendix B). Samples of about 6.8 mm diameter and thicknesses from 0.43 mm up to 0.68 mm were cut from the bulk material. It was important to ensure that the surfaces were parallel and smooth; this was done using a Logitech mechanical polishing machine which gave a surface flatness to within 0.25 μm. Much care was necessary in the sample preparation process since the ceramics were brittle.

Fig.7.3 shows the variation of the dielectric constant in the frequency range from 500 MHz to 9.34 GHz for the fully-nitrided samples. In order to compare the dielectric constant with that reported for the denser HPSN, account must be taken of the porosity of RBSN. The fully-nitrided samples measured had a porosity of 19.7 %. Walton [7.8] found that the dielectric constant of porous

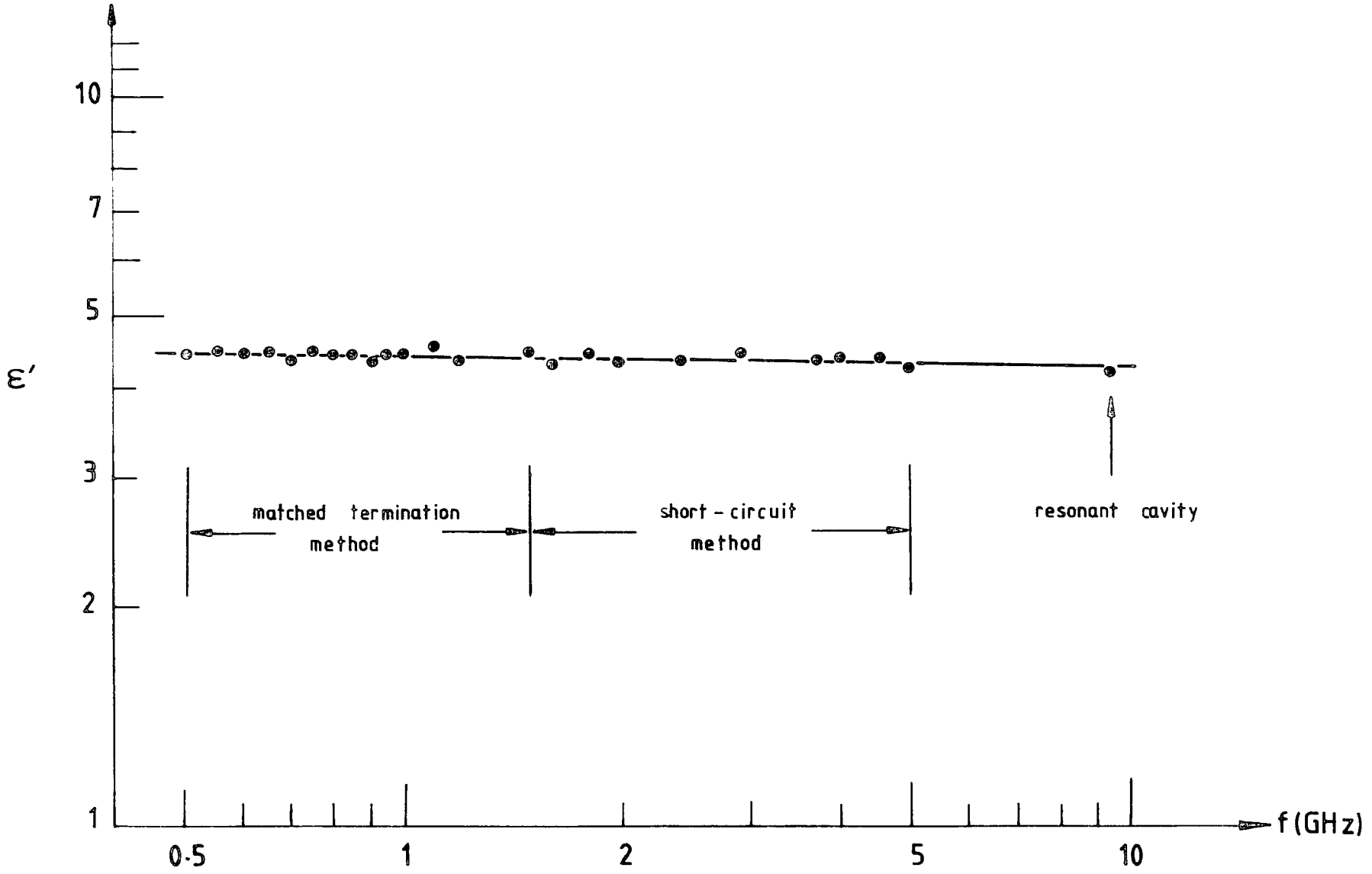

Fig. 7·3 Variation of dielectric constant with frequency for fully - nitrided (63·2 % weight gain) sample

low loss silicon nitrides follow the relation

$$\varepsilon'(p) = \varepsilon'(0)^{1-p} \qquad (7.2)$$

where $\varepsilon'(0)$ and $\varepsilon'(p)$ are respectively the dielectric constant of dense (zero porosity) and of that with a volume fraction p of pores. The quantity measured experimentally is in fact $\varepsilon'(p)$, (where in this case p = 19.7 %). This relationship is shown in Fig.7.4. To obtain $\varepsilon'(0)$, the point corresponding to given values of p and $\varepsilon'(p)$ is selected and $\varepsilon'(0)$ found by tracing back along the appropriate line to p = 0.

The reduced dielectric constant $\varepsilon'(0) - \varepsilon_\infty$, when plotted on a log-log scale against frequency, shows a linear variation, Fig.7.5, and is virtually independent of the measurement frequency. This frequency variation may be fitted with the Jonscher "universal dielectric response law", (section 6.4):

$$\left[\varepsilon'(0) - \varepsilon_\infty\right] \propto \omega^{n-1} \qquad (7.3)$$

where the exponent n had the value 0.98 ± 0.02.

7.2.2 LOSS FACTOR OF PBSN

The frequency variation of the loss factor for the fully-nitrided samples was determined using the matched termination method up to 1.5 GHz. Above 1 GHz up to about 8 GHz, the coaxial line resonance method was used. Values

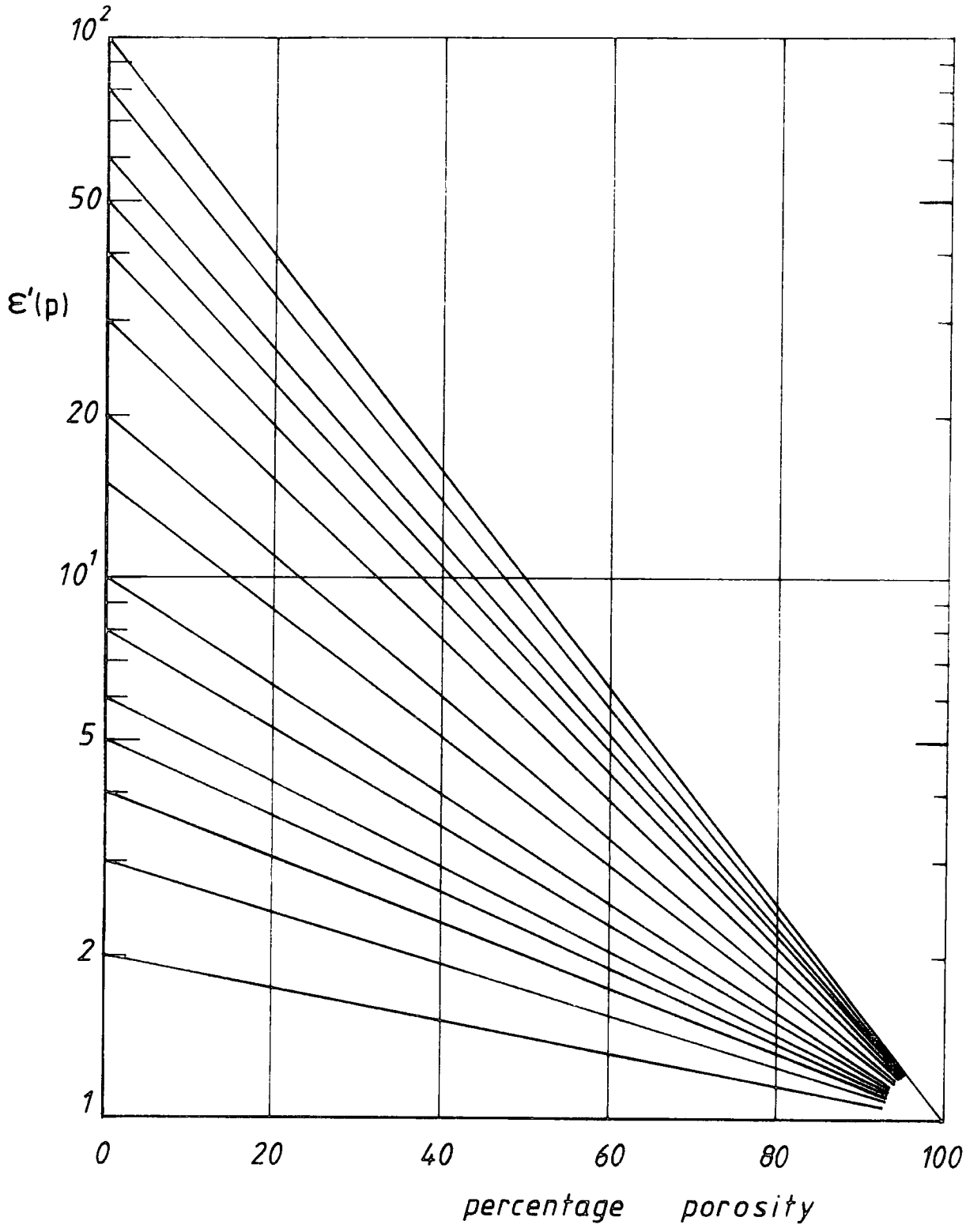

Fig.7·4 Dielectric constant as a function of volume percent of pores

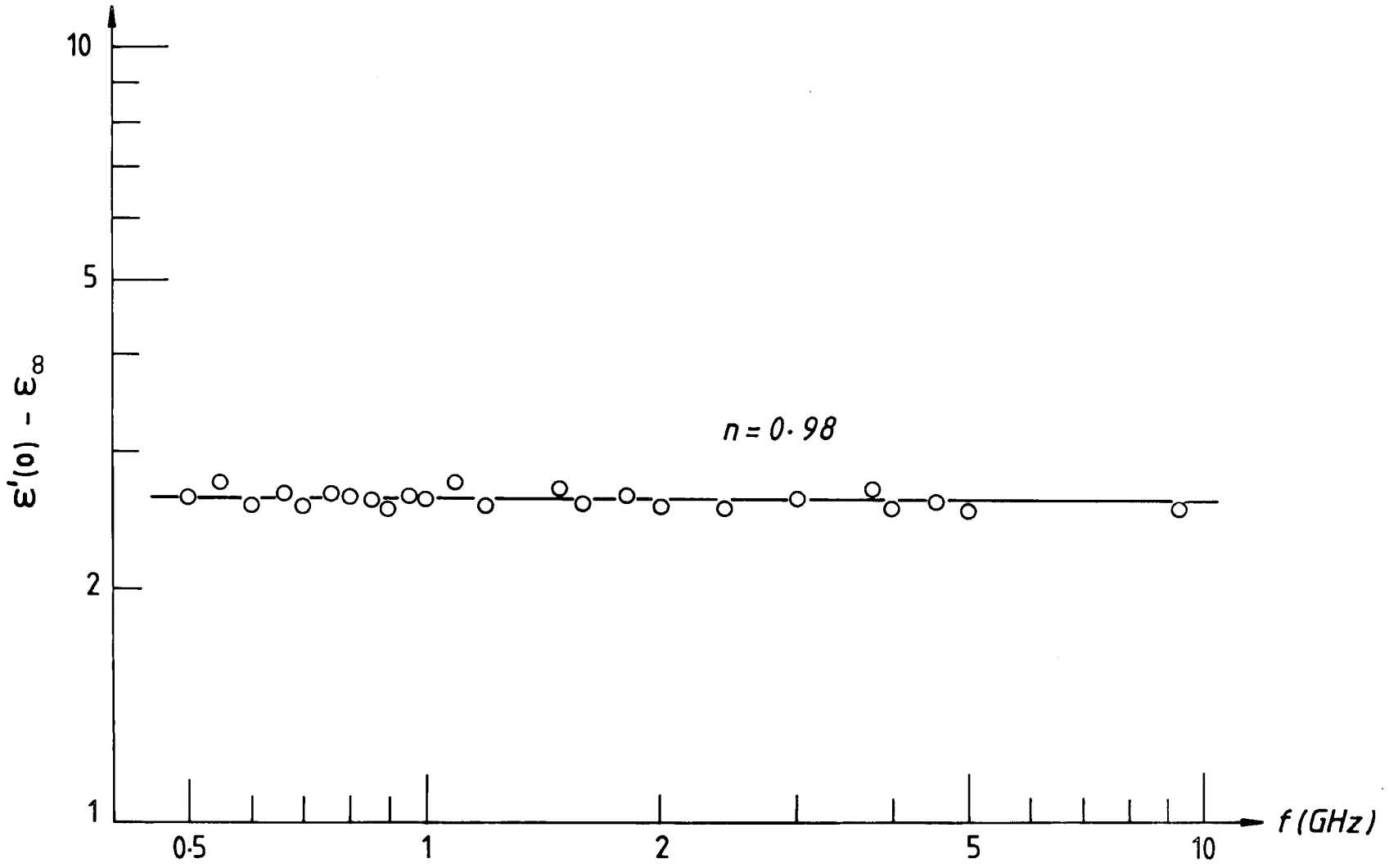

Fig.7·5 Variation of reduced dielectric constant with frequency for fully - nitrided sample

of the dielectric constant required for the determination of ε'' from about 6 GHz to about 8 GHz were obtained by interpolation between the measured values up to 5 GHz and that of the resonant cavity method at 9.34 GHz. The same coaxial line disc shaped samples were used in the resonant cavity method of measurement. A log-log plot of ε'' versus frequency in the measured range is shown in Fig.7.6. It is observed that ε'' is virtually constant throughout the frequency range, having a value $\sim 7 \times 10^{-3}$. Fitting with the universal dielectric response law for the loss component $\varepsilon'' \propto \omega^{n-1}$, gave the value of the exponent as $n = 0.97 \pm 0.02$, in close agreement with the value deduced from the variation of the dielectric constant with frequency.

As would be expected from the constancy of both the dielectric constant and loss factor, the loss tangent varies linearly with frequency as shown in Fig.7.6.

7.3 RESULTS: PARTIALLY-NITRIDED SAMPLES

7.3.1 DIELECTRIC CONSTANT

The partially-nitrided samples were again in the form of circular discs of about 6.8 mm diameter having thicknesses between 0.40 mm and 0.60 mm. Coaxial line and resonant cavity techniques were used as for the fully-nitrided samples. These partially-nitrided samples had weight gains from 38% up to 57% compared to the weight gain of 63.2%

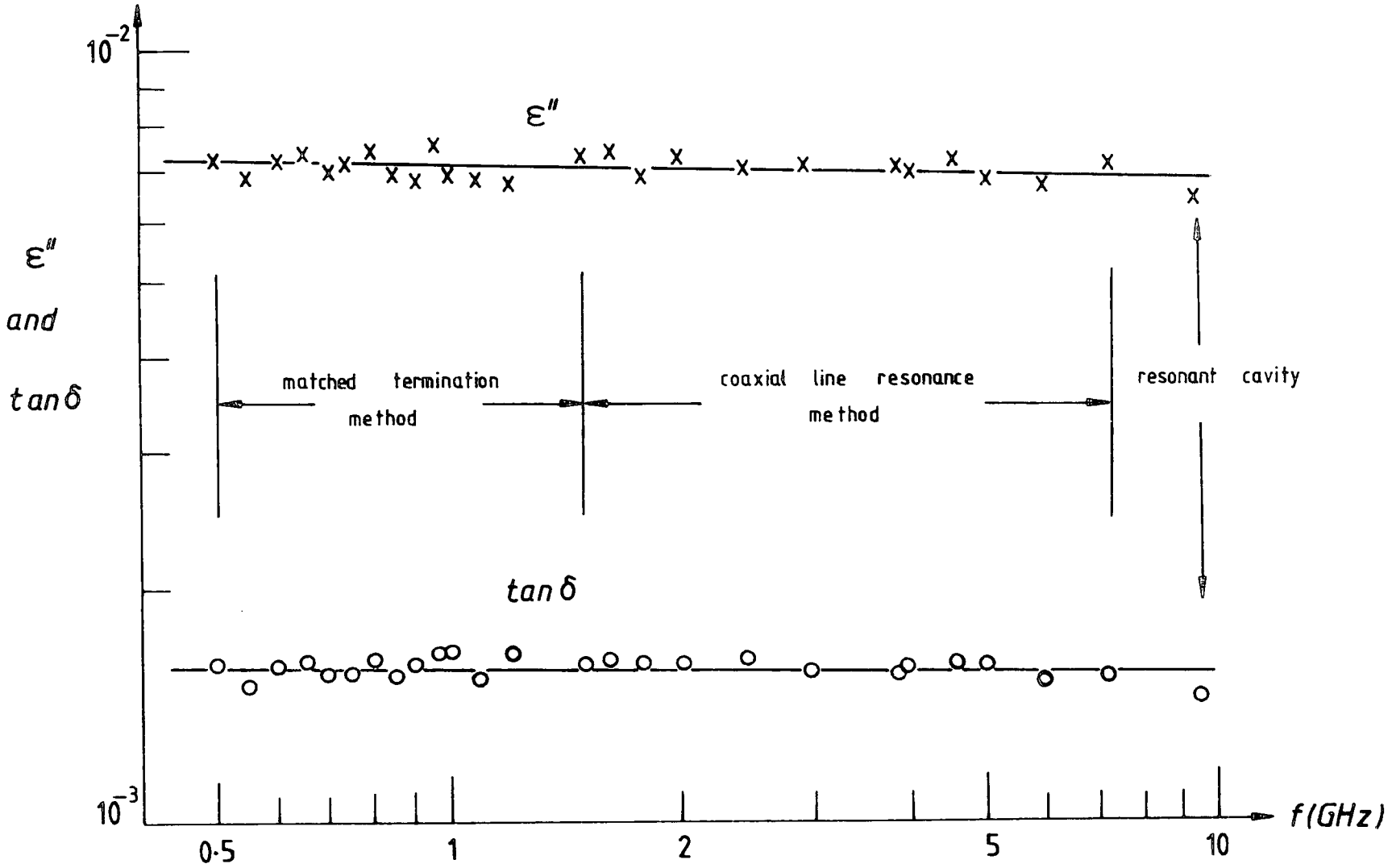

Fig. 7·6 Variation of ε'' and $\tan\delta$ with frequency for fully - nitrided samples

for the fully-nitrided samples. For all weight gains the matched termination method was suitable only up to about 1.5 GHz; above this frequency up to about 5 GHz the short-circuit termination method was preferable. Measurements become increasingly more difficult and less accurate as the weight gain decreased. It was impossible to obtain data for weight gains less than 38 % as the samples became very lossy and the equivalent circuit assumed for the short-circuit method is no longer valid. The variation of with frequency for these samples are given in Fig.7.7. An almost frequency independent behaviour is evident for all the various weight gains.

7.3.2 LOSS FACTOR

In the frequency range from 500 MHz up to about 1.5 GHz calculations of the loss factor were made from the measurements using the matched termination method. For all the lower weight gain samples, measurements using the short-circuit termination were relatively easier to perform since the losses were high, which gave low VSWR values. This method together with the coaxial line resonant method covered the range from 1 GHz up to about 8 GHz. It was found that these two methods gave good agreement for the higher loss samples. On the whole the loss factors obtained by the resonant cavity method at 9.34 GHz appeared slightly lower for all weight gains. Fig.7.8 shows the variations of the

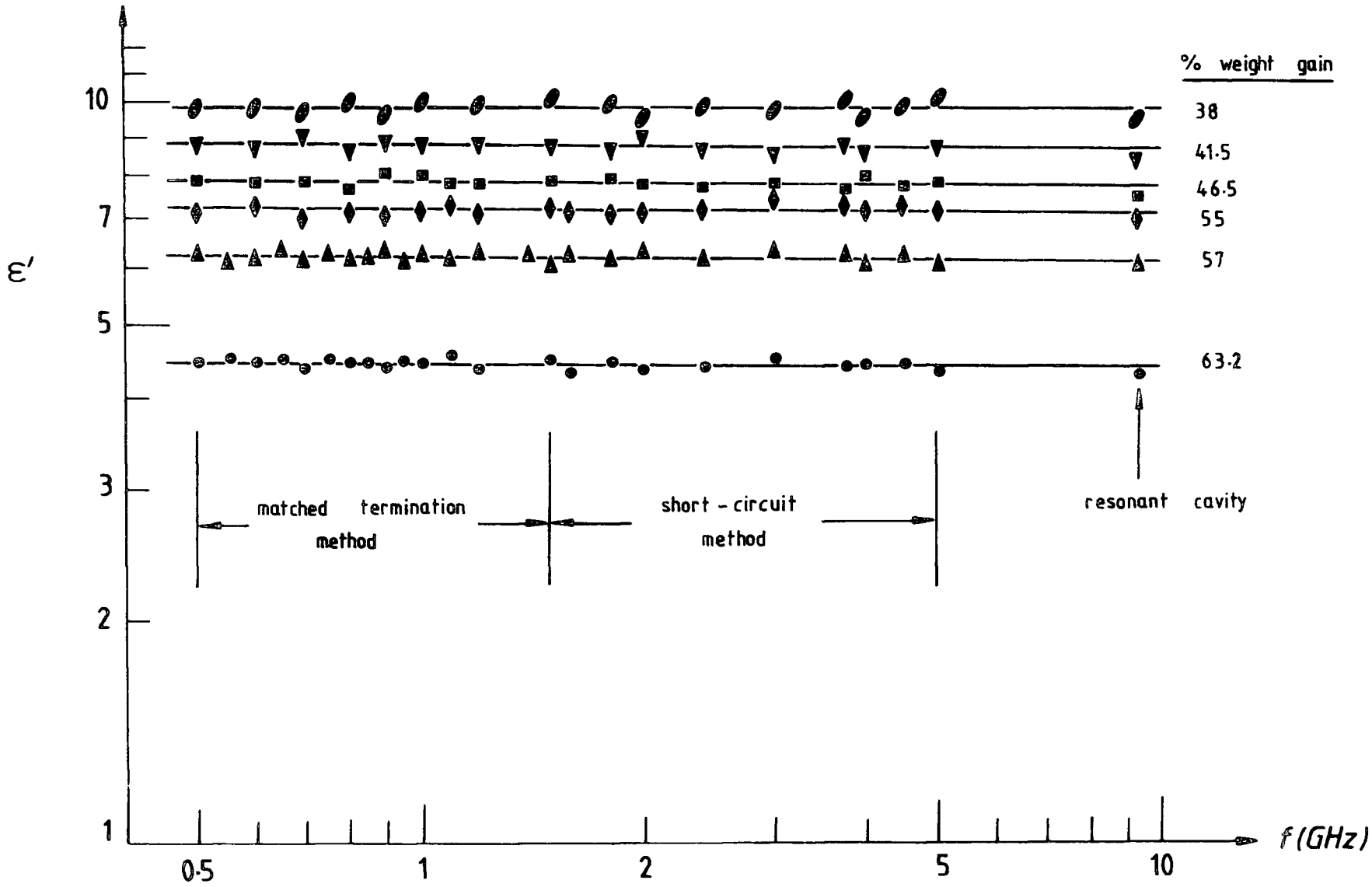

Fig. 7·7 Variation of ε′ with frequency for samples at different degrees of nitridation

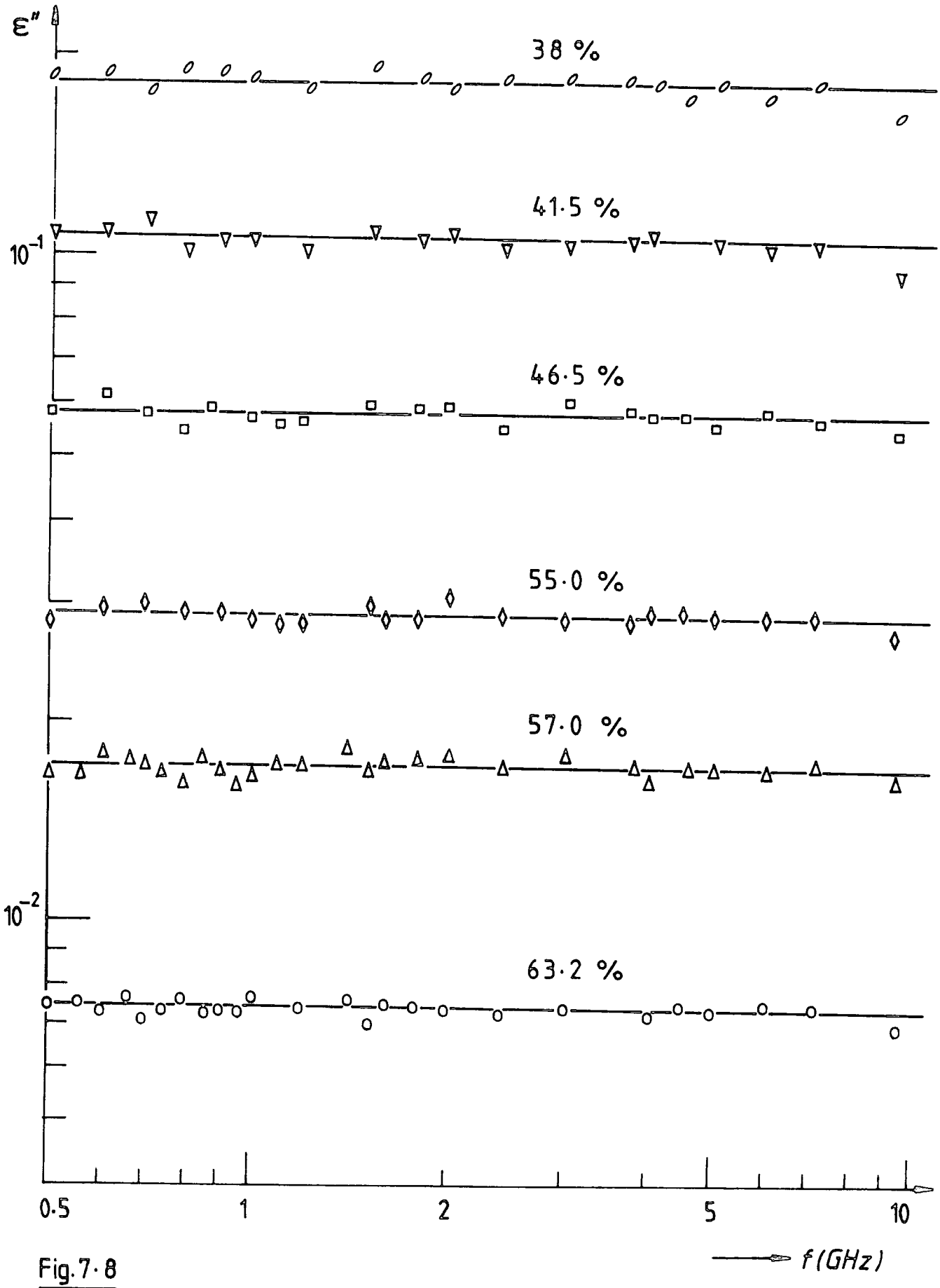

Fig.7·8

Dependence of loss factors on weight gain

loss factor with frequency for the range of percentage weight gains measured.

7.4 DISCUSSION

7.4.1 FULLY-NITRIDED SAMPLES

The measured dielectric constant of the fully nitrided samples, having 19.7% by volume fraction of pores, was virtually independent of frequency throughout the measurement range. The values obtained, between 4.50 and 4.65, were close to the limiting high-frequency dielectric constant, ε_∞ ($\simeq 4$), deduced from various optical measurements on thin film silicon nitrides [e.g. 7.1, 7.14]. Comparison with other reported results for both RBSN and HPSN, given in Table 7.5, shows that the $\varepsilon'(0)$ values in Table 7.4 agree reasonably well with the quoted figures for

Table 7.4 Dielectric Constants of Fully Nitrided Samples (Present Study)

frequency (GHz)	ε'(19.7 %)	ε'(0)
0.5	4.55	6.60
1.0	4.55	6.60
1.5	4.59	6.67
2.0	4.52	6.54
4.0	4.51	6.53
5.0	4.50	6.51
9.34	4.51	6.53

Table 7.5 Reported Values of the Dielectric Constant of Silicon Nitride

Frequency (Hz)	Dielectric Constant	Fabrication Method	Comments	References
$(8 - 10) \times 10^9$	4.5 - 5.6	Reaction-bonded	-	7.8
1×10^5 9.34×10^9	9.58 5.65	hot-pressed	5 $^{w}/_{o}$ MgO added	7.18
1×10^{10}	5.52 - 9.3 6.65 7.37	reaction-bonded hot-pressed	up to 5 $^{w}/_{o}$ MgO added	7.19
9.37×10^9	4.85 6.8 8.3 5.5 - 5.9	slip-cast flame-sprayed hot-pressed isostatically pressed	-	7.20

HPSN. In particular, the dielectric constants obtained here are in good agreement with the low loss silicon nitrides measured by Walton [7.8] . As can be seen from Table 7.5 the reported values (from 4.5 to about 9.5) vary greatly; this may be due to the diverse fabrication techniques employed. On the whole the more dense HPSN values are higher as would be expected. Another factor may be attributed to the free silicon content (see later).

The loss tangents of the fully-nitrided samples are compared in Table 7.6 with values reported for various silicon nitrides prepared by various fabrication routes, and

Table 7.6 Loss Tangents of Silicon Nitrides

Frequency (Hz)	tan δ	Fabrication Method	References
1.0×10^{9} 9.34×10^{9}	1.67×10^{-3} 1.58×10^{-3}	Reaction-bonded	Present study
9.37×10^{9}	7.0×10^{-3} - 1.7×10^{-2}	Hot-pressed	7.20
1.05×10^{5} 9.34×10^{9}	5.0×10^{-3} 4.02×10^{-3}	Hot-pressed	7.18
1.0×10^{10}	1.0×10^{-2} - 1.49×10^{-1}	Reaction-bonded	7.19

appears somewhat lower. The earlier silicon nitrides investigated by Messeir and co-workers [e.g. 7.19] and Perry and Moules [7.20] for radome applications were very lossy. The cause of this high loss have been under investigation and it was not until the mid 1970's that silicon nitrides with suitably low losses ($\tan\delta \lesssim 10^{-2}$) were produced.

7.4.2 PARTIALLY-NITRIDED SAMPLES

The variation of reduced dielectric constant, $(\varepsilon' - \varepsilon_\infty)$, with frequency could not be directly observed since no ε_∞ value was available for any of the partially-nitrided samples. Nevertheless, since ε_∞ is a constant quantity for each material, subtracting this from the measured dielectric constant would not alter the gradient of each of the plots in Fig.7.7. It can thus be inferred that the partially nitrided samples follow the universal dielectric response law ($\varepsilon' - \varepsilon_\infty \propto \omega^{n-1}$) with all n values close to unity. The variation of ε' with weight gain at any particular frequency is illustrated by the plot in Fig.7.9, where the value for pure silicon (i.e. 11.7), [7.21, 7.22] has also been included. The variation suggested by the curve indicates that the incremental change in ε' with increasing weight gain is much more pronounced at higher weight gains. Assuming that a decrease in weight gain represents an increase in free silicon content, this confirms that ε'

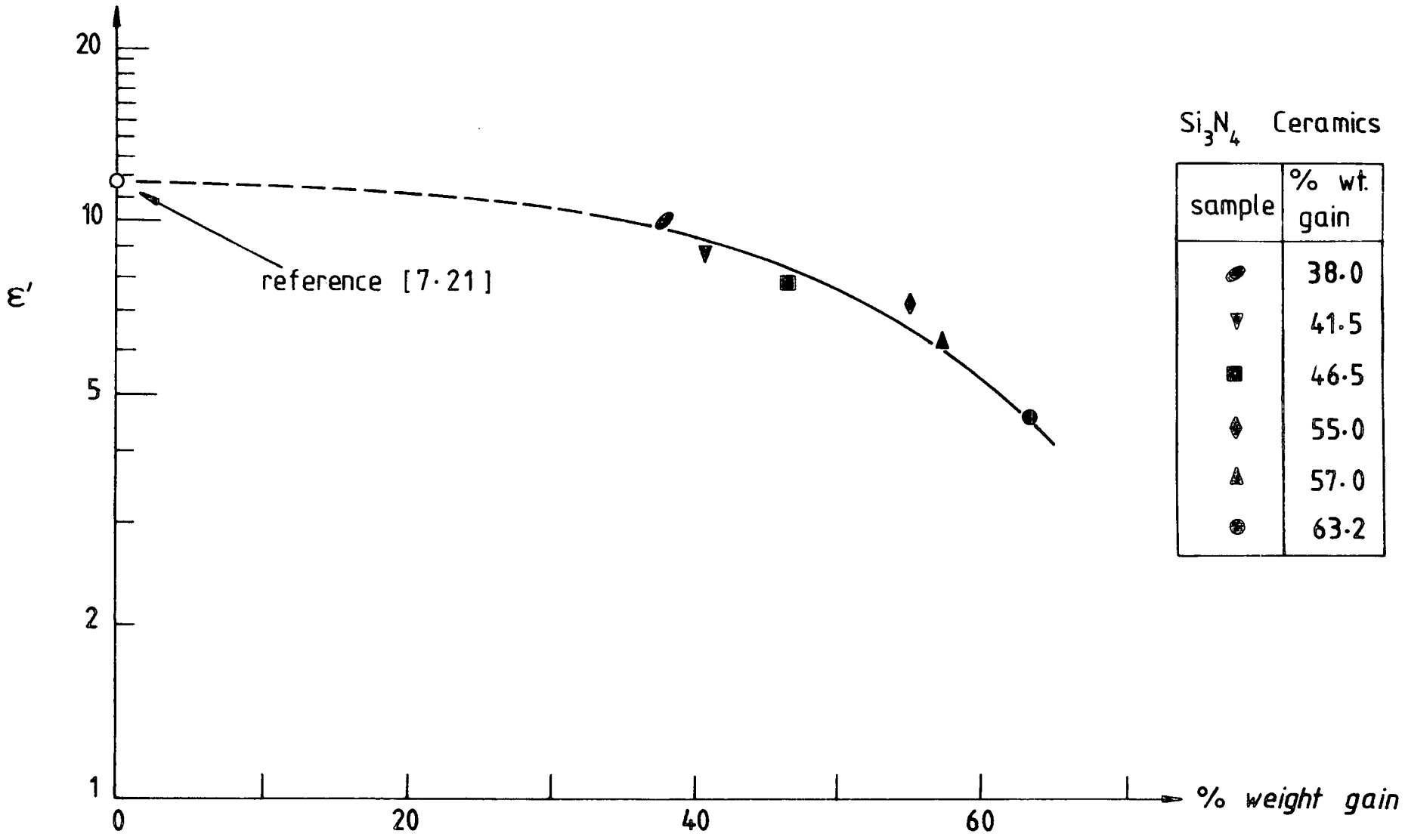

Fig. 7·9 The dependence of dielectric constant on percentage weight gain at 1 GHz

of silicon nitride is noticeably dependent on the free silicon content. Measurement of the dielectric constant can thus provide an estimate of the degree of nitridation.

Fig.7.8 shows that the loss factors of samples from the fully-nitrided to the lowest weight gain measurable spanned about one and a half decades from about 4.5×10^{-3} to 1.8×10^{-1}. At any particular frequency in the measurement range the variation of loss factor with weight gain is illustrated by the plot in Fig.7.10. In this plot the value of the loss factor of pure silicon (of resistivity 16,000 ohm-cm; [7.22]) is included in order to show the most likely shape of the curve. The loss data for the lowest weight gain measurable (38 %) is seen to depart considerably from the curve; this is probably due to the fact that measurements became less accurate as the samples became more lossy.

It is reasonable to attribute the large increases in dielectric constant and loss factor to the presence of free unreacted silicon, as indicated by Table 7.3. Moreover, ESR studies by Bushell [7.16] have shown that both pure silicon and fully-nitrided silicon nitride exhibit defect centre resonance lines which have slightly different g values; in his ESR examination of partially-nitrided samples Bushell showed that the relative proportion of the silicon and silicon nitride lines closely followed the

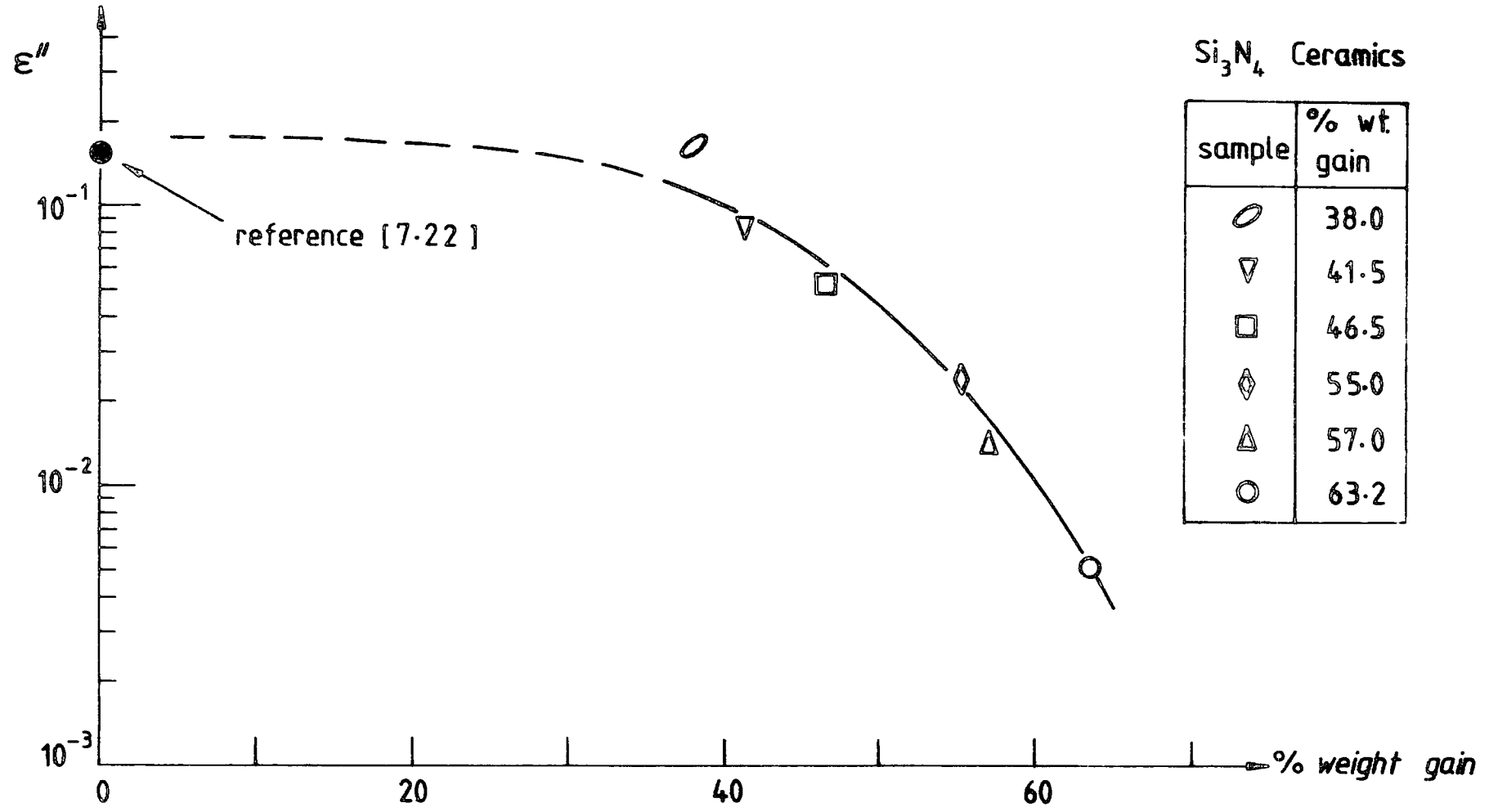

Fig. 7·10 The dependence of loss factor on percentage weight gain at 1 GHz

proportion expected from the known weight gains. This suggested that there was a close correlation between weight gain and free silicon content. The effects of free silicon on the dielectric properties of silicon nitride had also been observed by Messeir and co-workers [7.19] , and Perry and Moules [7.20] where dielectric constants between 4.8 and 8.3, and loss tamgents between 5.0×10^{-3} and 0.12 were reported for samples having densities of 2.2 to 2.6 g/cm^3. Not only is the effect due to free silicon observed in bulk materials but it is also noted by Sinha and Smith [7.23] that the dielectric constant of thin film silicon nitrides increased from about 6 to approximately 8 as the films become rich in silicon.

7.5 REFERENCES

7.1 Milek T.J. (Ed.)," Handbook of Electronic Materials ", Vol.3, IFI/Plenum, N.Y. (1971)

7.2 Morosanu C.-E.," The preparation, characterization and applications of silicon nitride thin films ", Thin Solid Films, vol.65,171(1980)

7.3 Ogawa H., Arizumi T. and Nishinaga T.," Preparation and properties of silicon nitride film and its applications ", Jpn. J. Appl. Phys., vol.10,1975(1971)

7.4 Aboaf A.J., Hammer R. and Crowder H.P.," Effects of insulator thickness fluctuations on NMOS charge storage characteristics ", IEE Trans. Electron. Devices, vol.19, 198(1972)

7.5 Swarop B.," Silicon nitride as a dielectric material ", Proc. 4th Interam. Conf. Mater. Technol., 224(1975)

7.6 Godfrey D.J.," Silicon nitride for engineering applications ", Tech. Pap. No. 740238 (1974)

7.7 Torti M.L., Alliegro R.A., Richerson D.W., Washburn M.E. and Weaver G.Q. in Proc. Symp. High-Temp. Mater. Gas Turbines, Sahu P. and Speidel M.O.(Eds.), (1973)

7.8 Walton Jr. J.D.," Reaction-sintered silicon nitride for high temperature radome applications ", Amer. Ceram. Soc. Bull., vol.53,255(1974)

7.9 Hardie D. and Jack K.H.," Crystal structure of silicon nitride ", Nature, vol.180,332(1957)

7.10 Forgeng W.D. and Decker B.F.," Nitrides of silicon ", Trans. AIME Metallurgical Soc., vol.242,343(1958)

7.11 Popper P. and Ruddlesdon S.N.," Structure of nitrides of silicon and germanium ", Nature, vol.179,1129(1957)

7.12 Kendall E.J.M.," The stabilization of silicon surfaces using silicon nitride ", J. Phys. D, Ser. 2, vol.1, 1409(1968)

7.13 Sokel R.J.," The electronic structure of silicon nitride ", J. Phys. Chem. Solids, vol.41,899(1980)

7.14 Moulson A.J.," Review - reaction-bonded silicon nitride: its formation and properties ", J. Mat. Sci., vol.14, 1017(1979)

7.15 Dalgleish B.J. and Pratt P.L.," The influence of microstructure on the strength of RBSN ", Proc. Brit. Ceram. Soc., vol.25,295(1975)

7.16 Bushell T.," Some Properties of Reaction-Bonded Silicon Nitride ", Ph. D. Thesis, University of Durham (1983)

7.17 Boyer S.M. and Moulson A.J.," A mechanism for the nitridation of Fe-contaminated silicon ", J. Mat. Sci., vol.13,1387(1978)

7.18 Sharif B.I.," Electrical Properties of Hot-Pressed

Nitrogen Ceramics ", Ph. D. Thesis, University of Durham (1977)

7.19 Messeir D.R. and Wong P.," Silicon nitride: a promising material for radome applications ", Proc. 12th Symp. Electromag. Windows, Georgia Inst. Tech., Harris J.N. (Ed.), (1974)

7.20 Perry G.S. and Moules T.R.," Microwave dielectric properties of silicon nitride ", Proc. 12th Symp. Electromag. Windows, Georgia Inst. Tech., Harris J.N. (Ed.), (1974)

7.21 Westphal W.B. and Sils A.," Dielectric Report ", M.I.T. AD - 746 686 and AFML - TR - 72 - 39 (1972)

7.22 Rao K.V. and Smakula A.," Dielectric anomalies in silicon single crystal ", J. Appl. Phys., vol.37,2840 (1966)

7.23 Sinha A.K. and Smith T.E.," Electrical properties of Si-N films deposited on silicon from reactive plasma ", J. Appl. Phys., vol.49,2756(1978)

CHAPTER 8

DIELECTRIC PROPERTIES OF OXYNITRIDE GLASSES

8.1 INTRODUCTION

8.1.1 OXYNITRIDE GLASS SYSTEMS

There are difficulties in producing fully dense silicon nitride by straightforward reaction-bonding or hot-pressing. Those arising in reaction-bonding have already been discussed in the previous chapter and some points relating to the hot-pressing techniques should be mentioned. Hot-pressing silicon nitride with small amounts ($\lesssim$ 2 $^{w}/_{o}$) of oxide additives such as magnesia, MgO, yttria, Y_2O_3, ceria, CeO_2, or zirconia, ZrO_2, [8.1 - 8.3] can achieve a fully dense product with high strengths up to 1000^{o}C. Silicon nitrides with less than 5 volume percent porosity can also be obtained by sintering with larger amounts (5 - 10 $^{w}/_{o}$) of oxide additives [8.4] . Magnesia reacts with the surface layer of silica which is always present on the nitride to give a grain-boundary phase, first thought to be a silicate liquid [8.1] , which cools to give a low softening-temperature glass. These types of grain-boundary phases cause the creep resistance of the high density product to decrease rapidly above 1000^{o}C. The liquid phase and the glasses that form from it are now established as oxynitrides [8.5 - 8.7] . With yttria

additive the Y-Si-O-N liquid yields highly refractory quarternary oxynitride phases giving improved high temperature properties [8.2] . Further efforts in the densification process led to the discovery that it is possible to replace silicon by aluminium and nitrogen by oxygen in silicon nitride without changing its structure [8.8, 8.9] . It is also found that silicon nitride may be "alloyed" with alumina and other metal oxides or nitrides to form what is known by the acronym "sialon", derived from the resulting Si-Al-O-N phases. From this development it is now possible to prepare bulk oxynitride glasses in the Mg, Ca, Y and Nd sialon systems [8.10] . These glasses are important because the high temperature strength and creep resistance of nitrogen ceramics depend markedly on the amount and characteristics of the grain-boundary glass [8.4] . They are also important in their own right since small amounts of nitrogen in oxide glasses have been reported to increase their viscosity and resistance to devitrification [8.11] .

Recently Thorp and Kenmuir [8.12] have reported measurements on the dielectric properties of Ca and Mg oxynitride glasses. Room temperature measurements of the dielectric constant and loss factor, using bridge techniques from 500 Hz to 10 kHz, showed that for each particular composition the data fitted well with the universal dielectric response law. It was also found that the addition of nitrogen in the glasses increases ε' and furthermore that changing

from Mg to Ca increased ε' in either the pure oxide or oxynitride glasses. These investigations have since been extended to cover two more new glass systems [8.13] , namely Y and Nd oxynitrides, together with further compositions in both the Mg and Ca oxynitride glasses. The present work is an extension to higher frequencies of the earlier studies carried out in this Department and was undertaken to see whether the trends of behaviour found in the lower frequency region also held over the frequency range from 500 MHz to 10 GHz.

8.1.2 GLASS COMPOSITIONS STUDIED

Oxynitride glasses of the form M-Si-Al-O-N (where the cation M = Mg, Y, and Ca) studied here have been prepared at the Crystallography Laboratory, University of Newcastle-upon-Tyne [8.14] . Table 8.1 shows the compositions of these glasses where it can be seen that the compositions were varied systematically. Each of the cation systems included an oxide glass without nitrogen. The oxynitrides of the systems are formed by substituting chemical equivalents of nitrogen for proportions of oxygen of the oxide glass. The percentage of oxygen replaced in this manner is given in Table 8.1 for each of the oxynitride compositions. Proportions of the other elements were held constant, although the decrease in the total number of atoms caused by the substitution of two nitrogen atoms for three oxygen atoms naturally increased the numerical values

Table 8.1 Compositions of the Mg, Ca and Y Oxynitride Glasses Studied

Sample	Composition in Atomic Percent							% Oxygen Replaced by Nitrogen (R)	ε_∞
	Mg	Ca	Y	Si	Al	O	N		
1	17.0	-	-	17.0	6.0	60.0	0	0	2.46
2	17.2	-	-	17.2	6.4	55.1	4.1	8.1	2.62
3	17.4	-	-	17.4	6.6	51.0	7.6	14.8	2.71
4	-	17.0	-	17.0	6.0	60.0	0	0	2.59
5	-	17.2	-	17.2	6.4	55.1	4.1	8.1	2.73
6	-	17.2	-	17.2	6.5	54.2	4.9	9.8	2.77
7	-	17.3	-	17.3	6.5	53.1	5.8	11.5	2.80
8	-	17.4	-	17.4	6.6	51.0	7.6	14.8	2.84
9	-	-	11.8	17.8	6.8	63.6	0	0	2.76
10	-	-	12.3	18.5	7.1	54.2	7.9	14.8	3.05

of their concentrations when expressed in atomic percent. The same pattern was followed between the different cation series, which therefore contained equal chemical equivalents of either Mg, Y or Ca. The ratio of total positive valences to total negative valences did not vary with either nitrogen concentration or cation type and was equal to one for all the materials studied. Table 8.1 also includes the limiting high-frequency dielectric constant, ε_{∞} , deduced from optical refractive index measurements [8.14] .

8.2 RESULTS

8.2.1 SAMPLES AND MEASUREMENT METHODS

Disc shaped samples of about 6.5 mm to 8 mm in diameter and thicknesses between 0.50 mm and 0.65 mm were cut from the bulk oxynitride glasses using conventional diamond wheel cutting techniques followed by diamond paste polishing to finishes of 0.25 μm. Besides being used for the coaxial line measurement techniques these same samples were also used in the cavity perturbation measurements at 9.34 GHz. In addition, cubic samples of sides about 2 mm to 5 mm were also used in the latter measurement method. The dielectric constants of the samples were determined using the short-circuit termination method from 500 MHz up to 5 GHz. These were used in the loss determinations using the coaxial line resonance method from 1 to 5 GHz. It was found that the matched termination

method was only applicable up to 1 GHz and more suitable for the lower dielectric constants. Above 5 GHz the VSWR measured by the coaxial line resonance method becomes very high thus effectively setting an upper frequency limit of about 5 GHz for the loss measurements on these glasses. All the measurements were made at room temperature.

8.2.2 MAGNESIUM OXYNITRIDE GLASSES

The dielectric constants of these glasses were found to be almost independent of frequency within the measurement range. Values of ε' ranged from about 5.6 to 6.5 for a series of oxynitrides having R between 0 % and 14.8 % (R is the percentage of oxygen replaced by nitrogen). The dielectric constants for the various compositions are given in Table 8.2 along with those for the Y and Ca oxynitride glasses. The variations of the reduced dielectric constants $(\varepsilon' - \varepsilon_\infty)$ with frequency are shown in Fig.8.1. According to Jonscher (section 6.4) the frequency dependence should follow $(\varepsilon' - \varepsilon_\infty) \propto \omega^{n-1}$ and the individual log-log plots for each of these compositions gave the n value of 1.0 ± 0.05. Fig.8.2 illustrates the changes of the loss factors with frequency, where it is evident that for all the compositions the n values deduced from the relation $\varepsilon'' \propto \omega^{n-1}$ gave the same n value 1.0 ± 0.05 as for the reduced dielectric constant versus frequency plots. Since the loss factor and dielectric constant are

Table 8.2 Dielectric Properties of Mg, Y and Ca Oxynitride Glasses at 1 GHz

Oxynitride Glass Systems	% Oxygen Replaced by Nitrogen (R)	ε'	ε''	$\tan\delta \times 10^3$
Mg	0	5.64	0.016	2.87
	8.1	6.18	0.021	3.32
	14.8	6.48	0.026	4.00
Y	0	6.60	0.017	2.51
	14.8	7.14	0.014	2.00
Ca	0	6.93	0.017	2.48
	8.1	7.22	0.020	2.81
	9.8	7.31	0.022	3.00
	11.5	7.39	0.023	3.10
	14.8	7.49	0.024	3.23

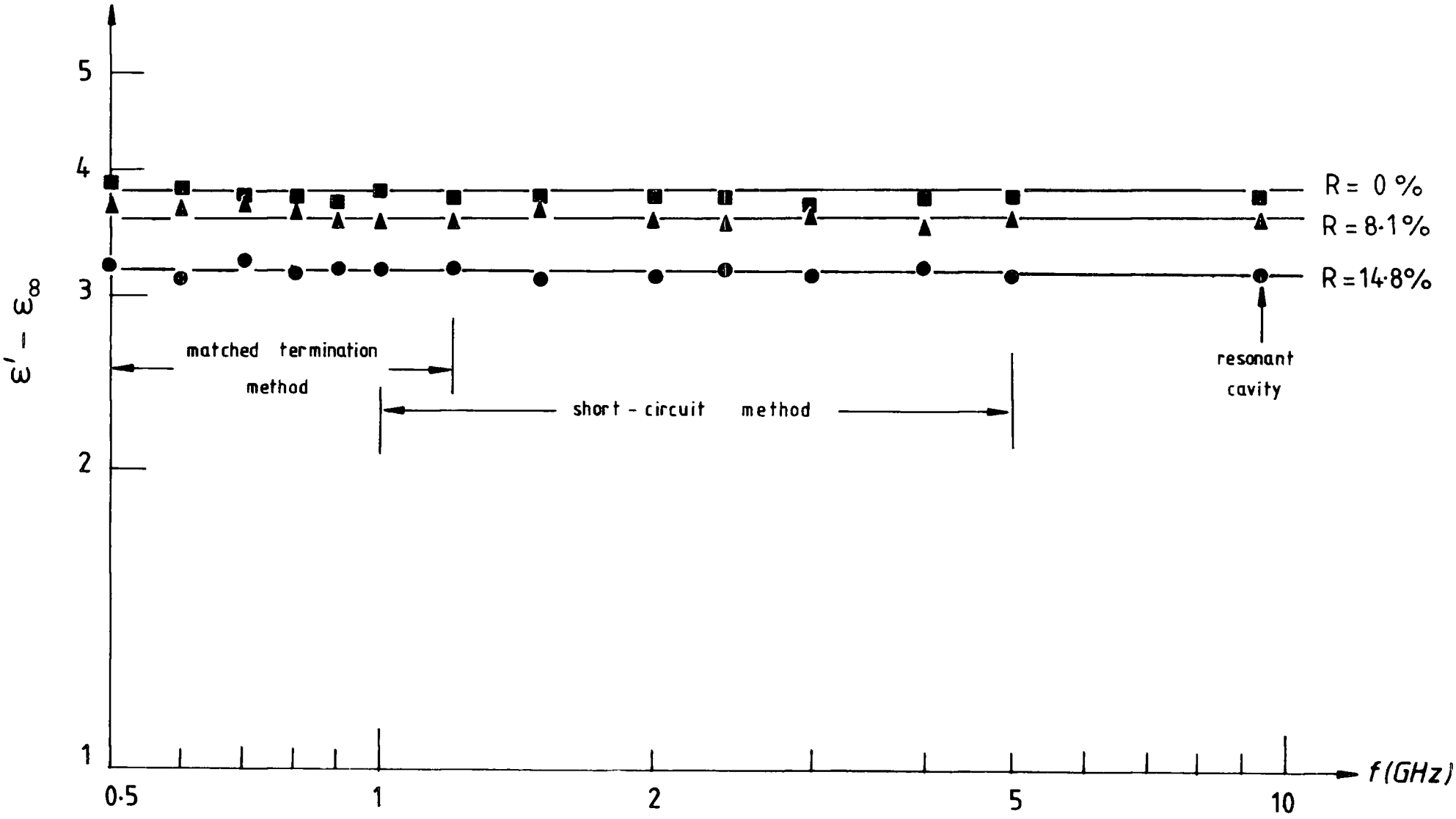

Fig. 8·1 Variation of reduced dielectric constant with frequency for magnesium glasses

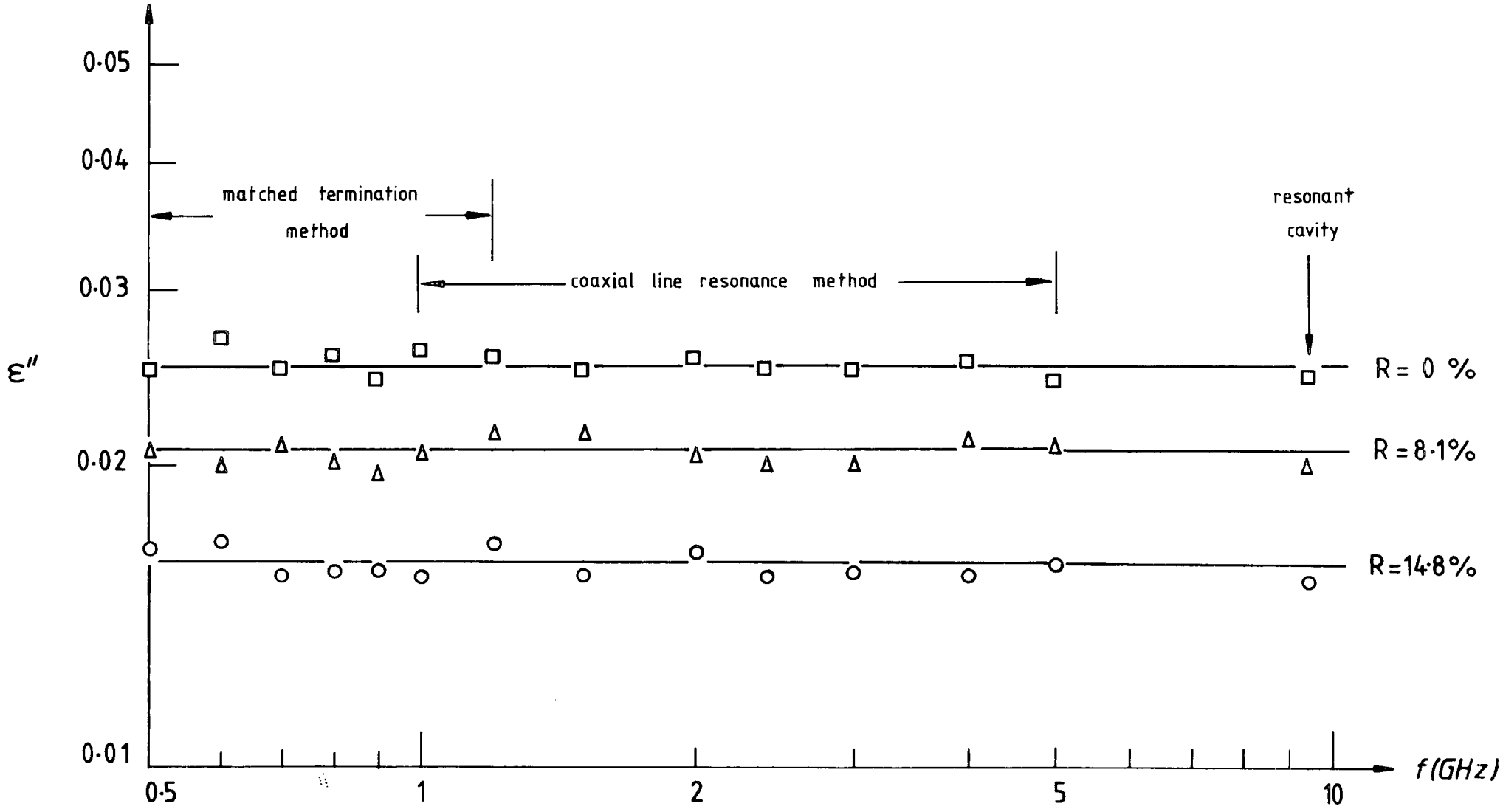

Fig.8·2 Frequency dependence of loss factor for magnesium glasses

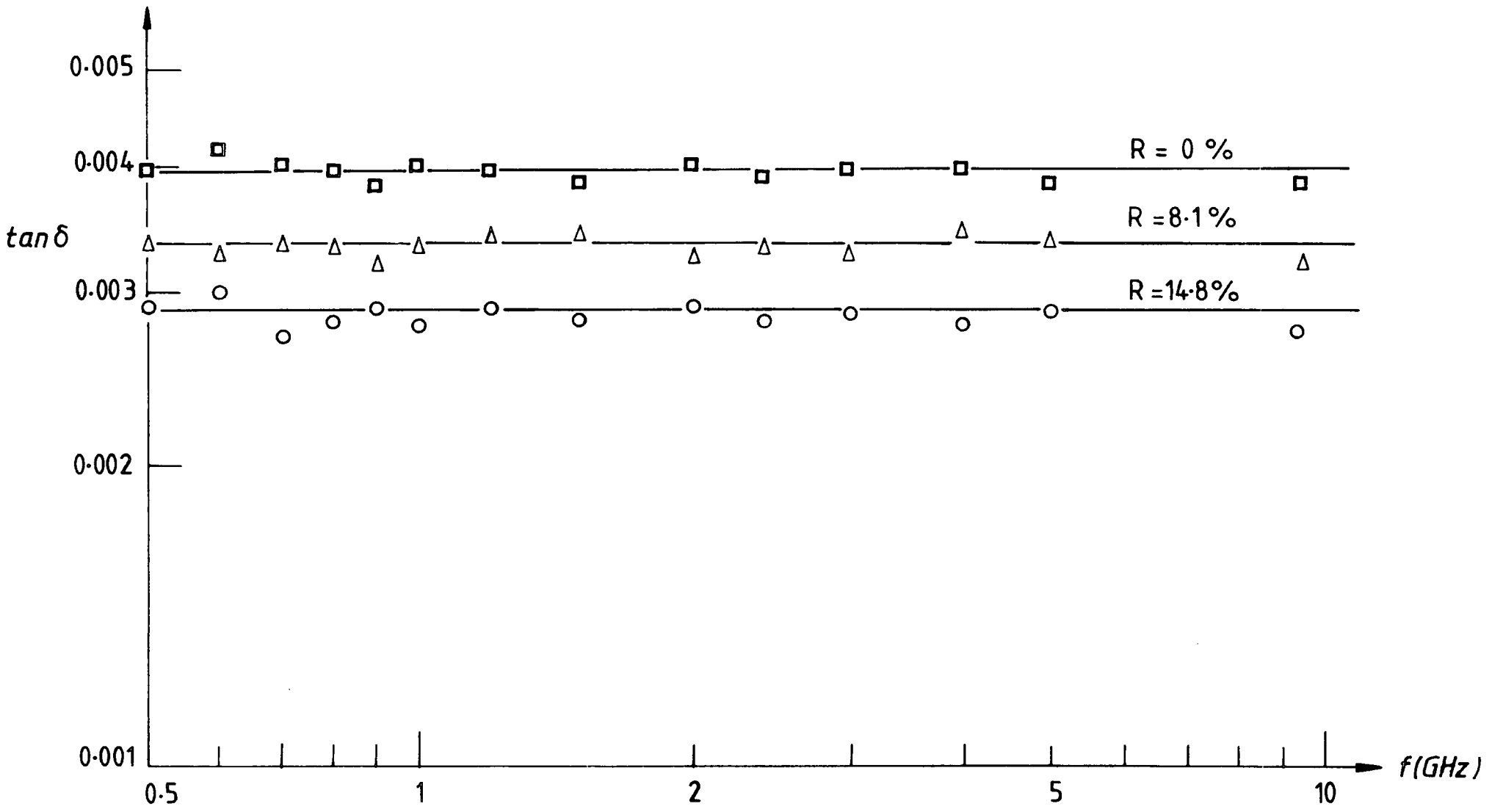

Fig. 8·3 Frequency dependence of loss tangent for magnesium glasses

almost independent of frequency, the loss tangent also follow this behaviour; Fig.8.3.

8.2.3 YTTRIUM OXYNITRIDE GLASSES

The dielectric constants of the yttrium oxynitride glasses studied are also almost independent of frequency in the measurement range, having values of about 6.6 and 7.2 for the compositions with R = 0% and R = 14.8% respectively. The slopes of the log-log plots of reduced dielectric constants with frequency gave n values close to unity, Fig.8.4. Again from the loss factor versus frequency plots in Fig.8.5, the slopes yield n values in agreement with those from the reduced dielectric constants versus frequency plots. The variation with frequency of the loss tangents for these glasses are shown in Fig.8.6.

8.2.4 CALCIUM OXYNITRIDE GLASSES

These glasses were found to have dielectric constants from about 6.9 to 7.5 for the five compositions for the range of R values similar to those for both the Mg and Y oxynitride glasses. Once again all the Ca oxynitride glasses showed linear variations of the reduced dielectric constants and loss factors with frequency, Figures 8.7 and 8.8. The n values deduced from both these sets of plots against frequency again gave values of 1.0 ± 0.05

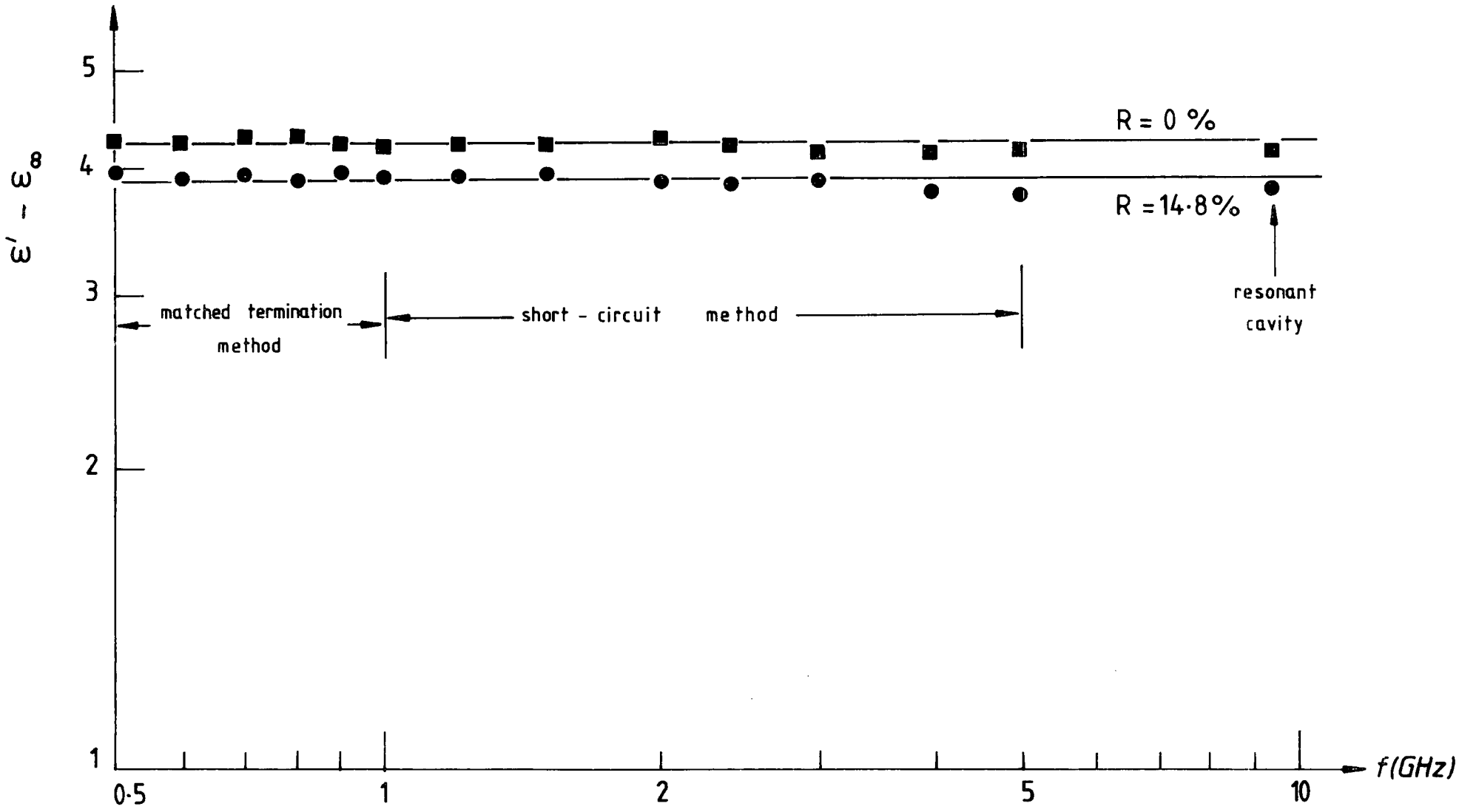

Fig. 8·4 Variation of reduced dielectric constant with frequency for yttrium glasses

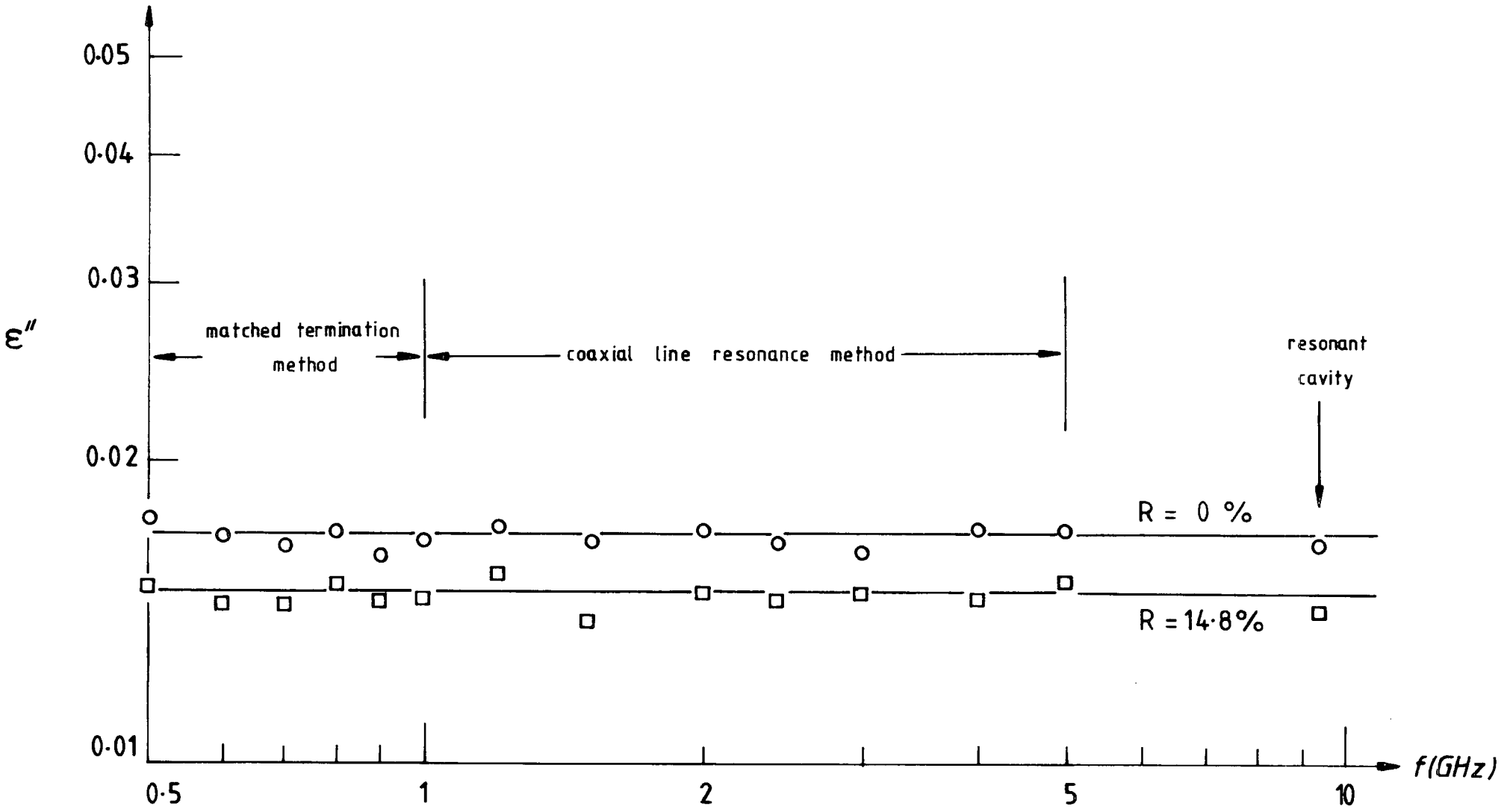

Fig.8·5 Frequency depedence of loss factor for yttrium glasses

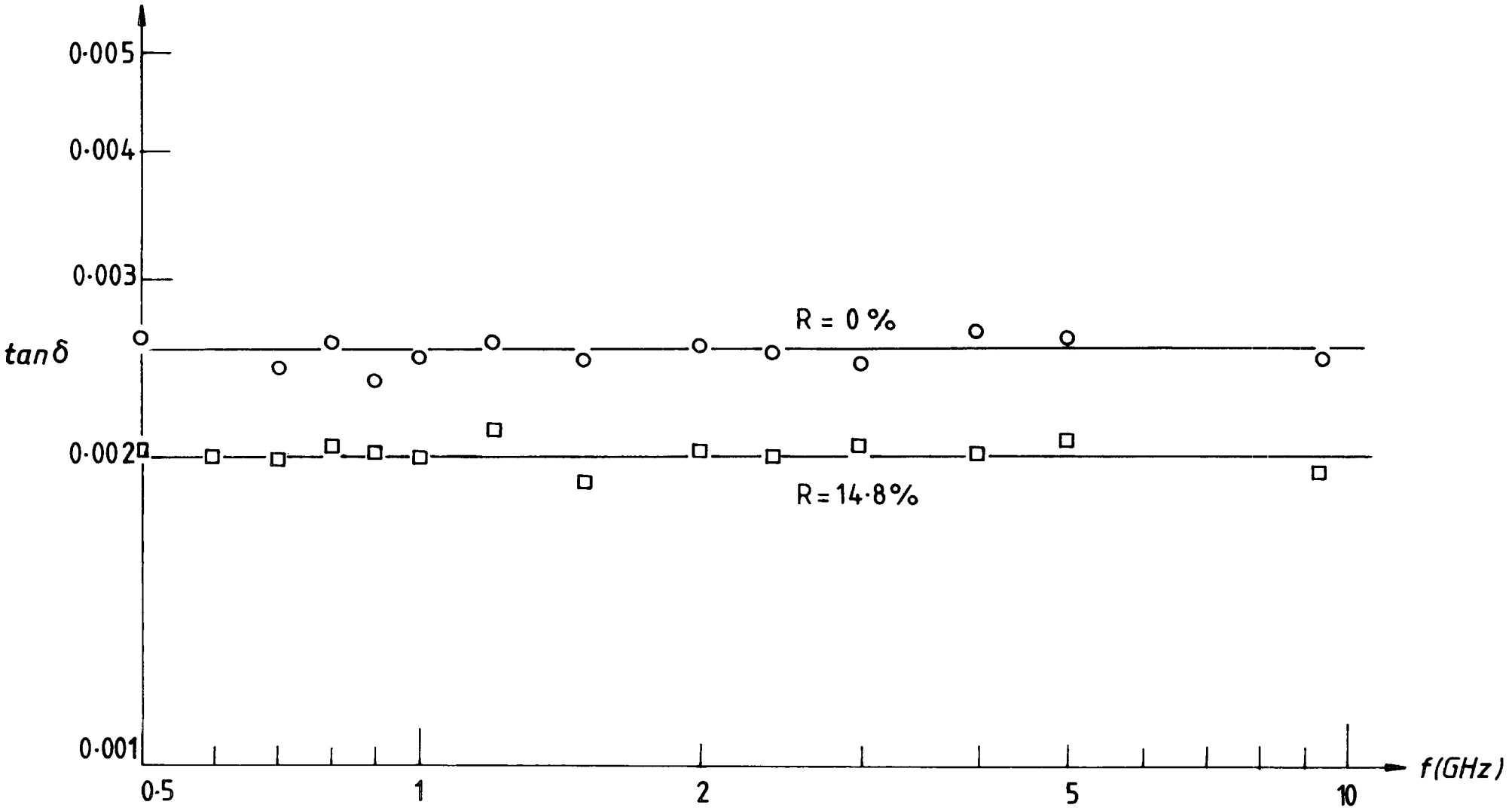

Fig.8·6 Frequency dependence of loss tangent for yttrium glasses

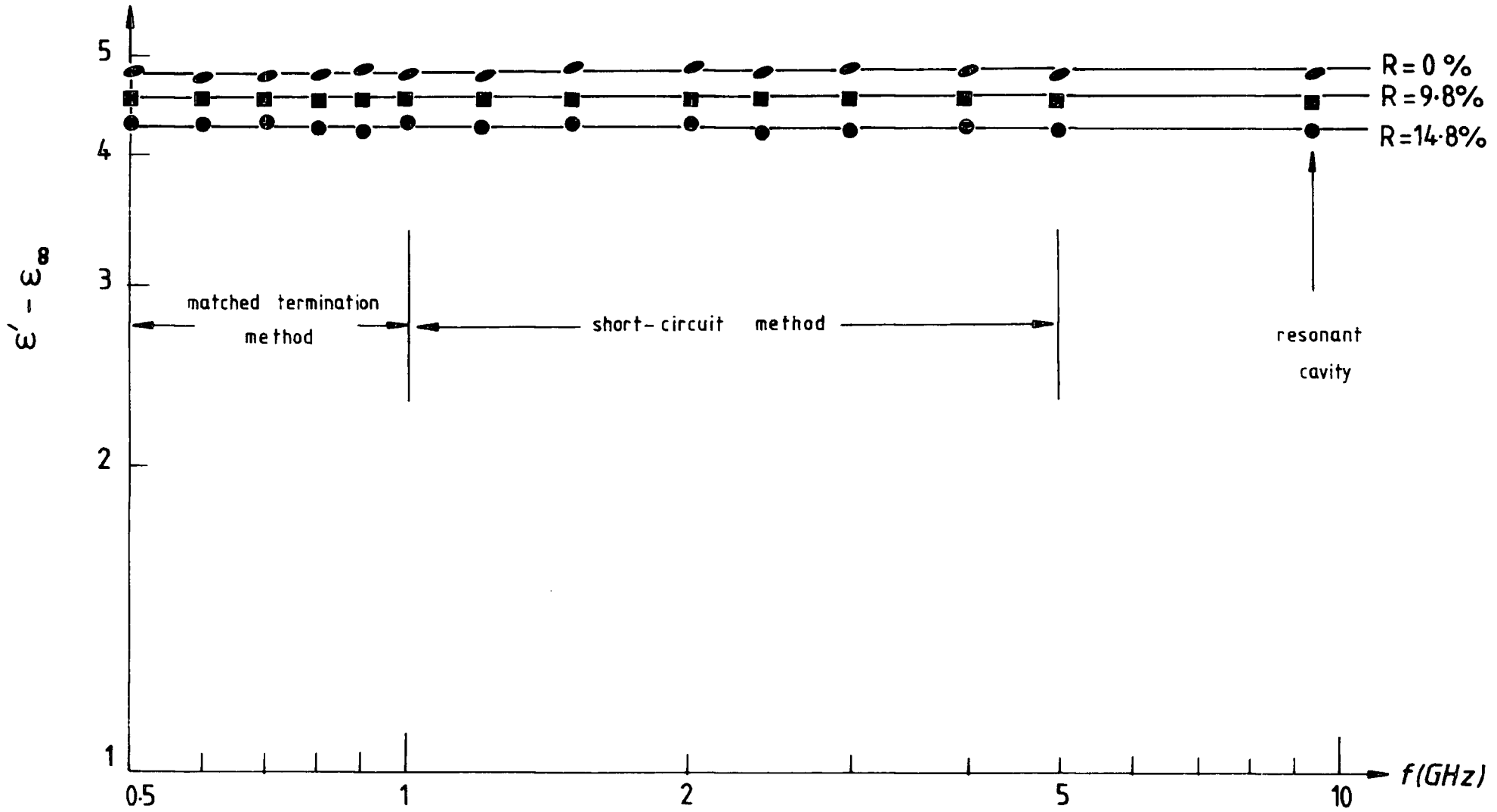

Fig. 8·7 Variation of reduced dielectric constant with frequency for calcium glasses

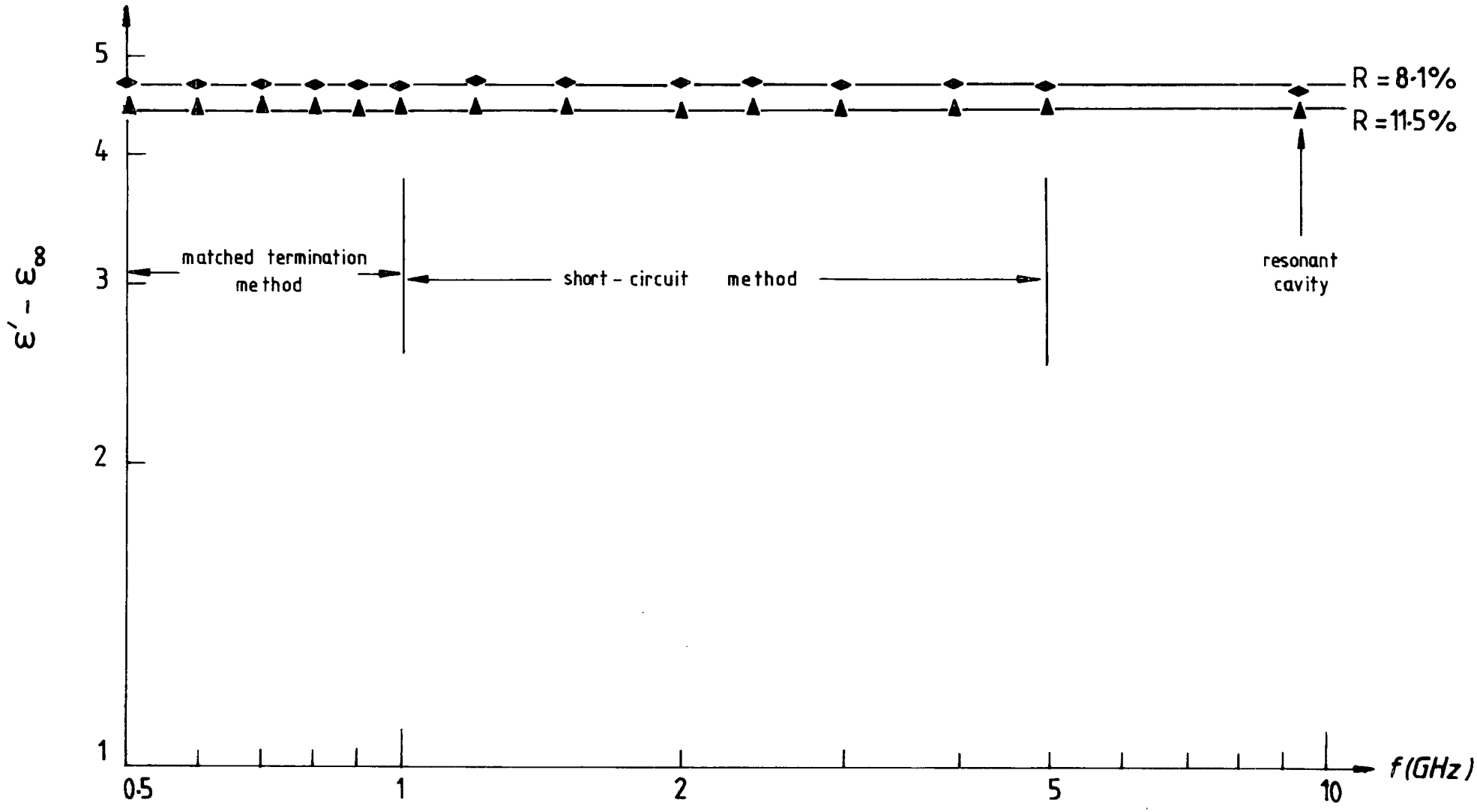

Fig. 8·7 (continued)

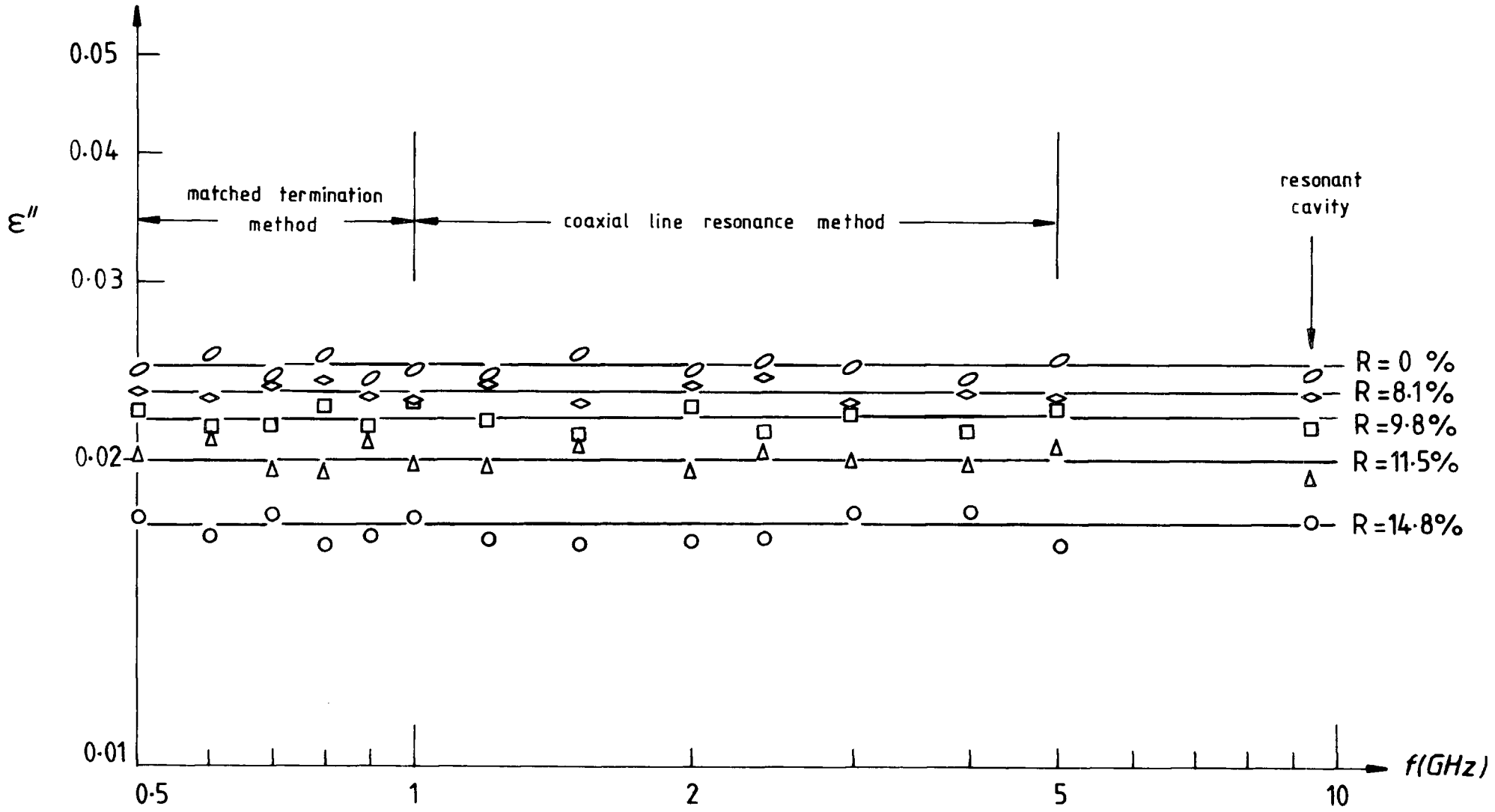

Fig. 8·8 Frequency dependence of loss factor for calcium glasses

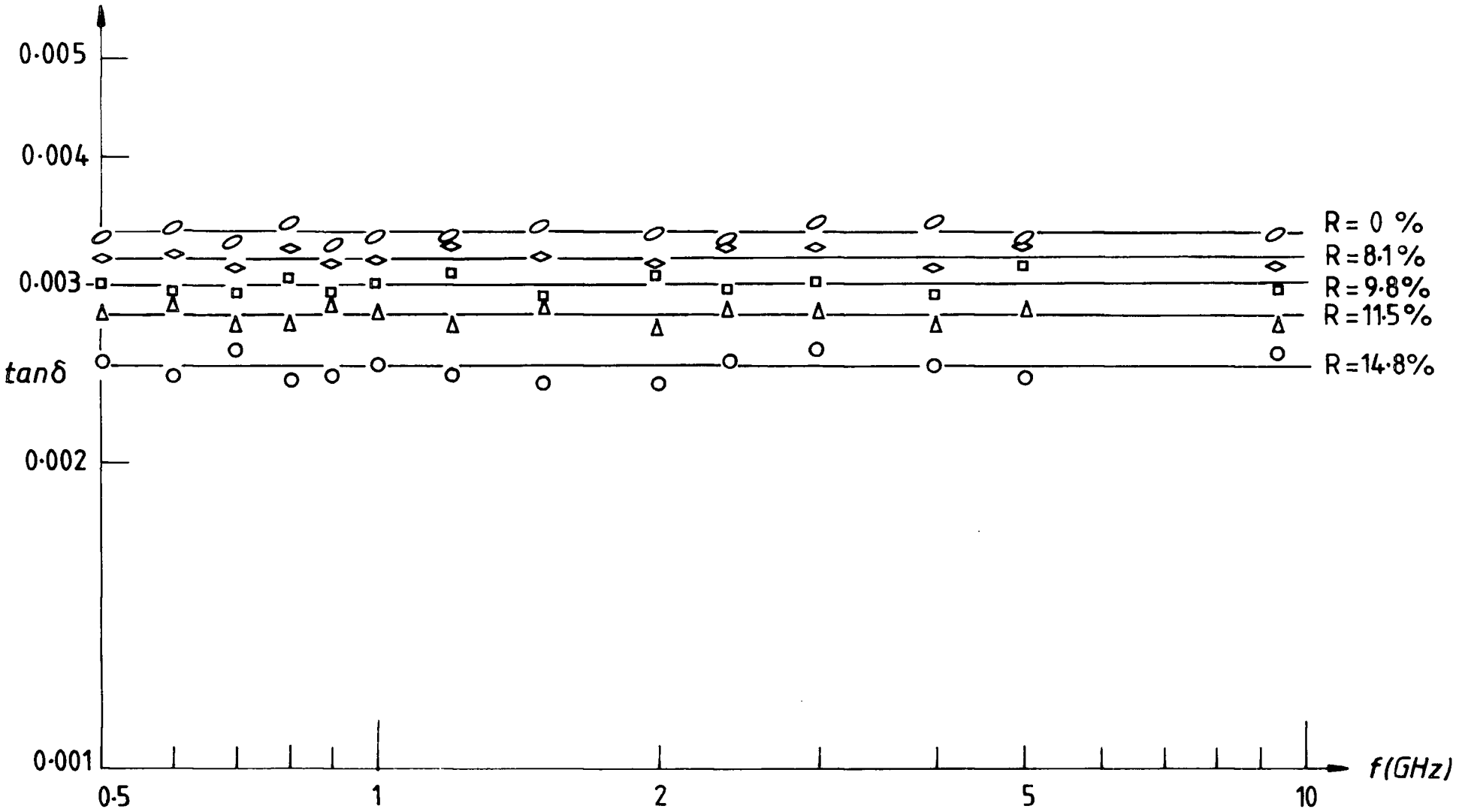

Fig. 8·9 Frequency dependence of loss tangent for calcium glasses

for all the five compositions. The loss tangent variations with frequency are given in Fig.8.9.

8.3 DISCUSSION

For all the oxide and oxynitride glasses studied it was found that for each composition the reduced dielectric constant $(\varepsilon' - \varepsilon_\infty)$ showed a linear variation with frequency. In all the systems, at any given frequency in the measurement range, the value of ε' was observed to depend on the composition, increasing as the nitrogen concentration increased. In addition, at each concentration, including the oxide glasses, ε' increased with cation type in the order Mg, Y, Ca. These are shown in Fig.8.10. Earlier Thorp and Kenmuir [8.12, 8.13] have observed the same trends in the variations of ε' on composition for Mg, Ca, Y and Nd oxynitride glass systems between 500 Hz and 10 kHz. They had also observed that ε' increased with cation type in the same order Mg, Y, Ca. The power law behaviour of ε' on frequency is in good agreement with the universal dielectric response law in solids in that $(\varepsilon' - \varepsilon_\infty) \propto \omega^{n-1}$, where the exponent n had the same value 1.0 ± 0.05 for all the compositions studied. Plots of the loss factors also showed linear variations with frequency for all the compositions. These plots again yield, from the dependence $\varepsilon'' \propto \omega^{n-1}$, n values similar to those found for the dielectric constant plots. Since the a.c. conductivity may

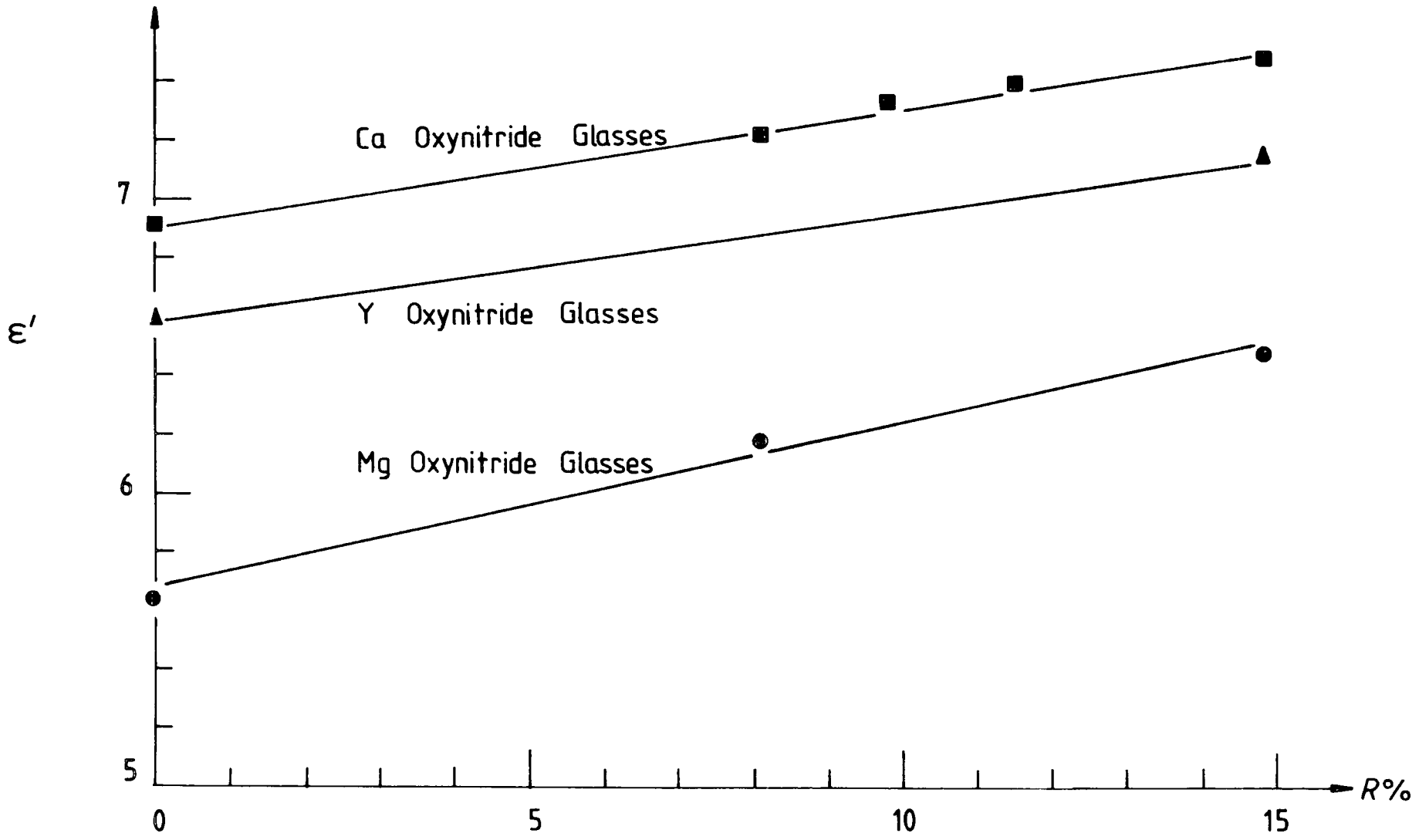

Fig.8·10 Variation of dielectric constant with % oxygen replaced by nitrogen in oxynitride glasses

be calculated from the loss factor through the relation $\sigma = \omega\varepsilon_o\varepsilon''$, it can be inferred that the variation of conductivity is also linear for each composition, giving a power law dependence $\sigma \propto \omega^n$, with an n value about 1. The fact that the same n value was found for all the samples suggests that, at room temperature for this frequency range, dielectric polarization and a.c. conductivity in all the compositions examined result from the same hopping mechanism, and that this mechanism is not changed by the substitution of nitrogen.

However, unlike the behaviour of the dielectric constant, the dependence of the dielectric loss on nitrogen concentration varied from one system to another. Substitution of 14.8 % of oxygen by nitrogen increased $\tan\delta$ by 39 % for magnesium glasses, by 22% for calcium glasses and decreased $\tan\delta$ by 16% for yttrium glasses, Fig.8.11. These figures may be compared with those of Thorp and Kenmuir [8.13] where increases of 55% and 13% for magnesium and calcium glasses, and a decrease of 20% for yttrium glasses were observed between 500 Hz and 10 kHz for the same increase in nitrogen concentration. It is interesting to note the close similarity between the values obtained in the two frequency ranges and further that the contrast in behaviour between the yttrium glass and the others has been confirmed. Similar dielectric behaviour have been noted by Loehman [8.15] and Leedecke and Loehman [8.16] . It was

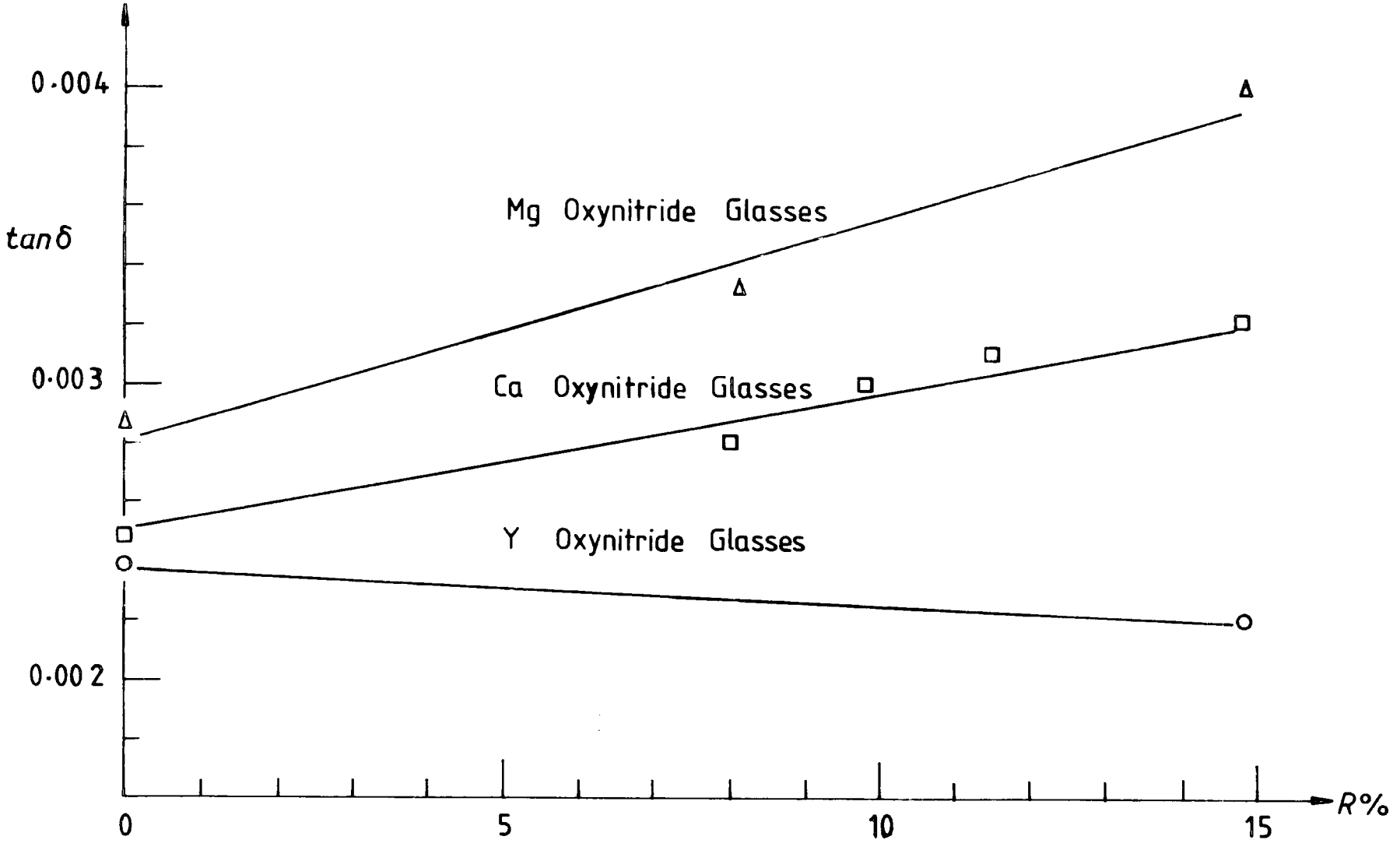

Fig. 8·11 Variation of loss tangent with % oxygen replaced by nitrogen in oxynitride glasses

reported that the dielectric constant increased when 1.5 atomic percent of nitrogen was substituted for the same amount of oxygen in a yttrium oxynitride glass. For this glass the loss tangent and room temperature a.c. conductivity decreased with nitrogen substitution by amounts larger than those observed by Thorp and Kenmuir and in the present case.

It is evident that substitution of nitrogen into oxide glasses increases the dielectric constant and produces changes in the loss in a manner which also depends on the other constituents of the glasses. Systematic variations in the compositions are necessary if the effects of nitrogen are to be distinguished. Oxynitride glasses may be prepared in which the dielectric properties can be controlled and hence enhance other physical properties, for example, by incorporating nitrogen the mobility of alkali ions in the material is reduced, increasing d.c. resistivity and reducing devitrification near electrodes due to electrolysis [8.11, 8.17] . It is also found that oxynitride glasses are harder and more refractory [8.11, 8.18, 8.19] .

Since the present measurements, made over the range 500 MHz to 9.34 GHz, and the previous observations, made by Thorp, Kulesza and Kenmuir [8.13] over the lower frequency region from 500 Hz to 20 kHz, were all taken with the same series of oxynitride glass samples a unique opportunity exists for assessing the dielectric behaviour over this very extensive frequency range. A number of important features are revealed.

For each individual glass composition the frequency

dependence of both the dielectric constant ε' and loss ε'' follows the variation expected from the Universal Law of dielectric response with the value of the exponent n being $n = 1.0 \pm 0.1$. Taking the results for all the individual compositions collectively reveals that this whole group of rigid ceramics gives dielectric behaviour corresponding to the limiting form of "lattice loss" [6.11] in which most dipolar processes have been eliminated and frequency independent loss is expected. This is not common though it is interesting to note that similar properties have been reported both for doped magnesium oxide, a rigid refractory oxide ceramic and for several sialon materials, high strength refractory ceramics containing oxygen and nitrogen [8.20, 8.21] .

A second point of interest is to note the range of value of ε' which can be obtained by compositional changes in the glass systems. At the lowest extreme one finds $\varepsilon' \simeq 5.6$ at 1 GHz for magnesium oxide glass and at the highest $\varepsilon' = 11.6$ at 1 kHz for a neodymium oxynitride glass containing 8.8 atomic percent nitrogen. This wide range suggests potential for the choice of special glasses where dielectric matching is important, e.g. in substrate materials for devices. In the oxide glasses ε' is dependent on the cation type and increases in the order Mg, Y, Ca, Nd while in all the systems the addition of nitrogen increases ε'. It should be noted however that there are limits to the latter method for increasing ε' since, depending on the particular system, the maximum nitrogen solubility lies in the range 10 - 15 atomic percent, the highest nitrogen containing glasses so far produced [8.14] being in the Y-Si-Al-O-N system. It would be of interest to compare simpler oxide and nitride

systems (e.g. Al_2O_3 and AlN ; SiO_2 and Si_3N_4) to find whether there are generalized behaviour rules for nitrogen substitution or whether the effects described above are specific to the oxynitride glasses examined here.

A third feature revealed by a comparison of measurements in the different frequency ranges relates to the cation order found to give increasing values of dielectric constant. This feature may most easily be demonstrated by reference to oxide glasses. At lower frequencies (i.e. 1.6 kHz, [8.13]) it can be stated quite definitely that ε' changes with cation in the order $Mg < Y < Ca < Nd$; here the differences in ε' between compositions are very much greater than any possible experimental errors so the trend is firmly established. A similar result has now been found at the higher frequencies (between 500 MHz and 10 GHz) and the coaxial line and perturbation measurements confirm that ε' increases in the order $Mg < Y < Ca$. However, the values of ε_∞ , obtained from refractive index measurements made in the visible range at wavelengths near 500 nm, determine the cation order for increasing ε_∞ as $Mg < Ca < Y < Nd$. Assuming the validity of the optical measurements [8.14] , which there is no apparent reason to doubt, this suggests a changeover in order between yttrium and calcium somewhere between the microwave and optical regions.

Some remarks may be made in conclusion regarding the influence of nitrogen substitution on the dielectric loss ε'' . Unlike the behaviour of the dielectric constant ε' the dependence of dielectric loss on nitrogen concentration varied from system to

system. The measurements in the lower frequency range showed that an increase in nitrogen concentration produced a relatively large increase in $\tan\delta$ in the magnesium glasses and a smaller though definite increase in the calcium glasses; by contrast a small decrease was observed in the yttrium glasses. The differences in behaviour has been confirmed by the new measurements in the higher frequency range. If the changes in dielectric loss are to be attributed to changes in chemical bonding there seems no obvious reason why the yttrium ion should differ so markedly from both calcium and magnesium. The value of $\tan\delta$ for yttrium oxynitride glasses can approach 0.001 which puts them in a competitive position relative to other materials (e.g. SiO_2) accepted as good insulators. It must be borne in mind however that, at the present stage of development of the preparative techniques for making the oxynitride glasses, there may be other impurities present at low levels and that the measured dielectric loss may be determined by these rather than being a direct monitor of the changes in cation-oxygen or cation-nitrogen bonding schemes. This re-emphasises the desirability for undertaking dielectric measurements on simpler oxide, nitride and oxynitride systems which can be obtained in a higher state of purity.

8.4 REFERENCES

8.1 Wild S., Jack K.H. and Latimer M.J.," Role of magnesia in hot-pressed silicon nitride ", Popper P. (Ed.)," Special Ceramics 5 ", Brit. Ceram. Res. Assn., 377(1972)

8.2 Gazza G.E.," Silicon nitride / yttria: potential gas turbine material ", U.S. Nat. Technol. Inform. Serv., AD Report No. AD - A025998(1976)

8.3 Buang K.B.," The Magnesium, Cerium and Zirconium Sialons ", Ph.D. Thesis, University of Newcastle-upon-Tyne (1979)

8.4 Gazza G.E.," Effects of yttria addition on hot-pressed silicon nitride ", Am. Ceram. Soc. Bull., vol.54,778(1975)

8.5 Terwilliger G.R. and Lange F.F.," Properties of sintered silicon nitride ", J. Am. Ceram. Soc., vol.57,25(1974)

8.6 Drew P. and Lewis M.H.," Microstructure of silicon nitride ceramics during hot-pressing transformations ", J. Mat. Sci., vol.9,261(1974)

8.7 Jack K.H.," Ceramics for High-Performance Applications ", Burke J.J., Corum A.E. and Katz R.N. (Eds.), Proc. 2nd Army Mater. Tech. Conf. (Brook Hill Pub. Co., Chestnut Hill, Mass.), 265(1974)

8.8 Oyama Y. and Kamigaito O.," Solid solubility of some oxides in Si_3N_4 ", Jap. J. Appl. Phys., vol.10,1637(1971)

8.9 Jack K.H., Technical Report, European Research Office,

United States Army, Grant No. DAERO-76-9-067

8.10 Jack K.H.," Nitrogen Ceramics ", Proc. NATO Adv. Study Inst., Riley F. (Ed.), (Noordhof, Leyden), 257(1977)

8.11 Elmer T.H. and Nordberg M.E.," Effects of nitriding on electrolysis and devitrification of high-silica glasses ", J. Am. Ceram. Soc., vol.50,275(1967)

8.12 Thorp J.S. and Kenmuir S.V.J.," Dielectric properties of some oxynitride glasses ", J. Mat. Sci., vol.16,1407 (1981)

8.13 Kenmuir S.V.J., Thorp J.S. and Kulesza B.L.J.," The dielectric behaviour of Mg-Al-Si, Ca-Al-Si, Y-Al-Si and Nd-Al-Si oxynitride glasses, to be published in J. Mat. Sci.

8.14 Drew R.A.L.," Nitrogen Ceramics ", Ph.D. Thesis, University of Newcastle-upon-Tyne (1980)

8.15 Loehman R.E.," Preparation and properties of yttrium-silicon-aluminium oxynitride glasses ", J. Am. Ceram. Soc., vol.62,49(1979)

8.16 Leedecke C.J. and Loehman R.E.," Electrical properties of yttrium-aluminium-silicon oxynitride glasses ", J. Am. Ceram. Soc., vol.63,190(1980)

8.17 Elmer T.H. and Nordberg M.E., Proc. 7th Int. Cong. Glass, Brussels, Belgium (Institut Nationale du Vere, Charleroi, Belgium), 30.1(1965)

8.18 Harding F.L. and Ryder R.J.," Effects of silicon nitride additions to a container glass batch ", Glass Technol., vol.11,54(1970)

8.19 Shillito K.R., Wills R.R. and Bennett R.B.," Silicon metal oxynitride glasses ", J. Am. Ceram. Soc., vol.61,537(1978)

8.20 Thorp J.S., Kulesza B.L.J., Rad N.E. and Kenmuir S.V.J., " High frequency dielectric properties of magnesia, iron/ magnesia and chromium/magnesia ", J. Mat. Sci., vol. 16, 1052(1981)

8.21 Thorp J.S. and Sharif R.I.," Dielectric properties of some hot-pressed nitrogen ceramics ", J. Mat. Sci., vol. 12, 2274(1980).

CHAPTER 9

CONCLUSIONS

For the most part in this thesis the relevant discussions and conclusions have been made at the end of the appropriate chapters. However, it is helpful in addition to make general comments and summary conclusions at the end of this work. Suggestions of possible improvements to the measurement methods developed are also outlined. As a whole the research suggests two main areas of interest firstly, the development and refinements of the measurement techniques and secondly, application of these to the measurements of the dielectric properties of materials in both solid and liquid form.

In an effort to reduce the VSWR to acceptable measurement levels, the matched termination was used. With the air gap spacings < 0.6 mm it produced values of VSWR of $\lesssim 100$ at frequencies of 500 MHz or higher. This is very much less than in the usual short-circuit method where the VSWR's are of the order of thousands. However, in the matched termination case at higher frequencies, the VSWR becomes too low when a material under test is introduced into the sample-holder. This increases the uncertainty in the standing-wave minima positions, consequently restricting the usefulness of the method to lower frequencies. Instead of the matched termination (Z_o), smaller resistive loads may be used to

terminate the sample-holder. These loads may be in the form of two matched terminating loads connected in parallel by a coaxial T-junction, giving half the initial value ($Z_o/2$). Calculations for loads of $Z_o/4$ up to $3Z_o/4$ showed that easily measurable VSWR values are obtained for an empty sample-holder with gap spacings of about 0.5 mm and for frequencies up to 8 GHz. The necessary equations for solving ε' and ε'' or $\tan\delta$ were not fully derived, however, since this would involve more detailed considerations of the equivalent circuit. This is one possible way which can be developed for dielectric measurements.

The coaxial line resonance method may be further improved and extended to cover good insulating low loss materials by re-examining the analysis of the equivalent circuit when a thicker sample is used. This will decrease the capacitance or equivalently increase the impedance due to the sample, hence lowering the maximum VSWR at resonance. Low loss materials having $\tan\delta < 10^{-3}$, which would normally give very high VSWR's, can thus be brought within the measurable range. It was found that even the low loss PTFE sample ($\tan\delta \sim 3 \times 10^{-4}$) of thickness 1 mm gave a maximum VSWR at resonance of 530 at 1 GHz (Appendix C). In comparison the short-circuit method would have given a VSWR of the order $\sim 2 \times 10^{4}$, which cannot normally be measured in practice because of overloading of the diode detector and very poor signal-to-noise ratio at the standing-wave minima. As the

sample thickness increases a rigorous treatment of the increased fringing-field effect is required before advantage can be taken of the reduced VSWR at resonance. This line of approach has not been undertaken since one of the primary aims of this research was to construct a suitable sample-holder and to test the matched termination and resonant line ideas. The validity of these ideas have been amply demonstrated by the good agreement with published data of a wide variety of materials from solids to liquids and spanning a wide range of loss.

In the nitrogen ceramics studied the results are best explained by the limiting case of the universal dielectric response law of Jonscher. A dependence of dielectric constant with frequency, i.e. $(\varepsilon' - \varepsilon_\infty) \propto \omega^{n-1}$, was observed for each of the samples where n was approximately unity. Similarly, for each sample the loss factor variation with frequency fitted the relation $\varepsilon'' \propto \omega^{n-1}$, where again n was close to unity. This corresponds to a frequency independent dielectric loss where most dipolar processes have been eliminated.

In the silicon nitride ceramics, chemical, X-ray or spectrographic analyses would be required to numerically relate weight gain with free silicon content. This would then enable weight gain to be a quantitative measure of the amount of free silicon. This in turn implies that the dielectric

constant or loss factor may be used as an indirect measure of the free silicon content which is responsible for the large variations in dielectric properties.

The measurements obtained from oxynitride glasses in which nitrogen was substituted for oxygen confirmed the trends observed at lower frequencies by Thorp and Kenmuir [8.12, 8.13] and others [8.15, 8.16] . In all the glasses, at any frequency in the measurement range, the dielectric constant increased with increasing nitrogen concentration. Also, at each nitrogen concentration the dielectric constant increased with cation type in the order Mg, Y, Ca. However, unlike the behaviour of the dielectric constant, the dependence of the loss factor on nitrogen concentration varied from one system to another. While the loss factor increased with increasing concentration in the Mg and Ca oxynitrides, the Y glasses showed a decrease. The anomalous behaviour exhibited by the Y oxynitrides have also been observed at lower frequencies [8.13, 8.16] . Systematic variations in compositions are necessary if the effects of nitrogen or any constituent on the dielectric properties are to be identified.

Some suggestions for improving the measurements of dielectric properties have already been described earlier. In this and the following paragraphs additional extensions of the methods which may be carried out in future are described.

A possibility that can be tested is to intentionally incorporate a standard material of known characteristics into the coaxial sample-holder. This may take the form of a capacitor in series and adjacent to the material under test. The geometry and dimensions of this combination of capacitances can be manipulated to produce the desired measurable VSWR.

Inserts constructed from material transparent to microwaves can be placed in the inner conductor gap of the coaxial sample-holder. This would be useful for the measurement of liquids and powders which are important in many industrial applications. In such a way more flexibility in sample thickness for optimum measurement conditions may be introduced. In addition, the meniscus effect and volatization problems associated with previous measurements, where the liquid is simply held in place by its surface tension forces, would be eliminated.

APPENDIX A

OPTIMUM CAPACITANCE CALCULATIONS

The frequency dependent real and imaginary components of the complex permittivity, from equation (2.9), are:

$$\varepsilon'(\omega) = \frac{2|\Gamma(\omega)|\sin[-\theta(\omega)]}{\omega C_o Z_o\left[1 + 2|\Gamma(\omega)|\cos\theta(\omega) + |\Gamma(\omega)|^2\right]} - \frac{C_f}{C_o}$$

$$\varepsilon''(\omega) = \frac{1 - |\Gamma(\omega)|^2}{\omega C_o Z_o\left[1 + 2|\Gamma(\omega)|\cos\theta(\omega) + |\Gamma(\omega)|^2\right]} \qquad \text{(A.1)}$$

The terms in the square brackets in the denominators can be written as $D(\omega)$. For clarity and convenience the frequency dependence will be dropped off hereafter and assumed understood. The uncertainties in ε' and ε'', assuming that C_f does not vary with frequency and the small uncertainty in C_f/C_o is negligible, are

$$\Delta\varepsilon' = \left[\left(\frac{\delta\varepsilon'}{\delta C_o}\Delta C_o\right)^2 + \left(\frac{\delta\varepsilon'}{\delta Z_o}\Delta Z_o\right)^2 + \left(\frac{\delta\varepsilon'}{\delta|\Gamma|}\Delta|\Gamma|\right)^2 + \left(\frac{\delta\varepsilon'}{\delta\theta}\Delta\theta\right)^2\right]^{\frac{1}{2}}$$

$$\Delta\varepsilon'' = \left[\left(\frac{\delta\varepsilon''}{\delta C_o}\Delta C_o\right)^2 + \left(\frac{\delta\varepsilon''}{\delta Z_o}\Delta Z_o\right)^2 + \left(\frac{\delta\varepsilon''}{\delta|\Gamma|}\Delta|\Gamma|\right)^2 + \left(\frac{\delta\varepsilon''}{\delta\theta}\Delta\theta\right)^2\right]^{\frac{1}{2}} \qquad \text{(A.2)}$$

where ΔC_o, ΔZ_o, $\Delta|\Gamma|$ and $\Delta\theta$ are respectively the uncertainties in the capacitance of the empty sample-holder, the characteristic impedance, the magnitude and phase of the reflection coefficient. It will be evident that

$$\frac{\delta\varepsilon'}{\delta C_o} = \frac{-2|\Gamma|\sin(-\theta)}{\omega C_o^2 Z_o D(\omega)} = \frac{-\varepsilon'}{C_o} \qquad (A.3)$$

$$\frac{\delta\varepsilon'}{\delta Z_o} = \frac{-2|\Gamma|\sin(-\theta)}{\omega C_o Z_o^2 D(\omega)} = \frac{-\varepsilon'}{Z_o} \qquad (A.4)$$

$$\frac{\delta\varepsilon'}{\delta|\Gamma|} = \frac{2(1-|\Gamma|^2)\sin(-\theta)}{\omega C_o Z_o D^2(\omega)} = \frac{\omega C_o Z_o \varepsilon'\varepsilon''}{|\Gamma|} \qquad (A.5)$$

and

$$\frac{\delta\varepsilon'}{\delta\theta} = \frac{2|\Gamma|\{(1+|\Gamma|^2)\cos(-\theta)+2\}}{\omega C_o Z_o D^2(\omega)}$$

$$= \frac{1+(\omega C_o Z_o)^2(\varepsilon'^2-\varepsilon''^2)}{2\omega C_o Z_o} \qquad (A.6)$$

Similarly

$$\frac{\delta\varepsilon''}{\delta C_o} = \frac{-(1-|\Gamma|^2)}{\omega C_o^2 Z_o D(\omega)} = \frac{-\varepsilon''}{C_o} \qquad (A.7)$$

$$\frac{\delta\varepsilon''}{\delta Z_o} = \frac{-(1-|\Gamma|^2)}{\omega C_o Z_o^2 D(\omega)} = \frac{\varepsilon''}{Z_o} \qquad (A.8)$$

$$\frac{\delta\varepsilon''}{\delta|\Gamma|} = \frac{2\{2|\Gamma|+(1+|\Gamma|^2)\cos(-\theta)\}}{\omega C_o Z_o D^2(\omega)}$$

$$= \frac{1+(\omega C_o Z_o)^2(\varepsilon'^2-\varepsilon''^2)}{2\omega C_o Z_o|\Gamma|} \qquad (A.9)$$

and

$$\frac{\delta\varepsilon''}{\delta\theta} = \omega C_o Z_o \varepsilon'\varepsilon'' \qquad (A.10)$$

Substituting equations A(3) to A(10) into equations A(2) we obtain

the fractional uncertainties:

$$\frac{\Delta\varepsilon'}{\varepsilon'} = \left[\left(\frac{\Delta C_o}{C_o}\right)^2 + \left(\frac{\Delta Z_o}{Z_o}\right)^2 + \left(\varepsilon''\omega C_o Z_o \frac{\Delta|\Gamma|}{|\Gamma|}\right)^2 + \left(\frac{1+(\omega C_o Z_o)^2(\varepsilon'^2-\varepsilon''^2)}{2\omega C_o Z_o \varepsilon'}\Delta\theta\right)^2\right]^{\frac{1}{2}} \quad \text{(A.11)}$$

$$\frac{\Delta\varepsilon''}{\varepsilon''} = \left[\left(\frac{\Delta C_o}{C_o}\right)^2 + \left(\frac{\Delta Z_o}{Z_o}\right)^2 + \left(\frac{1+(\omega C_o Z_o)^2(\varepsilon'^2-\varepsilon''^2)}{2\omega C_o Z_o \varepsilon''}\frac{\Delta|\Gamma|}{|\Gamma|}\right)^2 + (\varepsilon'\omega C_o Z_o \Delta\theta)^2\right]^{\frac{1}{2}} \quad \text{(A.12)}$$

The uncertainties ΔC_o and ΔZ_o result from the uncertainties in length measurements and for modern coaxial components may be assumed to be $\sim 1\%$, [1.17, 2.7]. The optimum values of $\omega C_o Z_o$, that is the values that give minimum values of $\Delta\varepsilon'/\varepsilon'$ and $\Delta\varepsilon''/\varepsilon''$, can be found by differentiating equations (A.11) and (A.12). After simplifying this lengthy process, certain conditions are found. The minimum of $\Delta\varepsilon'/\varepsilon'$ occurs when

$$\frac{1}{\omega C_o Z_o} = \left[\left(\frac{2\varepsilon'\varepsilon''}{\Delta\theta}\frac{\Delta|\Gamma|}{|\Gamma|}\right)^2 + (\varepsilon'^2 - \varepsilon''^2)^2\right]^{\frac{1}{4}} \quad \text{(A.13)}$$

and the minimum of $\Delta\varepsilon''/\varepsilon''$ occurs when

$$\frac{1}{\omega C_o Z_o} = \left[\left(2\varepsilon'\varepsilon''\Delta\theta \Big/ \frac{\Delta|\Gamma|}{|\Gamma|}\right)^2 + (\varepsilon'^2 - \varepsilon''^2)^2\right]^{\frac{1}{4}} \quad \text{(A.14)}$$

For lossless materials ($\varepsilon'' = 0$), equation (A.13) reduces to

$$\frac{1}{\omega C_o Z_o} = \varepsilon' \qquad \text{(A.15)}$$

Hence the optimum capacitance of the empty sample-holder is given by

$$C_o = \frac{1}{\omega Z_o \varepsilon'} \qquad \text{(A.16)}$$

It will be seen that equations (A.13) and (A.14) are identical if $\Delta\theta = \Delta|\Gamma|/|\Gamma|$ and the optimum value is obtained when

$$\frac{1}{\omega C_o Z_o} = \left(\varepsilon'^2 + \varepsilon''^2\right)^{\frac{1}{2}} \qquad \text{(A.17)}$$

For medium to low loss materials ($\varepsilon'' \lesssim 10^{-1}$) and for $\varepsilon' \gtrsim 3$, the conditions in equations (A.16) and (A.17) may be combined to give

$$\omega Z_o C_o |\varepsilon^*| = 1 \qquad \text{(A.18)}$$

The optimum capacitance of the empty sample-holder may thus be taken as

$$C_{opt} = \frac{1}{2\pi f Z_o} \cdot \frac{1}{\sqrt{\varepsilon'^2 + \varepsilon''^2}} \qquad \text{(A.19)}$$

APPENDIX B

CAVITY PERTURBATION METHOD

Measurements of dielectric properties at 9.34 GHz were carried out using a cubic cavity as previously described in references [7.18] and [2.8]. When a resonant cavity is perturbed by the introduction of a small sample its resonance frequency is lowered [B.1, B.2]. The change in resonance frequency is a function of the dielectric constant ε' and the change in cavity Q is a function of the loss factor ε'' of the material [B.1 - B.5]. In practice the resonance frequency and the loaded Q of the cavity with and without the the sample are measured. The results of the perturbation theory are expressed in the following form [B.1, B.2]

$$\frac{\Delta f}{f_o} - j\frac{1}{2}\Delta\left[\frac{1}{Q}\right] = \frac{(\varepsilon^* - 1)\int_{V_s} E_o E_s \, dV}{\int_{V_o} E^2 \, dV} \qquad B(1)$$

where

$$\Delta f = f - f_o$$

and

$$\Delta\left[\frac{1}{Q}\right] = \frac{1}{Q_s} - \frac{1}{Q_o} \qquad B(2)$$

The subscript s refers to the situation with the sample in the cavity and o refers to that of the empty cavity. V and f denote the volume and resonance frequency respectively, while E_s is the microwave field strength in the sample. For the

case of a rectangular or cubical cavity operating in the TE_{1on} mode equation B(1) reduces to the simpler forms

$$\frac{\Delta f}{f_o} = 2(\varepsilon' - 1)\frac{V_s}{V_o} \qquad B(3)$$

$$\Delta\left[\frac{1}{Q}\right] = 4\varepsilon''\frac{V_s}{V_o} \qquad B(4)$$

from which:

$$\varepsilon' = 1 + \frac{1}{2}\frac{\Delta f}{f_o}\frac{V_o}{V_s} \qquad B(5)$$

and

$$\varepsilon'' = \frac{1}{4}\frac{V_o}{V_s}\left[\frac{1}{Q_s} - \frac{1}{Q_o}\right] \qquad B(6)$$

As usual the loss tangent is calculated from $\tan\delta = \varepsilon''/\varepsilon'$.

In this method certain conditions must be met in order to satisfy the requirements of perturbation theory, namely:

(1) the Q of the cavity should be greater than 2000

(2) $\Delta f/f_o$ should be smaller than 0.005

(3) V_s/V_o should be less than 1/20.

A cubical cavity, of internal dimension 2.23 cm on a side, was constructed from copper, Fig.B.1. The Q of the empty cavity was approximately 3000. Cubic samples of sides about 2 to 5 mm gave the ratio $V_s/V_o < 1/80$. When the coaxial line disc-shaped samples were used here, the ratio $V_s/V_o < 1/60$. In both cases the volume ratios were well within the requirement (3) above. The sample was mounted at the centre of the cavity using a quartz rod, about half a millimetre

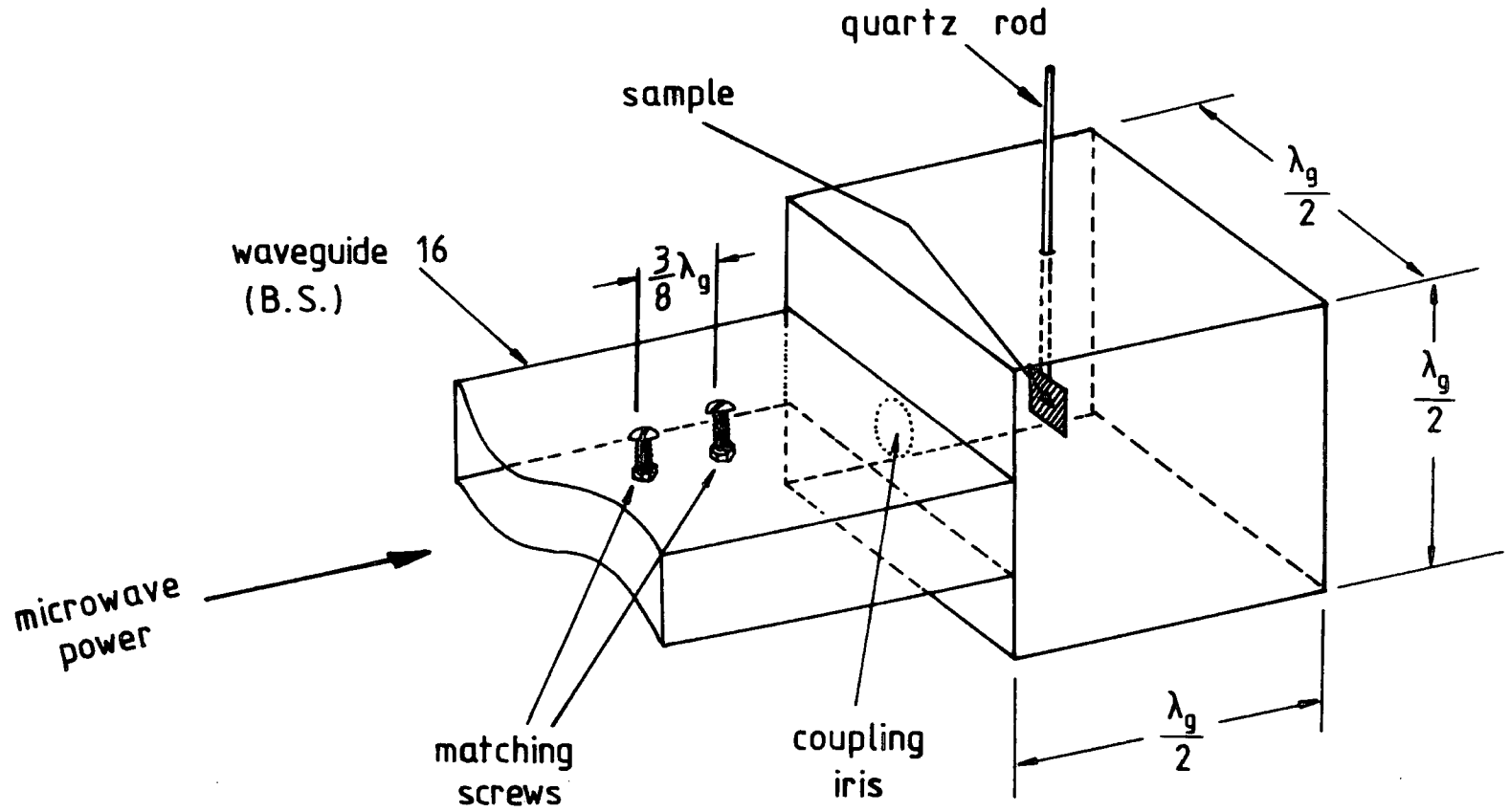

Fig. B·1 Cavity and sample arrangement for measurement of dielectric properties at 9·34 GHz

in diameter, so as to locate it at the position of zero magnetic field and maximum electric field [B.4]. A block diagram of the experimental set-up is shown in Fig.B.2, where the numbers denote the following:

1 : power supply

2 : reflex klystron

3 : modulator (RAMP generator)

4 & 7 : isolators

5, 8, 10 & 14 : attenuators

6 & 9 : directional couplers

11 : cavity wavemeter

12 : precision attenuator

13 & 15 : crystal detectors

16 : dual beam oscilloscope.

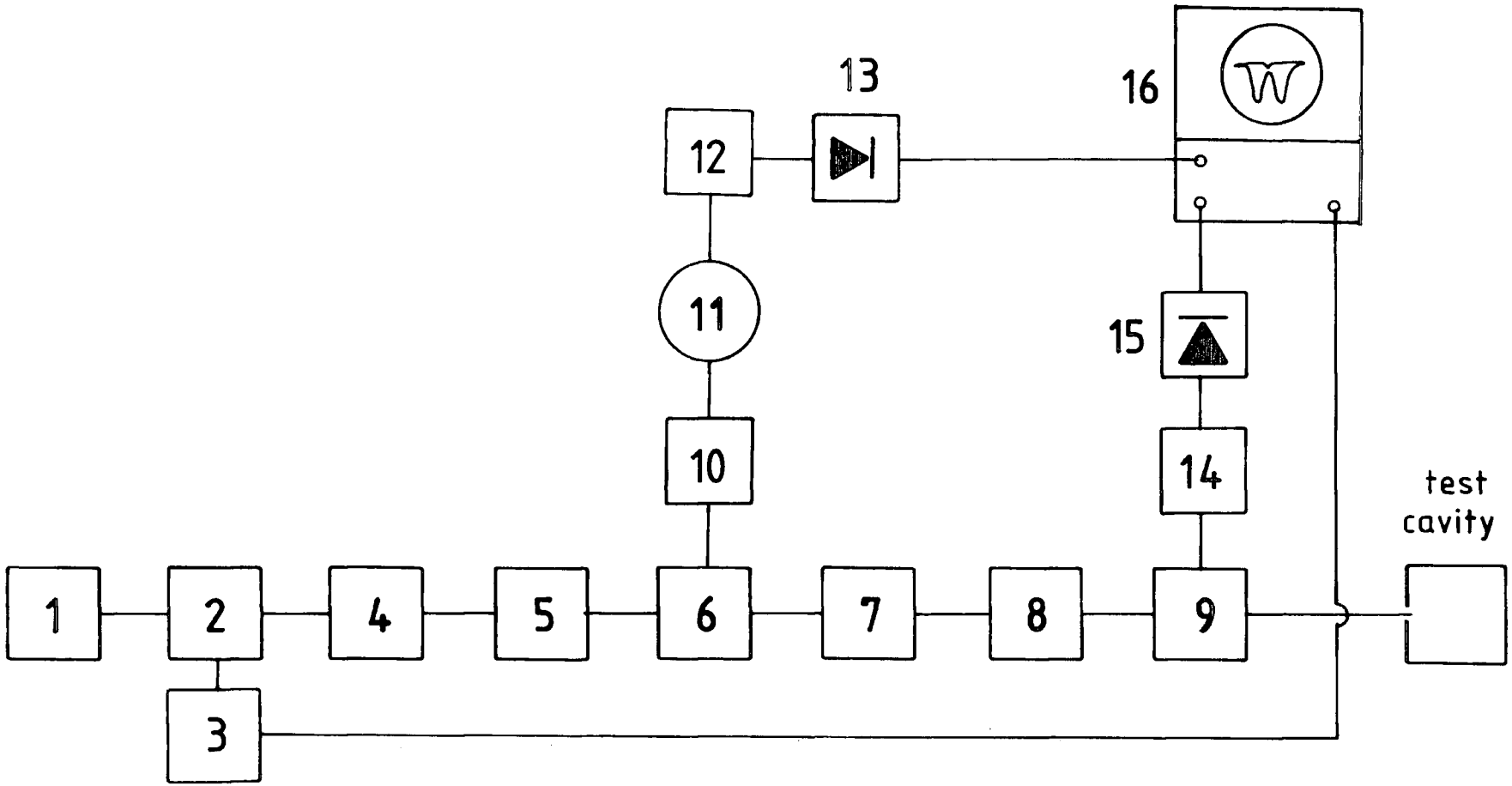

Fig. B·2 Block diagram of experimental set-up for the cavity perturbation method

REFERENCES

B.1 Sucher M. and Fox J. (Eds.)," Handbook of Microwave Measurements ", Vol.2, Polytechnic Press, Brooklyn, N.Y. (1963) chapt.8, 9

B.2 Kabashima S. and Kawakubo S.," A high frequency conductivity of Nio ", J. Phys. Soc. Jap., vol.24.493 (1968)

B.3 Casimir H.B.G.," On the theory of electromagnetic waves in resonant cavities ", Philip Res. Rep. No.6,162(1951)

B.4 Waldron R.A.," Perturbation theory of resonant cavities ", IEEE No. 373E, 272(1960)

B.5 Waldron R.A.," The Theory of Waveguide and Cavities ", Golden and Breach Science, N.Y.(1969)

APPENDIX C

Copy of Paper submitted for publication in the

Journal of Material Science

UNIVERSITY OF DURHAM

DEPARTMENT OF APPLIED PHYSICS AND ELECTRONICS

High Frequency
Measurements and
Applications Group

Report No. 23

COAXIAL LINE METHODS

FOR

DIELECTRIC CONSTANT MEASUREMENTS

by

B.L.J.Kulesza, J.S.Thorp and A. Bakar Ahmad

March 1983

1.0 Introduction

Two coaxial line techniques for the determination of complex permittivities of solids and liquids are described. Both methods use a coaxial sample-holder specially designed for this purpose, incorporating a parallel plate capacitor in series with the inner conductor.

The first, matched-termination method, is essentially a comparison technique using air as the reference dielectric. In this case, the changes in the voltage standing wave pattern are recorded when the sample material is inserted. Precise measurements of the reflection coefficient and shift in the standing wave minimum are of importance as the theory will show. In order to improve further the accuracy of measuring the Voltage Standing Wave Ratio, VSWR, its values are lowered by terminating the sample-holder with the characteristic impedance, Z_o.

In the second, the resonant line method, the characteristic impedance termination is replaced by an adjustable short circuit known as the reactive stub. After the test material is placed in the sample-holder the VSWR readings are taken and plotted against the varying stub lengths. Maximum occurs at resonance when the termination of the line is resistive and this value of VSWR, $VSWR_{MAX}$, is related to the loss tangent of the material, i.e. $\tan\delta = \frac{\varepsilon''}{\varepsilon'}$. The procedure can be successfully employed for low loss materials when the value of ε' is known ; possibly determined by the former matched-termination technique.

Both methods can be used for frequencies in the 200 MHz to 9 GHz range and normally require only conventional apparatus. It will be apparent from the following paragraphs, however, that better results are achievable with more sensitive instruments and higher precision components.

2.0 Coaxial Line Sample-Holder

The external and cross-sectional views of the sample-holder are shown in Fig 1 (a) & (b). It was made in brass with the internal and external diameters chosen to give theoretically a characteristic impedance, Z_o, of 50 ohms. The design was dimensionally based on the connector assembly of the General Radio slotted line system used in the measurements. Part of the inner conductor was

made replaceable to allow different sample thicknesses to be inserted also for a possible spring removal. The access to the gap is through a cut-out window on the outer conductor. When the sample-holder is in use a slide-on close-fitting ring clamps the window cover in place. Functional representation of the gap is given in Fig 1.(c).

The performance of the sample-holder was examined by measuring its VSWR over the operational frequency range when terminated with Z_o. The resulting plot in Fig.2 (a) for the unit with the gap closed satisfied the requirements adequately. Further, the deviation of VSWR from the calculated values as a function of the air gap spacing in Fig 2 (b) gave an additional check on the possible errors due to the sample-holder. These measurements helped in estimating the tolerances in the values of the reflection coefficient and later the accuracy of ε' and ε'' components of the complex permittivity constant. Such plots would normally be required at the frequencies of interest and for each sample-holder design. Calibration of sample-holders does not need any additional equipment or different procedures from those used in the actual dielectric measurements. The block diagram in Fig.3 shows the experimental apparatus and arrangement for the two methods.

3.0 The Matched Termination Method

3.1 Theory

The sample-holder with the material under test placed in the gap may be represented by an equivalent circuit of Fig.4. The series capacitance is given by $C_o \varepsilon_r^*$, where ε_r^* is the relative complex permittivity of the material, $\varepsilon'-j\varepsilon''$, and C_o in farads is a function of the air permittivity, ε_o, and the ratio of the cross-sectional area of the inner conductor, A, and the gap spacing, d, i.e. $\varepsilon_o \frac{A}{d}$. The fringing field capacitance, C_f, is associated with the inner conductor discontinuities (1,2).

When the sample-holder is terminated with the characteristic impedance,

the resulting line load may be approximated to, (3,4),

$$Z_L \approx \frac{1 + j\omega (C_o \varepsilon_r^* + C_f) Z_o}{j\omega (C_o \varepsilon_r^* + C_f)} \tag{1}$$

where ω is the radian frequency.

The reflection coefficient at A-A' may be expressed in terms of impedances (5) as

$$\Gamma_L = |\Gamma_L| e^{-j\Theta_L} = \frac{Z_L - Z_o}{Z_L + Z_o} \tag{2}$$

which for air dielectric, i.e. $\varepsilon_r^* = 1$, may be written as

$$|\Gamma_a| e^{-j\Theta_a} = \frac{1}{1 + j2\omega Z_o (C_o + C_f)} \tag{3}$$

and for dimensionally equivalent sample of material under test

$$|\Gamma_s| e^{-j\Theta_s} = \frac{1}{1 + j2\omega Z_o (C_o \varepsilon_r^* + C_f)} \tag{4}$$

Combining eqns (3) and (4) gives

$$\frac{|\Gamma_a|}{|\Gamma_s|} e^{j(\Theta_s - \Theta_a)} = \frac{1 + 2\omega Z_o C_o \varepsilon'' + j2\omega Z_o C_o \left(\varepsilon' + \frac{C_f}{C_o}\right)}{1 + j2\omega Z_o C_o \left(1 + \frac{C_f}{C_o}\right)} \tag{5}$$

On equating the real and imaginary parts and solving explicitly for ε' and ε'' we finally obtain

$$\varepsilon' = \frac{|\Gamma_a|}{|\Gamma_s|}\left\{\sqrt{\left(1+\frac{C_f}{C_o}\right)^2+\left(\frac{1}{2\omega Z_o C_o}\right)^2}\ \sin\Theta_s\right\} - \frac{C_f}{C_o} \qquad (6)$$

and

$$\varepsilon'' = \frac{|\Gamma_a|}{|\Gamma_s|}\left\{\sqrt{\left(1+\frac{C_f}{C_o}\right)^2+\left(\frac{1}{2\omega Z_o C_o}\right)^2}\ \cos\Theta_s\right\} - \frac{1}{2\omega Z_o C_o} \qquad (7)$$

where

$\Theta_s = 2\beta\ell_s$, ℓ_s is the standing wave minima location with the sample material as the dielectric

and $\beta = \frac{2\pi}{\lambda_g}$, λ_g being the wavelength.

Using Eqns. (6) and (7) or directly from eqn.4, we can get the following implicit relationship :-

$$\frac{\varepsilon' + {}^{C_f}\!/_{C_o}}{\varepsilon'' + {}^{1}\!/_{2\omega Z_o C_o}} = \tan\Theta_s \qquad (8)$$

leading to an approximation

$$\varepsilon' \simeq \frac{1}{2\omega Z_o C_o}\tan\Theta_s \qquad (9)$$

if

$$\frac{C_f}{C_o} \ll \varepsilon' \quad \text{and} \quad \varepsilon'' \ll \frac{1}{2\omega Z_o C_o}$$

The relationships between the reflection coefficient and the dielectric properties of the material under test, for a particular set of dimensions and frequency, are shown in Fig.5. The plots were obtained using eqns. (4) and (8), and require only the experimental values of the reflection coefficient magnitude and its angle to determine ε' and $\tan\delta$ for the sample material.

3.2 Measurements

In order to evaluate and determine the validity of the method, known well-documented materials were selected. The choice of a liquid as one material was deliberate, firstly as a new departure and secondly, because of the ease with which it can be placed in the gap of the sample-holder and maintained in position by means of its surface tension property. This gave also certain flexibility in the gap spacings and eliminated lengthy preparation of sample surfaces normally needed with solids.

Measurements were made using pure chlorobenzene for the liquid and a type of perspex PMMA (polymethyl-methacrylate) as the representative of solids.

The results for chlorobenzene covering the range 0.5 to about 3.0 GHz are given in Fig.6 (a) and compare favourably with the literature value for ε' of 5.7 (8,9,10). In the case of PMMA perspex, Fig 6(b), no precise data are available although the value of 2.6 for the ε' falls within the range of this type of materials (16, Moreno-plexiglas, p.204).

4.0 The Resonant Line Method

4.1 Theory

If the line is terminated with a reactance instead of the characteristic impedance, Z_o, standing waves will be produced along its length. Such termination can be achieved by using an adjustable lossless stub connected to the line as the load. The line, incorporating the sample-holder with air or material under test in the gap, presents a capacitive impedance (R and C in series). By varying the stub length a maximum reading in the voltage standing wave ratio, VSWR, will be observed when the inductance of the stub cancels the reactive part (C) of the line impedance. This condition of resonance results in a pure

resistance (R) which can be related to and deduced from the normalised minimum impedance value given by

$$\frac{R}{Z_o} = \frac{1}{VSWR_{MAX}} \tag{10}$$

according to transmission line theory (5). The equivalent circuit of the arrangement is shown in Fig.7 and produces the following relationships.

The impedance of the material sample may be written as

$$Z = \frac{1}{j\omega C_o \varepsilon_r^*} \tag{11}$$

where the symbols have the meanings previously defined.

On substitution for the complex permittivity

$$\varepsilon_r^* = \varepsilon' - j\varepsilon''$$

results in

$$Z = \frac{\varepsilon'' - j\varepsilon'}{\omega C_o (\varepsilon'^2 + \varepsilon''^2)} \tag{12}$$

which at resonance with the variable terminating stub gives on equating the real and imaginary parts

$$\frac{\varepsilon''}{\omega C_o (\varepsilon'^2 + \varepsilon''^2)} = R = \frac{Z_o}{VSWR_{MAX}} \tag{13}$$

and

$$\frac{\varepsilon'}{\omega C_o (\varepsilon'^2 + \varepsilon''^2)} = Z_o \tan \beta \ell_r \tag{14}$$

where

ℓ_r is the stub length at resonance.

Combining eqns. (13) and (14) leads to

$$\tan\delta = \frac{\varepsilon''}{\varepsilon'} = \frac{1}{VSWR_{MAX} \tan \beta \ell_r} \tag{15}$$

If, further, $\varepsilon'' << \varepsilon'$ approximations may be obtained

i.e.

$$\varepsilon' \approx \frac{1}{\omega C_o Z_o \tan \beta \ell_r} \tag{16}$$

and

$$\tan\delta \approx \varepsilon' C_o \frac{Z_o}{VSWR_{MAX}} \tag{17}$$

or

$$\varepsilon'' \approx \frac{1}{\omega C_o Z_o . VSWR_{MAX} . \tan^2 \beta \ell_r} \tag{18}$$

As can be seen from the above ε' may be determined from the resonant condition knowing only the relevant stub length, ℓ_r. On the other hand, for ε'' there is also a need to know the maximum value of VSWR measured at resonance. The value of $\tan\delta$ is given without any approximations by eqn.15 involving both parameters, $VSWR_{MAX}$ and ℓ_r.

4.2 Measurements

The apparatus arrangement was again as in Fig 3 which included the sample-holder without any modifications. The only difference was that now the line was terminated with an adjustable short circuit.

Chlorobenzene in cyclohexane solutions and water were used in the measurements as the liquid samples. As previously these were introduced into the gap of the sample-holder using a dropper and the stub was varied until a maximum reading in VSWR was obtained. The values of tan δ for pure and two solutions of chlorobenzene in cyclohexane, and pure distilled water were found in references

8,9,10 and 13, and 11 and 12, respectively, and plotted for comparison in Fig 8(a) and 8(b). The tan δ's for PMMA perspex were plotted against references 14, 15 and 16 in Fig 8(c).

The changes in the value of maximum VSWR over the frequency range 0.6 to 7.0 GHz for the two liquids are shown in Fig 9(a) and 9(b). Typical variations in VSWR plotted against the stub length are illustrated in Figs 10 (a), 10 (b), and 10 (c) for three solids, silicon, perspex and teflon.

5.0 Conclusions

The two methods just described, though independent, may be used for complementary measurements or mutual verification of results. These aims can be carried out with ease since the only difference between the two sets of apparatus is in the termination, i.e. matched load or variable short circuit stub.

The matched termination method produces reasonably accurate values of ε' as can be deduced from eqn.10 and amply supported by the results obtained for chlorobenzene and PMMA perspex shown in Figs 6(a) and 6(b), respectively. The values for ε'', on the other hand, were not in such a good agreement with the published information, for both materials although still very comparable. It suggests that the method using matched termination may be used with some confidence for finding ε'.

The resonant line method was essentially developed for the purpose of determining the values of tan δ in low loss materials. There are two parameters involved as shown by eqn.17, the maximum or the resonant value of VSWR and the resultant stub length. Representative examples of VSWR curves in order of increasing magnitudes for silicon, PMMA perspex and teflon, respectively are given in Figs 10(a), 10(b) and 10(C). Some difficulty may arise in measuring high VSWR values expected in the case of good insulators. Highly sensitive quality standing wave meters will normally have the range of 80 dB, 60 dB attenuator plus 20 dB on the meter scale. This would imply VSWR range of up

to 10^4 (20 dB ≡ a factor of 10) which, however, cannot be fully realised in practice because of overloading and noise-at-minima problems. A VSWR of 10^3 is possible with care allowing tan δ of 10^{-3} or less to be measured. There may also be additional difficulty of establishing graphically the actual $VSWR_{MAX}$ as is apparent in Figs 10(b) and (c) for perspex and teflon. If precise measurements are not possible around the peak, extrapolation of the slopes could give an estimate of the maximum value and the error involved.

REFERENCES

1. YOUNG L., "The practical realization of series capacitive couplings for microwave filters", Microwave J., 5, 79 (1962).

2. DAWIRS H.N., "Equivalent circuit of a series gap in the centre conductor of a coaxial transmission line", IEEE Trans.Microwave Theory and Techniques, 17, 127 (1969).

3. ISKANDER M.F. and STUCHLY, S.S., "Fringing-field effect in the lumped-capacitance method of permittivity measurement", IEEE Trans. Instrum. Meas. 27, 107 (1978).

4. VAN GEMERT M.J.C., "Theoretical analysis of the lumped capacitance method in dielectric time-domain spectroscopy", Adv.Molec.Relaxation Processes, 6, 123 (1974).

5. SUCHER M. and FOX J.(Ed), "Handbook of Microwave Measurements", 3rd edn. Polytechnic Press, Brooklyn N.Y. (1963).

6. SAAD T.S., "Microwave Engineers Handbook", Artech House Inc., Mass. (1971).

7. WINSCHEL B.O., "Standardization of precision coaxial connectors", Proc.IEEE 55, 923 (1967).

8. MARYOTT A.A. and SMITH E.R.,"Tables of dielectric constants of pure liquids", Nat.Bur.Stand., Washington D.C., NBS Circular No.514 (1951).

9. BUCKLEY F. and MARYOTT A.A., "Tables of dielectric dispersion data for pure liquids and dilute solutions", Nat.Bur.Stand., Washington, D.C., NBS Circular No.589 (1958).

10. Handbook of the American Institute of Physics, 2nd Edn., McGraw-Hill Bk.Co.1963.

11. HASTED J.B. in "Water: A Comprehensive Treatise", Vol.I Franks F.(Ed)., Plenum Press, N.Y. (1972) Chapt.7.

12. NIGHTINGALE N.R.V., SZWARNOWSKI S., SHEPPARD R.J. and GRANT E.H., "A coaxial line cell for measuring the permittivity of medium to high loss liquids in the frequency range 2 to 15 GHz", J.Phys. E., 14, 14, 156 (1981).

13. NICOL E.A. and HILL N.E., "Dielectric properties of simple liquids at high frequencies", J.Phys. C, 3, 2207 (1970).

14. VON HIPPEL A.R. (Ed), "Dielectric Materials and Applications", M.I.T.Press, Cambridge, Mass. (1954), p.334.

15. WUNDERLICH W., "The physical properties of polymethyl methacrylate", in "Polymer Handbook", BRANDRUP J. and IMMERGUT E.H.(Eds) 2nd Edn., Wiley Interscience (1975) p.V-55.

16. MORENO T., "Microwave Transmission Design Data", Dover Publications (1948).

(a)

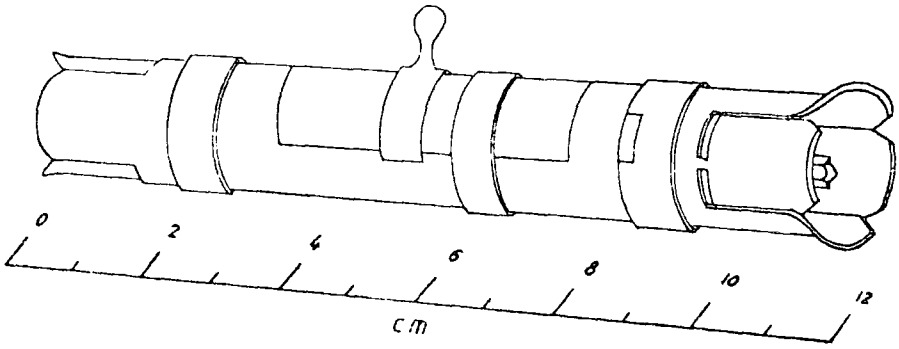

(b)

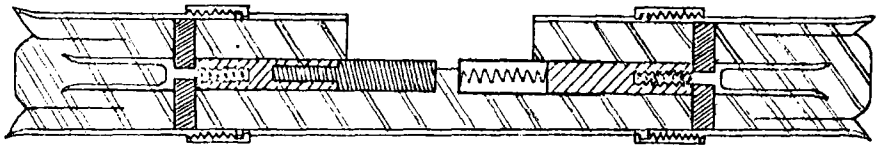

(c)

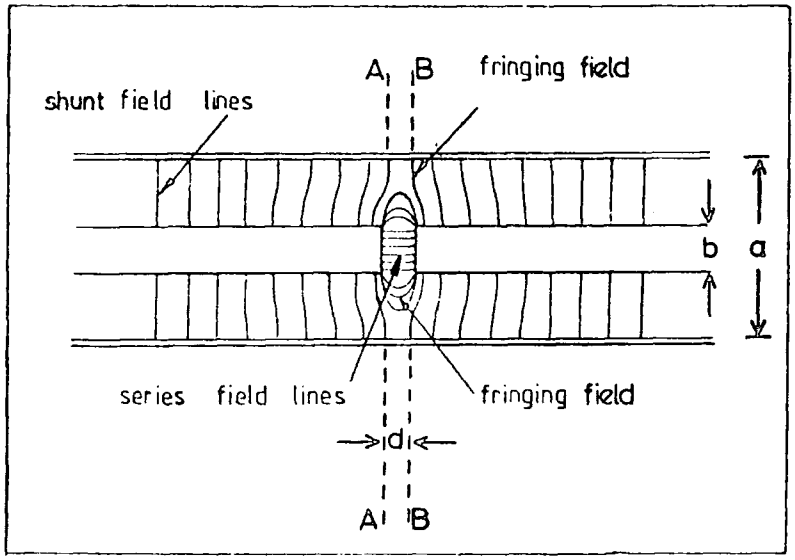

Fig. 1 (a) External view and (b) cross-section of sample-holder
(c) Electric field distribution.

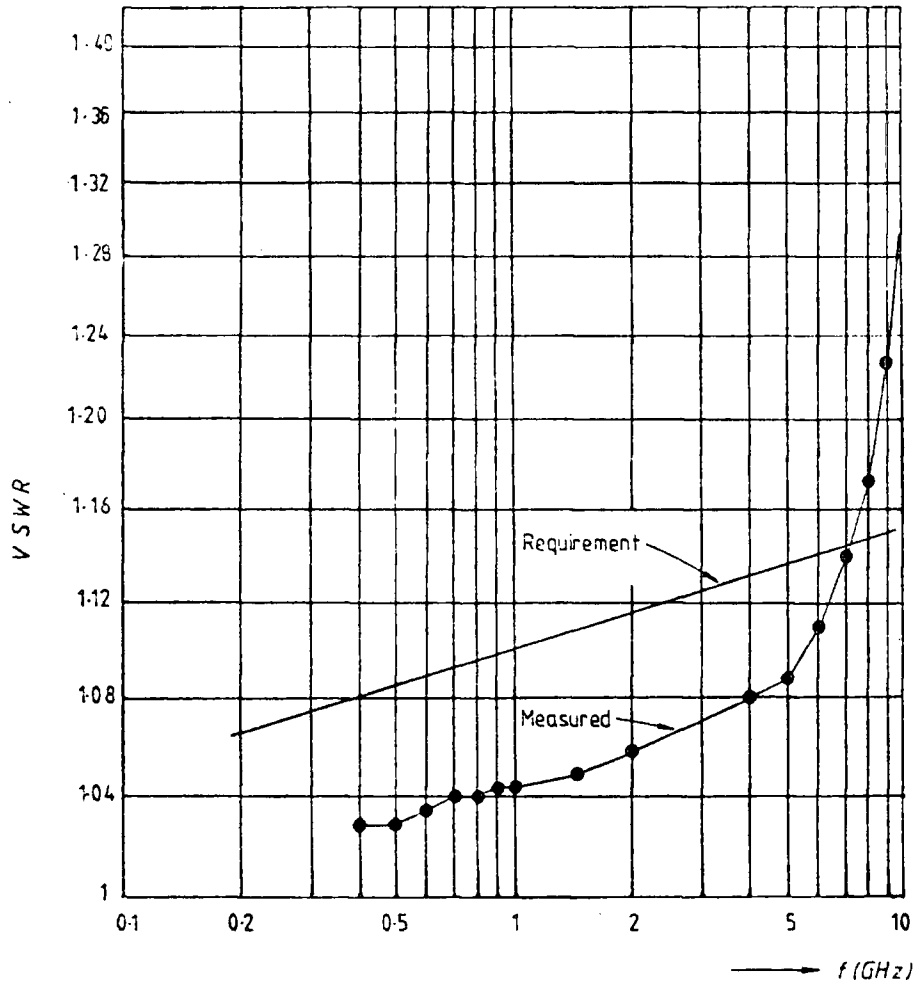

(a)

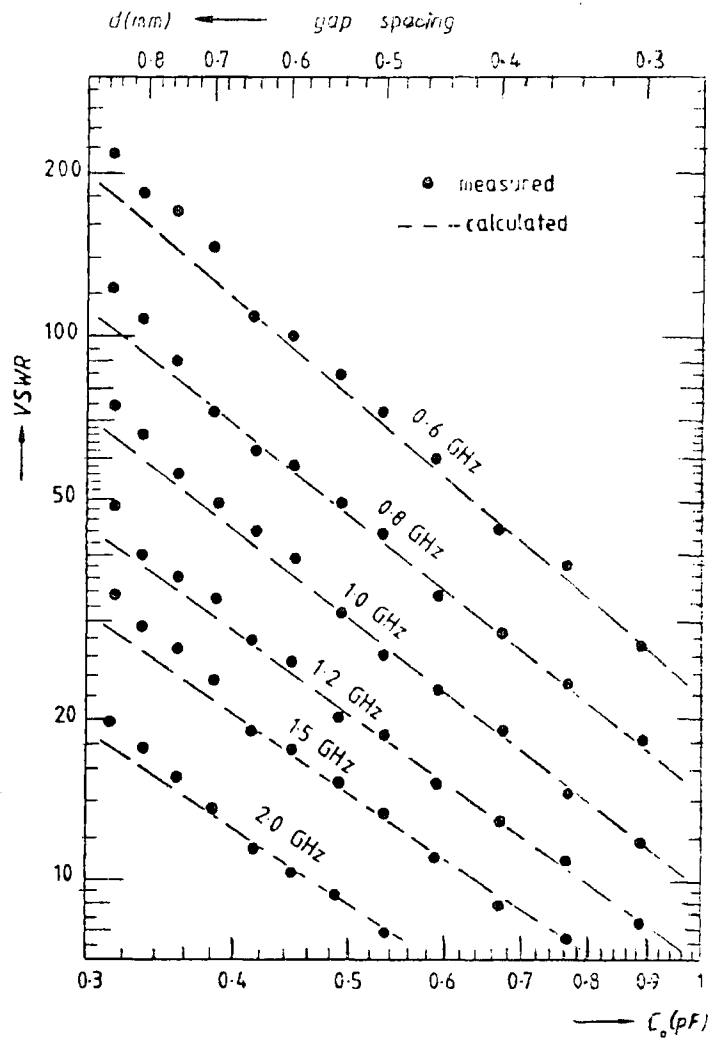

(b)

FIG.2. VSWR of the sample holde terminated with 50Ω at various frequencies for (a) Gap closed and (b) Different gap spacing

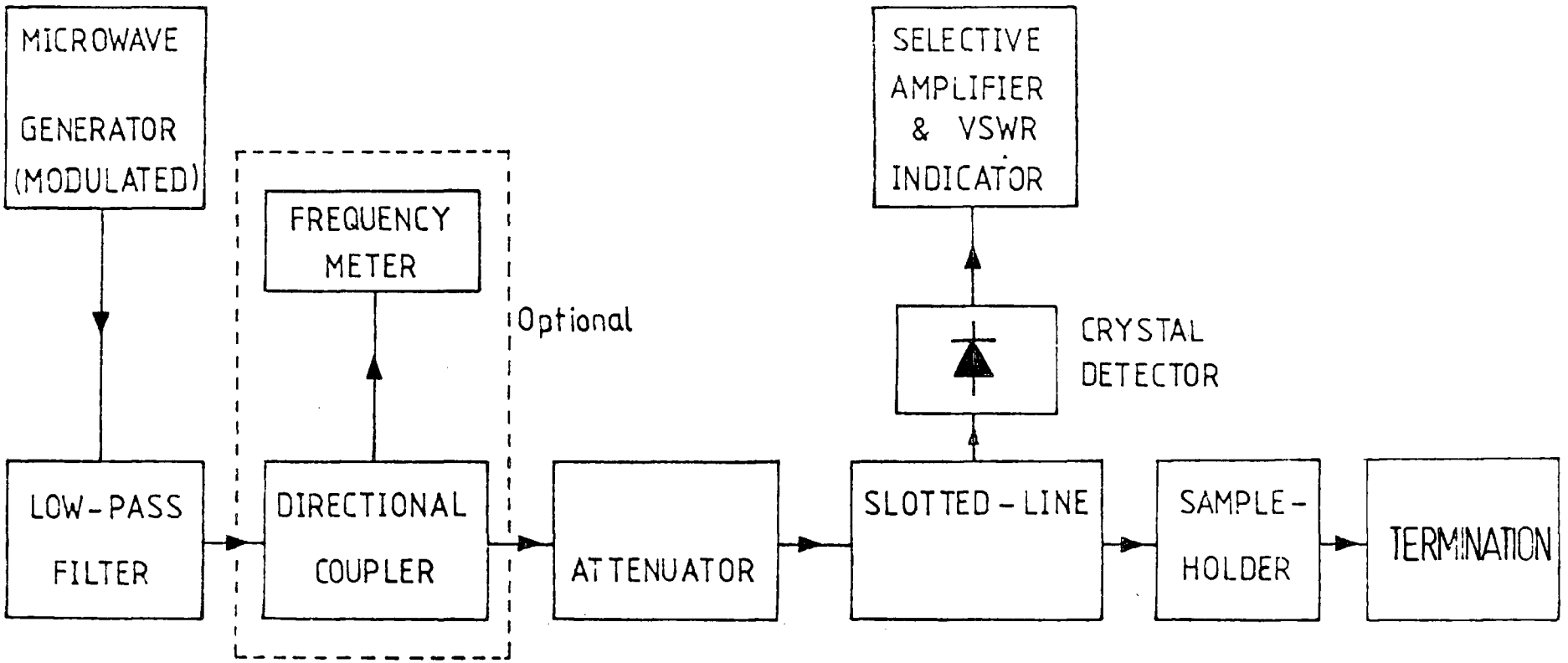

Fig 3 Block diagram of the coaxial line experimental bench.

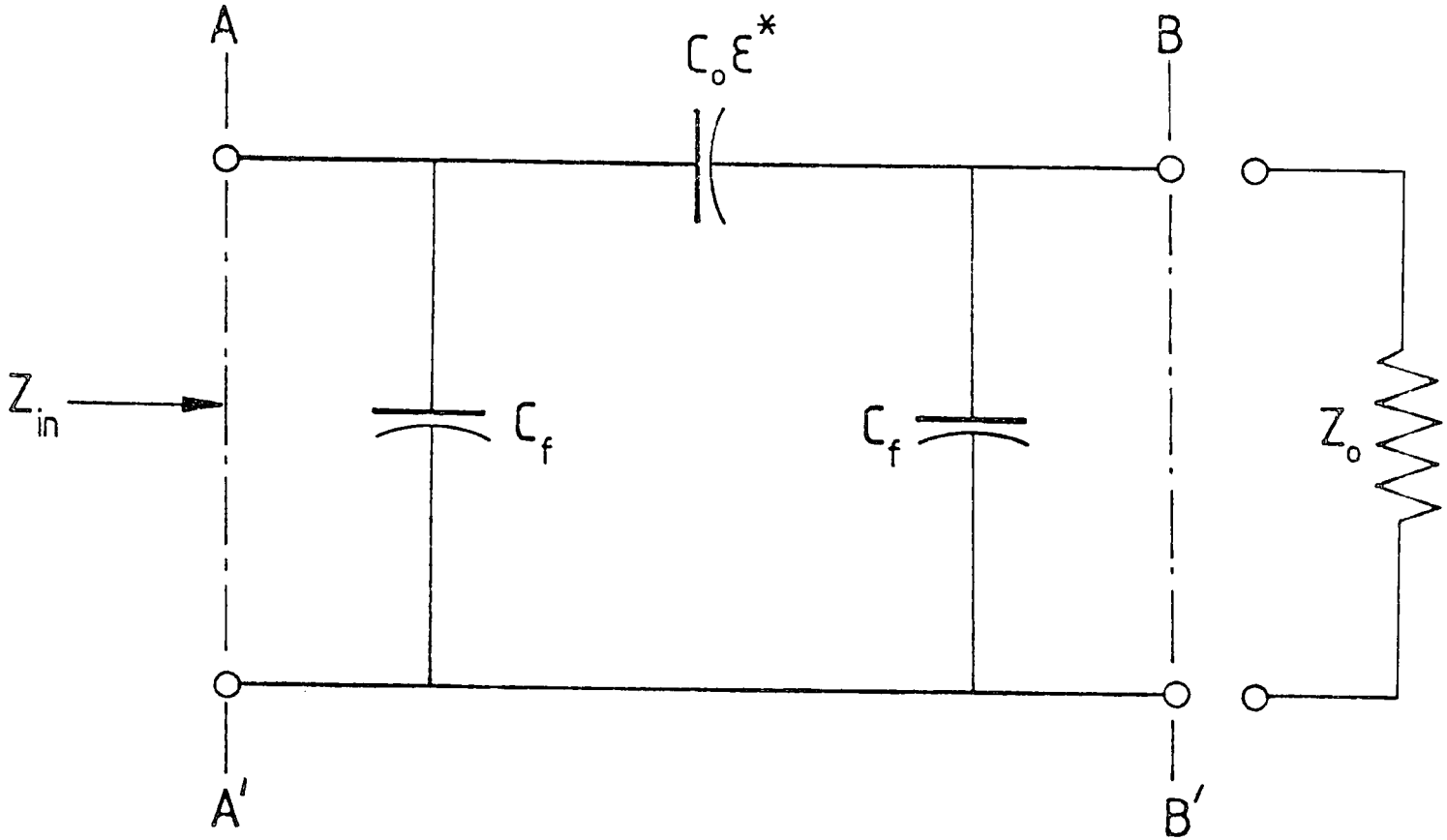

FIG. 4 The equivalent circuit for the Matched Termination Method.

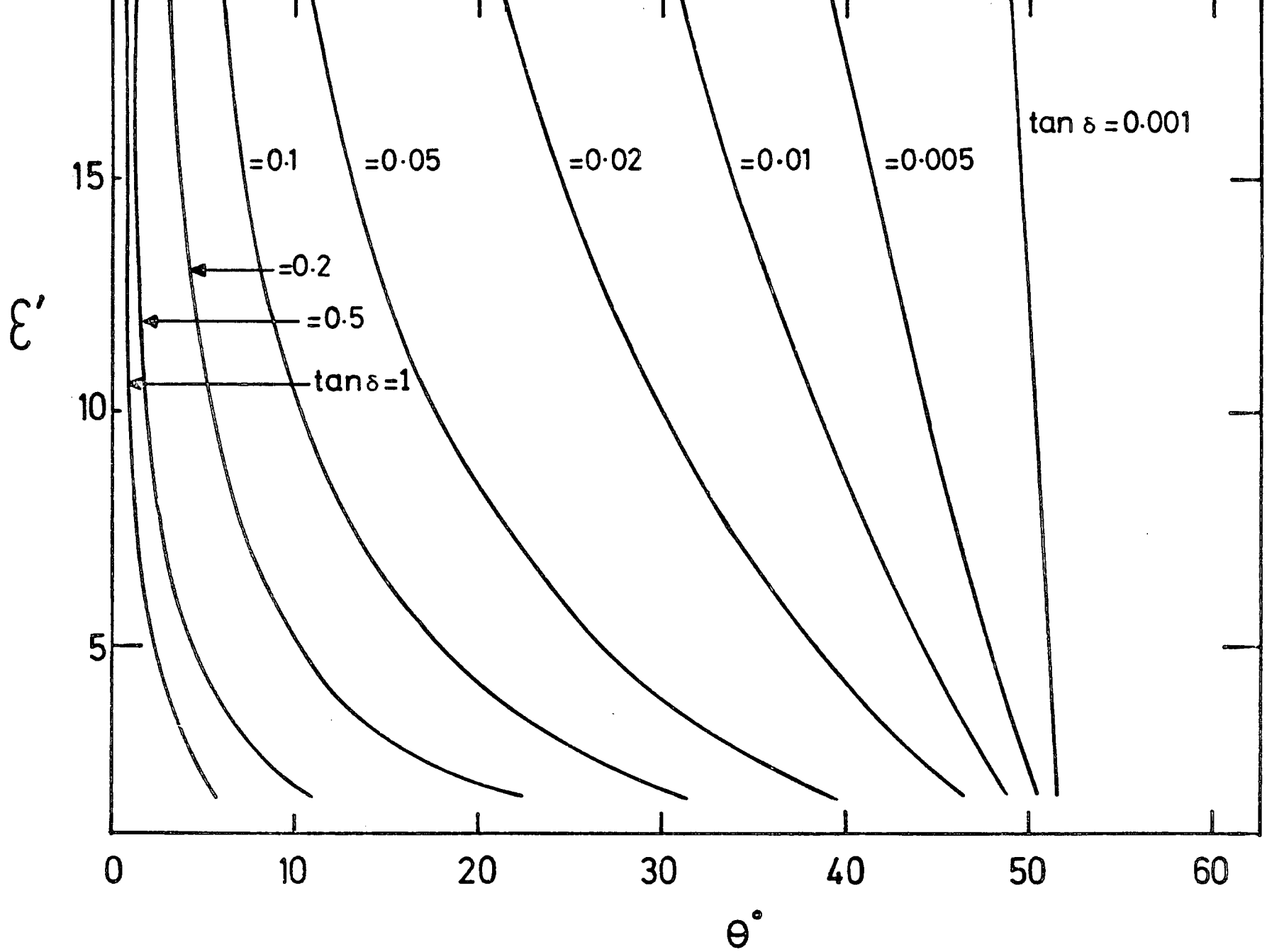

FIG.5. Interdependence of parameters in Eqn. 8 for 0·5mm gap at 500 MHz with C_f/C_o=0·112

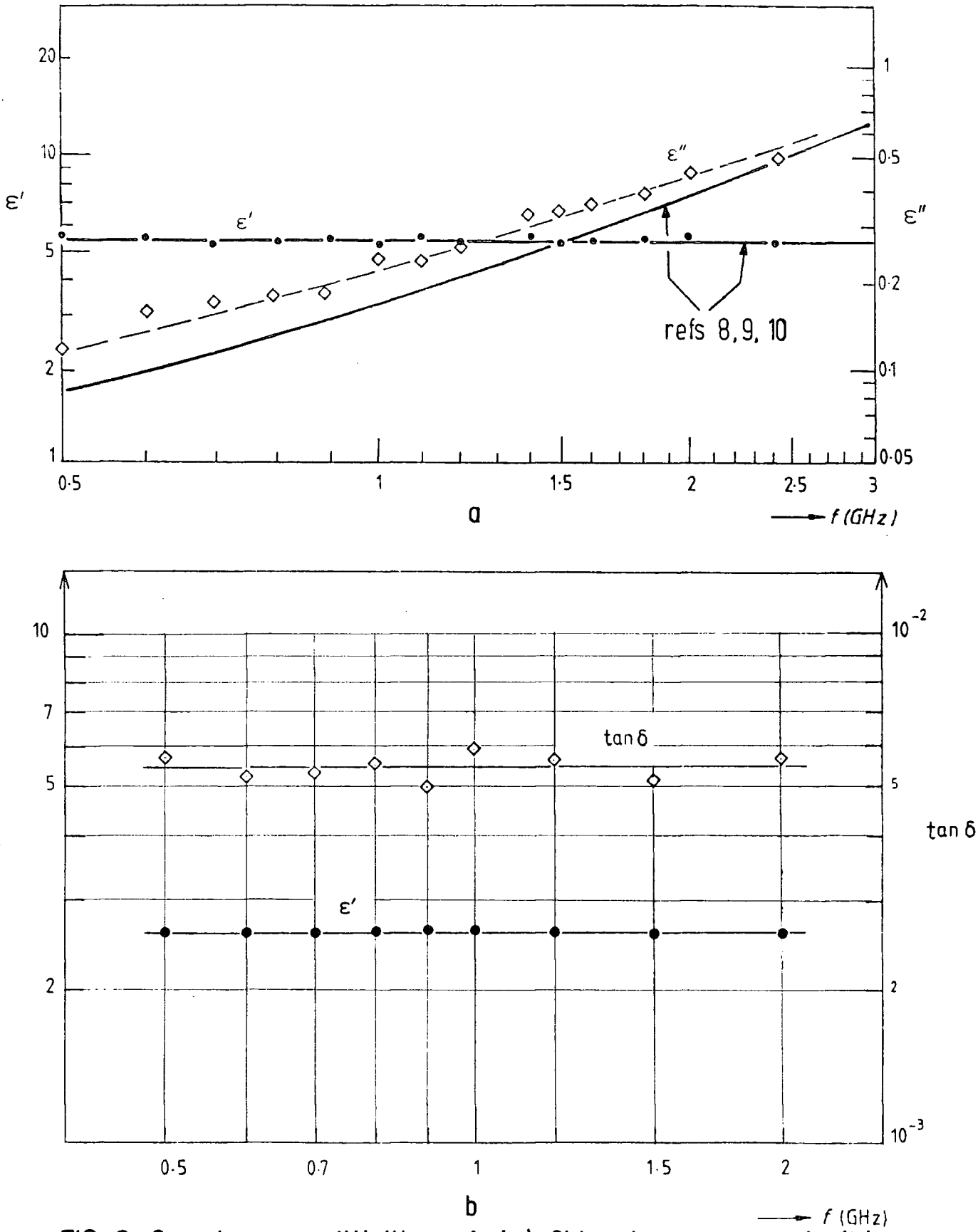

FIG. 6. Complex permittivities of (a) Chlorobenzene and (b) Polymethylmethacrylate (PMMA - perspex) determined using the Matched Termination Method.

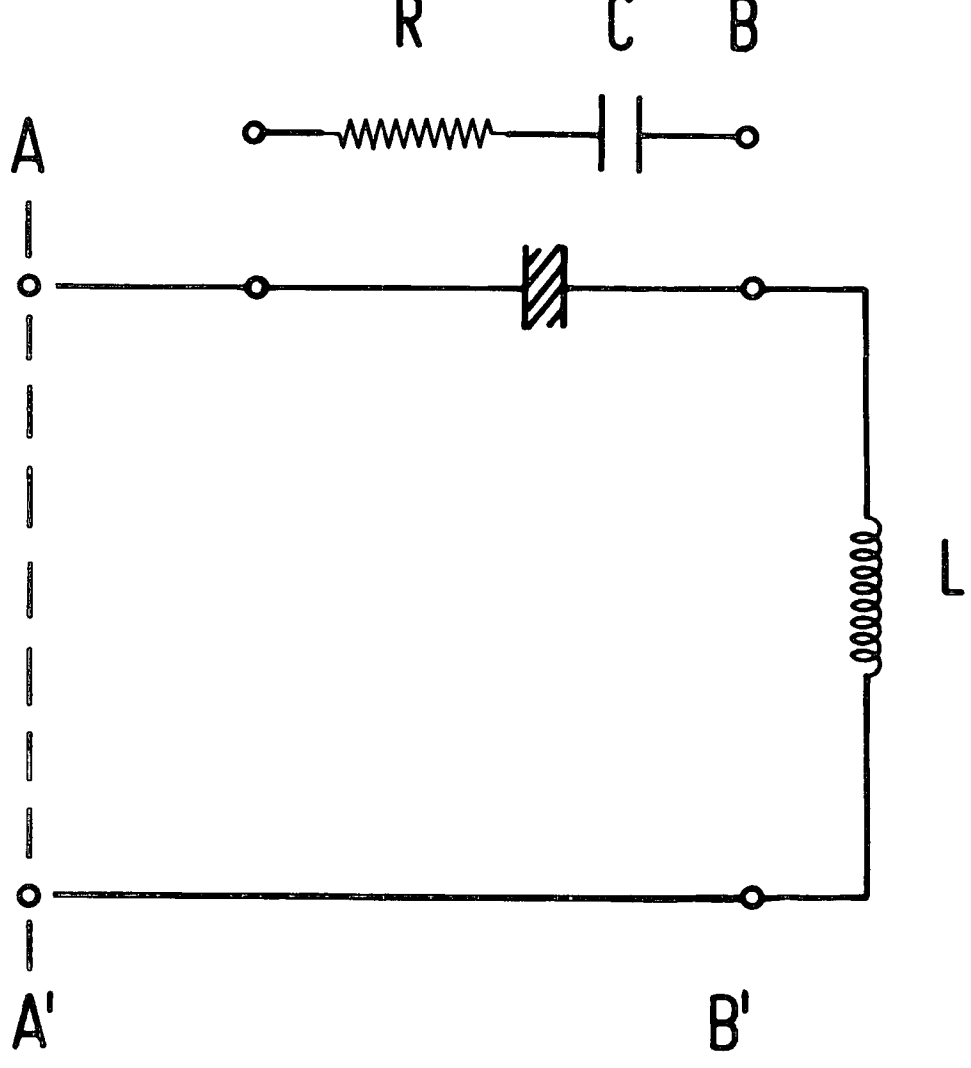

FIG. 7. The equivalent circuit for the Resonant Line Method .

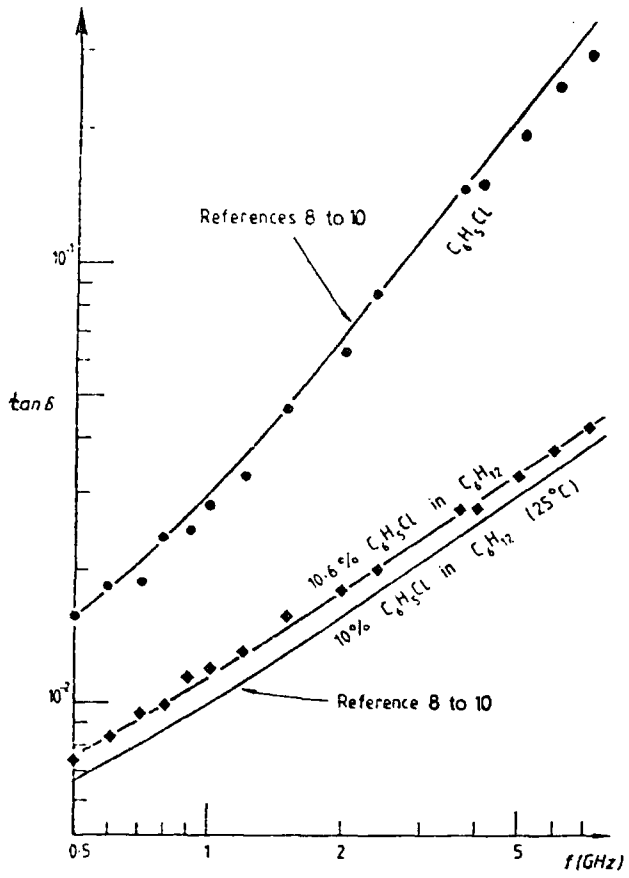

(a)

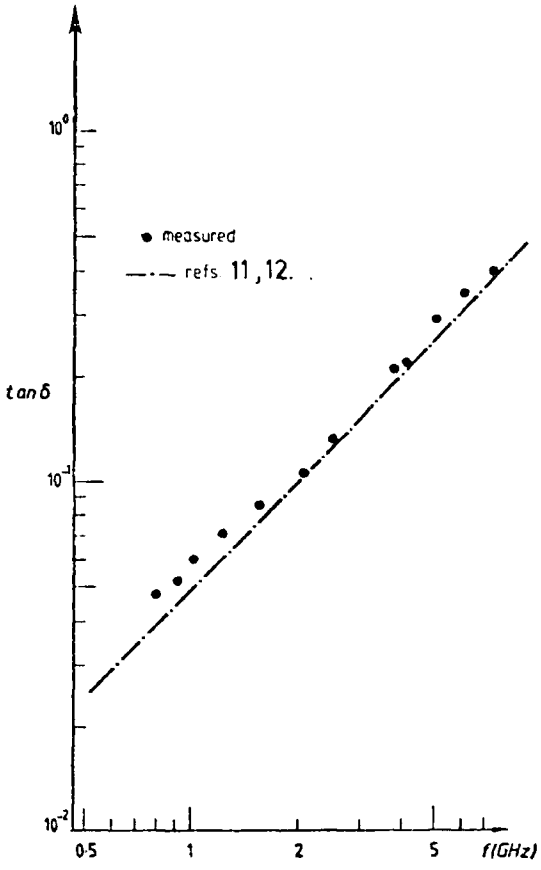

(b)

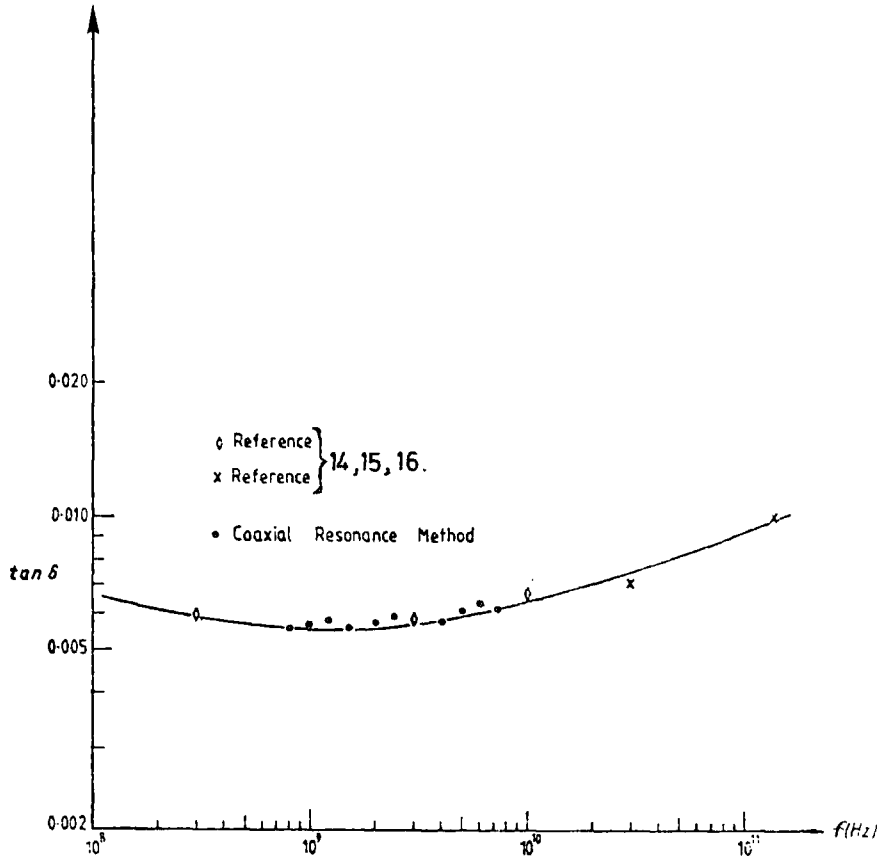

(c)

FIG. 8. Loss Tangent of;

(a) Chlorobenzene andchlorobenzene in cyclohexane solution. (b) Pure distilled water. (c) PMMA. Determined using the Resonant Line Method.

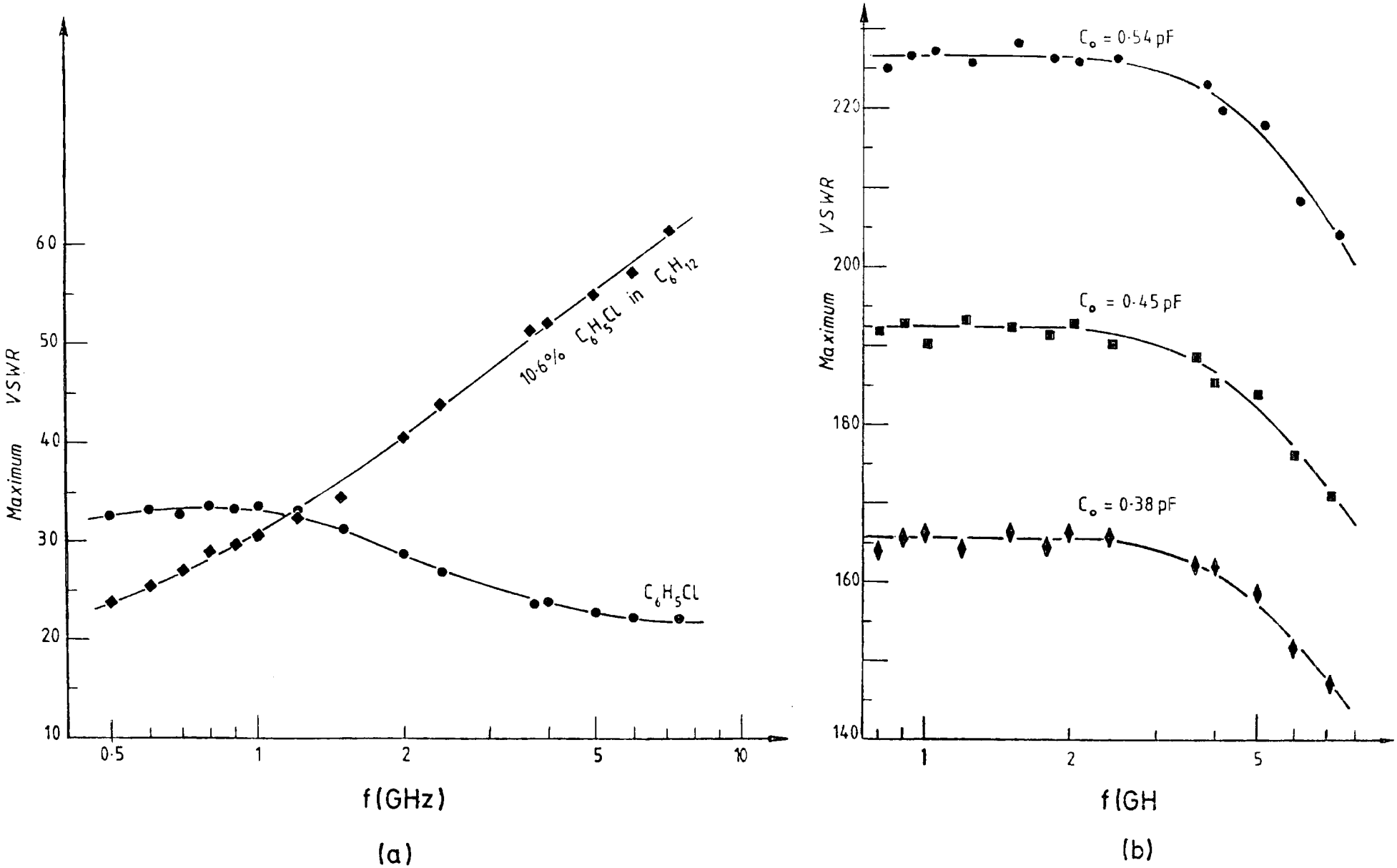

FIG.9. Maximum VSWR readings against frequency for (a) chlorobenzene and chlorobenzene in cyclohexane solution (b) Pure distilled water for three different gap spacings.

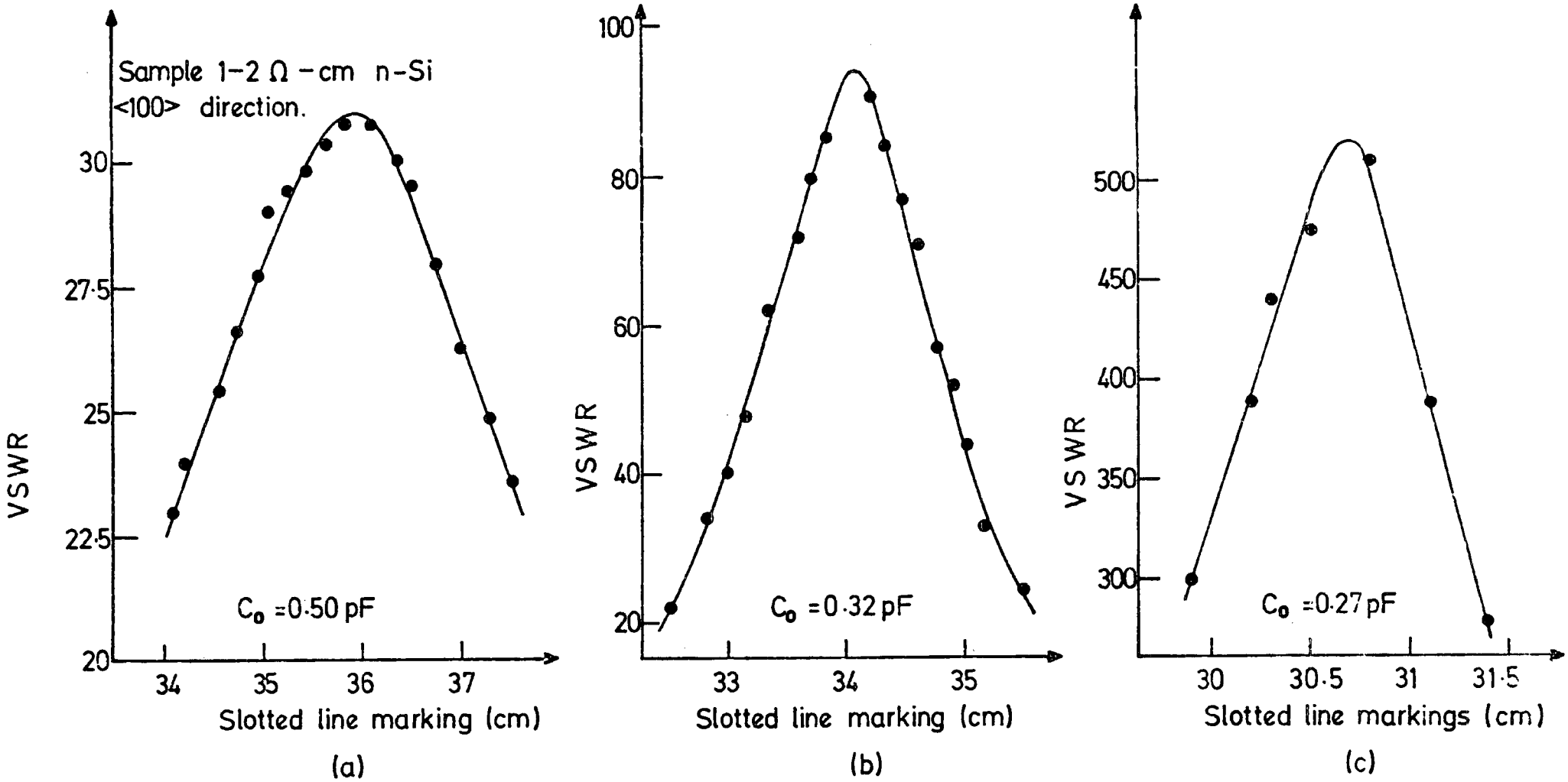

FIG. 10. VSWR Resonance curves for (a) silicon at 2 GHz, (b) PMMA at 2 GHz and (c) Teflon at 1 GHz.